A REVIEW OF RESEARCH ON AERONAUTICAL FATIGUE IN THE UNITED STATES

1999 - 2001

Compiled by
James L. Rudd
Air Force Research Laboratory
Wright-Patterson Air Force Base, Ohio, USA

FOR PRESENTATION AT THE MEETING
OF THE
INTERNATIONAL COMMITTEE ON AERONAUTICAL FATIGUE

25 - 29 JUNE 2001

TOULOUSE, FRANCE

TABLE OF CONTENTS

9.1. INTRODUCTION

1. Leading government laboratories, universities and aerospace manufacturers were invited to contribute summaries of recent aeronautical fatigue research activities. Their voluntary contributions are compiled here. Inquiries should be addressed to the person whose name accompanies each item. On behalf of the International Committee of Aeronautical Fatigue, the generous contribution of each organization is hereby gratefully acknowledged.

+ The Boeing Company – Commercial Airplane Group
+ NASA - Langley Research Center
+ Federal Aviation Administration
+ Air Force Research Laboratory
+ Fatigue Technology Inc.
+ University of Utah
+ The Boeing Company – Phantom Works
+ NASA - Glenn Research Center
+ Lehigh University
+ LSP Technologies Inc.
+ Honeywell Laboratories
+ Stress Wave Inc.
+ Purdue University
+ Rochester Institute of Technology
+ NASA – Johnson Space Center
+ U. S. Army Research Laboratory
+ Old Dominion University
+ Idaho National Engineering and Environmental Laboratory
+ University of Dayton Research Institute
+ Lockheed Martin Aeronautics Company
+ Analytical Processes Engineered Solutions Inc.
+ Gulfstream Aerospace
+ Ohio Aerospace Institute

2. The assistance of Ms. Charlotte Burns, Universal Technology Corporation, in the preparation of this review is gratefully appreciated.

3. Reference numbers are indicated as [ ]. For example, [1] is reference 1. References, if any, are listed at the end of each article. Figures are compiled at the end of the review.

9.2. OVERVIEWS

9.2.1 Comparison of Crack-Growth Lives for Fixed- and Rotary-Wing Aircraft

R.A. Everett, Jr., U.S. Army Vehicle Technology Directorate

In 1983, Sikorsky Aircraft was contracted by the U.S. Air Force to conduct a damage-tolerance assessment of selected HH-53 helicopter structure [1]. This study indicated that a few of the critical rotor components could be managed by damage tolerance if reliable detection of 0.13 mm and 0.25 mm long cracks were possible. Others would need to be redesigned. One of the objectives of the present work was to show the severity of the high cycle loading environment of the helicopter compared to that of fixed-wing aircraft and thus, the potential difficulty of applying a damage tolerance design to helicopters. This was accomplished by comparing crack growth times from an initial crack size of 0.38 mm to failure for a helicopter load spectra with that of a commercial transport and a fighter fixed-wing aircraft. This was done for a steel, an aluminum alloy, and a titanium alloy typically used in helicopters. Crack-growth lives were determined using the computer code FASTRAN [2], which uses a crack-closure concept based on a modified Dugdale strip-yield model and plasticity-induced closure.

In this study, the structural configuration was a 6.35-mm radius (r) open hole in a 3-mm thick plate (one-half width w = 25.4 mm). The crack geometry was defined as a corner crack growing from the hole with an initial crack size of 0.38 mm. The crack length (c_i) and depth (a_i) were assumed to be equal. This initial crack size is what one U.S. rotorcraft manufacturer uses for its damage tolerance designs. This size is also recommended by the U.S. Air Force for rotorcraft rotor components. For the 4340 steel used in this study, the ultimate strength was 1460 MPa with a ΔKeff threshold of 3.2 MPa-m$^{1/2}$. The helicopter load spectra used was Felix/28 [3], the commercial fixed wing transport spectra was called ComTran, and the fixed-wing fighter spectra was Falstaff [4].

The results of these comparisons are shown in Figure 1 for an applied gross stress (S_{max}) of 415 MPa, which is the maximum stress in the spectra. These results show how much more severe the high cycle rotorcraft spectra are than the fixed-wing aircraft when crack-growth lives to failure are compared. For the aluminum alloy 7075 similar results were shown while for the titanium alloy Ti-6Al-4V the difference in the crack-growth lives was even greater. In a damage tolerance assessment done by a major U.S. helicopter manufacturer on a main rotor spindle, the thickness at the critical crack location had to be increased by 38 percent to achieve an adequate crack-growth inspection interval. As shown in Figure 2, it would take about a 60 percent reduction in stress (to 165 MPa) in the above example to achieve an adequate inspection interval of about 1000 hours. Some helicopter manufacturers have stated that in order for damage tolerance to be applied successfully in rotorcraft, that a 40 percent stress reduction would be required from the safe-life design stresses. They also note that this needs to be done only in the critical crack location areas.

REFERENCES

[1] Tritsch, D. E.., Schneider, G. J., Chamber, G., and Lincoln, J. W., "Damage Tolerance Assessment of the HH-53 Helicopter," American Helicopter 46th Annual Forum Proceedings, Washington ,D.C., May 21-23, 1990.

[2] Newman,J. C., Jr., "FASTRAN-II - A Fatigue Crack Growth Structural Analysis Program," NASA TM 104159, Feb. 1992.

[3] Edwards, P. R. and Darts, J., "Standardized Fatigue Loading Sequence for Helicopter Rotors (Helix and Felix) Part I, Background and Fatigue Evaluation," Royal Aeronautical Establishment, TR 84084, Aug. 1984.

[4] van Dijk, G. M. and de Jonge,J. B., "Introduction to a Fighter Aircraft Loading Standard for Fatigue Evaluation, FALSTAFF, NLR, MP 75017U, May 1975.

9.2.2 A Critical Comparison between Mechanistically Based Probability and Statistically Based Modeling

Dr. D. Gary Harlow and Dr. Robert P. Wei, Lehigh University

Probability analyses are increasingly being used for reliability and durability predictions and risk assessments in the life-cycle design and management of aircraft and other engineered systems. A critical comparison between the mechanistically based probability approach and the statistically based modeling approach (used in current design methodologies) is made to show the urgent need for a change in design paradigm. The differences between the two approaches are illustrated by the flow diagrams in Fig. 3 and are demonstrated through the modeling of creep crack growth in a high strength steel, and the inferences drawn from these modeling approaches. Current methods for probabilistic design analyses are principally statistically and empirically based, and provide *ex post facto* parametric modeling of the observed phenomenon to reflect only those parameters that had been imposed in the development of the underlying experimental data. The mechanistically based probability modeling approach, on the other hand, differs significantly from these more traditional methods. It builds upon well-designed critical experiments to identify the key *internal* and *external* variables, and their variability, and entails the formulation of a mechanistic model to correctly represent the functional dependencies of the responses in terms of these key variables.

To highlight the difference between the two approaches, their difference is illustrated through modeling of creep crack growth in terms of kinetics in Fig. 4a and, in terms of the cumulative probability of failure at selected stress levels, in Fig. 4b. The mechanistically based probability model reflects the integration of a micromechanical model for creep crack growth with a dislocation-based model for creep. It seeks to transform mechanistic understanding of the processes of damage evolution into models that capture the functional dependence on the key *external* (*e.g.*, loading and environmental) and *internal* (*e.g.*, chemical and microstructural) variables. (Here, the external variables are stress, argon and 297 K, and the internal variables are process zone size (or, inclusion spacing, d_T), hardness σ^*, creep rate coefficient $\dot{A}^*$, and initial crack size, respectively.) It would provide probabilistic distributions that reflect the stochastic contributions from variations in only these variables. Once validated, it enables predictions beyond the range of typical data, facilitates predictions outside of the experiential base, and provides a quantifiable basis for assessment of risk.

Statistically based parametric approach, on the other hand, is predicated on the parametric representation of experimental data through regression analysis. As such, it can only capture the influences of those *external* variables that were utilized in gathering the data. The resulting parametric model is suitable only as an interpolative tool, and its use for predictions outside of the experiential base is fraught with danger. Because of model uncertainties and the inability to discriminate between variability associated with variations in key *internal* variables (which are seldom, if ever, defined), and that from uncontrolled variables and measurement errors, its suitability for use in risk assessment is uncertain. The approach could lead to conservative designs, or premature retirement of components and systems; both of which are costly. For example, for a design probability of failure of about 0.05 at 100 h, a reduction in design allowable stress from about 600 MPa for the mechanistically based probability approach to about 400 MPa for the statistical approach (or about 35 pct) would be required, see Fig. 2b. It is to be noted that, for the example given here, the data used in developing the statistical model had come from a limited number of well-controlled tests on a single material. As such, the indicated variability is principally associated with measurement errors. Its use as a measure of variability (*i.e.*, from *internal* variables) for reliability assessment is problematic.

Because it is the variability associated with the *internal* (*e.g.*, microstructural) *variables* that needs to be taken into account, it is essential to adopt the mechanistically based probability methodology for design.

REFERENCES

[1] D.G. and Wei, R.P. (2001). In *Probabilistic Methods in Fatigue and Fracture,* Vol. 200, pp. 119-138, A.B.O. Soboyejo, I.R. Orisamolu and W.O. Soboyejo (Eds.) Trans Tech Publications Ltd, Switzerland.

[2] Wei, R.P. (2001). In *Chemistry and Electrochemistry of Corrosion and Stress Corrosion Cracking: A Symposium Honoring the Contributions of R.W. Staehle*, pp. 263-278, Russell H. Jones (Ed.) The Minerals, Metals & Materials Society, Warrendale, PA 15086.Harlow

9.2.3 Development of Methodology for Establishing Durability and Damage Tolerance of Bonded Assemblies in Small Composite Aircraft

Mr. Peter Shyprykevich, FAA, AAR-430, (609) 485-4967

Recent developments in the small aircraft arena have featured significant growth in the use of bonded construction for joints and assemblies in composite airframe components. For example, there are currently about 14 general aviation (GA) class composite aircraft that have recently been or are currently being certified. Although with a few exceptions, larger aircraft such as transports have generally avoided bonded construction in flight critical areas, while small aircraft manufacturers have embraced bonding as an important element in achieving low manufacturing costs along with higher performance in composite aircraft.

The vigorous expansion of bonding for primary structure in the small composite aircraft has led to the investigation of several safety issues for bonded joints and assemblies, as the small aircraft industry is relatively unfamiliar with this type of construction. The issues include (1) the use of unusually large bond thicknesses— up to 0.1" or greater which some manufacturers have found cost effective; (2) the preparation of the surface, the most important factor in achieving structurally safe and durable adhesive joints; and (3) the design of the overall structure to provide damage tolerance for disbonds which might lead to loss of aircraft. An effort to address these issues supported jointly by the FAA and the NASA Advanced GA Transport Experiments (AGATE) consortium with the small airplane industry has been underway for some time. The effort involves activities in which the participants shown in Figure 5 are all involved. In this team effort, the FAA and NASA Langley jointly interact with the AGATE consortium. In addition, the FAA funds activities with Wichita State University (WSU) and the University of California at Santa Barbara (UCSB) through the FAA Airworthiness Assurance Center of Excellence (AACE). In particular, an effort on damage tolerance of bonded structure is being at UCSB and directly involves two small airplane manufacturers, Cirrus Design of Duluth, MN, and Pacific Aviation Composites of Bend, OR; both have recently certified small composite aircraft using significant levels of bonded construction. This effort is developing structural analysis and component modeling which, when combined with appropriate experimental efforts, will provide guidance to the industry and the FAA on design features for small composite aircraft. This will also help to insure structural safety and durability in this kind of construction. It is planned that this information will be incorporated into an FAA Advisory Circular.

An example of a typical application of bonded construction to small composite aircraft being investigated at UCSB is shown in Figure 6. Bonding together two premanufactured halves of a fuselage along the center line (C-L), as shown in the figure, has become common practice since it was first used in the 1980s. The safety issue of loss of the bond between the two halves under torsion loading is also under investigation in the USCB research.

9.2.4 Health and Usage Monitoring System (HUMS)

Dr. Dy Le, FAA, AAR-431, (609) 485-4636

The FAA and the U.S. Navy signed an Interagency Agreement and began a joint validation of the military and commercial Health and Usage Monitoring System (HUMS) for rotorcraft under the Defense Advanced Research Project Agency (DARPA) Dual Use Application Program. This joint validation is to address the draft Advisory Circular requirements and provide input for the certification of the HUMS installation and maintenance credits. (Figure 7.)

The FAA has also funded an investigation conducted by Bell Helicopter, Inc., on the application of usage monitoring on helicopter dynamic components and the analytical redesigns of four helicopter components to meet damage tolerance requirements.

The Bell effort will also develop mission spectrum data for modern helicopter usage to update the FAA Order 8110.9, Handbook on Vibration Substantiation and Fatigue Evaluation of Helicopter and Other Power Transmission Systems and the Civil Aeronautics Regulation (CAR) 6, Appendix A, Rotorcraft Airworthiness – Normal Category. The spectrum data will also be used to improve the accuracy of the analytical techniques used to predict crack growth in rotorcraft metallic and composite components. The results will be used to support the validation of the rotorcraft damage tolerance methodologies that can be used for regulatory compliance. (Figure 8.)

The actual flight spectrum of a particular aircraft is tracked using HUMS and the flight data recorder-equipped Bell 412 helicopter. Usage monitoring requires algorithms that define conditions based on measured parameters such as airspeed, altitude, roll angle, pitch angle, load factor, vertical velocity, and power setting. By monitoring these parameters on a flying aircraft, the maneuvers that are actually being flown by the helicopter are determined. The actual spectrum of the aircraft can then be generated.

Loads measured during the flight load survey and the actual aircraft spectrum from HUMS would be used for the analytical redesigns of four principal structural elements (PSE) in critical areas, Figure 9. Selected PSEs are the main rotor yoke, the main rotor spindle, the main rotor rephrase lever, and the collective lever.

Preliminary investigations and calculations using two flight missions compared to the FAA certification flight spectrum have been completed. The results of the calculations are presented in the following paragraphs.

Main Rotor Yoke
The goal was to analytically redesign the main rotor yoke, Figure 10, so that the crack growth life would be twice the retirement life of the yoke. The analytical results showed that to reach this goal required an increase in the thickness and there was an unacceptable weight increase as the thickness increased. Thus, the main rotor yoke may not be practically redesigned using a damage tolerance approach. An alternative approach may include another material, such as a composite configuration.

Main Rotor Spindle
The goal was to analytically redesign the spindle lugs, shown at cross-section A-A in Figure 11, so that no crack growth would occur assuming a 0.0015-inch initial flaw size for the most severe maneuver in the certification load level survey. Analytical results showed a weight increase of 4.6% was required with an inspection interval of 10,000 flight hours. Thus, due to the significant weight penalty, the spindle also may not be practically redesigned using a damage tolerance approach.

Main Rotor Rephrase Lever
The rephrase lever, Figure 12, was analyzed to determine the highest stressed location in the lever. This would be the location where the stress would exceed the crack growth threshold stress. The analysis identified the rephrase lever arm, section A-A in the figure, as the area with a highest stress level. The analysis showed that any crack at the location would lead to failure of the part unless the weight of the part was increased by 15%. Once again, the weight penalty is significant, leading to the conclusion that it may not be practical to redesign the main rotor rephrase lever using a damage tolerance approach.

Collective Lever
The collective lever, Figure 13, was also analyzed to determine the location in the lever that would produce a stress above the threshold stress for crack growth. The analysis identified a high-stress section near the area where the collective boost tube connects to the collective lever, section A-A as shown in figure 13. The analysis showed that any crack at the location would lead to failure of the part unless the weight of the part was increased by 15%. Once again, the weight penalty is significant, leading to the conclusion that it may not be practical to redesign the collective lever using a damage tolerance approach.

In summary, the preliminary analyses showed, for the four PSEs considered, it may not be practical to redesign them using a damage tolerance approach due to the severe weight required to meet the damage tolerance goals for each PSE. However, although the weight penalty was significant for each redesign, it is expected that for a new part that incorporates a damage tolerance approach from the beginning of the design process, the weight impact would be minimal.

9.2.5 Rotorcraft Fatigue and Damage Tolerance

Dr. Dy Le, FAA, AAR-431, (609) 485-4636

The Technical Oversight Group for Aging Aircraft (TOGAA), formed by the FAA to address aging aircraft issues, expressed concerns regarding the current Federal Aviation Regulation (FAR) 29.571, Fatigue Evaluation. They requested the helicopter companies to form a rotorcraft working group (RCWG) to review current fatigue and evolving damage tolerance methodologies being used by the U.S. and international helicopter manufacturers.

The RCWG was composed of representatives from major helicopter manufacturers in the U.S. and Europe. The group was tasked to conduct a study to review current fatigue and evolving damage tolerance methodologies and communicate their findings to the FAA and TOGAA. Participating U.S. helicopter manufacturers included Bell

Helicopter Textron, Inc., Sikorsky Aircraft Corporation, Boeing, and Columbia Helicopters. Participating European helicopter manufacturers included Augusta SPA, Westland Helicopters Ltd., and Eurocopter.

The RCWG conducted an in-depth study of the rotorcraft fatigue and damage tolerance methodologies currently in use in the rotorcraft. In the final report entitled *Rotorcraft Fatigue and Damage Tolerance* distributed in January 1999, the RCWG described various rotorcraft fatigue substantiation methods such as safe life, damage tolerance, and flaw tolerance. They concluded that both fatigue and damage tolerance methodologies would require some judgment and interpretation by an analyst. The RCWG recommended that the rotorcraft industry transitioning to damage and/or flaw tolerance should proceed cautiously while retaining the safe-life method. Additionally, the report recommended more research on damage and flaw tolerance to include the development of crack growth data and a software tool.

Based on the RCWG report, TOGAA made a recommendation to the FAA that a damage tolerance philosophy, if shown to be practical, should be used in the design and certification of rotorcraft structural components. In response to TOGAA's recommendation, the FAA initiated a rulemaking process to revise Federal Aviation Regulations (FAR) 29.571, Fatigue Evaluation, to include damage tolerance requirements in the design and certification of rotorcraft structural components.

The FAA, in collaboration with the rotorcraft industry and academia, then formulated a rotorcraft damage tolerance (RCDT) research roadmap outlining several critical areas of research needed for industry and the FAA to be able to design and certificate rotorcraft structural components using a damage tolerance philosophy.

Based on this jointly developed RCDT roadmap, the FAA and the rotorcraft industry have started several damage tolerance research efforts to support the development of new guidance material for the anticipated revision of FAR 29.571. Prioritized research tasks in the RCDT roadmap include development, assessment, and validation in the following areas:

Rotorcraft Damage Tolerance Guidelines
A set of rotorcraft airframe structure and dynamic structural components will be assessed to determine the practicality of using damage tolerance procedures for certification and continued safe operation of the rotorcraft.

Usage Monitoring
Actual mission spectrum data will be collected and used to validate the guidance material. The validated guidance material will be used to obtain the airworthiness approval to install Health and Usage Monitoring Systems (HUMS) on rotorcraft and for usage and maintenance credit validation for continued airworthiness on certain rotorcraft.

Equivalent Initial Flaw Size
The equivalent initial flaw size distributions that exist in newly manufactured and fielded parts will be determined, as this is required for damage tolerance designs. This information will be incorporated into advisory material.

Crack Growth Database
Various standard and nonstandard test methods will be reviewed to select best test methods for data such as through-crack, edge-crack and corner-crack geometries for incorporation into advisory material. Crack growth thresholds, short and long crack, and shot-peening effect data will be determined.

Nondestructive Inspections
Manufacturing and field inspection methods will be reviewed to ensure the required probability of detection.

Certification Testing
Qualification testing procedures and methodologies for fatigue crack initiation and propagation testing studies for rotorcraft metallic and composite material components will be investigated and/or developed.

Life Enhancement Methods
Life enhancement methods using shot-peening and cold working will be evaluated. Methods and practices such as crack arrest mechanisms that may effectively improve the damage tolerant capability of rotorcraft structure will be examined.

Fracture Mechanics Analysis
A computational system architecture with two- and three-dimension linear and nonlinear fracture mechanics analysis capabilities will be validated using established test data. The validated tool will be used in the damage tolerance analysis of airframe structure and dynamic (metallic and composite) components of rotorcraft and as a sanity check for other methodologies, unique to rotorcraft problems that could also be introduced. Stress-intensity factor solutions and residual stress effects on subsurface cracks due to shot-peening and cold working will be developed or determined.

Risk Assessment
Risk assessment data and historical safety data will be combined to review the risk assessment process currently being used in industry for certification. Probabilistic methods will be studied to remove conservatism while maintaining required safety.

Corrosion Control
Corrosion inspection methodologies and prediction tools will be assessed.

9.2.6 Rotorcraft Fatigue and Damage Tolerance
Dr. Dy Le, FAA, AAR-431, (609) 485-4636

One of the FAA's National Aging Aircraft Program Plan milestones is to review and update Title 14 Code of Federal Regulations Part 29 regulations and Advisory Circulars (ACs) regarding aging issues. The goal is to include damage tolerance (DT) requirements in Part 29.

In 2000, the FAA initiated several joint rotorcraft damage tolerance research efforts to support the implementation of DT requirements and the development or revision of applicable ACs. The FAA plans to implement the DT rule by fiscal year 2003.

The FAA, in collaboration with the U.S. rotorcraft industry and academia, revised the developed rotorcraft DT research roadmap outlining ten critical areas of research. Prioritized research tasks in the rotorcraft DT research roadmap include the development, assessment, and validation in the following areas.

Rotorcraft Specific Issues: Selected key principal structural elements (PSE's) where current DT methodology is known to give impractical inspection intervals (main rotor masts and other nonredundant, highly loaded components) are being evaluated. Various computational fracture mechanics capabilities, together with existing rotorcraft material and operational databases, are being used for the evaluation of PSEs.

Spectrum Development and Usage Monitoring: Approaches using the Health and Usage Monitoring System (HUMS) instrumentation and other techniques will be adapted and applied to obtain statistically valid data on various typical maneuvers flown in modern rotorcraft operations. These data will span the range of current and potential future missions (heavy lift, emergency medical service, offshore support, and corporate transport). Techniques will be developed to use this information in Safe Life and Damage Tolerance calculations for all aircraft types.

Equivalent Initial Flaw Sizes and Equivalent Initial Crack Sizes (EIFS/EICS): A statistically valid database of meaningful damage will be compiled from manufacturing, field operations, maintenance center experience, and targeted experiments. The data will be characterized in terms of structural type (airframe, rotors, drive system, flight control, and landing gear), material type (aluminum, titanium, and steel), the origin and character of damage (scratches, impact, nick gouge, and ding), and other considerations (design category of the component and the level of inspectability of the damaged area).

Crack Growth Database: Fatigue crack growth databases for rotorcraft applications will be developed by first developing a new standard test method. The developed method will then be used to generate reliable threshold and other types of short crack, long crack, and high R-ratio data to quantify the effects of shot peening and other surface treatments.

Nondestructive Inspections/Evaluations: Current available equipment and newly developed nondestructive inspection and evaluation (NDI/E) concepts will be examined for their potential to be applied to the component designs, materials, and the crack and blunt flaw sizes that occur in rotorcraft applications. Specific consideration will be given to evaluating current manufacturing technologies and practices; field deployment capabilities; probability of detection in the EIFS and EICS regimes; capability of detecting cracks in multilayered structural assemblies; fretting, corrosion, other noncrack damage; and capability of detecting damage at fastener holes without the need to remove the fastener in complex geometries.

Certification Testing: The basic principles associated with the design of practical qualification tests and experiments for fatigue crack initiation and propagation in safety-of-flight structures will be determined. The research will address the minimum number of component tests needed to verify the analysis, the appropriate testing requirements, the extent to which actual parts need to be tested versus coupons and subassemblies, and the quality and quantity of the data that enable reliable fatigue crack propagation and residual strength determinations to be developed.

Life Enhancement Methods: This research would identify, examine, and quantify the impacts of current life enhancement methods on fatigue life in rotorcraft by focusing on the development and validation of a generalized crack growth analysis model appropriate for all possible rotorcraft components and operating conditions.

Crack Growth Analysis: In coordination with the research at the U.S. Air Force and the National Aeronautics and Space Administration (NASA), a comprehensive database for the analysis of crack growth in rotorcraft materials and components will be established. Data will also be obtained to support the three-dimensional and nonlinear fracture mechanics computational models that will be developed to address elastic-plastic, large deformation, residual stress states due to surface treatments and contact or liftoff. In addition, spectrum interaction models appropriate for rotorcraft operating conditions will be developed and validated.

Risk Assessment Methods: The research will consist of three main steps. First, existing probabilistic risk assessment methodologies having some aspects in common with rotorcraft will be examined for a preliminary feasibility assessment. Second, historical safety data will be collected along with material and structural property uncertainties for trial calculations using one or more of these methodologies to refine these assessments. Third, the work required to expressly address all of the critical issues involved in rotorcraft damage tolerance will be scoped.

Corrosion Control: Existing work on corrosion morphology and characterization in other applications will be adapted to rotorcraft materials and components to determine where further original research should be focused. This additional research will likely be carried out on detection and evaluation, repair, and prevention that will include the development and verification of the next generation of durable corrosion prevention compounds.

9.2.7 Supplemental Inspection Document (SID) Development

Dr. Xiaogong Lee, FAA, AAR-431, (609) 485-6967

The primary objective of this research project is to provide the commuter industry with the necessary tools to perform damage tolerance analyses (DTA) as specified in the recently issued Notice Proposed Rule Making (NPRM) by the FAA. This newly proposed rule will require that all airplanes operated under 14 Code of Federal Regulations (CFR) Part 121, all U.S. registered multiengine airplanes operated under 14 CFR 129, and all multiengine airplanes used in scheduled operations conducted under 14 CFR 135 to include damage tolerance-based inspection and procedures in their maintenance or inspection program for all airplanes older than 14 years.

Damage tolerance-based inspections and procedures, incorporated into a SID, are the best way to assure the continued safety of the commuter fleet considering the overall costs, the impact on aircraft operators, and the aviation safety requirements mandated by Congress. To provide the commuter industry with proper guidelines in the SID development, the FAA initiated research to develop SIDs for two specific airplanes, the Cessna 402 and the Fairchild SA226/SA227, representing a wide spectrum of airplanes in the commuter fleet. The SID development for the Cessna 402, a nonpressurized airplane, was completed in 1998. In 1999, work continued on the development of the SID for the Fairchild SA226/SA227 airplanes and developing a SID Handbook.

The objective of the Fairchild SID development program was to establish supplemental structural inspections or modifications, based on a state-of-the-art DTA, which further assure the safety and structural integrity of SA226/SA227 aircraft in operation, Figure 14. The SA226 and SA227 designs were certified prior to FAR amendments requiring damage tolerant design and prior to the advent of modern DTA techniques. This program attempts to take full advantage of these developments by determining the crack growth life of critical areas of structure and then prescribing timely inspections or remedial structural modifications. Past work is not ignored in carrying out this process. Service history, previous fatigue tests, strain surveys, finite element analysis, and service bulletins all guide the analysis. New work has included material testing, additional strain measurements, and application of crack growth software. The structure has also been evaluated for susceptibility to widespread fatigue damage. It is expected that the DTA- based SID program will support their continued safe operation to 50,000 hours. The Fairchild SID development program consisted of three phases:

I. Identify principal structural elements (PSE's) and develop stress spectrums
II. Perform DTA and establish inspection intervals for each PSE's
III. Final documentation including the SID and final technical report

Phases I and II were completed in 1999 and the results were published in the FAA technical reports, DOT/FAA/AR-99/20, P1&P2, *Development of Supplemental Inspection Document for Fairchild SA226/SA227 Aircraft*, Part 1 and Part 2, September 1999.

The FAA research effort to develop a SID handbook will provide general guidelines to the commuter industry in the preparation of a DTA-based SID. It will give sufficient technical background information on the entire procedure of developing SID documents. Numerous references will be included to provide detailed information on the disciplines of stress analysis, loads analysis, and fracture mechanics. It is anticipated that the SID Handbook will be finalized and published in 2000.

9.2.8 Supplemental Inspection Document (SID) Handbook

Dr. Xiaogong Lee, FAA, AAR-431, (609) 485-6967

The Supplemental Inspection Document (SID) Handbook for Commuter Aircraft provides manufacturers, operators, and other engineering organizations with guidance to develop a damage tolerant SID for a commuter aircraft. The technical issues to be resolved, sources of critical engineering data, and the procedures to develop data are described in the handbook. The handbook also provides a systematic approach and step-by-step procedure for a SID development with technical details, which includes the following major steps:

- Identification of the critical areas of principle structural elements (PSE)
- Material data and material test procedures

- Stress spectrum development
- Crack growth analysis
- Initial and repeat inspection intervals
- Widespread fatigue damage assessment
- Inspection techniques and procedures
- Documentation of analytical results in a supplemental inspection document (SID)

The SID is the document that defines the continued structural integrity program. The intent of the SID is to supplement the existing maintenance program. Therefore, before writing the SID document, a review of the existing maintenance program is required to determine the areas where the existing maintenance program is lacking because of the data tolerance analysis (DTA). In addition, if a CAP (Continued Airworthiness Program) or other inspection document has been written for the airplane, the contents of the CAP or other inspection document should also be reviewed. The SID, at a minimum, must include the damage tolerance-based inspections and procedures needed for continued safe operation of the airplane.

To provide further guidance, specific examples of SIDs were developed for two types of commuters: the Cessna 402 and the Fairchild Metro SA226 and SA227 airplanes. Technical reports detailing the SID development for these two types of commuter airplanes (FAA technical report DOT/FAA/AR-98/66, Supplemental Inspection Document Program for the Cessna Model 402, and DOT/FAA/AR-00/18, Development of Supplemental Inspection Report for the Fairchild Metro SA226/SA227 Airplane) can be obtained from the National Technical Information Service (NTIS), Springfield, Virginia 22161.

9.2.9 Software and Digital Systems Safety (SDSS) Program
Mr. Charles Kilgore, FAA, AAR-421, (609) 485-6235

Software Mutation Testing: It has been identified that Modified Condition Decision of Coverage (MCDC) should be used as a structural coverage criterion because it attempts to provide a cost-effective form of logic verification and is required for Level A (safety critical) software. The Flight Safety Research Section published a report on “An Investigation of Three Forms of the Modified Condition Decision of Coverage (MCDC) Criterion.” This report compares three forms of MCDC, and investigates the adequacy of the different forms of MCDC in the software mutation, or fault injection, domain. Software mutation is one alternative that has been used within the software testing research community to evaluate the effectiveness of new testing methods and coverage criteria. MCDC is a software structural coverage criterion used in RTCA DO-178B; “Software Considerations in Airborne Systems and Equipment Certification.” It is used to assist with the assessment of the adequacy of the requirements-based testing process and can be considered to be a check and balance on the requirements-based verification process. This report provides justification why structural coverage, in general, and MCDC in particular, should be part of the software system development process. (Figure 15.)

9.2.10 Aging of Nonstructural Systems
Mr. Christopher Smith, FAA, AAR-433, (609) 485-5221

The Aging Nonstructural Systems Research Program (NSRP) formally got underway in FY99. The objectives of the NSRP are to develop technologies and techniques to ensure the continued safe operation of aircraft electrical and mechanical systems. Research results will be used in support of new and pending regulatory action and to facilitate compliance with new and existing regulations. FY99 NSRP research initiatives include development of an aging nonstructural systems test and validation infrastructure, development of wire testing equipment, assessment of visual inspection, and the development of aircraft arc fault circuit breakers.

The FAA and the USAF are jointly sponsoring a short-term effort to enhance an automated wire test system. The state-of-the-art equipment is being used to help baseline testbed aircraft and test articles and to establish a benchmark for future test equipment developed and tested under the NSRP. Fabrication of a laboratory aging wire test harness and interface cables for the DC-9 anti-skid system began in FY99 and will be completed shortly. The aging wire test harness and DC-9 anti-skid system wiring will be used to evaluate the wire test system as well as other emerging technologies.

In a joint program with the Office of Naval Research and the Naval Air Systems Command, the FAA is developing an aircraft arc-fault circuit breaker. An arc-fault is the undesired, momentary discharge of current from a conductor – i.e., a spark. This type of short circuit is particularly harmful because of the high temperature of the sparks it generates and the absence of any current excursions, which might trip standard thermal circuit breakers typically used on aircraft. Arc fault circuit interrupter (AFCI) technology has the potential to mitigate the consequence of wire failure without requiring the redesign of aircraft circuitry. A broad agency announcement was released and two companies have been selected to develop AFCI breakers. Contracts will be awarded before the end of calendar year 1999. Arc-fault characterization tests were completed this year. In addition, load characteristics were measured aboard a Navy C-9 (military equivalent of the DC-9). Both tests provide data essential to the successful development of an AFCI.

In FY99, the FAA acquired a 1971 Boeing 747 with over 100,000 hours of service. The 747 complements the Boeing 737 and the McDonnell Douglas DC-9 already in inventory at the FAA Airworthiness Assurance Nondestructive Inspection Validation Center (AANC). These aircraft are the testbeds that will be used in the research and validation of emerging nonstructural systems inspection and test technology. The aircraft will be used to support the aging nonstructural systems research program.

9.2.11 Fretting Fatigue: Current Technology and Practices
Dr. D.W. Hoeppner, Dr. Chandrasekaran Venkatesan and Dr. Charles Elliott, University of Utah

The staff of QIDEC completed the editing of the following book based on the Symposium on Fretting Fatigue held at the UU in September, 1998. ASTM STP 1367, **"Fretting Fatigue: Current Technology and Practices",** D. W. Hoeppner, Chandrasekaran Venkatesan, Charles Elliott, Editors, ASTM, Philadelphia, PA., January, 2000.

9.2.12 3rd International Symposium on Fretting Fatigue
Dr. David W. Hoeppner, University of Utah

Dr. Hoeppner is on the planning committee for the 3rd International Symposium on Fretting Fatigue to be held at Nagaoka, Japan on May 15-17, 2001. He will attend the meeting and present 3 papers related to fretting fatigue.

9.3. LOADS

9.3.1 Active Control of Weapons Bay Acoustics

Mr. Leonard Shaw, Air Force Research Laboratory

Active Weapons Bay Noise Suppression Program is an innovative program, which will result in a reduction in the acoustic levels (and associated damage) within an open weapons bay for all flight conditions and bay configurations. This technology could be applied to a variety of acoustic problems across many aircraft systems within their lifecycle resulting in reduced cost and improved performance. The objective of this critical experiment is to design, develop, and demonstrate active flow control for acoustic fatigue reduction in open cavities. Air Force systems that integrate active noise suppression will: reduce developmental costs, reduce fatigue damage to structure and components; facilitate the integration of new weapons; expand their weapon delivery envelope up to and including supersonic release; and enhance weapon separation. Such benefits will result in increased mission flexibility at a reduced cost through the lifecycle of the system.

Numerous actuators were considered for application to the weapons bay acoustic suppression problem. The chart in Figure 16 shows an evaluation of all of the ones considered compared to the no suppression case. The top three are seen to be some form of pulsed blowing. To date it has shown to be most effective under the widest test conditions.

Since pulsed mass injection was considered to be the most effective actuator, most of the wind tunnel testing was conducted using it. Figure 17 is a picture of the model which was used for most of the active flow control actuator evaluations. A wide range of frequencies and mass flow rates were tested. Different plenum and nozzle designs were also used to optimize performance. One of the major results of the evaluations is illustrated in Figures 18 and 19. In Figure 18 the two major acoustic tones in the cavity can be observed around 100 and 250 Hertz. Figure 19 shows how these tones are essentially eliminated with pulsed mass injection at the leading edge of the cavity. Future plans are to test this concept on a full-scale aircraft to evaluate acoustic suppression as well as store separation. Additional details of this effort can be found in the reference.

9.3.2 Advanced Actuators for Active Control of Sonic Fatigue Dynamic Environments

Mr. Leonard Shaw, Air Force Research Laboratory

Dynamic/acoustic environments, which cause sonic fatigue on aircraft structures, need to be controlled. If they are not the structure must be designed to withstand the higher loads resulting in a significant weight penalty. If the structure is not properly designed secondary structural failures will occur. Passive flow control techniques have not been able to provide sufficient control authority to effectively suppress the dynamic/acoustic environments. The objective of this effort is to develop advanced active flow control actuators and validate the effectiveness of active control of acoustic and dynamic flow environments.

The approach will consist of conducting an extensive survey to determine all of the current flow actuators, which are applicable to the dynamic environments causing sonic. Laboratory and flow tests will be conducted to evaluate the effectiveness of the various actuators. The most promising ones will be selected for further testing, optimization, and application to active control. New and unique actuators shall be considered and evaluated. A final recommendation will be given for the best actuator for the various flow environments and active control methodology. Data from flow tests will be provided to substantiate the recommendations.

Two separated flow environments were selected to evaluate the active flow control actuators. These being the downstream wake of a pod and the separated flow region downstream of a rearward facing ramp. These two configurations are shown schematically in Figures 20 and 21.

Numerous active flow control actuators were consider for potential application to these two environments. The ones selected for test and evaluation were steady state mass injection, pulsed injection, synthetic jets, and vibrating flaps. A typical downstream dynamic pressure environment for the pod is shown in Figure 22. The active flow control actuators will be utilized to suppress the magnitude of this environment as well as the dynamic pressures associated with the rearward facing ramp. Additional details about this research can be found in the reference below.

REFERENCE

[1] B, Maines, B. Smith, A.Cunningham, J. Jordan, and L. Shaw, "Establishing Bluff Pod Wake Characteristics for Flow Control," AIAA 00-2555, June 2000.

9.3.3 Characterizing Rotor Head Acoustics Environment for In-Flight Fatigue Monitoring

Mr. Jeffrey N. Schoess and Sunil Menon, Honeywell Laboratories

This paper summarizes the in-flight data analysis for the CH 46 rotor acoustic monitoring system (RAMS). This ambitious, 38-month, proof-of-concept effort, which was a part of the Naval Surface Warfare Center Air Vehicle Diagnostics System program, culminated in a successful three-week flight test of the RAMS system at Patuxent River Flight Test Center in September 1997. This paper presents recent data analysis of in-flight maneuvers, which characterizes the rotor head operation, and potential for on-rotor fatigue crack monitoring.

The RAMS system [1-6] employs a high-fidelity stress-wave AE-based measurement technology to "listen" to the acoustic sound to determine if a structural crack is initiated or propagating. AE is most commonly detected on metals during deformation caused by an applied stress. The "stress" waves are created by simultaneous motion of several dislocations (small regions of metal move the crack tip within a small volume of deforming material, or the relaxation of the elastic stress field in the metal is a lattice structure caused by the passage of a dislocation). The RAMS flight-test system was located on the rotor head and in the cargo bay. The on-rotor enclosure is physically mounted on the aft rotor hub and includes electronics for data multiplexing, passive band-pass filtering, signal amplification, an S-Band wireless transmitter, and drive electronics for a simulated crack generator (inject a fatigue fault). The simulated crack generator was mounted on the vertical hinge pin cap on one of the rotor arms.

The acoustic data analyzed for this paper were taken from flight tests conducted on September 5, 1997, and are referred to as Flight no. 5. During the course of this flight, acoustic data was collected while the helicopter performed several maneuvers such as climbing, descending, hover-in-ground-effect (HOGE) hover-out-of-ground-effect (HOGE). These maneuvers were performed in sequence, starting with ground turns, HIGE (stationary flight under 50 ft), HOGE (stationary flight above 50 ft), climb, straight and level, descent, and a straight-and-level maneuver at the end of the flight. Data were collected when the helicopter was doing ground turns and running in a straight-and-level manner during the flight.

The climb maneuver acoustic data are shown in Fig. 23. The spectrogram [7], a time-frequency representation of the acoustic data, is shown on top of the figure and the crack simulator command signal is shown on the bottom. The crack simulator signal is characterized as a square wave that is "on" for 10 ms and "off' for 15 ms. The climb flight maneuver puts "higher" torque loads on the helicopter rotor-head than straight-and-level. The straight-and-level data spectrogram shows the "footprint" of the crack generator signal (as vertical stripes). A helicopter "straight-and-level" sequence spectrogram is shown in Fig. 24.

From Figures 23-24, it is seen that the different flight maneuvers have different spectral features. The climb maneuver is observed to have the most spectral content of all the flight maneuvers, do to the high structural loads on the rotor-head as compared to the other maneuvers.

The RAMS system developed for crack detection on the rotor head was successfully flight tested on a CH46 Sea Knight helicopter. The acoustic data were collected under different helicopter flight maneuvers to determine the feasibility of detecting fatigue cracks during operational flight. Flight test analysis and fatigue component testing revealed a fatigue crack of 0.020 of an inch can be detected in actual flight conditions.

REFERENCES

[1] J. Schoess et al., "CH-46 Sea Knight Flight Test Results for the Rotor Acoustic Monitoring System (RAMS)," 1998 SPIE International Symposium on Smart Structures and Materials, paper no. 332951, San Diego.

[2] J. Schoess et al., "CH-46 Rotor Head Acoustic Fault Detection Analysis," 1999 SPIE International Symposium on Smart Structures and Materials, paper no. 3670.57, San Diego.

[3] J. Schoess, "Rotor Acoustic Monitoring System (RAMS)-A Fatigue Crack Detection System," America Helicopter Society (AHS) Forum 53, Virginia Beach, May 1, 1997.

[4] J. Schoess, "Rotor Acoustic Monitoring System," 53`° Meeting for Machinery Failure Prevention Technology (MFPT 53), Virginia Beach, April 19, 1999, pp. 175-184.

[5] J. Schoess, "Acoustic Fault Injection Tool (AFIT)," SPIN Conference on Sensory Phenomena and Measurement Instrumentation for Smart Structures and Materials, Newport Beach, March 1999, SPIE Vol. 3670.

[6] S. Menon, J. Schoess, "Stress-Wave Acoustics Analysis for the CFI-46 Sea Knight Rotor System", 54'" Meeting for Machinery Failure Prevention Technology (MFP 1' 54), Virginia Beach, April, 2000

[7] S. Mallm, A *Wavelet Totes of Signal Processing,* Academic Press, 1999.

9.3.4 Airborne Data Monitoring Systems

Mr. Thomas DeFiore, FAA, AAR-433, (609) 485-5009

The Federal Aviation Administration (FAA) has re-established a flight and ground loads data collection program for civil aircraft. The output from this Operational Loads Monitoring research provides the technical basis for Airframe Certification requirements. Subject research independently confirms and verifies original equipment manufacturers' (OEM) design assumptions and aircraft usage analysis. This is an essential part of the regulatory and certification activity of the FAA and is an essential input to confirming the continued safety and airworthiness of the civil transport fleet. This research provides the opportunity to identify operational problems or potentially hazardous operating conditions in a proactive manner.

Prior Data Collection

The initial phase of the research consisted of the acquisition and publication of a substantial quantity of data which had been previously collected yet not published. Data collected by NASA on large transports was analyzed and published; this included usage information of the B-727, B-747, DC-10, and L-1011. NASA had also collected but not published usage data on over 70 general aviation airplanes, both single and twin engine. These data were also analyzed and published. European data on the usage of the F-27 and the F-28 were similarly acquired, analyzed, and published.

New Technology

The second phase of the research included the incorporation of newer technologies and improving and enhancing both the data acquisition and analysis process. Included in this research were improved and simplified methods of analyzing and reporting gust loads, newer process of separating gusts from maneuver accelerations, and the development of methods to experimentally determine aircraft landing parameters from video image data. A user's guide for Federal Aviation Regulations (FAR) 23 loads was also developed. This document provides new technology for the small aircraft industry to predict aircraft loads from simple airplane data. Documentation of subject research is presented in formal publications.

New Data Collection

The third and most important phase of the research, which is ongoing, consists of the acquisition of new flight and landing load usage data for a wide variety of airplane models in a typical usage environment.

Large Transports

Digital Flight Data Recorder (DFDR) information for large transports was recorded on high-density Optical Quick Access Recorders. The B-737 model was the first model instrumented followed by the MD-82, B-767, and A-320. Major aircraft types were instrumented including twin engine on wing, twin engine in rear, wide-body aircraft, and airplanes with digital flight controls. Data from the three major manufacturers, Boeing, Boeing-Douglas, and

Airbus, were also recorded. Two data reports describing B-737 in service usage were published and one report was published on the MD-82. In FY00, a B-767 data report is expected. Reduction and analysis of data from the A-320 airplane will also commence in FY00.

Small Transports

Data from small airplanes are also being collected, reduced, and analyzed. Special loads recorders were installed on eight Cessna-172 airplanes and data are presently being processed and analyzed. BE-1900D DFDR data were offloaded and 900 flights were processed and analyzed. A draft report is available and newer recorders are being installed on BE-1900D aircraft. The Canadair Regional Jet airplane is being added to the program in late 2000. Again, both turboprops and jets used in regional service and data from a highly popular general aviation Cessna-172 are being collected and analyzed.

Landing Loads

Airplane landing parameter data (sinkspeed, velocity, pitch, roll, yaw, etc.) have been collected in video landing parameter surveys conducted at high-activity airports. Surveys have been conducted at the John F. Kennedy International Airport (JFK), Washington National Airport (DCA), Honolulu International Airport, London City Airport, and Philadelphia International Airport. Data reports for the JFK and DCA surveys have been published and formal reports for the other surveys will be forthcoming. A permanent video landing facility has been established at Atlantic City International Airport. Landing data from this facility have been used to verify video survey data accuracy by comparing them to the results from the Boeing flight test MD-90 airplane equipped with an advanced Internal Navigation System. Landing data are now being collected during both good and inclement weather conditions.

Advanced Research

In-service data collection will continue for quite some time. The final phase of the airborne data monitoring research involves special advanced studies on aircraft loads. Research has been conducted or is being initiated on the following areas: asymmetric buffet, statistical discrete gusts, time-phased vertical and lateral gusts, landing gear ground turning conditions, control system modification to reduce aft fuselage turbulence accelerations, and the conduct of a review of the continuous turbulence model.

Published Reports

The following is a list of reports published during FY99 in this research program. Only reports that are publicly available have been included.

- Report DOT/FAA/AR-99/14, *An Evaluation of Methods to Separate Maneuver and Gust Load Factors From Measured Acceleration Time Histories*, Final Report, April 1999.

- Report DOT/FAA/AR-99/27, *Prediction of Antisymmetrical Buffet Loads on Horizontal Stabilizers in Massively Separated Flows, Phase II*, Final Report, May 1999.

- Report DOT/FAA/AR-98/65, Statistical *Loads Data for MD-82/83Aircraftin Commercial Operations*, Final Report, February 1999.

- Report DOT/FAA/AR-98/28, *Statistical Loads Data for Boeing 737-400 Aircraft in Commercial Operations*, Final Report, August 1998.

- Report DOT/FAA/AR-97/106, *Video Landing Parameter Survey – Washington National Airport*, Final Report, June 1999.

9.3.5 Airborne Data Monitoring Systems
Mr. Thomas DeFiore, FAA, AAR-433, (609) 485-5009

The Code of Federal Regulations, Aeronautics and Space, Airworthiness Standards are replete with loads criteria much of which were generated prior to deregulation and in some cases prior to the design of both wide-body and fly-by-wire civil aircraft.

With the existence of (1) new technology, (2) newer operating rules and practices, and (3) the anticipated doubling of the air traffic within 10 years, a need exists to develop and implement a system to continuously validate and update the operational flight and ground loads airworthiness certification standards based on actual measured usage. (Figure 25.)

A research program, which provides a continuous supply of new in-service operational loads data is needed to ensure the appropriateness of the certification process for structural strength and fatigue life and to identify changes in-service usage trends. New flight loads data need to be collected for major airplane configurations including: twin engine on wing, twin engine in rear, wide bodies, airplanes with digital flight controls, regional jets, turboprops, and general aviation. Substantial quantities of large transport landing loads data, principally touchdown vertical velocity, are also needed for a wide variety of airports and airplane model types.

By taking advantage of newer technologies and improving, as well as enhancing, both the data acquisition and analysis process, safer and more optimally designed transports will continue to be made possible in the future.

The Federal Aviation Administration has reestablished an Operational Loads Monitoring Program, which includes both flight and landing loads data collection on civil transports.

Research Program: The initial phase of the research consisted of the acquisition and publication of a substantial quantity of data, which had been previously collected, yet not published. This included data from a number of prior NASA and European loads surveys.

The second phase involves developing and implementing new technology for obtaining, reducing, and analyzing operational loads data, Figure 26. Some of these enhancements included high-capacity optical disk recorders, simplified methods to analyze and report gust loads, newer methods to separate gust from maneuver c.g. accelerations, and methods to experimentally determine aircraft landing parameters from video image data. The third phase and most important phase of the research consists of the acquisition of new flight and landing load usage data for a wide variety of airplane models in typical usage environment. In-service data collection is expected to be a long-term effort.

The final phase of subject research involves the conduct of special advanced studies on aircraft loads. These include asymmetric buffet, statistical discrete gusts, time-phased vertical and lateral gusts, landing gear ground turning conditions, control system modification to reduce aft fuselage turbulence accelerations, and review continuous turbulence mode.

Research Program Output: The output from the Operational Loads Monitoring research provides the technical basis for airframe certification requirements. Subject research independently assesses the original equipment manufacturers' (OEM) design assumptions and aircraft usage analysis. This is a fundamental element of the FAA's regulatory and certification process and is an essential input to confirming the continued safety and airworthiness of the civil transport fleet. Subject research provides the opportunity to identify operational problems in a proactive manner. (Figure 27.)

Twenty-five formal loads-related FAA technical reports were published along with a significant number of technical papers.

- New in-service usage data is now published and available for transport airplanes: B-737, MD-80, B-767, and BE-1900D.

- Video Landing Parameter Survey reports were published for surveys at JFK and DCA.

Additional flight and ground data is continuously being collected, which will be documented in future technical reports. Airplane models B-747 and B-777 are expected to be added to the research program in FY01. New and improved methods of data reduction and analysis are also being developed and documented.

Three loads training seminars were conducted for FAA certification engineers. Periodic gust specialist workshops, which brought together international specialists in gust analysis and mitigation technology, were hosted. Interaction with ARAC loads committees was maintained.

Video Landing Survey Facility: The FAA has established a Video Landing Survey Facility at the Atlantic City International Airport (ACY) where high-resolution video images of typical landings are recorded. This facility enables the FAA to collect operational landing impact parameters year round under a wide variety of weather conditions. In addition to the regular commercial airplane arrivals at ACY, frequent US Air Force KC10 tankers and other large aircraft frequently conduct touch-and-go training at the airport. Inclement weather data collected at this facility will be used to supplement regular survey data collected during prior 10 to 12 day surveys. Over 800 video images have been captured thus far.

The following functions are performed at this video landing loads facility:

- High-resolution video images are recorded of typical landings at (ACY), Figure 28.
- Digitized images are analyzed to obtain landing contact parameters, i.e., sink speed, velocity, pitch, roll, yaw, etc.
- This facility, Figure 29, provides typical usage data to characterize the landing load environment for a wide variety of airplane models in both good and bad weather conditions at ACY. Output from the subject research facility forms the technical substantiation for assessing the validity of landing loads airworthiness certification standards.

BE-1900D Data Report: The FAA published its initial commuter airplane Operational Loads Monitoring report, DOT/FAA/AR-00/11, *Statistical Loads Data for BE-1900D Aircraft in Commuter Operation*. The output from subject Operational Loads Monitoring research provides the substantiation of the technical basis for airframe certification requirements and advisory materials. Subject research independently assesses the original equipment manufacturers' (OEM) design assumptions and aircraft usage analysis.

B-767 Data Report: The FAA published an Operational Loads Monitoring report for the B-767ER airplane, DOT/FAA/AR-00/10, *Statistical Loads Data for B-767-200ER Aircraft in Commercial Operations*. The collection, reduction, and analysis of substantial quantities of typical in-service usage information is a fundamental element of the FAA's regulatory and certification process and is an essential input to confirming the continued safety and airworthiness of the civil transport fleet. Subject research provides the opportunity to identify operational problems in a proactive manner.

Gust Specialists Workshop: The FAA conducted a Gust Specialists Workshop that brought together over 40 international specialists to review the results of a number of recently completed research studies and to propose and discuss new research. Alternative analysis methods and technical results for spanwise turbulence and both the linear and nonlinear Statistical Discrete Gust (STG) approaches were presented and discussed. Current and proposed new joint FAA, NASA, and Boeing research on turbulence mitigation was presented and evaluated. A follow-up workshop will be linked with a future ARAC meeting during the fall of 2001.

Operational Loads Monitoring Training Seminar: The FAA hosted an Operational Loads Monitoring Training Seminar at the William J. Hughes Technical Center. Students were exclusively FAA research, flight standards, and certification engineers. Principal topics presented included aircraft manufacturer OEM design loads processes, use of alternate gusts methods, multiaxis one minus-cosine gust model, review of operational loads data collected on the BE-1900 and B-767, data usage comparisons between and among models, development of storm turbulence constants, gust maneuver separation, and static aeroelasticity.

Operational Loads Monitoring Web Site: A web site has been established which more fully describes subject research and will permit the downloading of electronic copies of all loads technical reports. Web site address is: http://aar400.tc.faa.gov/aar430/430-programs/agingaircraft/olmp/olmpfinal.htm

9.3.6 Characterization of Lightning Environment

Mr. Anthony Wilson, FAA, AAR-421, (609) 485-4500

The Electromagnetic Hazards to Aircraft Systems program, AAR-421, conducts on-going research to characterize the lightning strike environment, Figure 30. Lightning strikes to aircraft are common, particularly when considered over a worldwide fleet or over a large production population. However, it is difficult to predict lightning strikes for specific aircraft, when lightning will strike an aircraft, and the precise characteristics of the lightning strike. Since the lightning strike effects on an aircraft vary widely, research continues to define the lightning environment and subsequently the lightning protection requirements.

The lightning protection requirements for aircraft, and the protection implemented on aircraft to meet these requirements, have evolved significantly over the last 35 years. Significant changes in requirements and protection have followed two well-known transport aircraft accidents. In 1963, a Boeing 707 crashed after it was struck by lightning. And again in 1976, a Boeing 747 crashed after it was struck by lightning. Both of these accidents resulted in extensive research into lightning characteristics, aircraft lightning protection requirements, and means to protect aircraft from catastrophic lightning effects. There are no recent catastrophic aircraft accidents due to lightning, but accidents continue, such as the February 1998 Fokker 100 accident which followed a lightning strike and subsequent brake system failure, and the January 1995 Aerospatiale AS332 helicopter ditching following a lightning strike.

Two distinct tasks have begun to define and characterize the lightning strike environment. The first element of this task has been to revitalize a program, which provided for airline participation in reporting of in-service lightning strikes. These lightning strike reports were sent to Lightning Technologies, Inc. who, under FAA sponsorship, analyzed the data and reported the results. In addition, LTI Inc. has contacted major airlines, regional airlines and business jet operators to solicit their participation in this reporting activity.

The second element of this task provides for the participation of on-going lightning characterization efforts. The International Center for Lightning Research and Testing at the University of Florida at Gainesville, under FAA sponsorship, are collecting lightning flash characteristics at a rocket-triggered lightning test facility at the Camp Blanding Army National Guard Base in north central Florida for both triggered and nearby natural lightning. This effort provides for the collection of lightning flash data to characterize the lightning current, waveform, energy, and pulse repetition characteristics as well as lightning electric and magnetic field waveforms from a few meters to 500 meters away from the flash. The University of Florida is in the process of analyzing the parameters of interest for aircraft protection, and the findings will be published in a FAA technical report.

9.3.7 Upgrades to the FAA Layered Elastic Design Program (LEDFAA)

Dr. Gordon Hayhoe, FAA, AAR-410, (609) 485-8555

In 1995, the FAA released a computer-based standard for airport pavement design. The new standard (LEDFAA) replaces previous FAA design standards for major airport pavements intended to handle traffic including the Boeing 777 airplane. In FY99, the FAA made a number of improvements to the LEDFAA program. Future releases of LEDFAA will include these improvements. In FY99, the FAA

- wrote and tested LEAF, a new structural analysis program for layered elastic pavement systems. LEAF replaces an older program (JULEA) as the main structural analysis module within LEDFAA. LEAF is designed to improve the performance of LEDFAA significantly on most personal computers.
- implemented full metric support in LEDFAA.
- made various enhancements to the LEDFAA user interface.

- implemented an improved procedure for computing the cumulative damage from different aircraft landing gear types.

9.3.8 Three-Dimensional Finite Element Pavement Model Development
Dr. David Brill, FAA, AAR-410, (609) 485-5198

The FAA continued to develop an advanced computer model for accurately predicting the response of airport pavement structures to complex vehicular loads. The advanced computer model, based on three-dimensional finite element technology, will be an integral part of future advanced pavement design procedures now in the development stage. The FAA field-verified the computer model by comparing its predictions with actual pavement measurements made at the FAA's instrumented runway at Denver International Airport, Figure 31. The FAA performed statistical analyses of the field data to show that the computer model predictions are realistic and in line with field measurements.

9.3.9 Cellular Cement Arrestor Bed
Mr. James White, FAA, AAR-411, (609) 485-5138

On May 8, 1999, an American Eagle commuter aircraft (SAAB 340) overran the end of runway 4R at JFK International Airport and stopped 250 feet into a cellular cement arrestor bed, less than 200 feet from the waters of Jamaica Bay, Figure 32. All 30 people on board escaped injury and the aircraft experienced only minor damage. This "save" marks the first operational use of a passive aircraft arrestor system developed and tested by the FAA, the Port Authority of New York and New Jersey, and Engineered Systems Company.

9.3.10 Canadian Design Standard Program (LEDCAN)
Dr. Gordon Hayhoe, FAA, AAR-410, (609) 485-8555

In cooperation with Public Works Government Services Canada (PWGSC), the FAA developed a computer program (LEDCAN) to perform airport pavement designs meeting Canadian design standards. The PWGSC provided funding for this work. The program is based on LEDFAA, the computer program for airport pavement design developed by the FAA. Both LEDFAA and LEDCAN implement layered elastic-based design principles to produce pavement designs for mixed aircraft traffic. Like LEDFAA, LEDCAN is user-friendly and runs in a Windows PC environment. LEDCAN is currently in a testing and evaluation stage with the final version to be ready for distribution in FY00.

9.3.11 Freezing Precipitation in Flight
Dr. Richard Jeck, FAA, AAR-421, (609) 485-4462

Freezing drizzle aloft has been suspected of causing several in-flight icing accidents and incidents over the past few decades. Most notable is the fatal Roselawn accident of October 1994 when a commuter airplane crashed near Chicago after holding in what may have been freezing drizzle in clouds at about 10,000 ft altitude.

In order to learn more about the occurrences and characteristics of freezing drizzle and freezing rain aloft, the Flight Safety Research Section has taken on the task of developing a centralized database of fine-scale measurements in these kinds of icing conditions.

Specially equipped research airplanes operated by NASA/Glenn, the Universities of Wyoming and North Dakota, and the Canadian Atmospheric Environment Service have obtained in-flight measurements in freezing precipitation in various parts of North America during the past 20 years. Relevant data from these flights are being collected and combined into a computerized database at the FAA William J. Hughes Technical Center.

An earlier study established where and how frequently freezing precipitation occurs at ground level in the eastern two-thirds of the United States. The new database under development here contains information on the vertical properties of freezing precipitation in selected geographic regions.

The database will show the amounts of freezable water that are available in these icing conditions and the range of temperatures and altitudes over which freezing precipitation has been recorded. Available droplet sizes are also recorded for use in computing where the resulting ice will form on wing and tail surfaces during flight.

In accordance with Task 9 of the 1997 *FAA In-Flight Aircraft Icing Plan*, the information collected in this database will be considered for possible expansion of the atmospheric icing conditions into which certain aircraft must be prepared and/or designed to fly.

9.4. Fatigue and Fracture

9.4.1 2xxx Series Extrusions - T-chord Evaluation
Dr. Michael P. Blinn, Boeing

Damage tolerant properties were determined for t-chord extrusions, both in the 2024-T3511 and 2224-T3511 alloys. In particular, both alloys' resistance to crack growth and fracture were evaluated using standard ASTM test methods (i.e. E 399, E 561, and E 647). In general, the main differences between the 2024 and the 2224 extrusions are: 1) tighter control of harmful elements (i.e. Fe, Si) and 2) variations in the processing.

In this study, there was a chance to compare a 2024 extrusion which had relatively low percentages of Fe and Si (sites for inclusions) against a similar 2224 extrusion. Figures 33 and 34 show the general shapes of the extrusions, location of the C(T) specimens, and the specimen orientation (T-L). The test results are listed in Tables 1 and 2. Statistically, there were 4 tests for each sample (alloy/thickness/test type combination) and the tests were performed at the same lab, with the same machines/personnel. The data presented are the average of the 4 tests, and there was relatively little scatter in any sample.

In summary, the 2224-T3511 extrusion showed more favorable crack growth and fracture toughness values, as compared to the 2024-T3511 extrusion. The roles that both the chemistry and processing had on the results are currently under investigation.

9.4.2 Fatigue Tests of K_t = 1.5 Coupons of VT22-1 Forging
Mr. Leon Bakow, Boeing

Screening fatigue tests were conducted to compare VT22-1 forging to baseline Ti 10V-2Fe-3Al forging and Ti 6Al-4V mill annealed plate.

Tests were on K_t = 1.5 flat edge notched 0.25 inch thick VT22-1, Ti 10V-2Fe-3Al and Ti 6Al-4V materials with and without shot peened surfaces. Tests were conducted at high and low maximum stress levels, at R = 0.10, for VT22-1 and Ti 10V-2Fe-3Al and at a low maximum stress level for the Ti 6Al-4V. Three heat lots of VT22-1 were tested and only one heat lot of the other materials.

The test data showed that:

1. For the shot peened specimens conducted at a high maximum stress, the three heat lots of VT22-1 and the Ti 10V-2Fe-3Al had equivalent fatigue test lives.

2. For the shot peened specimens at a low stress, the three heat lots of VT22-1 had equivalent fatigue test lives, while the T1 10V-2Fe-3Al test lives were higher and the Ti 6Al-4V lives were lower than the VT22-1.

For the specimens not shot peened, the lives of the VT22-1 specimens were higher than those of the Ti 10V-2Fe-3Al at both maximum stress levels, while the Ti 10V-2Fe-3Al and Ti 6Al-4V had equivalent lives at the lower stress level.

9.4.3 Anodize Effects on Aluminum Sheet Fatigue Properties
Mr. Mark Ofsthun, Boeing

Fuselage skins are clad with pure aluminum to increase resistance to corrosion. Some airlines like to polish these skins for reasons of appearance. Other airlines prefer to paint them (in essence doubling the corrosion resistance). In order to get the paint to adhere properly, a primer is required. However, even primer does not adequately ensure the structural integrity of the painted surface. Therefore, anodize is used, under the primer, to cause a chemical treatment of the aluminum surface. The anodize/primer/painting scheme is employed as a coating on many aircraft.

Anodizing can adversely affect the fatigue resistant qualities (durability) of a material. Figure 35 shows the effect that chromic acid, boric-sulfuric, and sulfuric acid anodizing has on the durability of aluminum, relative to an untreated surface. These three types of anodize leave an oxide layer over the cladding. The oxide layer is rather brittle, and the subsequent cracking that occurs manifests itself into the base material. This cracking of the anodized layer results in significant reduction in the durability of the aluminum beneath, with thicker oxide layers having the most detrimental effect. Thus, anodize treatments are typically not used on thin clad material because of their potentially damaging effects on the base material.

However, there is a type of anodize (phosphoric acid) that does not appear to have any detrimental effect on the durability of aluminum sheet. Phosphoric acid anodizing (PAA) has much less of an oxide layer on the cladding, yet meets the primer adherence requirements. Figure 36 shows the fatigue test results on the clad material, using PAA. Two types of testing, axial fatigue and flexure testing, both indicate that there are no detrimental effects on the 2024-T3 bare and clad sheet using PAA. It is advisable that new anodizes, and new applications of existing anodizes, be fatigue tested. PAA, for instance, has no apparent negative impact on the fatigue resistance of the 2024-T3 sheet. However, on the 7050-T7451 plate, PAA appears to cause significant pitting on exposed end grains, which is generally associated with fatigue problems.

9.4.4 Hemstitch Fatigue Evaluation

Mr. Mark Ofsthun, Boeing

Hemstitching is a machining method (also known as kellering) that refers to a surface topography. It is the result of an end mill cutter, with a radius, that is used to produce a machined surface (see Figure 37). There are two types of cutters: 1) a round ended cutter (ballnose), and 2) a radius ended cutter (bullnose). These two cutters are shown in Figure 38. Typically, the scallops left in a hemstitch surface are considered stress concentrations and are removed, by sanding, for appearance and fatigue quality. Boeing has done an extensive study to determine the effect on the fatigue resistant quality (durability) of the hemstitch surfaces.

In this fatigue evaluation, pure axial and bending specimens were used. Results of both types of specimens led to the same conclusions. A number of cutter configurations were evaluated for fatigue, and a number of aluminum alloys were tested. Findings from this study indicated that the stress concentration is at the scallop root radius, which is where the fatigue failures occurred. As long as the surface finish was the same as a conventionally milled surface, and the step-over to root radius ratio was less than about .2, no fatigue knockdowns were observed. Also, if the step-over to root radius was greater than 0.2 a small fatigue knockdown was observed, but shot peening the surface easily restored the fatigue resistant quality of the material. Testing indicated that specimens machined with a bullnose cutter had similar fatigue resistance as specimens machined with a ballnose cutter (provided the proper step-over to root radius was achieved).

The affects of sanding on the test results were particularly interesting. As discussed, sanding is generally done to improve appearance and to “restore” the fatigue resistance on the scalloped edges. In fact, in some cases the sanding resulted in a small knockdown in the fatigue life instead of improvement. Evaluating the specimen failures, tiny scratches in the surfaces were observed and are thought to contribute to the small knockdown in fatigue life. However, proper sanding techniques can improve the durability of the machined part. Fatigue tests indicated that two step sanding, with the final sanding done with ultra fine sandpaper, could restore the material's durability. A relative life plot of the trends observed in this test program is shown in Figure 39.

9.4.5 Effect of Hole Drilling and Finishing Processes on Fatigue Quality

Mr. Antonio Rufin, Boeing

A program is under way to support a decision on the potential replacement of conventional hole drilling and deburring operations in some 747 wing front spar assembly operations with a process involving integral ream/chamfer under local clamping. The program began as a generic evaluation of the effect on durability of hole deburring and clamping during drilling, using open-hole fatigue test coupons. The second phase of this effort shifted focus to the intended structural application, using prototype tooling and high-load transfer fastened test coupons. A third phase is in progress to expand coverage to include the full range of anticipated material thicknesses as well as a closer representation of the process that would be actually implemented in practice.

The following hole conditions were evaluated under Phase I: (a) No deburr, light clamping during drilling (baseline), (b) no deburr, moderate/high clamping force, (c) flat deburr (using sandpaper), light clamping, (d) rotary chamfer, light clamping, (e) hand chamfer ("Quick Burr"), light clamping, and (f) file, light clamping. Constant-amplitude fatigue tests were performed on specimens made from 7075-T6 and 2024-T3 bare aluminum sheet. The tests showed that application of a clamping force during drilling had a beneficial effect on fatigue life, which seemed more pronounced in 7075-T6 than 2024-T3. The positive effect of clamping was consistent with the lower interface burr heights observed in the clamped coupons. File deburr did not show a clear benefit relative to non-deburred for holes drilled without clamping, in either 2024-T3 or 7075-T6. Other deburring techniques generally demonstrated significantly improved fatigue performance relative to non-deburred holes drilled without clamping.

All Phase II test specimens were assembled using a prototype drill/chamfer tool using varying amounts of clamping and high-interference fastener installations, with and without sealant. Most of the fractures originated under the edge of fastener heads. The small number of bore-initiated fractures was attributed to the high quality of the holes processed with the prototype tool and the high amount of fastener interference (typically 0.003 inch [0.08 mm]). Specimens with holes reamed under maximum clamping produced the tightest fatigue life distributions. Clamping and no deburr (with and without sealant) resulted in the same fatigue quality as the baseline minimum clamping + deburr condition.

9.4.6 Fatigue Crack Formation Sites in 2024-T3 Aluminum

E.A. DeBartolo, Rochester Institute of Technology and B.M. Hillberry, Purdue University

The role of constituent particles in fatigue crack formation in several aircraft aluminum sheet alloys (2024-T3, 7075-T6, 2524-T3) has been well documented. In polished material, these particles are the dominant fatigue crack nucleation sites. When the material is rolled to sheet thickness, the particles often become cracked. Cracked particles have been shown to comprise about 90% of the nucleation sites, but only about 3% of the total particle populations in these aluminum alloys. The cracked particles are clearly among the largest particles present in the material (shown in accompanying particle size distributions for 2024-T3 aluminum: $\mu_{\text{all}} = 5.35\ \mu\text{m}^2$, $\mu_{\text{cracked}} = 90.53\ \mu\text{m}^2$), Figure 40, so it is not surprising that they are the critical fatigue features. In addition, since the particles themselves are cracked, they can be treated as existing fracture mechanics cracks in the material. This makes the distribution of cracked particles the correct distribution of potential nucleation sites; all cracked particles can be considered as existing cracks that could possibly cause failure. No threshold value is necessary since each cracked particle could result in a critical fatigue flaw. The sizes of cracked particles in three aluminum alloys have been measured and quantified [1], and have been used successfully to predict fatigue life distributions without the need for a threshold to truncate the particle distribution. The fatigue life prediction results and ΔK_{th} comparison with published data are presented in a poster at this ICAF Symposium.

REFERENCE

[1] E. A. DeBartolo and B. M. Hillberry, 2000, "A Model of Initial Flaw Sizes in Aluminum Alloys," Accepted to International Journal of Fatigue, February 2001.

9.4.7 Equivalent Initial Flaw Size Testing and Analysis

Capt Dan Schrage, Air Force Research Laboratory

The Equivalent Initial Flaw Size (EIFS) concept was developed nearly 30 years ago in an attempt to account for the initial quality, both manufacturing and bulk material properties, of the structural detail prone to fatigue cracking. Widespread use of this concept has not been realized due to the large amount of test data required to develop a reliable EIFS distribution. Since calculation of the EIFS is dependent on the crack growth model and all inputs to the crack growth model, the EIFS must be determined for each structural detail in question and all load spectra this detail may experience. Fuselage lap splice joints for transport aircraft are very similar across aircraft types and the loading spectrum is predominately constant amplitude as a result of cabin pressurization cycles. Thus, using the EIFS concept is acceptable.

Four types of flat, production like joints were fatigue tested with crack detection and measurement via the traveling optical microscope, eddy current rotating probe system, and scanning electron microscope. Novel techniques were employed to avoid edge cracking of the joints and multiple site damage (MSD) developed in all but two joints. A programmed loading spectrum was used to mark the fracture surface to aid in post-test crack history reconstruction using an optical and scanning electron microscope. As seen in the post-test fractographic evaluation, many of the crack nucleation sites were damaged by the large-scale plastic deformation of the rivet hole edge during fatigue or final fracture of the joint. In addition, crack face contact resulted in marring the fracture surface; in some cases obliterated the marker bands used for crack history reconstruction.

The mean EIFS for 48 cracks for which EIFS calculation were made was 21 μm with a standard deviation of 11.1 μm. However, the EIFS calculations are prone to compounding errors in the crack growth analysis due to the changing stress intensity factor solutions and stress fields as the crack gets longer. Therefore, only including EIFS calculations for crack length measurements less than 1.27 μm results in a mean EIFS of 12.7 μm with a standard deviation of 2.4 μm.

9.4.8 Advanced Fatigue Test Technologies
Dr. David W. Hoeppner, University of Utah

The University of Utah Structural Integrity Laboratory (SIL-one of the QIDEC laboratories) is conducting experiments in support of the Sverdrup Technology, Inc./Air Force Office of Scientific Research-sponsored Arnold Engineering Development Center research program for advanced fatigue test methodologies. Ti-6Al-4V titanium is being evaluated over a wide range of test conditions to investigate axial/torsional fatigue characteristics. SIL entered this ongoing research program in June 1998.The material characterization matrix comprises experiments with stress ratios ranging from R = -1.0 to R = 0.5 with varying ratios of tension to torsional loads. The matrix was developed to examine this material for biaxial fatigue characteristics in the high-cycle fatigue regime, to determine applicability of Miner's Rule (or load sequencing effects), and to investigate fatigue theory correlations. The test matrix was based upon the following parameterization:

$$\sigma_{eq} = \left[\sigma_{xx}^2 + 3\tau_{xy}^2\right]^{\frac{1}{2}} = \beta\sigma_e = \left[(\gamma\sigma_e)^2 + 3(\alpha\gamma\sigma_e)^2\right]^{\frac{1}{2}}$$

where
σ_{eq} = von Mises' Stress
σ_{xx} = Normal Axial Stress due to Tension
τ_{xy} = Shear Stress due to Torsion
σ_e = Material Endurance Limit
α = Shear-to-Normal Stress Ratio (= à on Plot)
β = von Mises Loading Factor
γ = Tension Loading Factor.

9.4.9 Fatigue Crack Closure at Threshold
John A. Newman, U.S. Army Research Laboratory (ARL) and Robert S. Piascik, NASA Langley Research Center (LaRC)

An advanced crack-closure model has been developed at LaRC. Here, interactions between plasticity-, roughness-, and oxide-induced crack-closure mechanisms (PICC, RICC, and OICC, respectively) are modeled resulting in accurate prediction of fatigue crack growth (FCG) threshold behavior. FCG threshold is an important design parameter in many engineering applications where fatigue-crack closure is known to be a first-order influence. Several closure models have been proposed, but most are limited because they do not consider multiple closure mechanisms. Crack closure at threshold is especially complex because multiple closure mechanisms contribute and interact; likely mechanisms include PICC, RICC, and OICC.

Several closure models have idealized rough cracks as two-dimensional sawtooths [1-4], schematically shown in Figure 41. This crack configuration is described by an asperity angle, α, and an asperity length, *g*, labeled in the figure. Due to their non-planar geometry, mixed-mode stresses exist at rough crack tips. Independent research at

LaRC [1] and by Parry, *et al*., [2] indicate that (a) rough cracks are subject to mixed-mode crack-face displacements and (b) sliding-mode displacements are greatest at the asperity nearest the crack tip (see Fig. 41). This implies crack-face contact (*i.e*. crack closure) is likely at the asperity nearest the crack tip. However, results for straight cracks (no roughness) indicate crack closure initially occurs at the crack tip itself [5]. In general, it is believed that crack closure may occur at either location depending on material, loading, and environmental conditions.

The new closure model described here computes closure loads at both the crack tip and at the asperity nearest the crack tip. The model considers only the highest value. Analytical results from the new closure model are compared with experimental near-tip closure measurements in Figure 42 for 2024-T3 aluminum alloy tested in laboratory air at R = 0.1 ($\alpha = 30^o$ and g = 10 μm with a 10 Å thick crack-mouth oxide layer). For convenience, these results are presented as R_{cl} (the stress-intensity ratio at the first occurrence of crack closure, K_{cl}/K_{max}) against K_{max}. At high values of K_{max}, R_{cl} is nearly constant and the initial crack-face contact is predicted to occur at the crack tip. As K_{max} decreases, a transition from crack-tip-contact to asperity-contact occurs at K_{max} = 3.9 MPa$\sqrt{m}$, coinciding with the discontinuous slope change of analytical results in Figure 42. Further reduction in K_{max} results in a rapid increase of R_{cl} until the crack completely closes at K_{max} = 2.8 MPa$\sqrt{m}$. Excellent agreement between analytical results and experimental data show the model is a good descriptor of near-crack-tip closure events. This model provides a more complete understanding of near-tip closure events at threshold.

REFERENCES

[1] J. A. Newman, "The Effects of Load Ratio on Threshold Fatigue Crack Growth of Aluminum Alloys," Ph.D. Dissertation, Virginia Tech, October 2000. Available online at http://scholar.lib.vt.edu/theses/available/etd-11012000-15010038/.

[2] M. R. Parry, S. Syngellakis, and I. Sinclair, "Numerical Modeling of Combined Roughness and Plasticity Induced Crack Closure Effects in Fatigue," *Materials Science and Engineering*, Vol. A291, 2000, pp. 224-234.

[3] S. H. Wang, C. Muller, and H. E. Exner, "A Model for Roughness-Induced Fatigue Crack Closure," *Metallurgical and Materials Transactions,* Vol. 29A, 1998, pp. 1933-1939.

[4] S. Suresh and R. O. Ritchie, "A Geometric Model for Fatigue Crack Closure Induced by Fracture Surface Roughness," *Metallurgical Transactions,* Vol. 13A, 1982, pp. 1627-1631.

[5] W. T. Riddell, R. S. Piascik, M. A. Sutton, W. Zhao, S. R. McNeill, and J. D. Helm, "Determining Fatigue Crack Opening Loads from Near-Crack-Tip Displacement Measurements," Advances in Fatigue Crack Closure Measurement and Analysis: 2nd Volume, ASTM STP 1343, American Society for Testing and Materials, West Conshohocken, PA, 1999, pp. 157-174.

9.4.10 Analyses of Near Threshold Fatigue Crack-Growth Behavior

J.C. Newman, Jr., NASA Langley Research Center

Crack-growth rate data in the near-threshold regime has generally been obtained with a load-reduction procedure that is based on the stress-intensity factor range changing at an exponential rate. The recommended normalized K-gradient, (dK/dc)/K, was -0.08 mm^{-1}. This is roughly equivalent to a 5% reduction in stress-intensity factor range for every 0.5 mm of crack extension. But from measurements and analyses of the crack-growth process using these load-reduction procedures, a rise in crack-closure behavior has been measured or calculated. The reason(s) for the rise have been debated for many years. Roughness- and oxide-induced closure has generally been the accepted reasons, but remote plasticity-induced closure (due to the residual plastic deformations) has also been suspected (see Ref. 1)

The objective of this work was to use a two-dimensional, plasticity-induced crack-closure model (FASTRAN) to study fatigue-crack growth and closure in 2024-T3 aluminum alloy under constant-R (load-reduction) threshold testing procedures. Analyses were conducted for a crack in a very large body. The effects of constraint (plane-stress/plane strain), stress ratio (R), stress level, and load-shedding rates on crack growth and closure were studied. The crack-tip-surface displacements, near threshold conditions, were computed to show the extent of the residual-plastic deformations along the crack surfaces. To simulate realistic crack-tip conditions, a high crack-front constraint factor (α = 2, nearly plane strain) was used in the crack-growth simulation. The constraint factor elevates the normal stresses in the crack-tip region. The configuration had a 13-mm sawcut (no plastic history). The cracked plate was pre-cracked under constant-amplitude loading ($R = S_{min}/S_{max} = 0$) to a crack length of 25 mm, and then the load-reduction procedure was applied. The crack-opening displacements (COD) along the crack surfaces are shown in Figure 43. The solid and dashed curves show the results at maximum and minimum applied stress, respectively. These results show that the crack surfaces were fully open at the maximum applied stress (7 MPa). But at the minimum applied stress (0 MPa), the crack surfaces near the start of the load-reduction procedure and at the crack tip (c = 54 mm) were closed. This remote closure caused a rise in crack-opening stresses near threshold conditions.

Crack-growth simulations were conducted under a high stress-ratio condition (R = 0.7) using two decay rates (γ) at a pre-cracking level of 135 MPa. The initial ΔK level and the initial crack-opening stress (the minimum applied stress) are shown as the solid triangular symbol in Figure 44. After pre-cracking, and as the ΔK values are reduced, both decay rates cause a rise in crack-opening stresses to occur at ΔK levels of about 2 MPa-m$^{1/2}$. The arrows indicate the values of the constraint factors from the analyses. The pre-cracking stage was conducted in the constraint-loss regime, but at realistic values of ΔK, and the minimum α value was about 1.5. The rise in crack-opening stresses at low ΔK values was caused by the remote residual-plastic deformations. Experimental crack-opening values from Donald and Paris [2], using an indirect method (see Ref. 1), are shown as circular symbols. These results show remarkable agreement, but requires further assessment because the model is averaging the constraint effects through the thickness and it does not model the plane-stress regions at the free surfaces. The model is also not accounting for any oxide-debris along the crack surface. Further study is needed to resolve these issues.

REFERENCES

[1] Newman, J. C., Jr., "Analyses of Fatigue Crack Growth and Closure Near Threshold Conditions for Large-Crack Behavior," *Fatigue Crack Growth Thresholds, Endurance Limits, and Design*, ASTM STP 1372, 2000.

[2] Donald, J. K. and Paris, P. C., "An Evaluation of DK_{eff} Estimation Procedures on 6061-T6 and 2024-T3 Aluminum Alloys," *Proceedings of Fatigue Damage of Structural Materials II*, Cape Cod, MA, September 7-11, 1998.

9.4.11 A Fracture Criterion for Thick Aluminum Alloys

M.A. James and J.C. Newman, Jr., NASA Langley Research Center

The critical crack-tip-opening angle (CTOA) fracture criterion has been successfully applied to thin-sheet (thickness < 2.5 mm) aluminum alloys for fuselage application. Further studies have been conducted to investigate the fracture behavior of compact and large middle-crack tension specimens made of 6.35-mm thick 2024-T351 aluminum alloy [1]. Tests were conducted on compact tension, C(T), specimens ranging in width from 51 to 152 mm and on middle-crack tension, M(T), specimens ranging in width from 76 to 1016 mm. Most of the M(T) specimens were allowed to buckle during the fracture tests.

Two elastic-plastic, finite element codes were used in this study: ZIP3D [2] and WARP3D [3]. A multi-linear representation of the uniaxial stress strain curve with the von Mises yield criterion was used in the analysis for both codes. ZIP3D employs the initial-stress concept and is based on incremental flow theory and small-strain assumptions and uses the engineering stress-small strain representation of the multi-linear stress-strain curve. WARP3D includes a large-strain formulation necessary to capture both geometric and material nonlinear response present for the unconstrained M(T) tests. For the large-strain analyses, WARP3D requires the true stress-true strain representation of the multi-linear stress-strain curve.

A summary of the experimental failure load results for different widths of C(T) specimens is shown in Figure 45. The critical CTOA is indicated by ψ_c. The critical CTOA value was determined from the finite-element analyses (with a straight crack front) by matching the average failure load for the 152 mm C(T) specimens. Both analysis codes were able to accurately predict the failure loads for the smaller width specimens, and both codes predicted a near linear relationship between failure load and specimen width. The larger compact specimen is recommended because the larger specimen has more contained yielding than the smaller specimens, which reach plastic collapse at lower loads. As a result, the failure load for the large C(T) specimen is more sensitive to changes in the critical CTOA value. Figure 46 is a summary of the measured and predicted failure stresses for the M(T) specimens. The differences between results from tests and the WARP3D analyses were less than about 3 percent. Figure 46 includes analysis results with and without anti-buckling guide plates to show the effects of out-of-plane deformations on the residual strength for each specimen width. Only one M(T) specimen was tested with guide plates – a single 1016-mm-wide specimen. The WARP3D analysis predicted the failure stress within about 2 percent. These results demonstrate the applicability of the critical crack-tip-opening angle (CTOA) fracture criterion from small laboratory specimens, such as the C(T) specimens, to large M(T) panels (restrained or allowed to buckle).

REFERENCES

[1] James, M. A., Newman, J. C., Jr., and Johnston, W. M., Jr., "Three-Dimensional Analyses of Crack-Tip-Opening Angles and δ_5-Resistance Curves for 2024-T351 Aluminum Alloy," *32nd Symposium on Fatigue and Fracture Mechanics*, ASTM STP 1406, 2001.
[2] Shivakumar, K.N. and J. C. Newman, Jr., "ZIP3D – An Elastic and Elastic-Plastic Finite-Element Analysis Program for Cracked Bodies," NASA TM 102753, 1990, NASA Langley Research Center, Hampton, Virginia.
[3] Koppenhoefer, K. C., A. S. Gullerud, C. Ruggieri, R. H. Dodds, Jr., "WARP3D -- Release 10.8 Users Manual," Department Of Civil Engineering, University of Illinois at Urbana-Champaign, Urbana, Illinois, 1998.

9.4.12 Elastic-Plastic Analyses of Crack Growth from Interference-Fit Fastener Holes

B.R. Seshadri, Old Dominion University and J.C. Newman, Jr., NASA Langley Research Center

Stress analyses of cracks growing from interference-fit fastener holes in a large plate (see Fig. 47) were conducted to study elastic stress-intensity factors and fatigue crack-closure behavior using a finite-element method [1]. The analysis approach sequentially carried out insertion of the interference-fit fastener and application of load (external traction and fastener load) to the plate, accounting for separation and progressive contact during loading and unloading at the fastener-plate interface. Both elastic and elastic-plastic stress analyses were conducted for various fastener interference levels and combined loading conditions. Crack growth and closure were simulated for various levels of interference.

To conduct the crack-closure analyses, a refined finite-element model was used. The model had about 4800 nodes and 7700 elements. The minimum element size along the line of crack growth was 0.1 mm. Symmetry in both configuration and loading was taken into consideration and only one-half of the configuration was analyzed. To obtain accurate fastener-plate contact results, the fastener-plate interface region was modeled with nodes at regular intervals of 3.75 degrees. A no-friction fastener-plate interface was assumed in the analysis. An initial crack of about 1-mm in length, emanating from the fastener hole, was created after applying the interference-fit fastener. Thus, the yielding in the plate due to the fastener interference was captured. To simulate crack growth and closure during cyclic loading, the crack-tip node was released at the maximum applied load in each of the cycles. The crack was grown in the model for 17 cycles. During unloading, displacements of the nodes along the crack surfaces were monitored to determine if the crack surfaces would close. Nodes were not allowed to penetrate the crack surfaces. During reloading, the crack-opening stress level (S_{op}) was determined as the applied stress level when the node closest to the crack tip opened.

The influence of the interference-fit level on the stabilized crack-opening stress levels (symbols) normalized by the maximum applied stress is shown in Figure 48. The fastener load was selected to be 40 percent of the total load and the model had two-symmetric cracks. The maximum applied stress level was one-half of the flow stress of the material with a minimum applied stress of zero ($R = S_{min}/S_{max} = 0$). For no interference, the crack-opening stress level was between the theoretical plane-stress and the plane-strain values (solid lines). But for higher interference levels, the stabilized crack-opening stresses were higher, indicating that the interference-fit fastener was keeping the crack surfaces from contacting and yielding the material in compression. This resulted in more residual plastic deformations along the crack surfaces and, consequently, higher crack-opening stresses. The higher crack-opening stress levels cause slower crack-growth rates for the same ΔK value. This is another beneficial effect of interference-fit fasteners on fatigue and fatigue crack growth lives.

REFERENCE

[1] Seshadri, B. R. and Newman, J. C., Jr., "Elastic-Plastic Finite-Element Contact Stress Analysis of Interference-Fit Tapered Fasteners," 4th Joint DoD/NASA/FAA Aging Aircraft Conference, May 2000, St. Louis, MO.

9.4.13 Three-Dimensional Mixed-Mode Fatigue Crack Growth
Scott C. Forth, NASA Langley Research Center

One of the goals of the NASA Inherently Reliable Systems Program is to develop the methodologies necessary to predict mixed-mode fatigue crack growth in aerospace structures. Experimental [1] and computational [2] methods were developed to model (3D) three-dimensional mixed-mode crack growth under fatigue loading [3]. The experiments utilized 7075-T73 aluminum forgings cut into modified ASTM E740 surface crack specimens (Figure 49) with precracks oriented at angles of 30, 45, and 60 degrees in separate tests. Progress of the evolving fatigue crack was monitored in real time using an automated visualization system. In addition, the amplitude of the loading was increased at prescribed intervals to mark the location of the 3D crack front for post-test inspection. In order to evaluate proposed crack growth equations, computer simulations of the experiments were conducted using a 3D fracture model based on the surface integral method. An automatic mesher advanced the crack front by adding a ring of elements consistent with local application of fracture criteria that govern rate and direction of crack growth. Comparisons of the computational and experimental results showed that the best correlation was obtained when K_{II} and K_{III} were incorporated in the growth rate equations.

To predict the behavior of mixed-mode cracks, the stress intensity factor range used to predict cyclic fatigue was modified to include mixed-mode effects. The following definitions of ΔK_{eq} have been proposed:

$$\Delta K_{eq} = \Delta K_I \qquad (1)$$

$$\Delta K_{eq} = \sqrt{\Delta K_I^2 + \Delta K_{II}^2 + \Delta K_{III}^2} \qquad (2)$$

$$\Delta K_{eq} = \sqrt{\Delta K_I^2 + \beta \Delta K_{II}^2} \qquad (3)$$

$$\Delta K_{eq} = \sqrt{\left(\Delta K_I + \left|\Delta K_{III}\right|\right)^2 + 2\Delta K_{II}^2} \qquad (4)$$

where equation (1) is the standard mode I definition, equation (2) is a curve fit to experimental data where $\beta = 0.4$ for aluminum, equation (3) was proposed by Gerstle [4], and equation (4) was obtained from the definition of energy release rate G for plane strain by setting Poisson's ratio equal to zero. Use of equation (4) assumes that energy required for advancing the crack tip straight ahead is equivalent to the energy available for propagating the crack at some other angle under mode I conditions.

Results for 7075-T73 aluminum suggest that reliance on mode I growth laws can lead to highly nonconservative predictions of fatigue life. Figure 50 is a comparison of the cracked specimen geometry and the prediction using the surface integral method. Figure 51 shows the accompanying data for the case of the crack at 60 degrees. Redefinition of ΔK_{eq} in terms of the mixed-mode stress intensity factors yields results that are both more accurate and conservative. A further study into other materials as well as more complex loading conditions will determine the true applicability of these empirical models.

REFERENCES

[1] Forth, S.C., L. H. Favrow and W. D. Keat, "Nonplanar Fatigue Crack Growth in 7075-T73 Aluminum", *The 2nd Conf. on Aging Aircraft*, Part II, 1998, p. 452 – 461.
[2] Forth, S.C. and W.D. Keat, "Growth of 3D Nonplanar Fractures Using the Surface Integral Method", *J. of Eng. for Gas Turbines and Power*, Vol. 119, No. 4, 1997, p 964-968.
[3] Forth, S.C., L.H. Favrow and W. D. Keat, "Mixed-Mode Crack Growth: An Experimental and Computational Study", *Fatigue '99 Conf. Proc.*, 1999, p. 2533 – 2538.
[4] Gerstle, W.H., "Finite and boundary element modeling of crack propagation in two- and three-dimensions using interactive computer graphics", Ph.D. Thesis, Cornell University, Ithaca, NY, 1986.

9.4.14 A Fracture Criterion for 3D Cracks in Brittle Materials

J.C. Newman, Jr., NASA Langley Research Center and W.G. Reuter, Idaho National Engineering and Environmental Laboratory

An International Cooperative Test Program on Surface-Crack Specimens [1] was conducted in the mid-1990's to study a wide range of surface-crack configurations made of a brittle material, D6AC steel, tested under remote tension and bending, see Figure 52. The nominal range of crack-configuration parameters tested were a/t from 0.25 to 0.85 and a/c from 0.2 to 1.0 with 2w = 51 or 102 mm and a thickness (t) of 6.35 mm. Tests were also conducted on through-the-thickness cracks in three-point bend specimens to determine the plane-strain fracture toughness, K_{Ic}.

In the last decade, the use of crack-tip parameters, such as the stress-intensity factor (K), and constraint parameters have been found to be necessary to characterize fracture of three-dimensional (3D) cracks. In the present study [2], the finite-width correction in the Newman-Raju stress-intensity factor equations for surface cracks was modified to apply for very large crack problems (c/w < 0.8). Also, elastic-plastic finite-element stress analyses of the surface crack in a plate subjected to tension or bending loads were conducted to determine a hyper-local constraint parameter (α_h) along the surface-crack front. The hyper-local constraint parameter is based on the average normal stresses acting over the plastic-zone region on a line perpendicular to the crack front and accounts for the triaxial stress state along the crack front.

A combination of the hyper-local normal-stress constraint factor, $\alpha_h(\phi)$, and the stress-intensity factor, $K(\phi)$, was used to determine the critical fracture location [2,3]. The objective was to develop a rationale to predict the critical location ϕ_c where fracture initiates. As a first approximation, the location where the product of K times α_h maximizes was used to predict the critical location. The rationale is that the region where the "stress-intensity factor and constraint" maximizes would be the most likely location for fracture to initiate. Figure 53 shows the plane-strain fracture toughness $(K_\phi)_{Ic}$ at the critical location (ϕ_c) from the test data on both surface cracks under tension and bending loads, and at the centerline of a three-point bend specimen. The critical values are plotted against the local constraint parameter. These results show that results for specimens with surface cracks under tension and bending fall together with the three-point bend specimen results to within ±20 percent. Surface cracks with high constraint fail at lower stress-intensity factors than specimens with lower constraint. These results demonstrate that the stress-intensity factor and a local constraint parameter can be used to predict the failure of surface cracks in brittle materials subjected to combined loading.

REFERENCES

[1] Reuter, W. G., Elfer, N., Hull, D., Newman, J., Munz, D., and Panontin, T., "Fracture Toughness Results and Preliminary Analysis for International Cooperative Test Program on Specimens Containing Surface Cracks," *Fatigue and Fracture Mechanics: 28th Volume*, ASTM STP 1321, 1997, pp. 146-166.

[2] Newman, J. C., Jr., Reuter, W. G., and Aveline, C. R., Jr., "Stress and Fracture Analyses of the Surface Crack," *Fatigue and Fracture Mechanics: 30th Volume*, ASTM STP 1360, 1999.

[3] Newman, J. C., Jr. "Irwin's Stress Intensity Factor – A Historical Perspective," *Fatigue and Fracture Mechanics: 31st Volume*, ASTM STP 1389, 2000, pp. 39-53.

9.4.15 NASGRO Enhancement

Dr. Xiaogong Lee, FAA, AAR-431, (609) 485-6967

NASGRO is a computer program package for general-purpose crack growth analysis. The program was developed by NASA at the Johnson Space Center (JSC) and has been continually enhanced over the past 15 years. The FAA has been working with NASA JSC to fund the continuing enhancement of NASGRO program and make it available to FAA Aircraft Certification Offices (ACO) and their Designated Engineering Representatives (DERs). Currently, the NASGRO v3.0 is publicly available and can be downloaded via the Internet from:
http://mmptdpublic.jsc.nasa.gov/nasgro/nasgromain.html.

The Federal Aviation Administration (FAA) requires that commercial aircraft certified under Part 25 of the Federal Aviation Regulations (FAR) meet damage tolerance requirements (DTRs). Damage tolerance requirements state that the residual strength of an airframe structural component shall not drop below that required to sustain limit load and that inspections must be scheduled to insure that the required level of residual strength is maintained. Currently, a Notice of Proposed Rulemaking (NPRM) No. 99-20 is being finalized which will require damage tolerance analysis (DTA)-based inspection programs on commuter-size airplanes. A DTA involves the development of crack growth curves and residual strength diagrams for individual structural components of an airframe. To produce crack growth curves and residual strength diagrams for a particular structural component, the engineer must perform a flight loads analysis, and then use the results in a fatigue and fracture mechanics analysis.

NASGRO is one of the available automated general-purpose programs capable of performing durability and damage tolerance analyses for cracked structures. The FAA-sponsored program enhancements have been focused on implementing capabilities to analyze cracked commuter aircraft structures, the development of Windows-based graphical user interface (GUI), and integration of the boundary element method (BEM) module for stress analysis and computing stress-intensity factors.

9.4.16 Crack Growth Analysis
Dr. Dy Le, FAA, AAR-431, (609) 485-4636

A damage tolerance assessment of rotorcraft airframe and dynamic structural components requires an accurate stress analysis of three-dimensional (3D) structural parts containing surface or internal flaws in nonuniform stress fields. A joint effort between the FAA, the University of California – Los Angeles, and the Rotorcraft Industry Technology Association (RITA) aims at enhancing the computational capabilities to provide the needed accuracy.

The University of California – Los Angeles, under FAA funding, is enhancing and validating computational capabilities using the Automated Global-Intermediate-Local Element (AGILE) computational methodology and helicopter manufacturers' full-scale crack growth data.

AGILE uses a hierarchical analysis, first developing a global model of the part being analyzed. From the analysis of this model, both a global stress distribution and the necessary boundary conditions for the intermediate analysis are obtained. The intermediate model is then developed by AGILE, and using the boundary conditions from the global analysis, a solution is obtained for the intermediate model. The analysis parameters for the global and intermediate models are automatically extracted by AGILE's postprocessing functionalities. Global and intermediate finite element analyses are currently performed using the Structural Analysis of Generalized Shells (STAGS) finite element shell program developed by Lockheed Missile and Space under funding from NASA. However, AGILE can incorporate other finite element analysis codes, both two-dimensional (2D) and 3D, and with linear and nonlinear capabilities; e.g., ANSYS, NASTRAN.

In the final step of the hierarchical analysis, a local model is used to obtain detailed fracture information in the vicinity of the crack. In AGILE, for linear analyses, the stress-intensity factors are calculated using the finite element alternating method (FEAM). FEAM uses superposition techniques and iterates between the finite element solution for the uncracked finite body and the analytical solution for an embedded crack in an infinite region. The FEAM allows the modeling of a substantial amount of crack growth to take place without the need for remeshing.

A Bell Helicopter Model 430 main rotor idler link was used to validate the AGILE computational capabilities, Figure 54. First, a global model of the idler link component was created and analyzed using NASTRAN. Then, the local model of the main rotor idler link was created and boundary conditions were transferred from the global model displacement and stress fields using AGILE. Finally, several crack configurations were analyzed with the use of the displacement discontinuity finite element alternating method (DDFEAM).

DDFEAM is an integration equation method used for an arbitrary nonplanar crack, utilizing a finite element model of an uncracked and crack body. It is more efficient compared to the traditional methods, in terms of both computational time and ease of use, because it does not require the user to model a crack tip explicitly in a mesh. It allows the user to calculate the fracture mechanics parameters accurately without excessive computational power.

Global Analysis: Figure 55, illustrates a global mesh of the main rotor idler link consisting of tetrahedral quadratic elements.

Local Analysis: A model for the local analysis of the idler link component for small and large cracks, as shown in Figure 56, is cut from the global model by two planes passing through the tube axis and by one cylindrical surface. The boundary conditions used for the local models were transferred from the analysis of the global model.

Fatigue Crack Growth Analysis Results: Figures 57-58 summarize the distributions of the crack growth angle and the stress-intensity factor range along the crack front.

The final configuration of the crack after fatigue precracking and predicted fatigue crack growth for the main rotor idler link component is shown in Figure 59.

9.4.17 Crack-Bulging Effects in Longitudinal Cracks in Pressurized Narrow-Body Aircraft
Dr. John G. Bakuckas, FAA, AAR-431, (609) 485-4784

Longitudinal cracks in pressurized aircraft fuselages are subjected to hoop load and bending. The interaction of these two loadings causes a bulging of the skin, which can significantly elevate the stress-intensity factor (SIF) at the crack tip and reduce the residual strength. One measure of the effect of bulging is the bulging factor, which is the ratio of the SIF at the tip of the longitudinal crack in a curved panel to the SIF for the same crack in a flat panel.

The damage tolerance design philosophy requires realistic stress state determination in the vicinity of cracks in airframe fuselages. However, few studies have been done to study the bulging effects for cracks in a narrow-body fuselage structure representative of commuter-sized aircraft and the consequence of not including these effects in the stress predictions and subsequent damage tolerance analysis. Of particular concern is the effect of bulging in a fuselage that has been repaired. Repairs add new flaw initiation sites to the structure and also can alter the bulging response to the structure.

To examine the effects of bulging on SIF and residual strength calculations in a repaired fuselage structure, the FAA has undertaken a study to calculate the bulging factors in narrow-body fuselages. The bulging factors were calculated using a nonlinear finite element analysis. The crack-tip SIFs were calculated using the Modified Crack Closure Integral Method. The bulging factors for a typical pressurized commuter fuselage were calculated. The effect of varying the crack length, internal pressure, stiffener placement, and the presence of a repair patch on the bulging factors was studied. Figure 60 shows typical results for a longitudinally stiffened fuselage containing a repair patch.

Once the parametric studies were completed, a database of bulging factors was developed for incorporation in existing repair methodologies. The database was generated in terms of several nondimensional parameters, a shell curvature and loading parameter $\alpha = (E_{skin} * t_{skin})/(pR))^{1/2} * (a/R)$, a stringer parameters, $\gamma = E_{stringer} * A_{stringer}/(E_{skin} * b * t_{skin})$, and a distance parameter, $\Delta = \delta/a$. Here, a is the half crack length, R is the fuselage radius, E is the modulus of elasticity, t is the thickness, A is the cross-sectional area of the stringer, δ is the distance of crack from one of the stringers, and p is the internal pressure. Figure 61 shows a nondimensionalized plot of the bulging factor for a typical case. For the case shown in Figure 61, the half-crack length, a was 1.5 in., the fuselage radius was 50 in., and the stringer spacing was 9 in.
The other quantities are varied to obtain the required non-dimensional parameters. The results show that for short cracks, the stringer parameter, γ, and the distance parameter, Δ, has minimal effect on the bulging factors.

The stress-intensity factors in all modes are being calculated and tabulated and will be used to obtain additional insight into crack propagation in pressurized fuselages and for use in damage tolerance repair analyses.

9.4.18 Laser Forming Technology
Dr. Kevin T. Slattery, Boeing

Laser Forming Technologies (Figure 62.)

- Builds Flanges/Stiffeners Onto A Wrought Substrate Using Electronic Model Like Stereolithography Using Titanium or Ni-Base Alloy Powders
- Uses An 18kw CO_2 Laser To Create A Melt Puddle, Future Machines To Be Higher Powered (~30kw)
- Near-net Shape (3:1 buy:fly) Material and Machining Cost Savings
- Minimal Or Generic Tooling Required
- Full-density Material

Demonstration and Characterization (Figure 63)

- Components as large as 96cm x 280cm and 300kg have been made
- Larger parts can be made by enlarging Ar chamber size
- Lead times as short as 8 weeks
- Mechanical Properties vs. Mill Annealed Forgings:
  - ~5% lower static properties
  - Equivalent fatigue crack initiation
  - Superior fatigue crack growth
  - Superior fracture toughness

9.4.19 Continued Development of the NASGRO Fracture Mechanics Software
J. Cardinal and C. McClung, Southwest Research Institute and R. Forman, NASA Johnson Spacecraft Center

The NASGRO (previously NASA/FLAGRO) computer code was first developed in the 1980s for fracture control analysis on NASA space hardware. More recently, additional funding from NASA, the FAA, and the USAF has supported substantial improvements in the code, especially for aircraft structures applications. Version 3.0 of the NASGRO fracture mechanics computer code was officially released to the public in early 2000. Version 3.0 contains many features not included in Version 2.0, including Windows GUIs for all modules, numerous load interaction models (both empirical and strip yield models), numerous new and improved stress intensity factor solutions, enhanced spectrum handling features, batch execution modes, an improved threshold equation, and a substantially improved materials data base.

Version 3.0 is currently available to the general public at no cost via a NASA web site: http://mmptdpublic.jsc.nasa.gov/nasgro/nasgromain.html. Since its first posting on the web in April 2000, the code has been downloaded over 1200 times (as of June 2001) by users in 44 different countries (60% of the downloads have been by US users). Users have identified their intended applications as space (25%), civil aviation (25%), university research (13%), DoD-USAF, DoD-Navy, DoD-other, petrochemical, nuclear, automotive, railroad, and other.

A growing interest in NASGRO among a variety of industrial users has motivated NASA to develop a new partnership with industry. NASA and Southwest Research Institute™ (SwRI™) have signed a Space Act Agreement under which SwRI and NASA will jointly develop future versions of NASGRO. Under the terms of this agreement, SwRI has formed a consortium of NASGRO users to provide guidance and support for future NASGRO development and user services. The consortium will identify and prioritize new NASGRO capabilities, provide a wider range of user support services, market the code to a wider audience, provide a stable supplementary revenue stream to expand and accelerate NASGRO enhancements, and promote direct technical interactions among fracture mechanics experts and practitioners. The consortium kickoff meeting was held in May 2001. At this writing, ten major aircraft, rotorcraft, and gas turbine companies from eight different countries have officially joined the consortium, and numerous other companies are currently completing contractual arrangements.

NASGRO Version 4.0 is currently in active development by NASA and SwRI. An early alpha version has already received limited distribution for evaluation purposes. Version 4.0 (Alpha) includes a substantially improved

Windows GUI and new stress intensity factor solutions, and many other enhancements are planned. The first formal release of 4.0 is currently planned for early 2002.

9.5. Widespread Fatigue Damage

9.5.1 Experimental Assessments of Multiple Cracking in Aircraft Fuselage Structure

Dr. John G. Bakuckas, FAA, AAR-431, (609) 485-4784

Overview: An experimental study was completed to determine the effects of multiple cracks on the fatigue crack growth and residual strength of curved fuselage panels. The data generated will support and validate analytical models developed under the sponsorship of the FAA to assess aging aircraft with multiple-cracking scenarios. The Full-Scale Aircraft Structural Test Evaluation and Research (FASTER) facility, Figure 64, was used for full-scale testing of curved panels under conditions representative of those seen by an aircraft in actual operation. The Remote Controlled Crack Monitoring (RCCM) system was used to track and record the formation and growth of multiple cracks in real time during a test.

Test Program: The test matrix for the four curved panels is shown below. Panel CVP1 contains a longitudinal lap splice with a lead crack in the outer critical rivet row. Panel CVP2 has a configuration similar to CVP1 with the addition of multiple small cracks. Panel CVP3 has a circumferential butt joint with a lead crack in the outer critical rivet row. Finally, panel CVP4 has a configuration similar to CVP3 with the addition of multiple small cracks.

Specimen	Joint Configuration	Initial Damage
CVP1	Longitudinal Lap Joint	Lead Crack Only
CVP2	Longitudinal Lap Joint	Lead Crack With Multiple Cracks
CVP3	Circumferential Butt Joint	Lead Crack Only
CVP4	Circumferential Butt Joint	Lead Crack With Multiple Cracks

The panels were subjected to three test types: (1) initial quasi-static loading to measure strains and ensure proper load introduction; (2) constant amplitude fatigue loading to measure crack growth; and (3) a postfatigue monotonic, quasi-static loading up to fracture to measure crack growth and residual strength. Representative results from this study include strains, crack growth, and residual strength.

Strain Survey: The measured and predicted hoop strain at gages in the middle of a skin bay in CVP1 (lead crack only) and CVP2 (lead crack and multiple cracks) panels are plotted in Figure 65 as a function of load step. The strains are nearly identical for both panels for all four runs indicating that small multiple cracks have no effect on the global strain response. As expected, there were no differences between panels tested when air or water was used to pressurize the panel. Predictions from analyses shown by the curves were in excellent agreement with the experimental data. Similar trends in strain gage data were obtained at the other gage locations in all panels. Measured strains were nearly uniform in the middle of the panel and in good agreement with the analysis. This provides confidence that the applied loads were introduced properly.

Fatigue Crack Growth: The effect of multiple cracks on the lead crack growth behavior is shown in Figure 66. The half-crack length, as a function of number of fatigue cycles, is shown for panels CVP1 and CPV2 under an applied load simulating a cylindrical pressurization. For CVP1, the vertical jumps indicate that the crack extended across a rivet hole. When this happened, the crack length increased instantaneously by the diameter of the rivet hole, thus the jump. As shown, the rate of crack growth increased as the crack tips approached the rivet holes. The horizontal segments shown in the plot indicate the number of cycles before the crack reformed on the opposite side of the rivet hole. As the crack length increased, the number of load cycles required for crack reformation (incubation period) decreased. For CVP2, which contained multiple cracks when the lead crack grew into the next rivet hole that contained a small crack, there was no incubation period since there was a crack tip already in place. As a result, the number of cycles to grow the lead crack to the final length (~12.5 inches) in CVP2 was approximately 40% less than that in CVP1.

Residual Strength: The effect of multiple cracks on the residual strength behavior is shown in Figure 67. For both the CVP1 and CVP2 tests, the central frame was saw-cut. Cylindrical pressurization was then applied quasi-statically, and the crack extension measured up to panel failure. In the initial stages of loading, slow stable crack extension was observed in both panels up to 10.25 psi pressure for CVP1 and 8.5 psi pressure for CVP2. Then, the crack grew rapidly until it reached the first intact frame for both panels. An increase of pressure was required to grow the cracks past the frames in both panels. The ultimate pressure at which the panels failed (residual strength) was 11.14 psi for CVP1 and 9.16 psi for CVP2. The presence of multiple cracks reduced the residual strength by approximately 20%.

9.5.2 Curved Panel Widespread Fatigue Damage (WFD) Evaluaton
Dr. Xiaogong Lee, FAA, AAR-431, (609) 485-6967

Four full-scale curved panels have now been successfully tested at the FASTER test facility at the FAA William J. Hughes Technical Center. The panels, fabricated by Boeing, are representative of narrow-body fuselage skin structure, two panels having circumferential splices and two with longitudinal splices. All four panels were fabricated with a saw-cut lead crack; in addition, two panels had multiple cracks saw cut ahead of the lead crack. The following table summarizes the panel configurations and test completion dates.

Spec. ID	Panel Description	Test Date	Residual Strength
CVP1	Longitudinal Splice—lead crack only	9/99	11.14 psi
CVP3	Circumferential Splice—lead crack only	2/00	17.9 psi
CVP2	Longitudinal Splice—lead and multiple cracks	6/00	9.08 psi
CVP4	Circumferential Splice—lead crack and MSD	9/00	21 psi

The finite element method (FEM) was used to analyze the curved panels and to calculate the crack growth rates and assess their residual strength. The public domain shell code STAGS was used for the analysis. Figure 68 shows a typical 3D FEM model used in the analysis. Crack-tip-opening angle (CTOA), developed by NASA, was used as the failure criterion in the analyses.

Figures 69 and 70 show the principal stresses at the inner surface of the curved panel with a two-bay lead crack. It was plotted in the deformed shape. Figure 70 is a close-up plot that shows the broken frame and shear clip, which are explicitly modeled.
Figure 71 shows the analysis results for curved panels CVP1 and CVP2. The intersection of the skin fracture and frame failure curves indicates predicted failure. For CVP1, the predicted residual strength is 10.68 psi, 5% less than the test result of 11.14 psi. The prediction for CVP2 is 9.58 psi, 6% higher than the test result of 9.08 psi.

Results from these analyses verify the accuracy of the FEM techniques used for the analysis.

9.5.3 Analysis of Aircraft Fuselage Structure Containing Cracks
Dr. John G. Bakuckas, FAA, AAR-431, (609) 485-4784

Overview: Analyses were conducted to predict the effects of multiple cracks on the fatigue crack growth and residual strength of curved fuselage panels that were tested using the Full-Scale Aircraft Structural Test Evaluation and Research (FASTER) facility. A total of four panels were tested, two panels with a longitudinal lap splice and two with a circumferential butt joint. For each joint configuration, one panel contained only a lead crack and the other contained a lead crack with multiple cracks.

Approach: Geometric nonlinear finite element analyses were conducted to predict the strain distributions and the fracture parameters governing the onset and growth of cracks. For fatigue crack growth predictions, the corresponding mixed mode stress-intensity factors (SIF) were calculated using the Modified Crack Closure Integral (MCCI) method. The SIF caused by tensile load, K_I, in-plane shear load, K_{II}, symmetric bending loads, k_1, and out-of-plane shear and twist loads, k_2, were calculated as shown in Figure 72. The SIF are related to the work done to close a crack of length Δa from the crack-tip nodal point forces, F, and the crack surface opening displacements, u.
For residual strength predictions, the critical crack-tip-opening angle (CTOA) fracture criterion and the computer code STAGS were used.

Finite Element Models: Details of the test panels were modeled using two-dimensional shell elements with each node having six degrees of freedom as shown in Figure 73. Beam elements were used to model the rivets that connect the substructures with the skin and the substructures to one another. The FASTER fixture loading conditions were simulated in the analysis.

Strain Survey Results: The measured and predicted hoop strain at gages in the middle of a skin bay in CVP1 panels are plotted in Figure 74. Measured strains were nearly uniform in the middle of the panel and in good agreement with the analysis. Similar trends in strain gage data were obtained at the other gage locations in all panels. This provides confidence that the applied loads were introduced properly and the models have enough fidelity to capture the mechanical response.

Fatigue Crack Growth Results: The measured and predicted fatigue crack growth behavior for CVP1 (lead crack only) and CVP2 (lead crack and multiple cracks) panels is shown in Figure 75. The number of cycles to grow the lead crack to the final length in CVP2 was approximately 40% less than that in CVP1 due to the presence of small multiple cracks directly ahead of the lead crack. The vertical jumps in the experimental data indicate the extension of the lead crack across a rivet hole for CVP1 or when the lead crack and multiple cracks linked up for CVP2. The horizontal segments shown in the plot for CVP1 indicate the number of cycles before the crack reformed on the opposite side of the rivet hole. For CVP2, there was no crack reformation.
In the analysis of both panels, the mode I SIF, ΔK_I, was used in a cycle-by-cycle crack growth model to predict the fatigue crack growth behavior. The rivet holes were not explicitly modeled in the finite element analysis. For CVP1, crack growth across rivet holes was accounted for by increasing the length of the crack by the diameter of the rivet hole. For CVP2, crack growth across the rivets was modeled by increasing the length of the crack by the diameter of the rivet plus the length of the small cracks at the rivet. The number of cycles just before and after crack growth across the rivet hole was assumed to be the same. The delay in crack reformation for CVP1 was not modeled. Only ΔK_I was used to predict crack growth since the SIF predictions indicated that it was the dominant SIF. There were indications of mode III from the Δk_2 calculated from analysis and from the crack-bulging deflection observed during the test which was not accounted for in the analysis due to the lack of experimental data. Good agreement was obtained between experiments and predictions relying on ΔK_I.

Residual Strength Results: The measured and predicted residual strength behavior for CVP1 is shown in Figure 76. In the initial stages of loading, slow stable crack extension was observed in up to 10.25 psi and 8 psi for the experiments and analysis, respectively. The crack then grew rapidly until it reached the first intact frame. An increase of pressure was required to grow the cracks past the frames. The measured and predicted residual strength were in good agreement with vales of 11.14 psi and 10.65 psi, respectively.

9.5.4 Experimental and Analytical Assessments of Multi-Site Cracking in Aircraft Fuselage Structures

Dr. John G. Bakuckas, FAA, AAR-431, (609) 486-4784

During FY99, an experimental and analytical assessment of multiple-site cracking in fuselage structure was initiated. The Full-Scale Aircraft Structural Test Evaluation and Research (FASTER) facility was developed to test full-scale fuselage panel specimens under conditions representative of those seen by an aircraft in actual operation. The facility includes the Remote Controlled Crack Monitoring (RCCM) system to track and record crack formation and growth during a test in real time. The facility also includes a test device developed to measure out-of-plane to determine the shape and extent of crack bulging. This device consists of an array of linear variable differential translation (LVDT) displacement transducers oriented normal to the panel surface, as shown in Figure 77.

The test program to assess multiple-site cracking in fuselage structure consists of both experimental testing using the FASTER facility and conducting finite element analyses of the test panels. The test program includes tests of four curved panels that are representative of generic commercial aircraft fuselage structure. In each test the strains, crack growth, and crack bulging will be measured.

As a part of the research program, a global-local hierarchical (GLH) analysis approach using the finite element method (FEM) was developed and used to calculate the strain distributions and the fracture parameters governing crack initiation and growth in the test panels. Figure 78 shows that GLH methodology that was used to analyze the test panels.

During FY99, the first of the four curved panels was tested. The panel was manufactured with a single 7″ crack in the outer rivet row of the longitudinal lap splice joint. The crack spanned an intact frame. The panel was first loaded statically to measure the strain distribution. Fatigue loading was applied to grow the crack to a predetermined length. The panel was then loaded statically until failure to measure the residual strength. The behavior of the panel was also predicted using the GLH methodology. The measured and predicted hoop strains in the middle of a skin bay of the panel are plotted as a function of load step as shown in Figure 79. Two repeat tests were run using air to pressurize the panel and two were run using water to pressurize the panel. The strains were nearly identical for all four runs. As expected, there were no differences in the results when air or water was used to pressurize the panel. The analytical predictions, shown by the curves, were in excellent agreement with the experimental data. The two analytical predictions were made using two independent analyses using different finite element codes and modeling procedures. This provides confidence that the FASTER boundary conditions are correctly modeled and that the models have enough fidelity to capture the mechanical response.

The crack extension was monitored with the RCCM system. Images from the RCCM system showed that the crack growth was generally collinear and symmetric. These images shown in Figure 80 show the crack extension from the two tips of the crack. When the crack tips propagated into a rivet hole, a number of additional fatigue cycles was required to start the crack growing on the other side of the hole. As the crack length increased, the number of fatigue cycles needed to start the crack growing again decreased. The fatigue testing was stopped after the two halves of the crack each reached lengths of approximately 12.5 inches, for a total crack length of 25 inches. The panel was then loaded statically until failure to determine the residual strength. For this test, the central frame was cut and the crack extension was measured up to panel failure. Slow stable crack growth was measured up to a pressure of 10.25 psi, at which point the crack grew unstably until it reached the first intact frame and was arrested. The pressure was increased to 11 psi before the crack grew past the frames. The panel failed at a pressure of 11.14 psi (the residual strength), shown in Figure 81. The final damage state included a skin crack approximately 68 inches and two broken frames, in addition to the frame that was cut. Further fracture analysis using the GLH approach is underway. Testing of the remaining three panels will be completed during the next year.

9.5.5 Multiple Site Damage in Aircraft Fuselage Skin Splices

Capt Dan Shrage, Air Force Research Laboratory

This test report is aimed at the experimental verification of analytical models that predict the residual strength of wide panel, aircraft representative structure subject to Multiple Site Damage (MSD). As today's transport aircraft become older, the possibility exists for predetermined analysis to be invalidated by the onset of MSD. MSD can be caused by cyclic loading of the fuselage structure during its life cycle and can pose a safety risk if not taken into consideration during repair and inspection procedures.

Four types of flat, production representative joints were tested for residual strength with existing damage configurations, accounting for narrow and wide body transport aircraft (Figure 82). The panels were fitted with anti-buckling guides in an attempt to remove the out-of-plane deformation during the testing. The resulting crack extension was recorded with a traveling optical microscope and each of the joints was instrumented with strain gages, both axial and rosettes. The joints were also instrumented with a crack opening displacement (COD) gage. The tests were displacement controlled, using a Linear Voltage Displacement Transducer (LVDT) which allowed the measurement of crack progression after the residual strength had been reached, as the load placed on the panel was dependent on achieving or maintaining a certain global linear displacement.

The average reduction in residual strength for the 0.050” size MSD was 21.45%, while the average for the 0.100” MSD was 27.88%. However, given the wide differences in the configuration of each joint type, such sweeping averages should not be applied across the board, but instead each joint type should be examined individually.

Additionally, the four types of flat, production representative joints were tested for residual strength with the resulting crack extension and displacements recorded using a new system with digital visual image correlation. This system can measure three-dimensional full-field displacements, as well as crack opening displacement (COD) and δ_5 measurements. Whereas the displacement fields can be transformed into strain fields, the specific measurements of deformation are used as failure criteria in many finite element analyses.

These eight panel tests were conducted without standard buckling guides and therefore are more representative of the failure modes seen in service. The out-of-plane displacement, normally restricted by the anti-buckling guides, is readily apparent during the tests and significantly increases our understanding of how aircraft splices fail in service. The results show there is reduction between 10-15% in residual strength when the tests are accomplished including the effects of out-of-plane bending.

9.5.6 Residual Strength Test and Analysis of Fuselage Splice Joints Containing Multiple-Site Damage
Dr. Paul W. Tan, FAA, AAR-431, (609) 485-6665

The FAA funded the United States Air Force (USAF) to test 12 flat panels to investigate the link-up and residual strengths of various fuselage splice joints containing a large lead crack with or without multiple-site damage (MSD). The experimental results will be used to validate fracture criteria developed by the FAA and NASA for thin sheet material such as the ligament yield criteria, the T* integral criterion, and the crack tip opening angle (CTOA) criterion. These criteria will be part of an integrated methodology to analyze the onset of widespread fatigue damage (WFD) in aircraft structures.

The flat panels consist of four different common types of splice joints. The splices represent three types of fuselage longitudinal splices and one type of fuselage circumferential splice. Four panels for each splice joint were tested, the first of which was the baseline panel with a lead crack and no MSD. The second and third panels had the same lead crack length as the baseline panel but with 0.05- and 0.10-inch MSD ahead of the lead crack, respectively. The fourth panel was a spare panel. The specimens were 48 inches wide and 72 inches long. The panels were tested with antibuckling guides.

The three longitudinal splice types were (1) a longitudinal lap joint with two finger doublers and a longeron, (2) a longitudinal lap joint without doublers but with a longeron, and (3) a longitudinal butt joint with a splice plate, a doubler and a longeron. The circumferential splice type was a circumferential butt joint with a butt splice plate and a finger doubler. The skins were made of 2024-T3 aluminum alloy, the longerons are made of 7075-T6 aluminum alloy, the doublers and splice plates were made of either 2024 or 7075 material.

The antibuckling guides were made of four pieces of half-inch-thick A36 steel plates with I-beam stiffeners. All specimens had eight strain gages, back to back, to determine if uniform load was being introduced in the splice joints and four gages to measure the effectiveness of antibuckling guides. The first specimen of each splice type had an additional 14 strain gages located in the tangential line of the critical rivet row to measure the secondary bending due to unsymmetrical geometry.

The residual strength of the panels with MSD was predicted using (1) the ligament yield criteria, (2) the T* integral and (3) the CTOA criteria. The predictions of all three methods correlated well with the test results. The fracture criteria and analysis procedures are briefly summarized in the following paragraphs.

Ligament Yield Criteria: In the ligament yield criteria, structural failure is assumed to occur when the applied stress reaches a level that causes consecutive link-ups between the lead crack and the MSD ahead of the lead crack. The stress, when individual link-up occurs, σ_{LU}, is assumed to be a function of the ligament yield stress, σ_{LY}. The ligament yield stress is estimated using Irwin’s plastic zone equation. The relation between the link-up stress and the ligament yield stress can be expressed as $\sigma_{LU} = C*\sigma_{LY}$. Several corrective factors C, available in the literature, were used to predict residual strength of splice joints with MSD, shown in Figure 83.

T* Integral Criterion: For T* integral criterion, the elastic-plastic finite element alternating method (EPFEAM) was used to analyze the stable tearing of a lead crack with MSD ahead of it. The analyses were performed on local models containing at least five fastener holes in the crack path. The boundary conditions of the local model were derived from results of nonlinear elastic-plastic analyses of global models. The T* resistance curves used in the analyses were based on analytical stress versus crack extension curves of a 48-inch-wide MT panel to simulate a true two-dimensional condition. The predicted residual strengths using T* integral criterion versus test results for the various types of panels are shown in Figure 84.

CTOA Criterion: For CTOA fracture criterion, a general purpose shell finite element code was used for the residual strength analysis. The global models were the same as those used in the T* analyses. The critical angles for the clad 2024-T3 aluminum alloys are 5.0 and 5.5 degrees for the T-L and L-T grain direction, respectively. The predicted residual strengths using CTOA Criterion versus test results for the various panels are shown in Figure 85.

9.6. Corrosion and Corrosion/Fatigue

9.6.1 The Transition of Corrosion Pitting to Surface Fatigue Cracks in 2024-T3 Aluminum Alloys

Dr. Paul N. Clark, University of Utah

Pitting corrosion experiments were executed to characterize the dynamics of accelerated corrosion for the combination of 2024-T3 aluminum and a 3.5% NaCl solution at room temperature.

A detailed corrosion protocol was developed to accelerate pitting corrosion on 2024-T3 aluminum. The developed protocol allowed for the relative control of pitting depth on fatigue dog-bone specimens. The protocol can be tailored to produce specific levels of corrosion damage.

Corrosion fatigue experiments were performed on specimens that had been prior corroded using the developed corrosion protocol. Pitting depths from approximately 40µm-200µm were examined for fatigue characterization. Corrosion pitting to surface fatigue crack transition was captured and fatigue crack growth behavior was documented. As well as the pit to crack transition, the short crack behavior to long crack behavior transition was captured and analyzed.
Fractographic analysis of corrosion fatigue specimens revealed that fatigue cracks nucleate, propagate and cause subsequent failure from accelerated prior pitting corrosion damage.

9.6.2 Evaluation of the Prior Corrosion Effects on the Fatigue Behavior of 7075-T651 and 2024-T351 Aluminum Alloy Specimens with and without Cold Worked Fastener Hole

Dr. Young-In Yoon, University of Utah

Corrosion fatigue experiments were performed on prior corrosion induced specimens with a simulated fastener hole. The specimens were manufactured from 7075-T651 and 2024-T351. The following were characterized at a maximum stress of both 25ksi and 35ksi, with a stress ratio of 0.1 in laboratory air at a frequency of 10Hz.

- Cold Working Without Prior Corrosion (Cx)
- Prior Corrosion Without Cold Working (PC)
- Cold Working before Prior Corrosion (Cx-PC)
- Cold Working after Prior Corrosion (PC-Cx)

The prior corrosion was introduced onto the precracked side of the center section of the specimens using an accelerated corrosion process involving and applied DC current, 3.5% NaCl solution and a carbon rod counter electrode.

In all cases, cold working the fastener hole increased the fatigue life of the specimens. The most significant increase in fatigue life was witness when comparing cold worked specimens without corrosion versus prior corroded specimens without cold working.

For all cases, a cold worked fastener hole showed an increase in fatigue life versus a fastener hole with prior corrosion but without cold working. An increase in fatigue life was shown whether the cold working was applied before or after the prior corrosion had been induced.

When tested at a maximum fatigue stress level of 35ksi both the 2024-T351 and 7075-T651 cold worked then subsequently exposed to prior corrosion (Cx-PC) exhibited an increased fatigue life when compared to specimens in kind that had been cold worked after exposure to prior corrosion (PC-Cx). However, at a reduced stress where the maximum fatigue stress was 25ksi the prior corroded and subsequently cold worked (PC-Cx) specimens showed and increase in fatigue life versus the cold worked and then prior corroded (Cx-PC) specimens.

There is an apparent threshold of corrosion damage that a cold worked fastener hole will withstand. This is dependent upon the stress range that the fastener hole will experience.

9.6.3 Modeling the Effect of Prior Corrosion on Fatigue Life Using the Concept of Equivalent Stress Concentration

C.A.Paul, Air Force Research Laboratory and J.P. Gallagher, University of Dayton Research Institute

The U.S. Air Force wants to reduce maintenance costs associated with its aircraft. One significant maintenance cost for older aircraft is associated with the actions of finding, assessing and repairing corrosion damage. If the Air Force wants to accurately determine the economic life of aircraft, it must include the effects of corrosion. The concept of an Equivalent Stress Concentration was investigated to determine if this approach can quantify the effect of prior corrosion on fatigue life. This concept is similar to a fracture mechanics-based analysis for durability assessment that establishes an Equivalent Initial Flaw Size (EIFS). The difference between an EIFS approach and the approach for this study was the application of strain-based fatigue analysis to establish an Equivalent Stress Concentration. An Equivalent Stress Concentration was also calculated using material data from Mil-Hdbk-5H. The results of a strain-based calculation for the Equivalent Stress Concentration are shown in Figure 86. In addition to the calculation of an Equivalent Stress Concentration, the pit dimensions were recorded and an analysis conducted to determine the existence of a correlation between pit depth and an Equivalent Stress Concentration. The Equivalent Stress Concentration was found to be a strong indicator of surface condition; however, no correlation was found to exist between pit depth and an Equivalent Stress Concentration for the limited range of measured pit depths. When the Equivalent Stress Concentration determined for the fatigue behavior of pre-corroded material is normalized to that of the non-corroded material, this normalized parameter becomes useful for estimating the effect of corrosion on fatigue life. The results of this normalization are shown in Figure 87.

9.6.4 Nature and Statistical Distribution of Damage in the Lower Wing Skin of a 24-Year-Old B707-321B Aircraft

Robert P. Wei, Mary C. Latham and D. Gary Harlow, Lehigh University - Research supported by the Air Force Office of Scientific Research

A more comprehensive metallographic examination and statistical analysis of damage in the fastener holes of the lower-wing-skin panels from a B707-321B aircraft was carried out. The aircraft (s/n 19266, line #531) had been in commercial service for about 24 years, from delivery in 1966 to termination in 1990, had logged 57,382 flight hours over 22,533 flight cycles. It was selected for a teardown inspection as a part of the J-STARS (Joint Surveillance, Target and Attack Radar System) program of the United States Air Force because it had the highest time for the 300 series aircraft in the inventory. The metallographic examinations included optical microscopy of the fastener hole walls at magnifications up to 150X to determine the size and distribution of damage, and serial sectioning and scanning electron microscopy of selected areas to characterize the nature and geometry of the damage. The extent and size of damage were found to be much more extensive than that indicated by the original J-STARS analyses; the under estimation is attributed to the lower-resolution (20X) optical technique used in the original teardown inspection program. Many more holes were found with damage, and the number of identifiable damage in some of the holes exceeded 60. Corrosion played a significant role in the nucleation and subsequent development of fatigue damage. The fatigue damage appear to have nucleated from prior corrosion damage and to have sustained further corrosion along their flanks (Figure 88). Many of the shallower damage appear to be the remnants of shorter cracks that have been dissolved away by corrosion. The evolution of damage was exacerbated by the use of steel fasteners, with over 40 percent of the fastener holes with steel fasteners exhibiting damage versus less than 10 percent of the others. The overall probability of occurrence (PoO) of damage had been found to be in good agreement with that predicted from a simplified mechanistically based probability model, proposed by Harlow and Wei, for pitting corrosion and fatigue crack growth, except for the fact that many of the smaller damage were missed by the initial optical inspection (Fig. 89). The measured distribution of damage within each fastener hole (not shown) was found to be in good agreement with those shown in Figure 89. Typical damage for a single corrosion-nucleated fatigue crack (Figure 90) and the linkup of adjacent cracks (Figure 91) tend to be elliptical in shape, reflecting the influence of the near-hole distribution of stresses. These findings suggest the need for further improvements of the predictive models (*e.g.*, to account for the multiplicity of damage in a single hole) in relation to the development of quantitative methodologies for life-cycle design and management of aircraft.

REFERENCES

[1] Harlow, D.G., Domanowski, L.D., Dolley, E.J. and Wei, R.P. (1999) "Probability Modeling and Analysis of J-STARS Tear-Down Data from Two B707 Aircraft", Proceedings of Third Joint FAA/DoD/NASA Conference on Aging Aircraft, Albuquerque, NM, September 20-23, 1999.

[2] Mary C. Latham, "Characterization of Corrosion Fatigue Damage in the Fastener Holes of a Boeing 707," M. S. Thesis, Lehigh University, 2001.

9.6.5 Structural Fatigue and Corrosion

Ms. Rosanne Weiss, FAA, AAR-424, (609) 485-4370

In the late 1980s after the Aloha Airline incident, the Federal Aviation Administration (FAA) and industry initiated a cooperative effort to establish programs and take actions necessary to ensure that the aging transport fleet remains airworthy. This cooperative effort was undertaken by the Airworthiness Assurance Task Force (AATF), now known as the Airworthiness Assurance Working Group (AAWG), and sponsored by both the Air Transport Association of America and the Aerospace Industries Association of America. The AATF initiated two tasks to assist with the Supplemental Structural Inspection Documents or Airworthiness Limitations

Inspections programs. These two tasks were the Structural Modifications Program (SMP) and the Corrosion Prevention and Control Program (CPCP). The FAA issued airworthiness directives mandating structural modifications and corrosion prevention and control programs for 11 aircraft models. These programs had been in place for 2 to 5 years when the FAA decided to conduct an overall assessment of the effectiveness of these programs.

A contract was awarded in late 1997 for this research. The purpose was to develop and analyze trends on fatigue and corrosion occurring in those structural details of aircraft that were included in the aging aircraft structural modification program and the corrosion prevention and control program.

Using the trends analysis results, the effectiveness of the SMP and CPCP were also examined.

The trends analysis was performed using the Boeing 737-200 series airplane as the prototype. The analysis was performed by identifying the structural components that should be analyzed using airworthiness directives and service bulletins and extracting relevant structural fatigue and corrosion service difficulty reports (SDRs) obtained from the FAA's SDR system for the applicable airplane and identified components.

A report titled "Trends on Structural Fatigue and Corrosion in Aging Commercial Airplane Fleets" was published in April 1999. This report documents the trends found for the Boeing 737-200 series airplane, Figure 92.

9.6.6 Probabilistic Corrosion Fatigue Analysis

Rigo Perez, Boeing

A probabilistic corrosion fatigue life prediction procedure, Figure 93, was developed to account for variation in the magnitude of corrosion. Model development utilized crack initiation and propagation analysis methods, in combination with statistical characterization of corrosion metrics, and corroded coupon fatigue test results.

Pits were measured on 7075-T6 sheets exposed to prohesion spray for various time periods. "Dog bone" fatigue test coupons were machined from the corroded sheets and tested in laboratory air at constant amplitude stress. Uncorroded specimens were also tested for comparison.

The measured pits were treated as initial cracks in a crack growth analysis of the dog bone coupon fatigue lives. The calculated lives were fitted with a Weibull distribution and compared with the test results. Ratios of the corroded and uncorroded coupon lives were used to generate effective stress concentration factors corresponding to the magnitude of corrosion. The corrosion was quantified in terms of a pit size norm metric, and relationships between the effective stress concentrations and the pit size norm values were formulated.

In the probabilistic corrosion fatigue life prediction approach, the effective stress concentration factors are used in combination with a strain life analysis to predict the number of stress cycles required to initiate a 0.254 mm crack. A deterministic crack growth analysis method was used to predict the number of cycles to grow a 0.254 mm crack to fracture. Total life is defined by the addition of the crack initiation and growth lives.

The accuracy of the method was assessed by comparing predicted fatigue lives with tests of corroded open hole 7075-T651 specimens. The results of the comparisons suggest that corrosion can be represented by effective stress concentration factors when analyzing structural life, Figure 94.

REFERENCES

[1] K.K. Sankaran, R. Perez, K.V. Jata, "Effects of Pitting Corrosion on the Fatigue Behavior of Aluminum Alloy 7075-T6: Modeling and Experimental Studies," Materials Science and Engineering, A297, 2001, pp. 223-229.

[2] M.E. Hoffman, P.C. Hoffman, R. Perez, K.K. Sankaran, H.G. Smith, Jr., "Impact of Corrosion on Structural Integrity," Symposium of the International Committee on Aeronautical Fatigue, 2001.

9.6.7 Corrosion Effects on Structural Integrity

Dr. E.J. Tuegel, Air Force Research Laboratory (Air Vehicles Directorate) and Dr. D.T. Peeler, Air Force Research Laboratory (Materials Directorate)

Corrosion cost studies were conducted for FY 1990 and 1997 to get accurate cost information not available from any automated USAF data system or combination of such systems. This detailed database breaks out corrosion costs by weapon system and quantifies the maintenance resources required under the current maintenance program. These two studies documented the baseline for the cost of corrosion maintenance alone, and established the cost trend over time. The data demonstrates that an improved corrosion management philosophy is needed. Rather than develop a new stand-alone corrosion management program, it is more effective to integrate corrosion management into the existing fatigue management program. This has the added advantage that the interaction of corrosion and fatigue can be managed within the same framework.

The U.S. Air Force Research Lab is executing a strategic technology plan to assess, model and mitigate the effects of corrosion on the structural integrity of aircraft. Elements of this plan, as shown in Figure 95, are to:

1. demonstrate and validate a framework for including the effects of corrosion in crack growth and residual strength analysis methods, including predicting the growth of corrosion damage;
2. improve nondestructive inspection techniques for finding corrosion on aircraft and quantifying it in a way that is meaningful for the analysis methods;
3. develop improved, environmentally compliant corrosion prevention/suppression coating systems; and
4. develop cost-effective repair and abatement options for corrosion damage and a trade study tool to help maintenance personnel choose the most appropriate repair.

As indicated in Figure 95, all of these elements are being developed to slip into the existing ASIP program, enhancing it and supporting the Force Structural Maintenance Plan.

Successful completion of this plan will enable the US Air Force to replace the current "Find & Fix" philosophy for corrosion maintenance with an "Anticipate & Manage" scheme. The successful integration of corrosion and fatigue into a single "Anticipate & Manage" maintenance program requires tools to place bounds on the threat posed to structural integrity by premature crack nucleation, faster crack growth, or loss of net section as a result of corrosion. Without these tools, maintenance personnel are forced to treat all corrosion as a serious threat and remove it, sometimes unnecessarily. In addition, models for corrosion growth are needed to be able to anticipate the development of corrosion.

The critical experiment of the technology plan is contained in the Corrosion Fatigue Structural Demonstration program. In this program, the framework for including corrosion into crack growth analyses and residual strength analyses is demonstrated and validated. Enhancements to the basic framework that increase its utility and effectiveness are being developed and validated in a complementary effort, Corrosion Fatigue Damage Management. Details of these various efforts are summarized in the following sections.

9.6.7.1 Corrosion Fatigue Structural Demonstration (CFSD)
R.P. Bell, D. Shelton and J.T. Huang, Lockheed Martin Aeronautics Co.

Lockheed Martin Aeronautics Company is the prime contractor on the CFSD Phase II program. In addition to program management, LM Aero's main task is to validate the corrosion fatigue analysis algorithms contained in the ECLIPSE™ software, and then integrate ECLIPSE™ into the tracking programs for both the C-141 and C-130.

The corrosion fatigue analysis algorithms will be verified via an extensive coupon and element test plan developed in coordination with the subcontractors, APES Inc., University of Utah and NRC-Canada. The test plan will involve specimens corroded in the laboratory as well as specimens removed from actual aircraft. LM Aero will also confirm the effects of corroded surface topography, and pillowing in lap joints, on stress intensity factors as implemented in ECLIPSE™ with independent finite element models. Verification of the algorithms and their implementation as judged by LM Aero, and the C-141 and C-130 ALCs, through correlation with test and service data is the criterion for integration of ECLIPSE™ into the respective tracking programs.

As part of the integration effort, LM Aero will determine the validity of the Environmental Severity Index (ESI) for predicting the relative severity of corrosion on C-141 and C-130 aircraft. The ESI concept is being developed by USAF under Corrosion Damage Management. The ESI for an individual aircraft is currently predicated on the base or bases of assignment for that aircraft. LM Aero will also develop a cost-benefit model that will determine the viability of different maintenance options, such as repair vs. replace vs. defer. The Return-On-Investment and Reliability & Maintainability improvements to USAF as a result of implementing these new corrosion fatigue methods will also be determined.

9.6.7.1.1 ECLIPSE™ Software
C.L. Brooks, S. Prost-Domasky and K. Honeycutt, APES Inc.

The inclusion of corrosion effects into a fracture mechanics-based life analysis requires consideration of both the direct physical degradation of the structure due to corrosion, and the synergistic effects of the corrosion process on crack propagation. The following corrosion effects are currently included in ECLIPSE™:

1) Environmentally Assisted Cracking: The increase in the basic crack growth rate (da/dN) resulting from exposure to corrosion environment, including humidity. This effect is often included in life estimates through the utilization of crack growth rates obtained from lab tests conducted in a similar environment. However, within ECLIPSE this phenomenon is approximated by using the cyclic crack growth rate in a standard environment for a specified number of load cycles and then applying a crack extension due to corrosion in actual environment for the time corresponding to the applied load cycles.
2) Geometric Decay: The overall dimensions of a structural part are decreased due to material loss from corrosion. This results in an increase in the gross stress in the part.
3) Local Geometric Stress Modifier/Riser: The corrosion process, not being uniform over the entire surface, roughens the surface of the material from the as-manufactured condition of the component. This "topography" effect produces an additional but relatively local stress gradient at locations of attack such as pits. These topographical features can exist in conjunction with geometric decay, larger stress concentrations such as holes, or both.
4) Pillowing: The corrosion by-products trapped in a confined space produce volumetric expansion and resulting pressure, or deflections, leading to a sustained stress. This sustained stress increases as corrosion by-products accumulate. These sustained stresses can produce cracking on their own, and combined with operational stress cycles, may result in faster cyclic crack extension due to the imposed tensile mean "pillowing" stress.

The effects of Geometric Decay, Local Geometric Stress Modifier and Pillowing are all seen in the stress intensity factor. The effect of Environmentally Assisted Cracking is accounted for in an additional crack extension added at specified increments to the cyclic crack growth.

The effect of increased crack closure due to the build-up of corrosion byproducts and debris in the crack is not included in ECLIPSE™ at this. This is a conservative approach since increased closure reduces the effective stress intensity and hence the crack growth rate. Without some criteria for determining when this build-up will occur and if it will be stable, it is imprudent to take advantage of this effect.

There is little data of known quality that can be used to verify and refine the models for the above behaviors. Within CFSD, test data will be obtained from both laboratory specimens and actual aircraft parts tested in the lab to further develop the algorithms in ECLIPSE™.

9.6.7.1.2 Corrosion Fatigue Data Development
Dr. D. Hoeppner and Dr. P. Clark, University of Utah

The University of Utah Structural Integrity Laboratory has been tasked with developing data to refine several of the models in ECLIPSE™. The UU experimental effort is in the following areas:

1) Growth of pits on 2024-T3 and 7075-T6 aluminum in various environments under no load, sustained load, and cyclic load. Pit growth characteristics are evaluated by observation in the scanning electron microscope and also in the confocal microscope. Data on the size and depth of pits can be obtained with these techniques for use in developing the model of how the Local Geometric Stress Modifier/Riser evolves.
2) Transition of pits into cracks in 2024-T3 and 7075-T6 aluminum under various laboratory environments and for varying levels prior corrosion. These tests will provide data for how the Local Geometric Stress Riser nucleates a crack and how the model should account for the transition to a crack.
3) Growth of “short crack” in 2024-T3 and 7075-T6 aluminum in humid air and 3.5% NaCl solution, and with varying levels of prior corrosion. The results will be used to refine the crack growth rate models for “short cracks” especially for Environmentally Assisted Cracking. Short crack tests using specimens with prior corrosion will demonstrate the effect of the Local Geometric Stress Riser on short crack growth rates.
4) Growth of long cracks in 2024-T3 and 7075-T6 aluminum in humid air and 3.5% NaCl solution, and with varying levels of prior corrosion. The results will be used to refine the crack growth rate models for long cracks especially for Environmentally Assisted Cracking. Tests with prior corrosion will demonstrate the effect of the Local Geometric Stress Riser on long crack growth rates.

In addition, Dr. Hoeppner has been developing a common terminology to aid in the communication between the various organizations.

9.6.7.1.3 Discontinuity State Metrics
G. Eastaugh, Institute for Aerospace Research, National Research Council Canada

The NRCC Institute for Aerospace Research is performing the following experimental work in support of ECLIPSE™ model development:

1) Identifying the initial discontinuity state (IDS) of 2024-T3 and 7075-T6 aluminum. In the absence any manufacturing defects or corrosion, fatigue cracks will nucleate at a discontinuity that is inherent to the material and thus part of the IDS distribution. Quantitative metallography is performed to identify the types of discontinuities and their respective sizes. Fatigue tests of dogbone-type coupons with subsequent fractography will identify those discontinuities at which crack nucleation occurs. Figure 96 shows micrographs of a crack nucleation site at a constituent particle in 7075-T6 during pilot testing. These results will be used in the model for crack nucleation of a pristine part, that is, without any manufacturing flaws or corrosion.

2) Nucleation and growth of fatigue cracks 2024-T3 and 7075-T6 with different levels of prior corrosion. This condition is referred to as a Modified Discontinuity State. Both artificially and naturally corroded material will be tested. The naturally corroded material will come from fuselage skin splices removed from aircraft. Prior to testing the severity of the corrosion for each specimen will be characterized by thickness mapping and profilometry traces. The results of these tests will help to define corrosion metrics for NDI, provide a means to correlate artificial and natural corrosion, and establish the interactions between the effects of Geometric Decay and the effects of the Local Geometric Stress Riser.

3) Generic Multi-Site Damage 2024-T3 splice element tests. The splice elements are pre-corroded using a procedure developed by the NRCC to produce corrosion in the joint that is representative of service corrosion. In addition to the Geometric Decay and development of Local Geometric Stress Modifiers, there is build up of corrosion byproducts in the joint leading to Pillowing. Prior to testing the amount of pillowing is measured and the joint is inspected with several different NDI methods. During the test, a record of the cracking and subsequent growth is made. After the test is complete, the joint is disassembled for detailed fractography, thickness measurements and profilometry. These data will be used to refine the Pillowing model in ECLIPSE™.

NRCC is also performing the following modeling activities:

1) Supporting the modeling of fuselage splices by supplying stress data for corroded and non-corroded splices on some aircraft. The data will include pre-stresses caused by the riveting process, friction effects, and corrosion pillowing. As far as possible, the data will be supplied in parametric/generic form covering a variety of splice geometry and corrosion severity.

2) Developing an analytical model of crack nucleation and growth in the presence of exfoliation. This is being developed in a program separate from CFSD. However, the model will be validated under CFSD with fatigue testing of coupons containing exfoliation machined from aircraft wing skins. The model will also be integrated into ECLIPSE™ during CFSD.

At the same time, work is being performed in collaboration with SAIC, AP/ES Inc. and Lockheed Martin to develop relationships between the corrosion metrics used for modeling and the measurement capabilities of current and future field NDI technologies. All corroded specimens are subjected to various NDI by NRCC and SAIC. The NDI measurements of corrosion damage will be compared with the high-resolution measurements made by NRCC after the specimens are dismantled. This information will be analyzed to determine the corrosion metrics to be inferred from each NDI technology. These metrics will then be correlated statistically with the actual corrosion damage topography used in modeling. This will enable the current state of a structure to be more readily determined when there is corrosion present.

9.6.7.2 Corrosion Fatigue Damage Management
Dr. D.T. Peeler, Air Force Research Laboratory

Concurrent management of corrosion and fatigue damage ("Anticipate & Manage") requires significant development of tools and data beyond those in CFSD. Existing tools and data used to support corrosion prevention and control ("Find & Fix") are not sufficient to support concurrent management of corrosion and fatigue. Corrosion severity has not been tied to its impact on structural integrity, or its likelihood of occurrence. Instead, corrosion severity has been classified in relative terms. Developments in corrosion science and engineering, as well as laboratory capabilities, make it now possible to construct the tools and data needed for comprehensive corrosion fatigue damage management.

Comprehensive corrosion fatigue damage management requires integration of new prevention, assessment and management technologies into the Force Structural Maintenance Plan (FSMP) and supporting tools. Figure 97 shows examples of each of these technologies that must be integrated into the FSMP of the "Anticipate & Manage" scheme. A multidiscipline technical team was formed to demonstrate the feasibility of integrating the necessary technologies into an analytical tool to assess and manage the structural impact of corrosion and fatigue on specific critical aircraft structure. The ability to anticipate and manage corrosion fatigue damage was successfully demonstrated on a 1x1 KC-135 lap joint.

A schematic of the integrated computer code developed for the feasibility demonstration with the important algorithms and their relationships identified is presented in Figure 98. The structural integrity module is ECLIPSE™; the cost module uses the cost of corrosion database described earlier. The key algorithms in this program are being refined as the application of the code is extended to wing structure, critical attachments and empennage structure. The integrated code provides a framework with sufficient flexibility to incorporate improvements in each of the key algorithms as this effort progresses.

The enhanced capabilities afforded by the proposed "Anticipate & Manage" scheme for corrosion fatigue and the integrated analysis tool are best illustrated by comparing the differences in the maintenance process when an aircraft is inducted into PDM as depicted schematically in Figure 99. The "Anticipate & Manage" side appears to be more complex, but this just reflects the availability of more maintenance options as a result of introducing new technologies. Corrosion inspections move from general visual inspection of the entire airframe for corrosion to focused inspections for both corrosion and fatigue based upon historical knowledge of corrosion and fatigue susceptible structure, and an understanding of the difference between superficial, cosmetic damage and structurally significant degradation. Time spent finding corrosion and fatigue will focus on areas of structural significance and NDI capabilities will be directed towards finding the damage feature(s) that characterize the damage and its criticality to the structure in that location/component. The "Damage Assessed" box represents the ability to use the NDI data to support a structural assessment of the current condition, both for residual strength and remaining life. In addition, the current structural state will be projected forward to a future state for a selected interval of time (*e.g.*, a PDM interval) as a result of anticipated environmental exposure and flight hours. Maintenance decisions can then be optimized for time, cost, longevity, risk, etc., expanding "repair" options. New data management tools will archive (corrosion and fatigue damage mapping), retrieve and manipulate sequential NDI assessments of damaged and repaired structure, so that the historical record can be used to support future repair decisions and refine elements of the analytical tools with actual service data. Finally, the tools will enable the effects of unfound corrosion and fatigue on residual strength and durability to be assessed, making possible more informed decisions regarding the need for additional inspections that may impact flow days.

9.7. Joints

9.7.1 Fatigue Analyses of Riveted Lap-Joints Under Severe Environment

J.C. Newman, Jr., R.S. Piascik and C.E. Harris, NASA Langley Research Center

A series of tests were conducted by Furuta, Terada and Sashikuma [1] to study the fatigue behavior of countersink riveted lap-joint panels exposed to laboratory air or to a corrosive salt water environment. Figure 100 shows the configuration of the four types of 2024-T3 (Alclad) panels tested: Type 1 - two rivet row, Type 2 - three rivet row, Type 3 – three rivet row with thin-straight tear straps, and Type 4 – three rivet row with non-uniform thickness tear straps. Testing was conducted at constant amplitude loading which simulated the fuselage skin stress. Tests were conducted under ambient (laboratory air and room temperature) conditions and under a corrosive environment. For the corrosive environment, the lap-joint panels were immersed in circulating 3.5% NaCl solution.

The objective of this work [2] was to apply “small-crack theory” and small-crack-growth-rate data under the various environments to calculate the fatigue life of the lap-joint panels. The remote stress due to rivet load (S_p), by-pass stress (S_b) and remote bending stresses (S_M) were used in the life analyses of Furuta’s panels. The riveted joint was assumed to be a neat-fit joint and an interference level was not used in the calculations. The two-rivet row (Type 1) had a 50% rivet and by-pass stress; whereas, the three-rivet row (Types 2-4) had 37% rivet stress and 63% by-pass stress. Only Type 1 panel was considered with and without bending. Schijve’s [3] rivet-rotation correction bending equations were used to estimate the bending stresses.

Figure 101 shows that the fatigue life of Type 1 panels exposed to salt water (square symbols) is about 1/3 of the fatigue life in ambient laboratory air (circle symbols). The FASTRAN predictions, for salt-water (dashed curve) and laboratory-air (solid curve) environments agreed well with the experimental results. Here, the fracture mechanics based calculations assumed a corner crack in a neat-fit riveted-loaded straight shank hole (rivet clamp-up and interference-fit stresses were assumed to be small). The 6 μm radius equivalent-initial-flaw-size (EIFS) used for each FASTRAN calculation is consistent with laboratory observations; 6 μm radius constituent particles and corrosion pits are observed at small-crack initiation sites in fatigue test coupons exposed to laboratory air and salt water.

The excellent agreement between these tests and the calculations were somewhat surprising because the riveted lap-joint configurations were expected to have clamp-up and interference-fit stresses. Also, manufacturing defects in these joints were expected to be much larger than 6 μm, such as those observed (50 to 100 μm) on an actual fuselage joint [2]. It could be that using a smaller flaw size (EIFS) and neglecting the clamp-up and interference-fit stresses compensated each other in the final results. Further study is required to measure flaw sizes in the range of 6 to 200 μm on riveted lap-splice joints to resolve these issues.

REFERENCES

[1] Furuta, S., Terada, H. and Sashikuma, H., “Fatigue Strength of Fuselage Joint Structures under Ambient and Corrosive Environment,” *ICAF 97 – Fatigue in New and Ageing Aircraft*, EMAS, Ltd., West Midlands, UK, 1997, pp. 231-249.

[2] Harris, C. E., Piascik, R. S. and Newman, J. C., Jr., “A Practical Engineering Approach to Predicting Fatigue Crack Growth in Riveted Lap Joints,” NASA/TM-2000-210106, May 2000.

[3] Schijve, J., “Some Elementary Calculations on Secondary Bending in Simple Lap Joints,” NLR TR 72036U, 1972.

[4] Newman, J. C., Jr. Harris, C. E., James, M. A. and Shivakumar, K. N., “Fatigue-Life Prediction of Riveted Lap Joints using Small-Crack Theory,” *ICAF 97 – Fatigue in New and Ageing Aircraft*, EMAS, Ltd., West Midlands, UK, 1997, pp. 523-552.

9.7.2 Fatigue Evaluation of Machine Riveted Body Longitudinal Joints
Tom Sovar, Gulfstream Aerospace (Formerly of Boeing)

The durability analysis system used for Boeing Commercial Transports makes a distinction between which side of the riveted detail will tend to be fatigue critical based on the specific application. Twenty-four fastener, three row, single shear lap joints were fatigue tested to evaluate the benefits of precision controlled machine riveting compared to hand riveting using fine grain 2017 alloy rivets. Additionally, the orientation of the rivets was changed to control the critical location of the joint with respect to the non-countersunk head side or the countersunk head side, shown schematically in Figure 102. The hole tolerance range was also evaluated. Finally, the method used for fatigue testing small-scale lap joints was validated. This testing method required that the test specimens be fatigue loaded in an unrestrained condition as shown in Figure 103. However, the edge fasteners of the test panels were to be slightly over-driven compared to the rest of the rivets in the same row and the joint was to be clamped tightly, as shown in Figure 104, to prevent edge cracking. This latter practice is a modification of a technique used by Mueller [1].

Precision controlled machine riveting of body structure can provide a tremendous improvement in fatigue life, when compared to hand installation. This must be qualified by stating that this is only true if the machine riveting process incorporates significant support of the riveted skins during the drilling operation so that the formation of burrs is minimized. Also, the resultant holes are more consistent, and held to a tighter tolerance due to the lack of skin deformation as the holes are drilled. Other critical characteristics include optimum drill feed and speed, and finally more consistent squeezing of the rivet. For these coupons, overdriving to a non-countersunk button size of 1.4D or 1.5D improved the countersunk head locations more than the non-countersunk button locations. This is likely due to the increased uniformity of hole fill on the countersunk side of the riveted joint. The standard hole tolerance ranges tested did not demonstrate a significant difference in fatigue response.

Both overdriving and properly installed edge blocks are required to prevent cracking from occurring first at the edge rivets. Simply using tape to shim any small gaps and tightly torquing small C-clamps (by hand) can be the difference between getting, or not getting, cracks that occur at the edge first.

REFERENCE

[1] Mueller, R.P.G., “An Experimental and Analytical Investigation on the Fatigue Behavior of Fuselage Riveted Lap Joints,” Delft University, 1995, page 258.

9.7.3 Crack Growth and Residual Strength Testing of Large Panels with Z-section Stiffeners
Suzanne Masterson, Boeing

Fastener shear transfer capability, FSTC, below a certain limit begins to impact the residual strength of a built-up panel. As FSTC gets lower, a threshold is reached at which the fasteners local to the skin crack fail before the skin or stringers, reducing the amount of load that results in total panel failure.

Two built-up panels representing lower wing skin to Z-stringer connections were tested to determine whether the currently used threshold of FSTC was too high. Skin and stringer material and dimensions were identical for both panels, except one was fastened using 7/16 inch rivets and one with 3/8 inch rivets. A failed panel is shown in Figure 105. Each panel was initially damaged by a saw cut through the central stringer and attached skin midway between fasteners. The first panel was cut to 2 inches, and crack growth data was taken during constant amplitude cycling until the crack had reached 2 stringer bays in length. The predicted and actual crack growth matched very well as shown in Figure 106. The second panel was cut to 7.5 inch and cycled to a length of 2 stringer bays with no crack growth data taken.

The panel with 3/8 inch rivets, which fell below the FSTC threshold, failed under a tension load of 1447 kips. The panel with 7/16 inch rivets, which was slightly above the FSTC threshold, failed at 1664 kips, 15% greater than the first panel failure load. The failure prediction for both panels using standard prediction methods was 1559 kips. The residual strength of the panel below the FSTC threshold can be better predicted by treating it as a skin panel with no attached structure. This gives a prediction of 1460 kips, which is only 2% higher than the test result.

9.7.4 Effect of Bolt Type, Splice Thickness, and Percent Coldwork on High Load Transfer Joints

Helen Chapman, Boeing

A test program is underway to evaluate the fatigue performance of lower side-of-body joints. A typical joint is shown in Figure 107. The following conditions are being evaluated as part of the test program: effect of percentage hole coldwork expansion, tee-chord thickness, and bolt torque.

A high load transfer test coupon, Figure 108, was designed to simulate the joint. Phase 1 of the test program determined that changing the bolt type from titanium to steel and thus increasing bolt torque by a factor of nearly 2.0, increased the life by nearly 70 percent. Phase 2 of the test program focused on the effect of percent hole coldwork expansion on life. Three percent nominal coldwork expansion, using the split-sleeve process, improved the life by approximately 35 percent. Phase 3 explored the effect of increasing the tee-chord thickness while keeping the applied loading the same. Initial results suggest that increasing tee-chord thickness by roughly a third increases the life by about 20 percent, but further evaluation is still underway.

9.7.5 Full-Scale Aircraft Structural Test Evaluation and Research (FASTER) Facility

Dr. John G. Bakuckas, FAA, AAR-431, (609) 485-4784

The Full-Scale Aircraft Structural Test Evaluation and Research (FASTER) facility, Figure 109, located at the Federal Aviation Administration (FAA) William J. Hughes Technical Center, is capable of testing full-scale fuselage panel specimens under conditions representative of those experienced by an aircraft in actual operation. The FASTER test fixture features a unique adaptation of mechanical, fluid, and electronic components and is capable of applying internal pressurization and longitudinal, hoop, frame, and shear loads to a curved panel. As shown in the exploded view on the right, the fixture consists of a base structure, a hoop load assembly, a longitudinal load assembly, a pressure box, a frame load assembly, and a shear fixture assembly. The FASTER facility also includes a computerized instrument control and data acquisition system.

Loads can be applied dynamically or statically. The hoop and longitudinal stresses are simulated by the controlled application of distributed loads around the perimeter of the test panel. An innovative shear load application system was developed that uses two load distribution points in the longitudinal direction at the edges of the specimen. The force is applied as a couple and is reacted by a couple in the hoop direction which creates a close approximation to uniform shear distribution in both the applied and reacted couples.

All forces are generated using water and air as the fluid medium. The external loads are generated by applying water pressure to bladder type actuators, which are controlled by pressure activated dome valves. The dome valves are automatically controlled by electro/pneumatic (E/P) control valves. The E/P valves are driven by a computer control system in a closed-loop configuration. The operator can control the loads, speed, and type of test. Data from strain transducers, load transducers, pressure transducers, etc., are displayed on color monitors in real time and stored for off-line analysis.

Acceptance testing was conducted to verify that the FASTER test fixture met the specified design and operational requirements. Each of the load assemblies was loaded to the full-scale levels to demonstrate that the fixture could sustain the appropriate design limits. Both quasi-static and durability loadings were conducted using water and air to pressurize the panel. For the durability test, the system had to demonstrate that a complex loading spectrum could be applied at a frequency of 0.2 Hz for a continuous 12-hour period.

A panel with a radius of 66" and a skin thickness of 0.05" was used in the acceptance test. The panel was cut from the fuselage of a narrow-body aircraft and contains six frames (labeled F1 through F6) and seven stringers (labeled L3 through L9) shown in Figure 110. The panel contained a longitudinal lap splice located along stringer L7. The panel was instrumented with 50 strain gages on the fuselage skin, frames, and stringers.

The test fixture met all of the design and operational requirements. During the test, in general, a uniform strain distribution was measured in the middle of the panel, i.e., away from the edge of the panel by a minimum of one stringer or frame spacing, the effect of the panel boundary was no longer seen in the strain distribution. In addition, strain measurements were highly repeatable. Representative results are shown below. The hoop strain measured in the center of the panel is plotted as a function of load step. As shown in Figure 111, measurements from each of the tests were nearly identical for each test.

9.8. Testing

9.8.1 Aft Pressure Bulkhead Test (See Section 9.8.2, also)
Dr. Xiaogong Lee, FAA, AAR-431, (609) 485-6967

A full-scale test of an actual aft pressure bulkhead was conducted at the US Air Force Research Laboratory, Wright Paterson Air Force Base (WPAFB), in Dayton, Ohio, under funding by the FAA.

The objective of this test was to generate widespread fatigue damage (WFD) test data on a realistic structure to verify NASA- and FAA- developed prediction models. The specimen, about 10 feet long with an enclosed volume of about 2000 ft^3, was the aft section of a retired DC-9-30 fuselage, no. 48. Before being retired, the airplane had 57,757 landings with approximately 60,583 flight hours. The skin is 0.04 inch thick made of aluminum (AL 2014-T6).

The test article, shown in Figure 112, was attached horizontally to a strong back at its forward end. A 10.5-inch saw-cut crack was introduced along the end row of fastener holes in the dome skin to fuselage T-attachment, Figure 113. In addition, thirty-one 0.05-inch small cracks were introduced ahead of each lead crack tip. Figure 113 also shows the strain gauges that were installed in front of the crack tips to monitor the strain and stress levels before the final failure.

The test was successfully completed in April 2000. The specimen failed at 9 psi due to a fast fracture. A fractographic study of the test is underway, but the fracture surface appears to be dominated by Mode I cracking.
The finite element method was used to model the bulkhead and predict its residual strength. The public domain shell finite element code, STAGS, was used with the crack-tip-opening angle (CTOA) crack growth criterion as implemented in the STAGS code. The predicted results are plotted in Figure 114 showing the predicted failure at 9.34 psi, which is within 4% of the actual test results.

9.8.2 DC-9 Aft Pressure Bulkhead Residual Strength Test (See Section 9.8.1, also)
Capt Dan Schrage, Air Force Research Laboratory

This test report presents the background, set-up and test results of the DC-9 Aft Pressure Bulkhead Residual Strength Test. The purpose of the test was to validate the analytical methods of determining Widespread Fatigue Damage (WFD) and Multiple Site Damage (MSD) effects on the residual strength of a complex aft pressure bulkhead structure.

The test article was approximately the aft 10 feet of a DC9 fuselage incorporating the aft pressure bulkhead (Figure 115). This particular aircraft had 57,757 landings and 60,583 flight hours. When mounted on a fixture plate, the enclosed volume was approximately 700 ft^3. The test article preparation by Boeing included a) cutting the fuselage section to a manageable size, b) installing a structure forward of the bulkhead to facilitate mounting the test article and c) creating the MSD and lead crack in the pressure web (Figure 116). AFRL/VAS at Building 65, WPAFB received the prepared test article and mounted it to a fixture plate fabricated locally. Government technicians installed all instrumentation and completed the mechanical, electrical and pneumatic systems installations as required.

The primary data to gather from the test were the strains at a variety of locations on the bulkhead pressure web. They were placed in various locations away from the MSD to validate global finite element models generated by Boeing Long Beach, as well as between the rivets manufactured with MSD. From this strain data, the following information about the aft pressure bulkhead would be derived; the residual strength, the stress distribution around the lead crack, the growth rate of the lead crack, and the stress level at link-up of crack between fastener hole.

9.8.3 Longitudinal Test of a B737 Fuselage Section
Gary Frings, FAA, AAR-431, (609) 485-5781

In June 1999, the final FAA technical report *Longitudinal Acceleration Tests of Overhead Luggage Bins and Auxiliary Fuel Tank in a Transport Airplane Airframe Section*, DOT/FAA/AR-99/4, was published. This report documents the results of three separate longitudinal accelerations of a B737 fuselage section with overhead bins and auxiliary fuel tanks onboard. The fuselage section, shown in the photograph in Figure 117, was nominally accelerated to 6, 9, and 16 g's. At the 6 g level the auxiliary fuel tank broke free of the airframe and was not used in subsequent tests but both bins remained attached. At the 9 g level both bins remained attached to the fuselage. At the 16g level one of the bins separated from the airframe section. These and other results documented in the final report will aid FAA certification engineers in reviewing the certification requirements for overhead bins and auxiliary fuel tanks.

9.8.4 Longitudinal Acceleration Test of a B737 Fuselage Section
Gary Frings, FAA, AAR-431, (609) 485-5781

The FAA technical report "Longitudinal Acceleration Test of Overhead Luggage Bins and Auxiliary Fuel Tank in a Transport Airplane Airframe Section, Part II," DOT/FAA/AR-99/4,II, provides detailed analysis data of the results of three separate longitudinal accelerations of the Boeing 737 Model 200 fuselage section shown in Figure 118. These tests were documented in the FAA technical report DOT/FAA/AR-99/4 published in June 1999.

The transport airframe section was configured with a 120-inch overhead stowage bin attached to the left/pilot side, a 60-inch overhead stowage bin attached to the right/copilot side, and a 500-gallon auxiliary fuel tank attached underneath the airframe's passenger floor section. The fuselage section was accelerated to 6, 9, and 16 g's. During the 6-g test, a peak acceleration of 6.1 g's was reached with a velocity of 23 ft/sec. During the 6-g test, the auxiliary fuel tank broke free of its mounting and was not used in subsequent tests. The 9-g test saw a peak acceleration of 8.2 g's with a velocity of 32.2 ft/sec. The 16-g test reached a peak acceleration of 14.2 g's with a velocity of 41.7 ft/sec. Both bins remained attached to the fuselage during the 6- and 9-g tests. However, during the 16-g test, the 60-inch bin remained attached but the 120-inch bin detached from the fuselage. A load comparison between the static and dynamic 6-g tests is provided in the report. The results documented in the report will aid FAA certification engineers in reviewing the certification requirements for overhead stowage bins and auxiliary fuel tanks.

9.8.5 757-800 Fuselage Fatigue Test
John E. Goethe, Boeing

A 737-800 fuselage was subjected to durability testing for two lifetimes (150,000 cycles) followed by crack growth and damage tolerance testing in Everett, Washington. The test was accomplished to validate the fuselage structure for all models in the new 737 family (i.e. 737-600/700/800/900). Planning activities began during the summer of 1996 and testing was completed in June 2000. Structure teardown investigations are in progress during the first quarter of 2001.

The primary purpose of the 737-800 Fuselage Fatigue Test during the first two lifetimes was to identify potential fuselage fatigue design and production issues in advance of the fleet. The objective of the crack growth and damage tolerance testing was to investigate the threshold at which wide spread fatigue damage might occur and to demonstrate that damage was detectable by visual and non-destructive inspection methods.

The test article was a structurally complete fuselage. Structure outside of the scope of testing was omitted from the test article. The general test setup is shown in Figure 119. A variable amplitude flight load spectrum was applied to the fuselage in a cyclic manner. Each flight contained simulated loads for taxi, takeoff, climb, cruise, descent, landing and return taxi. Test loads were derived from the 737-800 short flight fatigue mission. These loads were applied to the fuselage through a series of load fittings (Figure 120) to simulate body shear and bending. Cabin pressurization was provided by an air system (Figure 121). Gear and empennage loads were also applied.

The fatigue test demonstrated that the fuselage structure for the new 737 airplanes is well designed and durable. The test has resulted in hard evidence that the structure will be trouble free and that the inspection programs to maintain airplane safety have been validated.

9.8.6 Remote Controlled Crack Monitoring (RCCM) System
Dr. John G. Bakuckas, FAA, AAR-431, (609) 485-4784

In support of the Federal Aviation Administrations (FAA) National Aging Aircraft Research Program (NAARP), the Full-Scale Aircraft Structural Test Evaluation and Research (FASTER) facility was established at the FAA William J. Hughes Technical Center for testing fuselage panels under conditions representative of those experienced by an aircraft in actual operation. The FASTER facility, shown in figure 122, is used to generate data to support and validate analytical models being developed under the sponsorship of the FAA to assess aging aircraft with multiple-cracking scenarios, Figure 122. A key component of the FASTER facility is the Remote Controlled Crack Monitoring (RCCM) system developed to track and record the formation and growth of cracks in real time during a test. The RCCM system was upgraded to measure multiple crack lengths.

The RCCM, Figure 123, system is a stand alone, computer-based video data acquisition system capable of monitoring the entire fuselage panel test surface at several levels of magnification with a field of view ranging from 0.05" up to 14". The system consists of cameras mounted to two computer remote controlled, high precision x-y-z translation stages as shown below. The cameras on each stage are used to monitor formation and growth of a crack. Two black and white RS-170 format analog cameras are mounted on each stage. A high magnification zoom lens (narrow-field-of-view (NFOV) lens) is attached to the first camera and provides a field of view ranging from 0.05" to 0.5". A zoom lens (wide-field-of-view (WFOV) lens) is attached to the second camera and provides a field of view ranging from 2" to 14".

Video data acquisition and reduction software provides real-time crack length measurement capabilities from the cameras on each stage with a 0.0001" resolution. Up to 360 of the 768- by 493- pixel digital images can be captured continuously and stored in bitmap format at a rate up to 30 frames per second. The software can playback the stored images. In addition, direct hook-up to monitors and video control recording (VCR) equipment is provided for continuous real-time monitoring and recording.

Digital images taken from the RCCM system were used to measure crack growth from a crack located in the outer critical rivet row in a longitudinal lap joint in a fuselage panel. As shown in Figure 124, the crack grew from the notch in a co-linear manner. This data verified predictive models developed by the FAA to assess cracking in fuselage structure.

9.8.7 Response Testing at the National Airport Pavement Test Facility (NAPTF)
Dr. Gordon Hayhoe, FAA, AAR-410, (609) 485-8555

The FAA conducted the first set of full-scale pavement tests in August-September 1999 at the National Airport Pavement Test Facility. The FAA worked closely with the Boeing Company in planning and executing these tests. These pavement response tests subjected the nine test pavements to slow-moving rolling loads simulating aircraft landing gears. The test vehicle, Figure 125, simulated different types of landing gears ranging from simple dual (two-wheel) gears to more complex B-777 landing gears (six wheels). Instruments embedded in the pavement structure automatically recorded the responses to the load as the test vehicle traveled along the test pavement. Among other results, the data collected in these experiments will lead to a better understanding of how multiple wheels in large aircraft gears interact with each other at different levels of the pavement structure.

9.8.8 National Airport Pavement Test Facility (NAPTF) Dedication
Dr. Satish Agrawal, FAA, AAR-410, (609) 485-6686

The FAA completed construction of its new National Airport Pavement Test Facility (NAPTF) in FY99 and dedicated the facility on April 12, 1999, Figure 126. As part of a Cooperative Research and Development Agreement (CRDA) between Boeing Co. and the FAA, Boeing provided one-third of the total $21 million construction cost. The NAPTF is designed to provide high quality, accelerated test data from rigid and flexible pavements subjected to simulated aircraft traffic. The major features of the NAPTF are:

- Fully enclosed instrumented test track, 900 feet long by 60 feet wide.
- Computerized data acquisition system.
- Rail-based, electrically powered test vehicle capable of simulating aircraft weighing up to 1.3 million pounds.
- Twelve test wheels capable of being configured to represent two complete aircraft landing gear trucks having one to six wheels per truck.
- Wheel loads independently adjustable up to 75,000 pounds per wheel.
- Controlled aircraft wander simulation.

9.8.9 Development of a Fire Test Method and Criteria for Thermal Acoustical Insulation Resistance to In-Flight Fire

Timothy Marker, FAA, AAR-421, (609) 485-6469

Fiberglass bat-type insulation is used extensively throughout the fuselage of commercial aircraft. It serves two main purposes thermal and acoustical suppression. Fiberglass batting, using a very small fiber diameter, is a highly efficient thermal barrier and acoustic attenuator. Typically, the insulation blankets consist of fiberglass batting encapsulated in plastic moisture barrier film coverings. Film covering materials have consisted predominantly of polyethylene terephthalate (PET), polyvinyl fluoride (PVF), and to a lesser degree, polyimide.

Currently, a vertical Bunsen burner test is the only FAA requirement for all thermal acoustic insulation materials, including those used to insulate ductwork beneath floors, behind the sidewall, and in the cheek areas. Although these materials are required to meet this flammability test, some have been found to propagate fire under certain conditions. Several fire incidents/accidents between 1993 and 1995 focused attention on the flammability of the insulation materials. Following this, a series of tests were run which exposed the inability of the vertical Bunsen burner test method at discriminating between materials that allow flame propagation and materials that do not. A test originally developed by the aircraft manufacturers, involving the placement of flaming cotton swabs on the film surface, was evaluated and seemed to provide a more realistic assessment of the material performance [reference DOT/FAA/AR-97/58, Evaluation of Fire Test Methods for Aircraft Thermal Acoustical Insulation]. However, large-scale tests and in-service experience indicated that the cotton swab test was not severe enough, so research continued on the development of a more realistic test. After conducting a variety of mock-up tests in small-, intermediate-, and full-scale test rigs, the flame characteristics of the very thin film coverings were more fully understood, and a decision was made to use a radiant panel test apparatus for determining the fire resistance of insulation blankets.

The radiant panel test apparatus that has been proposed for evaluating the flammability of insulation blankets is shown in Figure 127. This test equipment was originally used for measuring the critical radiant flux of horizontally mounted floor-covering systems according to ASTM E648, which exposed a test sample to a flaming ignition source in a graded radiant heat energy environment. The critical radiant heat flux can be described as the heat flux level below which flame spread will not occur. This test has been adapted for evaluation of the flammability of thermal acoustical insulation covering films, as it offers the possibility of recording flame propagation velocity, the time of ignition, and the burn length at different heat fluxes. The test also provides the level of incident radiant heat energy on the covering film at the most distant flameout point, which is the critical heat flux measurement, in Btu/ft^{2}sec (kW/m^2). On August 12, 1999, the FAA issued an Airworthiness Directive requiring the replacement of metalized PET insulation blankets with materials shown compliant with the radiant panel test adopted by the FAA for evaluating the flammability performance of thermal acoustic insulation materials.

Prior to testing, the radiant panel was calibrated to determine the heat flux as a function of distance from the point of initiation of flaming ignition. This is referred to as the flux profile. The heat flux was measured using a 0 to 10-mV range heat flux transducer at 10 positions along the horizontal incident surface at a distance of 2 inches between each position (Figure 128).

During the FAA's evaluation of the radiant panel test, a number of aircraft films were tested. The initial results in terms of burn length and critical heat flux are shown in Figure 129. Overall, the results were consistent with what was observed during the mock-up intermediate- and full-scale fire tests. In addition, physical effects such as melting, contraction, and the behavior of the reinforcing scrim, which play an important role in the flammability of the thin films, can be readily observed and better understood. Finally, the test appears to be repeatable, which is an important consideration when the output is a proposed requirement.

A finalized test procedure has been adopted. During the test, a 10-inch wide by 40-inch long sample is clamped to a sliding platform with test samples typically consisting of two layers of fiberglass batting with film covering. After the temperatures within the test chamber stabilize, the sample is inserted into the test chamber via the sliding platform, and the chamber door is closed. Simultaneously, the pilot burner flame is brought into contact with the specimen. A burn length of less than a 2-inch radius is the proposed acceptance criteria. In effect, the proposed criteria prevents ignition under the specified in-flight fire exposure condition. This test method will also be included in a planned Notice of Proposed Rulemaking (NPRM), expected to be issued in the early part of 2000, which specifies new stringent flammability criteria for insulation blankets.

9.8.10 Development of a Fire Test Method and Criteria for Thermal Acoustical Insulation Burnthrough Resistance
Timothy Marker, FAA, AAR-422, (609) 485-6469

Fuselage burnthrough refers to the penetration of an external postcrash fuel fire into an aircraft cabin. The time to burnthrough is critical because, in survivable aircraft accidents accompanied by fire, ignition of the cabin materials may be caused by burnthrough from burning jet fuel external to the aircraft. Thermal acoustical insulation, typically comprised of fiberglass batting encased in either a polyvinyl fluoride (PVF) or polyester terephthalate (PET) moisture barrier, can offer additional protection if the material is not physically dislodged from the fuselage structure.

Full-scale testing using surplus aircraft has confirmed the burnthrough sequence of events as a large external fire penetrates into an aircraft cabin. In addition, full-scale tests conducted in a fuselage test rig have also highlighted the effectiveness of alternate insulation materials at significantly delaying or preventing the penetration of an external fuel fire into an aircraft cabin [reference DOT/FAA/AR-98/52 Full-Scale Test Evaluation of Aircraft Fuel Fire Burnthrough Resistance Improvements]. By delaying the burnthrough event, passengers can be afforded additional time to evacuate an aircraft, thus reducing fatalities. For this reason, a standardized laboratory test method was developed for evaluating the burnthrough resistance of thermal acoustic insulation blankets. Over 50 laboratory-scale tests were conducted in various-sized test rigs in an effort to establish a repeatable test condition that was representative of the threat likely to occur from a large external fuel fire. During the testing, it was determined that the method of attaching the insulation to the test rig structure played a key role in the effectiveness of the insulation material. In addition, the composition of the insulation bagging material, normally a thermoplastic film, may also be an important factor.

The fire threat was replicated in the lab using an oil-fired burner situated adjacent to a sample holder. This burner equipment is currently in use for other FAA test methods, such as the seat-fire blocking test and the cargo liner flame penetration resistance test. The test sample holder is oriented 30^o with respect to vertical to better simulate the area of a fuselage that would likely be impacted during a postcrash fuel fire. The sample holder also incorporates three steel Z-frame vertical formers spaced 20 inches on center, typical of the construction used in large commercial aircraft fuselage. A total of six horizontal hat-shaped stringers were bolted into place as shown in Figure 130. This configuration allowed the installation of two between-frame blankets that could be tested for burnthrough resistance. The test burner is aimed at the center of the test frame (Figure 131). Two heat flux transducers are mounted on the cold side of the sample holder to monitor the amount of radiant and convective heat flux passing through the test sample. A pass/fail criteria of 2.0 Btu/ft^2 sec on either transducer has been established.

In order to develop a test condition that was most representative of full-scale conditions, several tests were performed using Alclad aluminum skin identical to that used in the full-scale tests. During full-scale tests, the Alclad material failed in approximately 55 seconds, which was the target for the lab-scale testing device. During the baseline trials, the burner fuel flowrate, intake air velocity, and position respective to the test frame were modified in order to obtain the appropriate condition (Table 3). By increasing the fuel flowrate to 6 gallons per hour and positioning the burner cone 4 inches from the sample holder frame, the proper 55-second burnthrough time was achieved. This condition produced a flame temperature and heat flux output of 1900^{o}F and 13.5 Btu/ft^{2} sec, respectively, measured at 4 inches from the burner cone exit plane.

After finalizing the fire exposure condition, trials were run using a combination of aluminum skin and thermal acoustic insulation. However, it became evident that the use of the aluminum skin created a cumbersome test, as it was difficult to quickly and realistically mount and remove the aluminum skin each time, so the configuration was simplified to involve the insulation materials only. Originally, to specify the burnthrough protection needed based on an analysis of past accidents, the pass/fail criteria was set at 5 minutes with the aluminum skin and insulation materials combination, but this was adjusted to 4 minutes in the absence of the skin. The realistic test configuration further highlighted the importance of attachment of the insulation. As it appeared, some current original equipment manufacturer (OEM) designs allowed for easy flame penetration along the seam area where the two between-frame blankets join along the vertical former. As a result, a standardized attachment system was used to prevent early failure along the center vertical former. Future guidance material will be developed to evaluate OEM insulation attachment designs in order to prevent these types of failures in service.
Additional tests were run using a variety of insulation materials, in which the results correlated well with previous full-scale tests using identical materials (see Figure 132). This test method has been incorporated into a planned Notice of Proposed Rulemaking (NPRM) for new insulation flammability requirements, which is expected to be released in the latter part of 1999.

9.9. Composites

9.9.1 Probabilistic Methodology for Composite Airframe Structures

Peter Shyprykevich, FAA, AAR-430, (609) 485-4967

To date, the design practice for composite aircraft structures has followed the traditional approach used for designing metallic airframes. In that approach, a safety factor of 1.5 is applied to the loads to account for any uncertainties in design and 'A' or 'B' basis material properties are used for strength to reflect material variability. Because of higher scatter in composite properties and the sensitivity of composite structures to environmental effects and impact damage, large knockdown factors are required to obtain positive margins of safety. This approach, in essence, reflects a "worst case scenario" at each design condition. In other words, knockdown factors for temperature, moisture, scatter, and loading are accumulated in a way that is not reflective of actual aircraft usage and results in a conservative design. A reliability-based design methodology has the potential to significantly reduce this weight penalty by considering probabilistic distributions of loads, strength, damage occurrences, and environment, and establishing reliability of the structure at a prescribed level consistent with safety requirements. Probabilistic design is the stochastic interaction between the strength variability of the structure and the expected variability of loads that stress the structure. A flow chart of the total design process is shown in Figure 133. Probability of failure occurs at the intersection of the operating stress and material strength probability density functions.

In 1993, the FAA initiated a study into probabilistic design methods with an ultimate goal of establishing the applicability of probabilistic design methods in the design and certification of civil aircraft. The study was completed in FY00 with the following results:

- making methodology accessible by developing a primer and software
- fying the level of conservatism in deterministic design approach
- increasing confidence in the probabilistic approach through application of the methodology
- understanding acceptable limits and usage of the methodology
- setting requirements for statistical data-bases
- establishing guidance for certification.

The work has been documented in the FAA Technical Reports *Development of Probabilistic Design Methodology for Composite Structures*, DOT/FAA/AR-95/17, *Probabilistic Design Methodology for Composite Structures*, DOT/FAA/AR-99/2 and a technical paper *Computer Methods in Composite Materials IV*, CADCOMP98. WTT Press Computational Mechanics Publication. In FY00, two software codes, MONTE and ProDeCompoS, which were developed previously to calculate the reliability of composite airframe structure, were evaluated as to their validity and usefulness. After validation, the software was used to perform sensitivity studies on key parameters and apply the design methodology to aircraft wing configuration of different aircraft classes to compare deterministic and probabilistic approaches.

As a probabilistic approach requires more data to implement, effort was also expended in data gathering and synthesis. A search of available United States and Russian aircraft in-service data was gathered (a sample for AN-124 is shown below) to obtain exceedance curves for damage occurrences versus size of damage for several types of damage. Other data that were obtained included damage size versus probability of detection for different nondestructive inspection techniques, effectiveness of repair, and residual strength versus damage type and size.

The methodology has been developed with sufficient confidence that the FAA can accept the probabilistic approach if offered in the certification process by the industry.

9.9.2 The Development and Use of a Common Database for Composite Materials

Peter Shyprykevich, FAA, AAR-430, (609) 485-4967

A major barrier to lowering the cost of using composite structural materials in commercial aviation has been the cost of certification. To a large extent, the high certification cost has been due to the need for individual manufacturers to develop extensive and costly data on mechanical and chemical properties of the composite materials selected in

aircraft construction. In the conventional approach, each company is required to develop a complete database; even if several companies desire to apply the same material to a number of components each company is required to develop the same database. Thus, the considerable effort involved in generating the database has to be duplicated several times.
The Advanced General Aviation Technology Experiments (AGATE) consortium, under sponsorship and participation of the FAA, developed a common database and guidelines for its generation and use for certification of small aircraft. Because the companies agreed to use a common material for each of their applications, only one database development was required. The cost of generating the database is then shared by the companies in the consortium, resulting in sizeable savings. The conventional and AGATE certification procedures are compared in Figure 134.

In the conventional approach shown on the left, individual companies are required to develop the total database. In the AGATE process shown on the right, the group of small aircraft companies making up the consortium agree to use a common material for each of their applications, therefore only one database development is needed. It is estimated that after the development of a common database, the certification cost of each company is reduced from $350,000 to $50,000, with a concurrent reduction in time to complete the development of the property base from as much as 24 months to as little as 6 months. The developed methodology may also be used by material suppliers to qualify a material system to be used by future customers.

The developed common database guidelines include types and number of mechanical tests, test methods, and environmental conditions. Methods to reduce the test data to the level of obtaining ‘A’ and/or ‘B’ basis values include statistical procedures that allow pooling across different environments for the same failure modes in order to increase sample sizes to estimate material variability. Either Weibull or normal distribution statistics can be used. For the normal distribution, knockdown factors from mean value to ‘A’ and ‘B’ basis lamina allowables were developed that are based on a large sample size for variability and a small sample size for the mean. The concept of establishing large sample (population) variability for particular failure modes has implications for the statistical significance of design allowables for notched and unnotched laminates where the test samples are historically small.

In order to utilize the database, each company must demonstrate that their processing of the identical composite material results in mechanical properties that are the same as in the database. Equivalency tests, along with statistical acceptance criteria, were developed that would perform that function. In addition, the developed acceptance criteria can be used by the manufacturing company to control the quality of future incoming materials.

The developed methodology, documented in the FAA Technical Report *Material Qualification and Equivalency for Polymer Matrix Composite Material Systems*, DOT/FAA/AR-00/47, resulted in the issuance of a policy by the Small Aircraft Directorate with an associated technical protocol. Advanced Materials Research Program personnel from the William J. Hughes Technical Center participated in a workshop that presented this new policy to industry and FAA certification personnel.

9.9.3 Damage Accumulation in Composite Structures Under Repeated Loads
Peter Shyprykevich, FAA, AAR-430, (609) 485-4967

Composite materials and the subsequent laminates and structures made from them behave differently from metals under repeated load (fatigue) regimes. For instance, low amplitude cyclic loads are damaging to metals while they are not damaging to composites, and although composites are less fatigue critical than metals, large amplitude cyclic loads can cause cracks, splits, and delaminations. Thus, there is a need to determine qualitatively which repeated loads cause damage in composites and to use that information to develop realistic and economical fatigue test protocols for the aircraft composite structure certification.

The main goal, a study done at the University of California at Los Angeles under an FAA grant, was to determine the effects of various loading parameters on damage growth as a function of strain level. The threshold strain levels below which fatigue damage does not accumulate were also defined so that low-strain cycles could be eliminated from a loading. As low-strain cycles are generally numerous, a great amount of testing time could potentially be saved if these cycles were eliminated.

In the study, a significant database was developed by testing carbon/epoxy specimens to simulate damage initiation sites commonly found in composite aircraft structures. Three damage types were tested: (1) unnotched laminates to simulate free edge damage, (2) laminates with center holes to represent notch stress risers, and (3) laminates containing barely visible impact damage. The test loading for the test program consisted of constant- amplitude fatigue with and without pre-load, low-high and high-low constant amplitude blocks, various stress ratios, and a transport wing spectrum with and without elimination of low loads.

The test data was analyzed and threshold strain levels were obtained for the three damage initiation sites. The threshold strain levels for damage initiation for open-holed specimens were determined from fatigue test data such as that plotted in the top of Figure 135. The plot shows that initiation of fiber splitting and its growth is a function of strain amplitude. When the data is replotted in terms of strain range (as shown in the bottom of Figure 135) except at high strain levels, that data collapsed into one area whether the fatigue cycling was tension-tension, compression-compression, or tension-compression. The conclusion that can be reached from these plots is that a minimum threshold strain can be established such that if it is not exceeded in real usage, damage will not grow around open holes. Similar results were obtained for unnotched and impact damaged specimens.

The threshold strain data from this study can serve as a guideline to determine the load levels that can be eliminated from spectrum loading. A comparison of damage growth in full and modified spectra indicated that the two lowest load levels of a typical wing load spectrum (which represent 98.7% of testing time) could be deleted without any significant influence on damage propagation and fatigue life. For the quasi-isotropic specimens tested, the threshold load levels for no damage growth correspond to a strain range of 0.2% and a maximum fatigue strain of 0.3% for both open-holed and impacted specimens. These research results showed that low-level fatigue cycles have no effect on damage accumulation and therefore can be eliminated from the test protocols, saving significant testing time.

9.9.4 Damage Tolerance of Stitched Composite Wing Structures

Dr. Dan Adams, University of Utah

Dr. Dan Adams is investigating the damage tolerance of stitched composite wing structures under quasi-static and fatigue loading. The objective of this study is to assess the increase in damage tolerance of composite structures by incorporating through-the-thickness stitching. Of particular interest is the use of stitching in the stiffener flange/wing skin junctions to suppress delamination growth. A finite element based modeling techniques has been developed to predict delamination growth behavior in stiffened composite structures that utilize stitching. Research is also being performed to evaluate the use of through-the-thickness stitching to increase the damage tolerance and energy absorption characteristics of composite sandwich structures.

9.9.5 Fatigue Damage and Compressive Residual Strength of a Woven PMC Subjected to Cyclic Hygrothermal Conditioning

M.G. Castelli and J.C. Thesken, Ohio Aerospace Institute, NASA Glenn Research Center

An experimental investigation was conducted to characterize the elevated temperature, fully reversed, fatigue response of a hygrothermally conditioned, carbon fiber reinforced epoxy composite. The material is a 5 harness satin weave in a high temperature epoxy matrix: AS4/PR500. Its response, elastic modulus and residual compressive strength, were recorded as a function of fatigue cycle. Baseline unconditioned material is compared to material exposed to 12 khrs of hygrothermal cycle (HC) mission conditioning. The HC mission was an 85 % nominal relative humidity at 30 °C (85RH/30 °C) exposure combined with a daily "mission cycle" consisting of a 90 minute exposure at 121 °C. The HC conditioning employed was selected to be representative of a static component in the propulsor region of a gas turbine engine. Results of the experimental effort included the development of a dogbone specimen geometry verified for fully reversed fatigue and compressive static tests without anti-buckling guides. Fully reversed fatigue data revealed a deterministic stress-life response (see Figure 136). The 12 khrs HC conditioned material experienced an 11% strength degradation when compared to baseline data prior to mechanical fatigue loading. Residual compressive strength measurements were made at specified degradation levels of modulus and are correlated with elastic modulus. As shown in Figure 137, this correlation showed a clear degradation in residual strength due to the HC conditioning. Work is underway to characterize material conditioned to 30 khrs.

ACKNOWLEDGEMENTS

The authors acknowledge Chris Burke for technical assistance in the laboratory, Rod Ellis for project guidance and oversight, and also Ron Cairo, Rajiv Naik, and Ken Tosi of Pratt & Whitney for numerous interactions on the project. The work was performed under the NASA cooperative research grant NCC3-821.

*Paper to appear in the *Proc. of the 10th Int. Conf. on Fracture,* Dec. 2-6, 2001, Hawaii.
**Author to whom correspondence should be addressed: j.c.thesken@grc.nasa.gov

9.10. Life Enhancement/Repair

9.10.1 A New Cold Working Process

Michael Landy, StressWave, Inc.

A new cold working process for improving the fatigue lives of holes in components and built-up metal structures has been developed by StressWave, Inc. of Kent, Washington. The patented process produces residual compressive stresses and fatigue performance comparable to, or better than, those produced by mandrel methods and is designed primarily for automated fastening and assembly environments. The StressWave process eliminates the need for close-tolerance starting holes and associated hole cutting tools, consumable split sleeves, split or solid mandrels, liquid lubricant cleanup and off-line processing steps. Automation and significantly lower processing cost will lead to a more usage of cold working and result in greater structural integrity. The benefits and associated cost savings satisfy many aspects of continuous improvement program initiatives.

The StressWave process treats individual components as well as built-up structure. It has been shown to effective in thin (1.6mm) 2024-T3 sheets and thick (25mm) stackups of 2000 series alloys resulting in minimum life improvement factors (treated life: non-treated life) of 3:1. As an example, S-N curves for treated and non-treated 6.35mm holes in a 4.8mm 2024-T3 aluminum sheet are shown in Figure 138. Stackups may be treated either with or without wet sealants. Testing in titanium open hole specimens has demonstrated better than 5:1 life improvement factors for the conditions tested.

The process works by treating the metal prior to drilling the hole into the structure using devices called indenters. This has the advantage of eliminating the close-tolerance starting holes (0.075mm range) and associated tooling and labor steps. The indenters are specially shaped to provide a large and controllable zone of residual compressive stress in the area surrounding the fastener hole as shown in Figure 139. The process works a large range of strain rates from quasi-static to highly dynamic. Compressive residual stresses are formed consistent with mandrel cold working.

In a typical automated production application, the indenters are positioned with initial touching contact concentric to the targeted hole position. One of a number of specially designed end effector devices shown in Figure 140 actuates the indenters to a prescribed depth into the surfaces of the part. The action of the opposing indenters creates dimples on each side of the material that are completely removed during the hole machining operation.

The process takes advantage of the near incompressible behavior of the material during yielding. During the indentation process the workpiece material flows radially away from the dimple as a result of the high degree of axial compression that occurs. The magnitude of the radial flow, for a given hole diameter, is similar to that produced by the mandrel cold working processes. However, the axial compression of the material minimizes the surface upset (the so called “volcano effect”) that is a limitation of the mandrel processes.

An important benefit of the StressWave process is that it does not use expendable sleeves, lubricants, or any of the related dimension-specific tools such as solid or split tapered mandrels and nosecaps. Elimination of the sleeve and/or split mandrel means that there are no longer axial ridges or discontinuities inside the hole.

One of the biggest potential benefits of StressWave is the elimination of off-line processing. Most mandrel cold working operations are performed off-line because of the difficulty in automating the basic processes. The simplicity of the StressWave process makes it perfectly suited for automation, and allows keeping major structural assemblies such as aircraft wings in the automated manufacturing cell instead of in an off-line pick-up station.

9.10.2 Laser Peening for Fretting Fatigue Resistance

A.H. Clauer and D.F. Lahrman, LSP Technologies, Inc.

Fretting fatigue tests were conducted on laser peened Ti-6Al-4V specimens in an Air Force SBIR Phase I program to assess the effects of laser peening on fretting fatigue resistance. The objective of the program was to evaluate laser peening as a treatment to increase the fretting fatigue resistance of dove tail slots in aircraft gas turbine engine disks, and of dove-tail attachments on blades. The tests were conducted on fatigue specimens machined from forged Ti-6Al-4V plate. The specimens were laser peened at LSP Technologies and tested at the Purdue University Fatigue Laboratory.

For the test, a dog-bone tensile fatigue specimen was contacted with Ti-6Al-4V pads on opposite sides of the laser peened gauge length as shown in Figure 141. The pads were machined from the same plate as the tensile specimen. The test enables both the cyclic load on the fatigue specimen and the contact load between the pads and the fatigue specimen to be controlled. Two laser peened specimens were tested. The results were compared to fretting fatigue results of the same material tested in the untreated condition available from other test programs.

The first test, LSP1, was tested at a stress amplitude of 48.6 ksi, R=0.5, and a nominal contact pressure of 55 ksi. This was a condition under which untreated specimens failed at about 10^5 cycles. The result, shown in Figure 142, was no failure after 10^6 cycles. The second test, LSP2, was then tested at a stress amplitude of 38.8 ksi, but R=0 and a contact pressure of nominally 75 ksi. This was a condition under which untreated specimens failed at about 20,000 cycles. This specimen also did not fail after 10^6 cycles. In Figure 142 these results are shown as the two runout points in the upper right corner, with LSP2 being the upper point. The other data points are fretting fatigue results using the same test on untreated material and the solid curve is the uniaxial fatigue curve for this material. The data are plotted vs. the equivalent stress, which accounts for both the cyclic stress on the fatigue specimen and the surface contact stresses from the pads to describe the localized stresses leading to fretting crack initiation and growth[1].

The surface of the wear scars was examined using scanning electron microscopy. Surface cracks were found only in LSP2, in the lower edge of the wear scar. This specimen had the highest contact stress. LSP2 was then sectioned through the wear scar and examined metallographically. The surface cracks had propagated only a short distance into the surface as shown in Figure 143. The longest crack, shown in Figure 143, extended only 70 to 80 μm into the surface after 10^6 cycles, a condition for which untreated specimens failed completely at about 20,000 cycles. LSP1 showed no surface cracking after 10^6 cycles, even though untreated specimens failed after about 100,000 cycles at the same test conditions.

The above results clearly show that the LaserPeen™ process is very effective in increasing the resistance to fretting fatigue failure. The first specimen tested demonstrated that a significant component of this increase is due to difficulty in initiating fatigue cracks by at least an order of magnitude in life. The second specimen tested supports this and also suggests that crack propagation is substantially inhibited.

Reference

[1] Murthy, H., Farris, T.N., and Slavik, D.C. "Fretting Fatigue of Ti-6Al-4V Subjected to Blade/Disk Contact Loading," Proceedings of Symposium on Developments in Fracture Mechanics for the New Century, Conference on Materials Science for the 21st Century to celebrate the 50th Anniversary of Japan Society of Materials Science, Osaka, May 2001, In-Press.

9.10.3 Fatigue Evaluation of Flap Peening

Irfan Rosidi, Boeing

Almen strips have been commonly used to measure the intensity of peening process. In the case of flap peening, the peening intensity at certain coverage depends on the flapper size and flapper RPM. Boeing has developed a chart of “Flapper RPM vs. Almen Intensity” for several flapper sizes at 100% visual coverage (see Figure 144). This will save time and money needed to do Almen test verification.

A test program is underway to evaluate the fatigue performance of new proposed flap peening procedure versus conventional shot peening, per BAC 5730, using notched (Kt=1.5) test specimens (see Figure 145). These specimens were fabricated out of 2324-T39 plate, 7075-T651 plate, Ti 6AL-4V (mill annealed) plate, 15-5PH (180-200 ksi) steel plate, and 4340M (275-300 ksi) steel plate. They will be fatigue cycled at a constant amplitude load that will give a fatigue life between 100,000 to 1,000,000 cycles.

9.10.4 Improved Method Being Developed for Surface Enhancement of Metallic Materials

T.P. Gabb, P.S. Prevey, J. Telesman, P. Kantzos and P. Bonacuse, NASA - Glenn Research Center

Surface enhancement methods induce a layer of beneficial residual compressive stress to improve the impact (FOD) resistance and fatigue life of metallic materials. Shot peening is a traditional method of surface enhancement, in which small steel spheres are repeatedly impinged on metallic surfaces. Shot peening is inexpensive and widely used, but the plastic deformation of 20 to 40 percent imparted by the impacts can be harmful. This plastic deformation can damage the microstructure and severely limit the ductility and durability of the material near the surface. It has also been shown to promote accelerated relaxation of the beneficial compressive residual stresses at elevated temperatures. Low-plasticity burnishing (LPB) is being developed as an improved method for the surface enhancement of metallic materials.

LPB is being investigated as a rapid, inexpensive surface enhancement method under the NASA Small Business Innovation Research program, with supporting characterization work performed at NASA. Previously, roller burnishing had been employed to refine surface finish. This concept was adopted and then optimized as a means of producing a layer of compressive stress of high magnitude and depth, with minimal plastic deformation (ref. 1). A simplified diagram of the developed process is given in Figure 146. A single pass of a smooth, free-rolling spherical ball under a normal force deforms the surface of the material in tension, creating a compressive layer of residual stress. The ball is supported in a fluid with sufficient pressure to lift the ball off the surface of the retaining spherical socket. The ball is only in mechanical contact with the surface of the material being burnished and is free to roll on the surface. This apparatus is designed to be mounted in the conventional lathes and vertical mills currently used to machine parts. The process has been successfully applied to nickel-base superalloys by a team from the NASA Glenn Research Center, Lambda Research, and METCUT Research, as supported by the NASA Small Business Innovation Research Phase I and II programs, the Ultrasafe program, and the Ultra-Efficient Engine Technology (UEET) Program.

A comparison of the residual stresses and plasticity produced by shot peening and LPB on the nickel-base alloy IN718 is shown in Figure 147. The residual stress and plasticity profiles were measured using x-ray diffraction peak shift and broadening after repeated removal of surface material by electropolishing. LPB clearly can produce deeper compressive residual stresses with much less plasticity (percent cold work) than shot peening. The high-cycle fatigue resistance of this alloy increases with the application of this LPB treatment. Shot peen and LPB-treated high-cycle fatigue specimens were exposed at 600 °C for 10 hours and then tested at room temperature. LPB-treated specimens had 2 to 5 times longer lives, even with surface scratches normal to the load axis to simulate foreign object damage. The shot-peened specimens failed at the scratches at lower fatigue lives. Crack-growth specimens were notched, precracked, and LPB treated. The notch was then machined away before crack growth testing at room temperature. The LPB treatment was highly effective, completely arresting crack growth into the material. This LPB process has been successfully applied to several nickel, titanium, and aluminum alloys (ref. 2) used in aerospace gas turbine engine and airframe applications. LPB has recently been shown to be surprisingly effective for treating corroded airframe materials after extended service, restoring fatigue lives to original (uncorroded) levels. LPB processing is now being extended to other alloys and applications.

References

[1] Prevey, P.S., et al.: FOD Resistance and Fatigue Crack Arrest in Low Plasticity Burnished IN718. Proceedings of the 5th National Turbine Engine High Cycle Fatigue Conference, Chandler, AZ, 2000.

[2] Prevey, P.S.; and Cammett, J.: Low Cost Corrosion Damage Mitigation and Improved Fatigue Performance of Low Plasticity Burnished 7076–T6. Proceedings of the 4th International Aircraft Corrosion Workshop, Solomons, MD, 2000.

9.10.5 Bushing Qualification

Mark Ofsthun, Leon Bakow and Antonio Rufin, Boeing

In a few specific single-pin joints, shrink-fit installed bushings have been found to be prone to shift ("migrate") under high loads or vibration (Figure 148). Although the bushings are trapped and movement is restricted, migration is a concern because it can lead to corrosion and possibly affect durability. In a shrink-fit installation, the bushing has an outer diameter that is initially slightly greater than the receiving hole diameter. The bushing is dipped in liquid nitrogen, allowing it to be inserted in the hole before the bushing warms back up to ambient temperature. At ambient temperature, the bushing is held in place by mechanical interference. Drawbacks of this process include the following:

- low interference levels (and hence, limited bushing retention capability),
- potentially scored holes - caused by having to press bushings that warm up prematurely during installation,
- moisture entrapment - due to the presence of condensation on the cold surface of the bushing during installation.

A recent study evaluated baseline shrink-fit bushing installations against the Fatigue Technology Incorporated (FTI) ForceMate™ system in terms of bushing retention (push-out force, torque, and resistance to vibration) and fatigue. With the FTI process, an initial clearance-fit bushing is expanded into the hole by pulling a tapered mandrel through it. This process is illustrated in Figure 149. ForceMate generates much higher bushing interference levels than shrink-fitting, resulting in greater bushing retention and, usually, improved fatigue life.

In this test program, 7150-T77511 aluminum extrusion and Ti-6Al-4V mill annealed titanium forging stock were used to make the test coupons. Three types of bushings were evaluated in the tests: single-piece, two-piece nested, and three-piece nested (Figure 150). Bushings were made from 15-5PH corrosion resistant steel and aluminum-nickel-bronze (Al-Ni-Br).

In the static push-out tests, the bushings were forced out using a cylindrical pin driven by a load frame actuator. For this portion of the tests, only one- and two-piece bushings were tested, as three-piece bushings were expected to perform similarly to two-piece bushings in terms of push-out capabilities. For single-piece installations in aluminum, the ForceMate-installed bushings produced a roughly six-fold increase in push-out force, regardless of bushing material. For the two-piece installations, the push-out forces roughly trebled with ForceMate.

The purpose of the static rotation (torque) tests was to compare the different bushing configurations and their ability to resist rotation. For these tests, the bushings were designed with a special flange capable of accommodating a torque wrench. Torque was applied to the bushings and the amount of torque required to cause the bushings to rotate was recorded. Only one- and two-piece bushings were tested. Three-piece bushings were again assumed to perform similarly to their two-piece counterparts. For single-piece Al-Ni-Br bushing installations in aluminum, ForceMate increased the torque by a factor of about 5.5. For the two-piece bushings, the increase was a factor of approximately 4.5 with Al-Ni-Br bushings, and just under 3.0 for 15-5PH bushings. With single-piece 15-5PH bushings in titanium, the torque for the ForceMate bushings was about four times greater than for shrink-fit bushings.

The vibration tests qualitatively evaluated bushing retention using a procedure sometimes employed to evaluate fastener stability in extreme vibratory environments. The test specimen consisted of a circular plate with four subscale bushings in it. The plate was subjected to repeated pounding at high frequency by a rivet gun operating at full force. When the test is used to evaluate blind fasteners, 20 minutes are considered to be an adequate demonstration of retention capability for structural use. In this instance, 15-5PH ForceMate installed bushings greatly outperformed shrink-fit bushings, enduring more than two hours of vibration. For the Al-Ni-Br bushings, however, the improvement was much smaller, but there was also less scatter with ForceMate.

The fatigue tests were performed under constant-amplitude loading using symmetrical two-lug fatigue coupons made from aluminum and titanium. The aluminum lugs were tested with all three bushing types and both aforementioned bushing materials. Expecting better fatigue lives out of the ForceMate installations, shot peening of the lug bores (currently required in production for this application in aluminum) was done on shrink fit bushed holes only. The titanium lugs were tested only with single-piece bushings, but with both bushing materials. No shot peening was required for the titanium lugs.

In the fatigue tests, ForceMate significantly outperformed shrink-fit bushing installations, without exception. In titanium, the lowest ranked ForceMate specimen produced a nearly four-fold increase in fatigue life over its shrink-fit counterpart. In aluminum, with a 24 percent higher maximum net stress, specimens with ForceMate bushings consistently outlasted coupons with shrink-fit bushings by factors of three or more.

In conclusion, the ForceMate process was subjected to a variety of tests to qualify it as a possible substitute for shrink fit bushings on a specific application where higher bushing retention was desired. In every test conducted, the ForceMate process demonstrated superior performance over shrink fit installations. Ancillary benefits of the ForceMate process for this application include relaxation of lug manufacturing tolerances and elimination of a number of manufacturing steps (including shot peening of aluminum lug bores), resulting in reductions of labor costs and manufacturing flow time.

9.10.6 Effects of Cold Expansion Processes on Damage Tolerance

Len Reid, Fatigue Technology Inc.

Recent tests have been performed to evaluate the effects of FTI's cold expansion processes on the crack growth lives and damage tolerance of different configurations. Testing has included cold expansion of thin sheet material, cold expansion of short edge margin specimens, and FTI's ForceTec® rivetless nutplates in short edge margin. The following are summaries of these tests.

Thin Sheet Testing

A multi-phase test program was performed to evaluate the effectiveness of FTI's Split Sleeve Cold Expansion™ (SsCx™) process in extending the fatigue lives and the crack growth lives of thin sheet specimens (0.040-inch thick) under high-cycle loads typical for helicopter applications. The 2024-T3 aluminum specimens were tested in various configurations including zero-load transfer with open and filled holes, load transfer assemblies and lap-joint assemblies. The specimen holes were tested in either the non-cold expanded or the cold expanded conditions. In addition, specimens were tested with smooth holes (no flaws) or with 0.010-inch long notches or pre-cracks at the holes. The notches simulated damage that may occur during manufacturing or fastener installation; the pre-cracks simulated damage that may not be completely removed during repair and rework. The results of this program demonstrated that cold expansion greatly enhanced the durability and damage tolerance of these structures. In some specimens, the fatigue strength was improved more than 200%. Cold expansion also slowed the crack growth near the hole in the slow crack region of the ΔK vs. da/dN curves. The data did not show any significant difference in behavior between the notched specimens and the pre-cracked specimens.

Low Edge Margin Testing

This test program was performed to determine the crack growth of low load transfer specimens with short edge margin holes. The specimens were made from 7178-T651 aluminum material. While the main objective of this program was to obtain actual data in order to model the crack growth of this material using crack growth prediction software, some comparisons were made between the results for the non-cold expanded specimens and the results for the cold expanded specimens. The fastener holes in the specimens were tested in either the non-cold expanded condition or the cold expanded condition. The holes in the non-cold expanded specimens had an edge margin of 2.0. The holes in the cold expanded specimens had edge margins of 2.0, 1.5, 1.2 or 1.0. All specimens were tested with a 0.050-inch by 0.050-inch pre-crack at one hole in the main specimen component. The pre-cracks were made before the specimens were cold expanded or assembled. The specimens were tested using either the upper-wing spectrum loads or the lower-wing spectrum loads for a military transport aircraft. The results of this test show that cold expansion greatly improves both the fatigue lives and the crack growth lives of these short edge margin specimens. The cold expanded specimens with edge margins of 2.0, 1.5 and 1.2 all showed an increase in fatigue lives and slower crack growth than the non-cold expanded specimens with edge margin of 2.0. The cold expanded specimens with edge margin of 1.0 had fatigue lives and crack growth similar to the non-cold expanded specimens.

Damage Tolerance Testing of FTI ForceTec Rivetless Nutplates

This test program was performed to determine the crack size at non-cold expanded holes that would result in comparable fatigue lives to holes that have 0.050-inch by 0.050-inch pre-cracks and are installed with ForceTec rivetless nutplates. All specimens were manufactured from 7075-T6 aluminum. The non-processed specimens were tested with two different hole diameters: the starting hole diameter for ForceTec and the final inner diameter of the rivetless nutplate. The non-processed specimens were tested with 0.010-inch and 0.050-inch corner cracks. All specimens had edge margins of 1.9 or 2.6; the specimens were manufactured with short edge margins to promote cracking at the same location for all specimens. All specimens were tested with constant amplitude and the fatigue and crack growth data were recorded during testing. In addition, FTI used several different methods for predicting and modeling the crack growth of the different configurations. Results show that non-processed specimens with the same hole diameter as the ForceTec starting hole diameter and 0.010-inch corner cracks had similar fatigue lives to the ForceTec specimens with 0.050-inch cracks. In addition, the specimens were used to validate an FEA model used to predict the residual compressive stress from cold expansion and also an FTI program (FTISTRS) developed to predict crack growth through the residual stress and compare these to the actual crack growth curves generated from the test data. The results show that the FEA model produced a comparable stress field to the test data, however the FTISTRS program tended to slightly over predict crack growth lives. More work is continuing to develop this program.

9.10.7 Effects of Cold Expansion Processes in Anodized Material

Len Reid, Fatigue Technology Inc.

Testing has been performed to determine the effects of using FTI's cold expansion processes in anodized material. Anodizing is known to cause early cracking and reduced fatigue lives in aluminum alloy structures. However, the effect of combining the two processes was unknown and testing had been performed to investigate the combination of these processes.

Effects of Anodizing and SsCx

This test program was performed to determine the effects of anodizing on the fatigue lives of 7075-T651 specimens with open holes. The specimens holes were tested in the non-cold expanded condition or the cold expanded condition. Specimens were tested with bare and anodized surfaces. Because it was unknown when anodizing would occur with respect to machining and cold expansion of the holes, different specimen configurations were anodized before or after hole machining, and before or after cold expansion. When the bare specimens were compared, the cold expanded specimens showed 12:1 fatigue life improvement over the non-cold expanded specimens. When the anodized specimens were compared, the cold expanded specimens showed approximately 3:1 fatigue life improvement over the non-cold expanded specimens. In addition, the anodized cold expanded specimens had significantly shorter fatigue lives than the bare cold expanded specimens.

Anodized Aluminum Lug Specimens with FTI ForceMate® Bushings

This test program was performed to evaluate the use of FTI ForceMate® bushings in lugs prepared with and without anodized surfaces (no configurations with shrink fit bushings were evaluated). The lug specimens were manufactured from 7075-T73 aluminum and the bushings were manufactured from 17-4 PH stainless steel. Three different specimen conditions were tested: bare surface, anodized surface including the hole surface, and anodized surface and bare hole (the anodized layer was removed before bushing installation). The specimens were installed with standard size ForceMate bushings using standard ForceMate tooling. The lug specimens were pin-loaded and constant amplitude fatigue tested. Results show that anodized specimens had significantly lower fatigue lives than the bare specimens with ForceMate bushings. Further studies can be undertaken to compare these results to traditional shrink fit bushing installations.

9.10.8 RAPID For Commuters (RAPIDC)
Dr. Xiaogong Lee, FAA, AAR-431, (609) 485-6967

Several major enhancements have been added to the RAPIDC program in 2000. The program development was focused on damage tolerance analysis (DTA) assessments of antenna installations.

A finite element analysis (FEA) capability was incorporated in RAPIDC software to analyze layered sheet structures with discrete joints between sheets. Thin sheets are modeled with plane stress elements, which are connected to each other through a shear spring element. An automated model generator has been incorporated in RAPIDC for fast preprocessing.

RAPIDC can analyze doublers with elliptical, teardrop, or sausage shapes. With the FEA capability in RAPIDC, there is no need to generate and store large amounts of data. Instead, all the parameters, such as fastener loads, critical fastener locations, stress gradients, and stress-intensity factors needed for the analysis are generated as needed shown in Figure 151, the circular and rectangular (square) shapes are now available in RAPIDC v1.0. The elliptical, sausage, and teardrop shapes are being finalized and will be incorporated in RAPIDC v1.2, which will be beta-tested in January 2001.

A survey of commercial repair stations was completed to gain a better understanding of repair practices and existing repairs. Information on common types of repairs on various types of aircraft, the repair procedure, airplane configurations, usage, and specifications was compiled. Figure 152 shows some of the repairs and a sausage- shaped antenna installation mounting plate found during the survey. In addition, software demonstrations were made at each survey site and feedback was received to define areas for improvement. This survey also increased awareness of the RAPIDC software and sparked interested from the potential users.

A major enhancement, “joint relocation capability,” was added to the RAPIDC design process. This capability allows the user to place fasteners as they really are found in an operational environment rather than the straight line previously required by the program. This feature was critical for the design of the elliptical, sausage, and teardrop doublers.

9.10.9 RAPIDC Repair Tool for Commuter Aircraft
Dr. Xiaogono Lee, FAA, AAR-431, (609) 485-6967

RAPID is a simple, fast, and user-friendly damage tolerance analysis (DTA) design tool for fuselage structural skin repairs developed by the FAA. It automatically performs static strength and damage tolerance analyses for fuselage structural skin repairs to optimize the designs of inspectable structural repairs. In 1999, the RAPID development program has been focused on the commuter category airplanes and significantly enhanced for application to commuter aircraft.

The newly developed RAPIDC Version 1.0 consists of the following four major components:

- Windows^{TM} -based with point-and-click graphical user interface (GUI);
- Advisory system to provide repair guidelines;
- Extensive material and fracture parameter database;
- Automated static strength and damage tolerance analysis to quickly assess skin repairs and antenna installations.

A generic load spectrum for commuter category airplane operations, based on data available in the FAA report AFS-120-73-2, was implemented. Up to six flight profiles can be inputted by the user to generate load spectra. The stress spectra is then computed based on the repair locations and the load spectrum. The program also allows the user to input their own stress spectra if they are available for specific applications. Crack growth analyses can be performed by applying either the simplified method or cycle-by-cycle analysis. In RAPIDC Version 1.0, a total of 12 basic repair cases will be available including two types of antenna installations (circular/elliptical and square/rectangular) as shown in figure 153.

RAPIDC v1.0 is scheduled to be released in January 2000 and will be available at the FAA website http://www.asp.tc.faa.gov/rapid/

9.10.10 Damped Bonded Patch Repairs
Theodor H. Beier, Boeing

Damped boron composite repairs have been developed to repair sonic fatigue cracking of aircraft skins in situ, and reduce vibratory response to preclude additional damage, Figure 154. These repairs out performed other damped, doubler, and strengthened replacement repair concepts by a factor of greater than 6.

The response data presented shows a reduction in response of the panel at its fundamental frequency of 1.5 orders of magnitude with little detrimental panel stiffening. Stiffening risks driving the damage into adjacent structure. A broadband response reduction near an order of magnitude is exhibited also, which is very difficult to achieve.

The pre-cured repair consists of several boron plies to restore the strength of the cracked skin, a high performance damping pack, and boron constraining layers on the outside. The damping pack is a proprietary combination of layers of damping material and interleaved composite layers to enhance shearing of the damping material. The damping pack can be adjusted to compensate for the temperature range at which best performance is required.

9.11. Nondestructive Inspection

9.11.1 Thermography Used for Composite Inspections

David Galella, FAA, AAR-433, (609) 485-5784

The Nordam Group, working with Thermal Wave Imaging, Inc., Wayne State University, and the Airworthiness Assurance Nondestructive Inspection (NDI) Validation Center (AANC), completed a technology transfer project to use thermography for inspection and certification of composite structures. Nordam operates an aircraft manufacturing, maintenance, and repair depot. In its repair division, the thermography system will be used to conduct pre- and postrepair damage assessments of composite parts control surfaces, engine nacelles, and access doors. In its manufacturing division, Nordam has obtained Cessna approval to use thermography as an authorized method of inspecting newly manufactured control surfaces.

The use of thermography replaces the "tap" test and ultrasound immersion inspections for finding disbonds and delaminations within composite parts. As a replacement for the tap test, thermography has the advantage of providing a permanent visual record of a defect rather than relying on the transient sound of the tap as heard by an inspector.

Thermography can inspect for disbonds and delaminations with a reliability similar to immersion testing but without the potential of water intrusion into honeycomb parts. The Thermal Wave Imaging systems is commercially available from Thermal Wave Imaging, Inc. (Figure 155.)

9.11.2 Semiautomated Ultrasonic Tap Tester

David Galella, FAA, AAR-433, (609) 485-5784

Several challenging ultrasonic inspections for composite structures have been identified by the aircraft operators and manufacturers (OEMs). Working in cooperation with the Commercial Aircraft Composites Repair Committee (CACRC) and inspection managers from US and foreign carriers, researchers from Iowa State University (ISU) conducted informal surveys of over 40 organizations to better define the needs required to develop an automated tap tester. Based on these needs, an affordable, simple to use, quantitative system with imaging capability has been developed by ISU as part of the Airworthiness Assurance Center of Excellence (AACE) and Center for Aviation System Reliability (CASR) programs.

Based on a mechanical model, tap test data are converted to local spring stiffness of the part, which provides an indication of the severity of a flaw or damage. There has been close interaction with the airlines, OEMs, and the military during the development of the instrumented tapper. For example, the prototype has been tested at Northwest Airlines on CACRC composite standard specimens. A considerable number of tests have been conducted on composite repair samples, manufactured parts, and real aircraft structures provided by Boeing, FAA AANC (for CACRC), Northwest Airlines (also for CACRC), Lockheed-Martin, Northrop Grumman, VisionAire, and Wichita State (composite repairs). Samples covered both composite and metal honeycomb structures and a variety of defect types including disbond, delamination, crushed core, impact damage, and anomalies in composite repairs. The tapper system was field tested four times on helicopter blades and engine decks at the Iowa Army National Guard Aviation support facility.

Based on results to date and enthusiasm shown by the industry, it is anticipated that the tapper will be beneficial in both the manufacturing of new parts and the maintenance, repair and inspection of existing parts.

The system consists of a highly portable, battery-operated laptop PC and a semi-automated tapper imaging system with a dedicated circuit to measure the impact duration and convert it to digital data. Software was developed within the Microsoft Excel environment for data acquisition, image display, and converting impact duration image to a local stiffness image. A grid printed on a transparency was used as the "encoder" in the manual tap scan. A mechanized scanner is also under development.

Field demonstrations have been done at Northwest, TWA, and American Airlines (AA). Beta site testing of the system began at American Airlines in July 1999. Delta Airlines and Boeing will also participate in the demonstrations.

The inspection done at AA were for disbond detection in the heater blanket (a 5- ft. x 9-ft. thin aluminum honeycomb sandwich with imbedded heating wires) glued onto the top surface of MD80 wingskins to prevent icing in front of the engines. Tests performed at TWA were for the detection of disbonds on B767 elevators. (See Figure 156.)

9.11.3 Rotorcraft Validation and Nondestructive Inspection (NDI) Assessment
Dr. Dy Le, FAA, AAR-431, (609) 485-4636

Current available equipment and newly developed nondestructive inspection and evaluation (NDI/E) concepts are being examined for their potential applications to component designs, materials, and the crack and blunt flaw sizes that occur in rotorcraft.

Phase II Testing of the Composite Rotor Hub Fatigue: Phase II testing of the composite rotor hub fatigue, damage tolerance, and nondestructive inspection program was completed. Four rotor hubs were fabricated with an array of flaws and tested in the biaxial flex beam test rig shown in Figure 157.

The implanted flaws (0.25-inch-square Teflon inserts) were half the size of the flaws used in the Phase I test specimens. Hand-held, pulse-echo, ultrasonic inspections were conducted during the fatigue tests to obtain flaw growth versus damage tolerance data. The strain field was assessed before the fatigue test; the strains were quite similar to last year's specimen responses. The strain survey was repeated after fatigue testing and flaw growth so that the data could be related to the NDI results. Delamination flaws grew much faster than the growth rate obtained in Phase I test specimens. All four Phase II test specimens reached flaw runout (7 to 9 inches delamination length) in a fraction of a segment, although fatigue testing continued up to one full segment (140,000 cycles per segment). It is believed that the test specimen fabrication process produced resin-starved rotor hubs. This would account for the rapid breakdown of the resin/fiber layers and initiation of interply delaminations. Test coupons will be cut from the failed rotor hubs to determine the ratio of resin to fiber content. Subsequent fatigue tests showed that, despite the extensive delamination flaws in the rotor hubs, the hubs were able to withstand flapping angles in excess of 3 times normal flight loads (36^{o}) while maintaining the necessary axial loads for flight (31,000 pounds).

Inspection of Helicopter Tension Straps: Recent in-service failures of the tension straps, Figure 158, that connect the rotor blade to the engine mast have focused attention on a need for either improved NDI or a more frequent replacement of the straps. The FAA investigated the capability of NDI methods for the tension straps. The investigation revealed that it is difficult to acquire a clear signal with ultrasonics (UT) due to the high noise levels associated with the construction of these parts. It was concluded that even large flaws would not be easily detected in the noisy UT signals.
Neutron Radiography (NR) showed some promise and an ability to differentiate the wire wrap from the protective coating. Without some sort of NDI reference standard or a well-characterized flawed part removed from a helicopter, it is not possible to be more specific about the capability of NR. It is believed that NR would require an area of approximately two square millimeters of damage to produce a detectable density change. Since the wires are only 0.006 inch in diameter, the damage would have to cover about 90 wires in a single area.

The investigation revealed that it is extremely difficult to inspect the tension straps due to the manufacturing process for the straps. Composite tension straps are being recommended to replace the existing ones.

9.11.4 Rotorcraft Assessment and Validation of Nondestructive Inspection Methods
Dy Le, FAA, AAR-431, (609) 485-4636

A research task in the assessment and validation of nondestructive inspection (NDI) methods for rotorcraft is underway to support the FAA rulemaking process and the development of guidance material with the anticipated revision of Federal Aviation Regulations (FAR) 29.571, Fatigue Evaluation, to include damage tolerance requirements for rotorcraft.

Accurate and reliable methods to find damage or flaws in rotorcraft structures due to manufacturing and/or operations are needed. Manufacturing and field inspection methods will be reviewed to ensure the required probability of detection (PoD) of initial flaw sizes. The effort is being conducted at the FAA Airworthiness Assurance NDI Validation Center (AANC).

A biaxial fatigue rig, shown in the schematic drawing in Figure 159, was built to test rotorcraft flex beams and is now fully operational. Two composite rotor hub specimens can be tested simultaneously. Axial and torsional loads can be dynamically and simultaneously applied to simulate the centrifugal force and flapping motion of the rotor hub.

Fatigue testing of the first set of three composite (fiberglass and glass-carbon) flex beams was completed. The specimens prototyped a critical portion of the main rotor hub to assess NDI sensitivities with respect to typical flaws. Pulse-echo and ultrasonic inspection techniques were used. The correlation between structural integrity and inspection sensitivity is being done.

The probability of flaw detection study for corrosion in thin gauge material was also performed on the blind test specimens with three layers of 0.0016-inch-thick skins. Sixteen specimens were produced, eight each of two-layer and three-layer skins. Dual frequency eddy-current inspections were conducted by Bell and the AANC (AANC used Nortec $19e^2$ and Bell used Hocking Phaseac 2200 equipment). The dual frequency eddy-current technique was able to detect 5% material loss in one-, two-, or three-layer stack-ups. The desired detection level for cumulative material loss over the thickness of the joint is 10%. The test specimens contained 47 flaw sites and the composite results from Bell and AANC showed that 81% of the flaws were detected. These results were obtained for flaws that were about one inch in diameter; it is anticipated that the desired detectable flaw size would be two inches or greater in diameter.

9.12. Engines

9.12.1 Characterizing Aeroacoustic/Combustion Loads for Aging Aircraft Sustainment

Leonard Shaw, Air Force Research Laboratory

The Air Force needs to be able to predict the dynamic loads associated with aging aircraft problems. Currently these loads cannot be predicted for all the various dynamic loads associated with aging aircraft. The goal of this work is to characterize these loads and format them on a CD-ROM for easy access. When completed the aging aircraft community will be able to readily and reliably predict the loads contributing to fatigue cracking of aircraft structure. The objectives of this effort are to formalize and compile an extensive aircraft acoustic loads data-base, develop an OASPL acoustic loads prediction methodology, develop modal characteristics for frequency and amplitude, and conduct a sensitivity analysis of structural response to acoustic spectra. The approach will consist of developing a database of all available loads data for attached and separated flows, cavities, engine inlet/combustion /nozzle, and exhaust plume (screech). The database will be then be enhanced by utilizing a novel prediction technique, which was developed by the principal investigator and is based on first principles. Sensitivity analysis of structural response to different acoustic spectra will be conducted. The results will then be formatted into a CD-ROM for application to aging aircraft loads prediction.

The novel prediction technique is the following equation:
Where:

$$\mathbf{SPL} = \mathbf{OASPL} + 10\ \mathbf{Log}_{10}\left[\frac{\zeta\ \mathbf{bw}}{(1 + (\pi/2)^2\ \zeta^2\ \mathbf{f}^2)}\right]$$

- **bw** Is Bandwidth (Hz)
- **f** Is Frequency (Hz)
- **OASPL** and ζ Are Parameters (Stored In the Database) Based on Flow Similarity and Geometry
- ζ= (ζ-Heat Release, Characteristic Length, and Velocity)
- NOTE: ζ**f** = Strouhal Number

The chart in Figure 160 shows a wide source of aeroacoustic data all normalized to essentially one curve using the novel technique. By normalizing the aeroacoustic and dynamic loads from various sources on aircraft, predictions becomes more reliable. It will permit the summary of very extensive data bases into a tool readily usable by the aircraft designer.

9.12.2 Ceramic Inclusions in Powder Metallurgy Disk Alloys: Characterization and Modeling

P. Bonacuse, US Army Research Laboratory, Vehicle Technology Directorate at NASA Glenn Research Center; Pete Kantzos, Ohio Aerospace Institute at NASA Glenn Research Center; Jack Telesman, NASA Glenn Research Center

Powder metallurgy alloys are increasingly used in gas turbine engines, especially as the material chosen for turbine disks. Although powder metallurgy materials have many advantages over conventionally cast and wrought alloys (higher strength, higher temperature capability, etc.), they suffer from the rare occurrence of ceramic defects (inclusions) that arise from the powder atomization process. These inclusions can have potentially large detrimental effect on the durability of individual components. An inclusion in a high stress location can act as a site for premature crack initiation and thereby considerably reduce the fatigue life. Because these inclusions are exceedingly rare, they usually don’t reveal themselves in the process of characterizing the material for a particular application (the cumulative volume of the test bars in a fatigue life characterization is typically on the order of a *single* actual component). Ceramic inclusions have, however, been found to be the root cause of a number of catastrophic engine failures. To investigate the effect of these inclusions in detail, we have undertaken a study where a known population of ceramic particles, whose composition and morphology are designed to mimic the “natural” inclusions, are added to the precursor powder. Surface connected inclusions have been found to have a particularly large detrimental effect on fatigue life, therefore the volume of ceramic “seeds” added is calculated to ensure that a minimum number will occur on the surface of the fatigue test bars. Because the ceramic inclusions are irregularly shaped and have a tendency to break up in the process of extrusion and forging, a method of calculating the probability of occurrence and expected intercepted surface and embedded cross-sectional areas were needed. Figure 161 shows a derivation for the intercepted surface area for an arbitrarily shaped and oriented ellipsoid cut by a plane. We have developed a Monte Carlo simulation to determine the distributions of these parameters and have verified the simulated results with observations of ceramic inclusions found in macro slices from extrusions and forgings. Figure 162 shows a comparison of the observed intercepted areas of a seeded extrusion and the simulated intercepted area distribution. The ultimate goal of this study will be to use probabilistic methods to determine the reliability detriment that can be attributed to these ceramic inclusions.

9.12.3 Fatigue of Graphite Fiber/Polyimide Composites for Reusable Launch Vehicle Applications

Cheryl L. Bowman, NASA Glenn Research Center and Michael G. Castelli, Ohio Aerospace Institute

Background Polyimide matrix composites have been used successfully in aeronautic engine applications at temperatures of 290-315°C. Extending these materials to Reusable Launch Vehicle applications will require higher operating temperatures for shorter duration. In this program, an eight-harness satin weave T650-35/PMR-II-50 composite has been tested at temperatures of 260-480°C. Composite quality was characterized through destructive and nondestructive techniques. Uniaxial tension, creep, and tension-tension fatigue tests were conducted in the temperature range of 260-480°C on dry specimens. Ultimate tensile strength (UTS) degradation at temperatures below 480°C was minimal; the elastic modulus was essentially constant below 385°C. Furthermore, the temperature for onset of steam delamination was determined as a function of moisture content and heating rates (0.6°C/min to 6°C/min). Fatigue properties of moisture-saturated material is currently being explored as well as alternate composite lay-ups to avoid steam delamination.

Dry, Low Cycle Fatigue Evaluation Isothermal, low cycle fatigue tests were performed between 260 and 482°C. Initially zero-tension (R=0) fatigue tests were performed to define the upper limit of this composite’s usefulness and for experimental convenience. Although the fatigue loading was only tensile, both tensile and compressive elastic moduli were measured throughout the fatigue tests as an indication of progressive damage. At 315°C (600° F), fatigue tests were conducted with maximum stresses ranging from 380 to 585 MPa and interrupted prior to failure (lives of 4.6×10^4 to 3.4×10^5 cycles). The percentage of degradation in both the tensile and compressive moduli evaluated at 315°C is listed in Table 4. In this table, the fraction of UTS is a comparison between the maximum stress in the fatigue test to the UTS measured on a separate tensile-to-failure test. The loss of elastic modulus (E^T for tension, E^C for compression) is based on the original specimen moduli measured at the beginning of the fatigue test. These results suggest the dry composites can easily withstand R=0 mission cycles on the order of 100-1000 missions at 315°C. More aggressive temperatures and fatigue loads were likewise investigated. Cycles-to-failure at 370°C (700° F) data are shown in Figure 163 and greater than 10,000 cycles were achieved for a maximum load which was aproximately 80% of the UTS. Figure 164 shows the modulus degradation (incremental tensile modulus normalized by initial modulus) as a function of number of cycles between 315 & 427°C. At temperatures as high as 370°C the zero-tension fatigue durability may be sufficient for 1000 mission cycles. This survey of PMC properties at aggressive use-temperatures suggests that further investigation is warranted for RLV applications.

Reference

[1] C. Bowman et al., “Characterization of Graphite Fiber/Polyimide Composites for RLV Applications”, in *Proceedings of the 46th International SAMPE Symposium*, (SAMPE, Covina, CA, 2001).

9.12.4 Uncontained Turbine Engine Research
Mr. William Emmerling, FAA, AAR-432, (609) 485-4009

Task I - Debris Characterization and Vulnerability Analysis
Uncontained turbine engine events have caused catastrophic results to aircraft. The FAA saw a need to update advisory material relative to uncontained turbine engine failures, Figure 165.

The Aviation Rulemaking Advisory Committee (ARAC) was tasked to update Advisory Circular (AC) 20-128, *Design Considerations for Minimizing Hazards Caused by Uncontained Turbine Engine and Auxiliary Power Unit Rotor and Fan Failure*. The ARAC group determined that there was a need to better characterize the types of failures, number of fragments, velocity of fragments, and damage caused by these fragments.

However, much of the data needed to do this has been collected by engine and airframe manufacturers who consider this data to be proprietary. Therefore, in 1995, the FAA William J. Hughes Technical Center entered into an interagency agreement with the Naval Air Warfare Center, Weapons Division (NAWCWD), China Lake, CA, to gather the data and conduct an analysis which could then be used to update AC 20-128. The data was given freely to the Navy for analysis because this organization had pre-existing nondisclosure agreements with most engine and airframe manufacturers and could therefore respect the proprietary nature of this data. The data has now been analyzed and the results have been made available to members of the ARAC to use for the update of AC 20-128.

Additionally, the characterization will also be used to prepare stochastic models of uncontainment events of various types to be used with vulnerability assessment tools. These tools (FASTGEN 3 and COVART 4.0) have been used by the military to assess the vulnerability of their aircraft to hostile threats. By modifying this code for use by civilian airframe manufacturers, the vulnerability analysis of a commercial airframe to the threat from uncontained engine debris can be conducted. (See Figure 166.)

The NAWCWD and their support contractor, The Service Engineering Company, have already identified certain modifications to this code. These modifications are being made. In addition, initial testing of the vulnerability assessment was undertaken to obtain comments from commercial airplane manufacturers. Boeing commercial divisions have conducted initial evaluations of the vulnerability assessment tools under contract from NAWCWD. Both contractors have provided recommendations that will improve the ability of the tools to assess aircraft vulnerability to uncontained engine debris threat.

The resulting vulnerability assessment tools will enhance the safety of commercial aircraft by providing the means to critically examine the threat posed by uncontained engine debris and allow steps to be taken to mitigate the threat.

Several reports were completed during 1999 as the result of years of effort in support of developing the revisions to AC 20-128 *Design Precautions for Minimizing Hazards to Aircraft from Uncontained Turbine Engine and Auxiliary Power Unit Rotor Failure*.

Two reports from the Naval Air Warfare Center, Weapons Division, China Lake, California, provide data on the historical events for large and small engine uncontained events, and a third report documents air gun tests to refine penetration equations used for aircraft vulnerability analysis. These reports are DOT/FAA/AR-99/7, DOT/FAA/AR-99/11, and DOT/FAA/AR-99/19, respectively, and are contained on the CD-ROM with this report. (Figure 167.)

Task II – Aircraft Material Penetration Analysis
Lawrence Livermore National Laboratory (LLNL) and industrial partners AlliedSignal Engines, Boeing Commercial Aircraft Group (BCAG), United Technologies, and Pratt & Whitney (P&W) have showed the need for improved analysis tools for evaluating the mitigation and containment in advanced turbofan engines.

Although various experimental data have been obtained, the methodology has not yet been developed that is needed to implement a calibrated system for the design and certification of means to maximize engine debris containment and minimize uncontained engine debris hazards to the aircraft. The development and validation of the tools necessary to numerically simulate the containment and assess the vulnerability of aircraft to uncontained engine debris are the objectives of this effort. The numerical methodology will be based on a fundamental understanding of material properties, failure mechanisms, and structural dynamics that will be benchmarked against experiments, as opposed to just empiricism. The result will be analytical tools that will be useful to engine as well as airframe manufacturers for predicting the design of a cost-effective aircraft structure mitigation and/or engine containment system. The validated toolbox will be applicable to vulnerability analysis of the overall system structure.

The analytical tools which are being developed will predict the interaction between a liberated fan blade and the engine containment casing, fragmentation, subsequent behavior of aircraft structures in the event of perforation, and the velocities and associated energies of the uncontained fan blade mass. In addition, the developed computational tools will be available to aircraft and engine manufacturers to assess more general problems of single or multiple fragment effects. With sufficient industrial use and validation, this collection of robust simulation tools will form part of the certification process. The mechanism for the transition from simulation tools validated for use in design and analysis to the incorporation of simulation tools into a certification process will be determined by the aviation community as a whole.

The final report from Lawrence Livermore National Laboratory for the work performed under subcontract to AlliedSignal Aerospace has been completed (*FAA Debris Mitigation Phase 1 Impact Test Report*, DOT/FAA/AR-99/54). Impact tests were performed to obtain needed data for proper calibration of LL-DYNA-3D analysis of aluminum 2024 and titanium 6-4.

Task III – Armor Material Development and Analysis
Over the years, several civil aircraft accidents with catastrophic consequences have occurred when fragments from in-flight engine failures damaged critical aircraft components. To reduce the probability of such incidents in the future, the FAA is sponsoring research to develop and apply advanced technologies and methods for mitigating the effects of uncontained engine bursts. In support of this FAA objective, SRI International is conducting a research program to evaluate the ballistic effectiveness of fabric structures made from advanced polymers and to develop a computational ability to design fragment barriers. (See Figure 168.)

Since the previous progress report, SRI has solved several problems associated with the crimped geometry and interaction of woven yarns. When an orthotropic model is invoked and direction-dependent yarn properties are specified, the yarn, as it is loaded, exhibits no appreciable stiffness until it straightens. The analytical behavior of this model was examined in simple simulations of single yarn response to axial and transverse loads and found acceptable. (See Figure 169.)

SRI evaluated the ballistic response of fabrics-to-fragment impact, examined fabric deformation and failure using quasi-static penetration tests, and measured the tensile properties of yarns and fibers. They focused on three commercially available high-strength polymer materials—PBO (Zylon), aramid (Kevlar), and polyethylene (Spectra).

Several reports were completed in 1999 which document the progress made in modeling and designing armor fabric barriers to protect aircraft systems from the majority of fragments liberated from an uncontained engine failure. The majority of fragments, as described in the China Lake reports, are relatively small and can be defeated with ballistic fabrics in combination with the existing structure. (See Figure 170.)

The largest fragments, like the disc found in the farmer's field after the Sioux City, Iowa, accident, would not be stopped by these materials. However, the loss of all hydraulic systems in that accident was attributed to smaller debris liberated by the failure rather than a direct hit by the large piece. The reports are DOT/FAA/AR-99/8 Part I and II. A full-scale test of fabrics in an aircraft structure is described in report DOT/FAA/AR-99/71, printed in November 1999. (See Figure 171.)

The final result of this effort in uncontained turbine engine research will be a validated tool kit to improve the certification process and provide a means of compliance with the proposed revision to AC 20-128 that will include design for multiple fragment threat.

9.12.5 Enhanced Turbine Rotor Material Design and Life Methodology
Mr. Joseph Wilson, FAA, AAR-432, (609) 485-5579

The commercial service experience of turbine powered aircraft has shown that despite the current rigorous 'safe-life' design approach toward failure critical components, material and manufacturing anomalies can reduce structural integrity and increase the risk of failure. The FAA, working closely with the engine industry through the Rotor Integrity Subcommittee of the Aerospace Industries Association, has developed supplemental design and lifing methods that formed the basis for this research program. The Turbine Rotor Material Design Program is aimed at developing a standardized, damage tolerance-based, probabilistic risk assessment and life management code to address the structural integrity issues of failure of critical turbine rotors in aircraft engines.

The FAA marked the release of a software code, called "Design Assessment of Reliability With Inspection (DARWIN)" with a workshop and training session for industry and government users on May 18-20, 1999, at Southwest Research Institute (SwRI) in San Antonio, TX. Attendees included nine engine manufacturers from Canada, Europe, and the United States as well as representatives from the FAA, Transport Canada, NASA, and the US Air Force. The new DARWIN computer design tool will improve the structural integrity of turbine engine rotor disks used in commercial aircraft engines by assessing rotor design and life management considering the uncertainties in hard-alpha material defect (size, location, and occurrence rate); stresses, crack growth, inspection effectiveness, and shop visit time. DARWIN integrates production related anomaly distributions, finite element stress analysis, fracture mechanics analysis, nondestructive inspection simulation, and probabilistic analysis to assess the risk of rotor fracture. It computes the probability of fracture as a function of flight cycles, considering random defect occurrence and location, random inspection schedules, while being aided by a user-friendly, sophisticated graphical user interface to handle the otherwise difficult task of setting up the problem for analysis and viewing the results. This technology is a result of a four-year research, engineering, and development grant with SwRI. In this grant, SwRI developed the tool in collaboration with engine manufacturers AlliedSignal, Rolls-Royce-Allison, General Electric, and Pratt & Whitney.

The first phase of the program focused on the presence of melt-related defects, known as hard alpha defects, found in titanium alloys, Figure 172. DARWIN will be enhanced to handle manufacturing and maintenance-induced surface anomalies in all rotor disk materials and inherent anomalies in cast/wrought and powdered metal nickel rotor disks in Phase II of the Turbine Rotor Material Design program which is currently underway.

The engine companies can use the code with their design systems as a means to meet the requirements of an anticipated FAA Advisory Circular on enhanced life management (reliability) and damage tolerance. The anticipated outcome, when implemented, is a reduction in the uncontained rotor disk failure rate while providing more realistic inspection schedules. (See Figure 173.)

9.12.6 Engine Titanium Consortium
Mr. Richard Micklos, FAA, AAR-432, (609) 485-6531

The FAA Engine Titanium Consortium (ETC), composed of researchers from Iowa State University, AlliedSignal, General Electric Aircraft Engines, and Pratt & Whitney, was conceived to develop equipment, techniques, and procedures to inspect critical jet engine rotating parts, focusing primarily on hard alpha defects in titanium. Although these defects are very rare, undetected hard alpha in these critical components can fail with tragic results. The DC-10 Sioux City, Iowa, accident was caused by an undetected "hard alpha" defect.

Fiscal Year 1999 was a transition year for ETC. The initial 5-year program, ETC Phase I, was completed, and a new 5-year effort was initiated. The Phase II efforts have raised the bar on the inspection of titanium billet. Work has also been expanded to include the inspection of titanium forgings as well as nickel billet. Phase II also addresses the development of ultrasonic and eddy-current techniques and equipment for in-service and shop inspections. Work that specifically addresses the eddy-current inspection of bolt holes is included. In-service work also addresses cleaning and drying procedures to enhance Fluorescent Penetrate Inspection. Additional quantification of inspection system performance is included.

During this transition, the funding mechanism was changed from the research grant used in Phase I to a contractual mechanism through the Airworthiness Assurance Center of Excellence in Phase II. This generated the development and introduction of an enhanced program management structure, which includes more senior industry input to develop a more efficient and cost-effective program. A program facilitator was also added to the ETC II program management team to assure the management team presents a unified position to the FAA and the industry review board.

The work of the Consortium is sub-divided into several focus areas. The first is the inspection of titanium billet. This is performed at the material manufacturers' site to identify hard alpha during the initial manufacturing stage. A multizone ultrasonic inspection technique was developed in Phase I that has demonstrated the ability to find hard alpha inclusions that were missed by conventional inspection techniques. This system has also been used successfully to find high-density inclusions in billet material. These efforts include fundamental studies into the metallurgical and acoustic properties of titanium to aid in inspection system design.

The second focus is in-service inspection. Here, new techniques and equipment are being developed to enhance engine component inspection capability at the repair or overhaul shop. The ETC has developed a portable eddy-current scanner, with an associated data acquisition capability. This versatile devise permits a more cost-effective, automatic inspection of design features of engine disks.

The ETC portable scanner has been introduced into inspections performed by original equipment manufacturers (OEMs) on their engine components. Use of the system by overhaul shops is expanding, and it is currently being used by the US Army in the inspection of helicopter turbine engines.

The final area is directed towards determining the capability and reliability of inspection systems. This work includes determining the Probability of Detection (PoD) and Probability of False Alarm (PoF) of inspection systems. A methodology to predict the PoD of inspection systems has been developed and is undergoing evaluation. Part of this work includes verification of the methodology using specially developed test specimens, including fabricated billets with known defects. Parts of this verification work will be continued in Phase II.

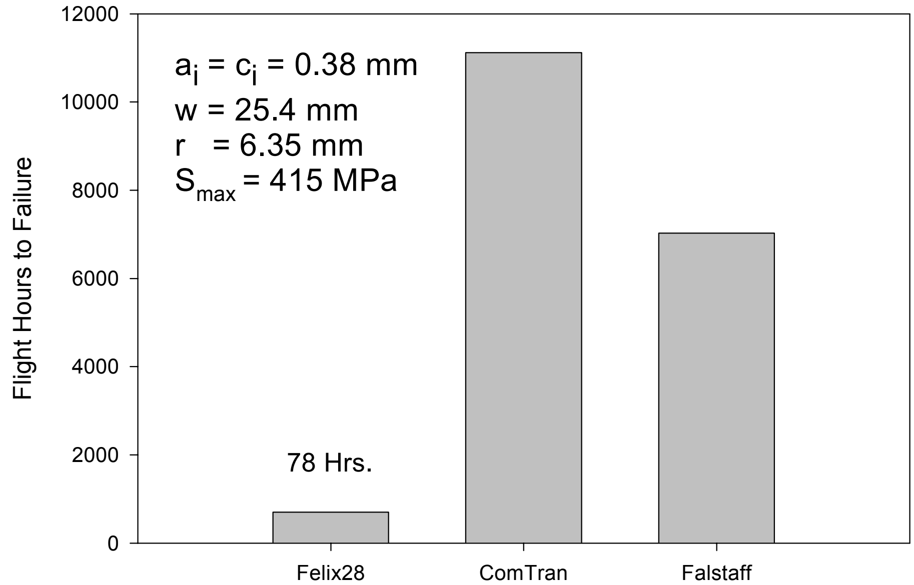

Figure 1. Rotor-wing and fixed-wing crack-growth life comparisons

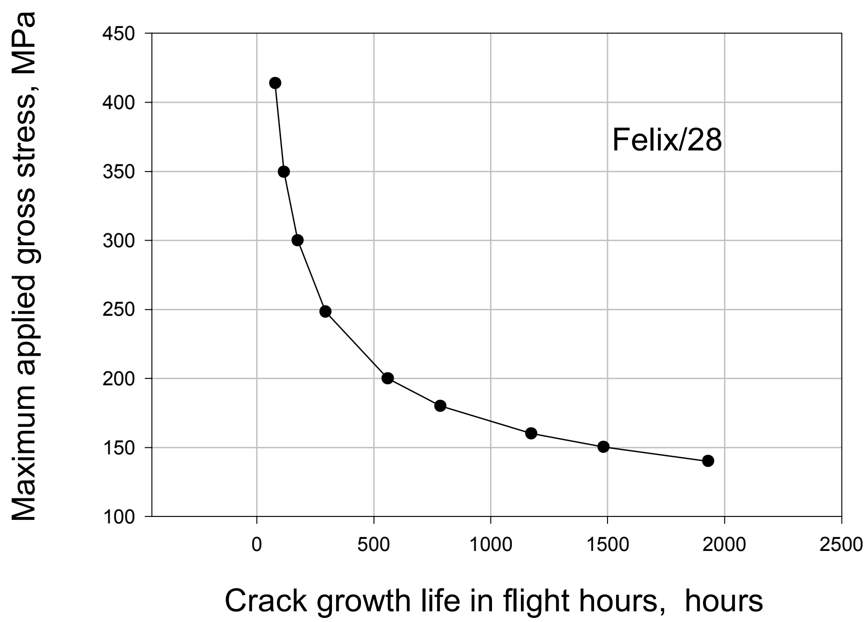

Figure 2. Effects of maximum applied stress on crack-growth lives

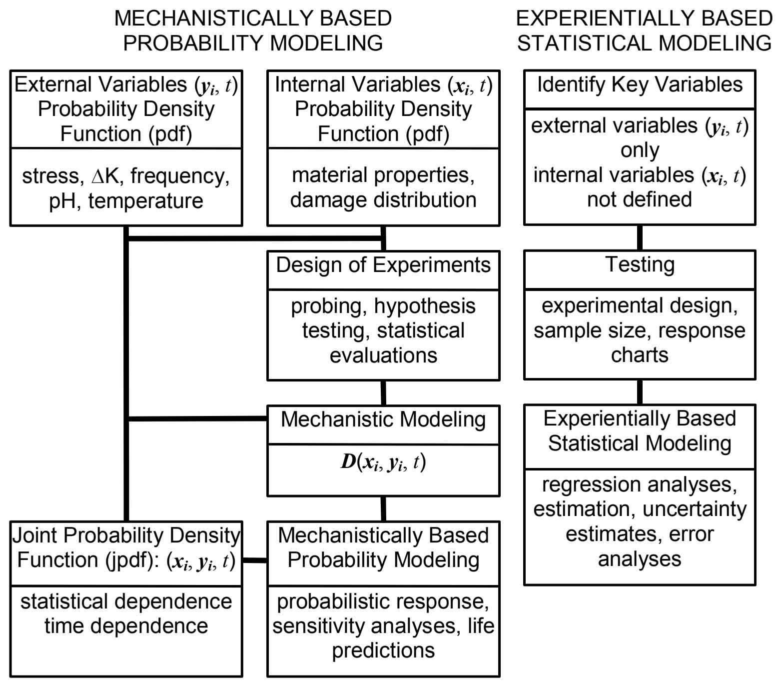

Figure 3. Flow diagrams showing the difference between the mechanistically based probability and experientially based statistical modeling approaches.

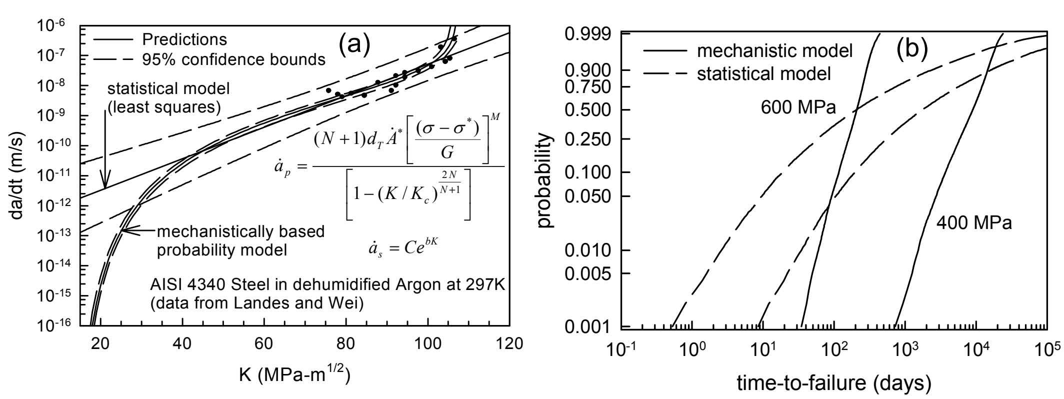

Figure 4. Comparison between mechanistically based probability and statistically based models (a) for crack growth kinetics, and (b) in terms of the cumulative probability of failure at selected stress levels.

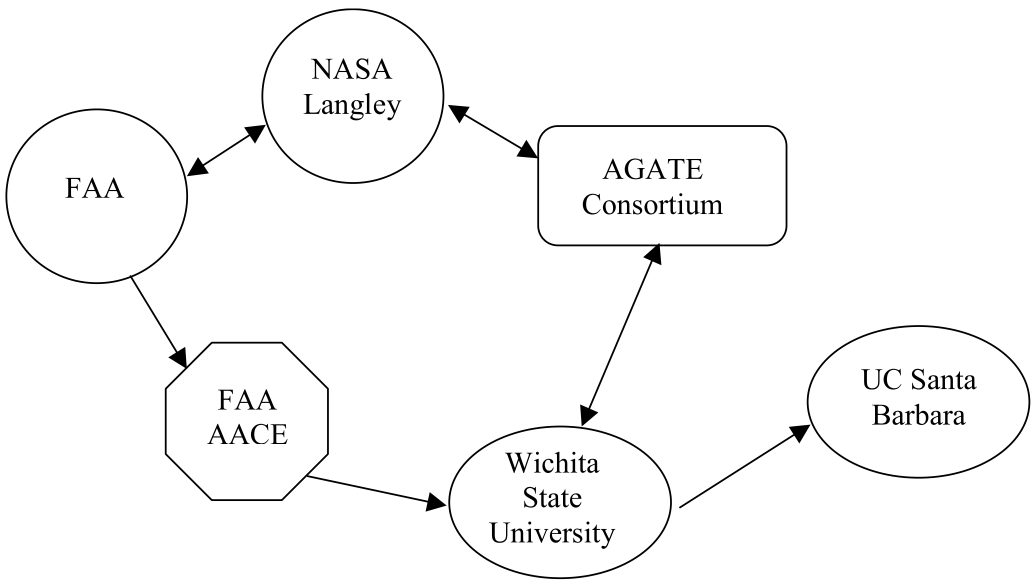

Figure 5. Participants in FAA supported efforts on bonded structure for small composite aircraft

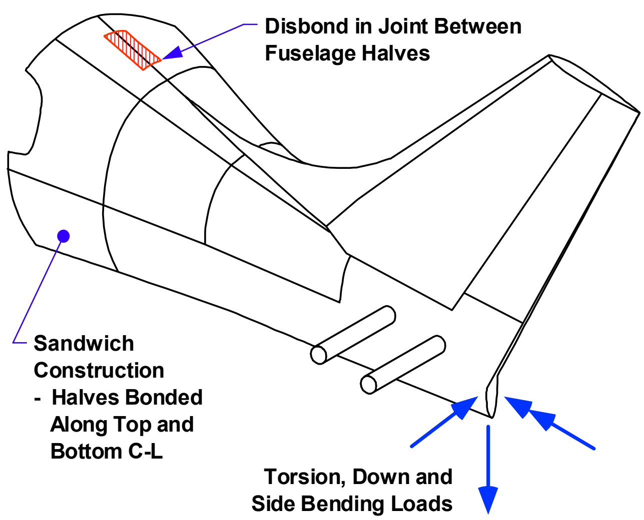

Figure 6. A typical application of bonded construction to small composite aircraft being investigated at UCSB

Figure 7. FAA S-76 HUMS-equipped helicopter

Figure 8. Petroleum Helicopters Inc. aircraft used to collect mission spectrum data

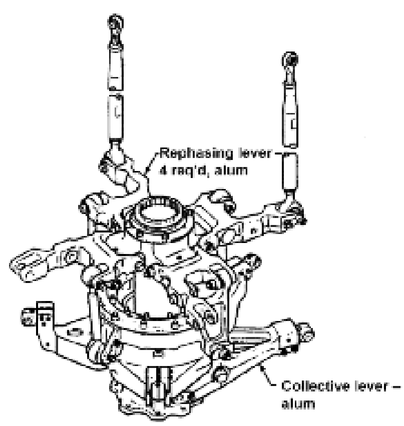

Figure 9. The four principal structural elements selected for damage tolerance study

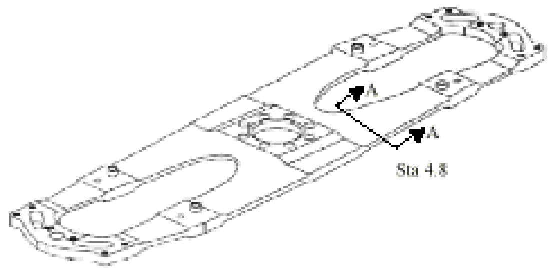

Figure 10. Main rotor yoke

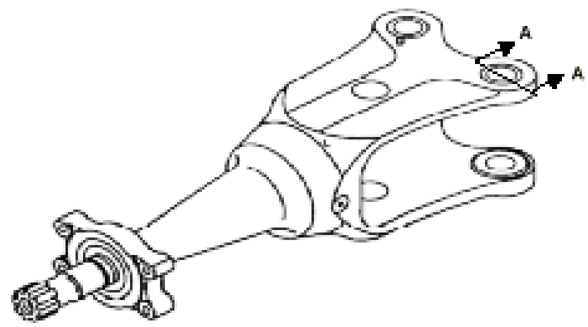

Figure 11. Main rotor spindle

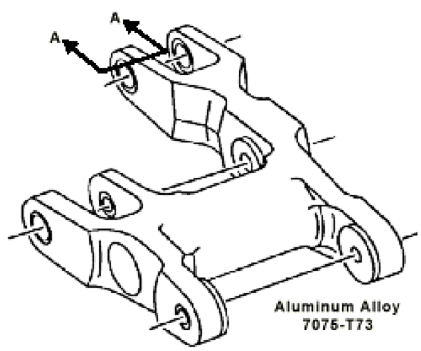

Figure 12. Rephrase lever

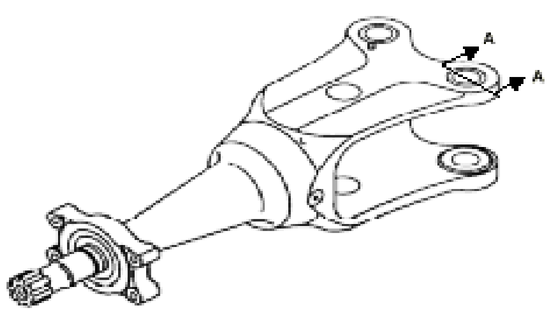

Figure 13. Collective lever

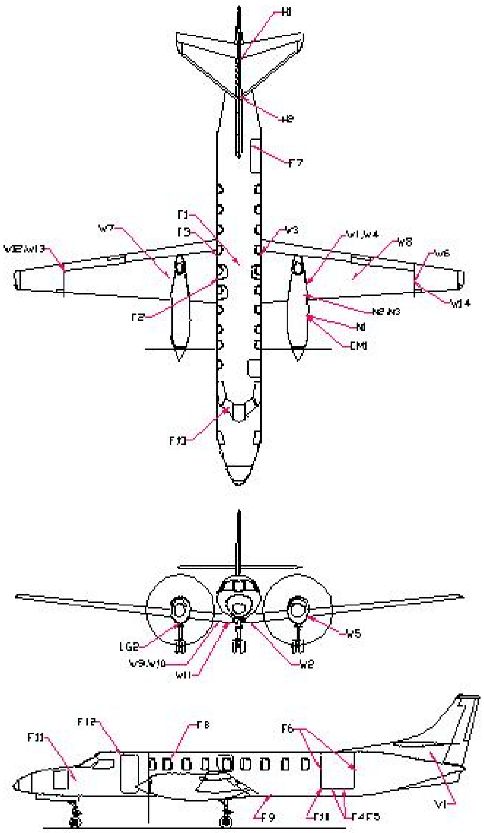

Figure 14. Fairchild SA226/SA226 PSEs and their locations

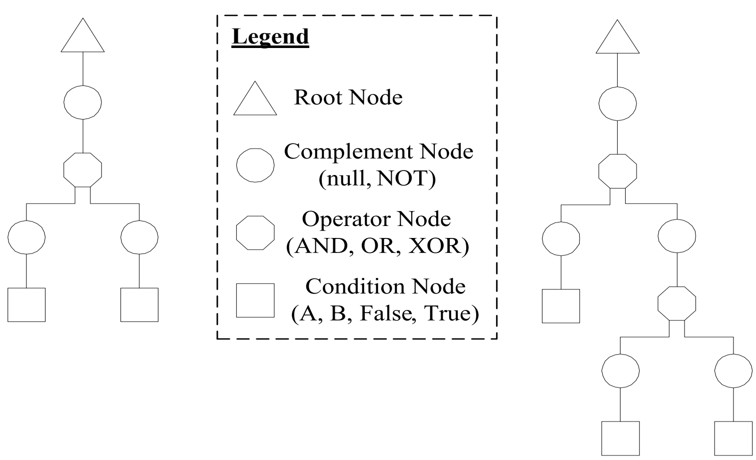

Figure 15. Modified Condition Decision of Coverage

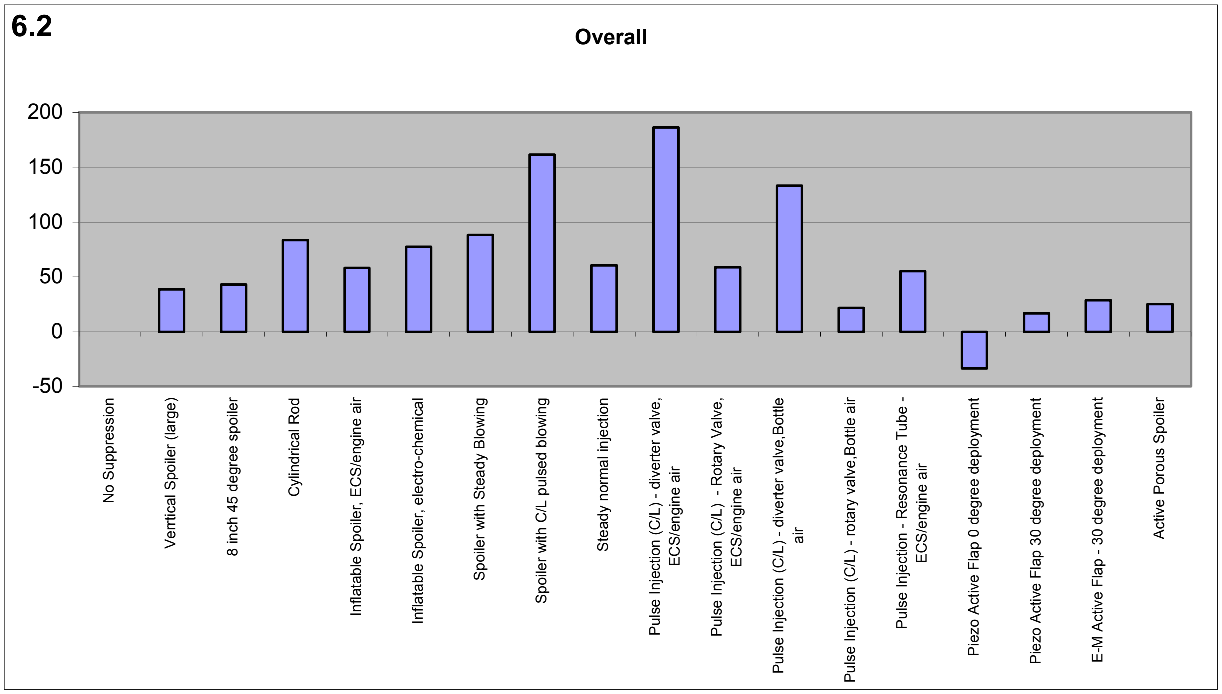

Figure 16. Chart showing evaluation of various potential actuators Vertical axis is a "Measure of Merit."

Figure 17. Photo of cavity used to evaluate the active flow control actuators

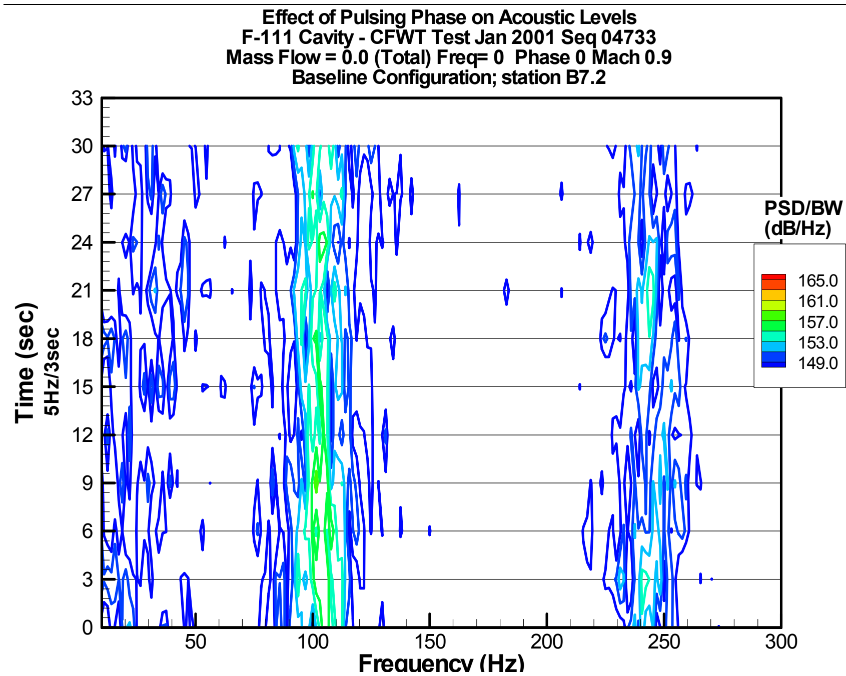

Figure 18. Chart showing major tones in the spectrum

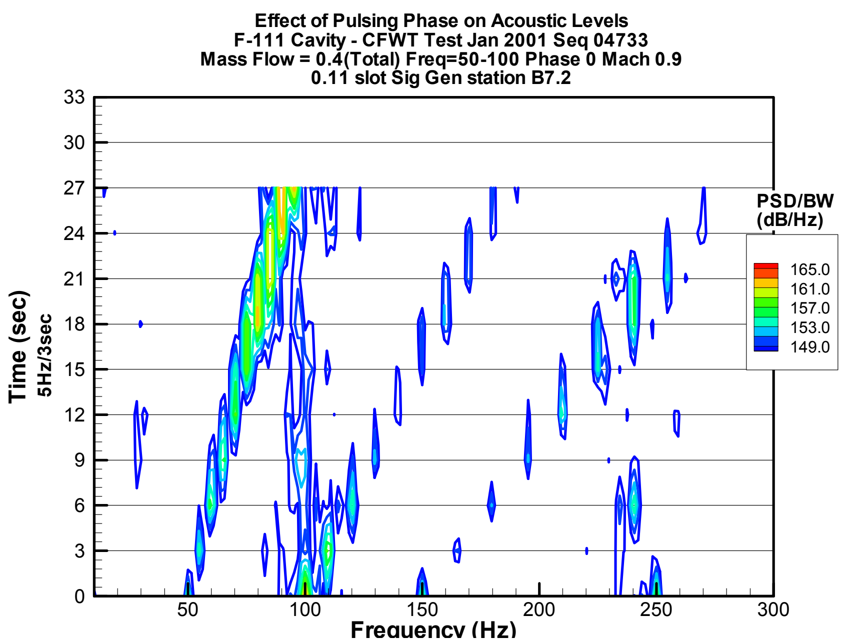

Figure 19. Chart showing effect of pulsed blowing on major tones

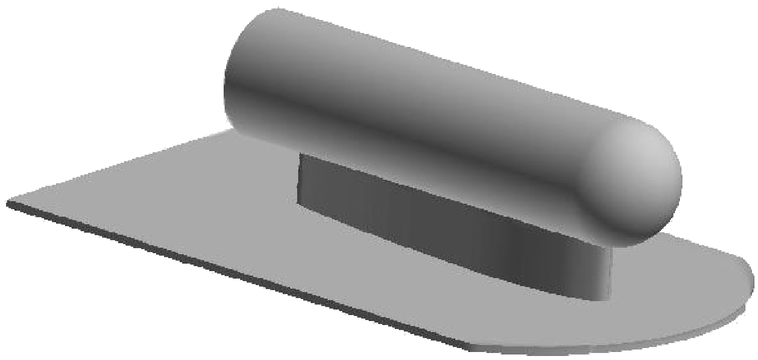

Figure 20. Drawing of pod configuration

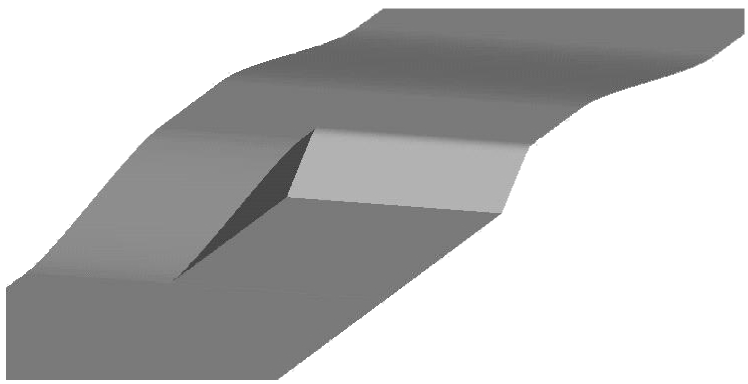

Figure 21. Drawing of the rearward facing ramp

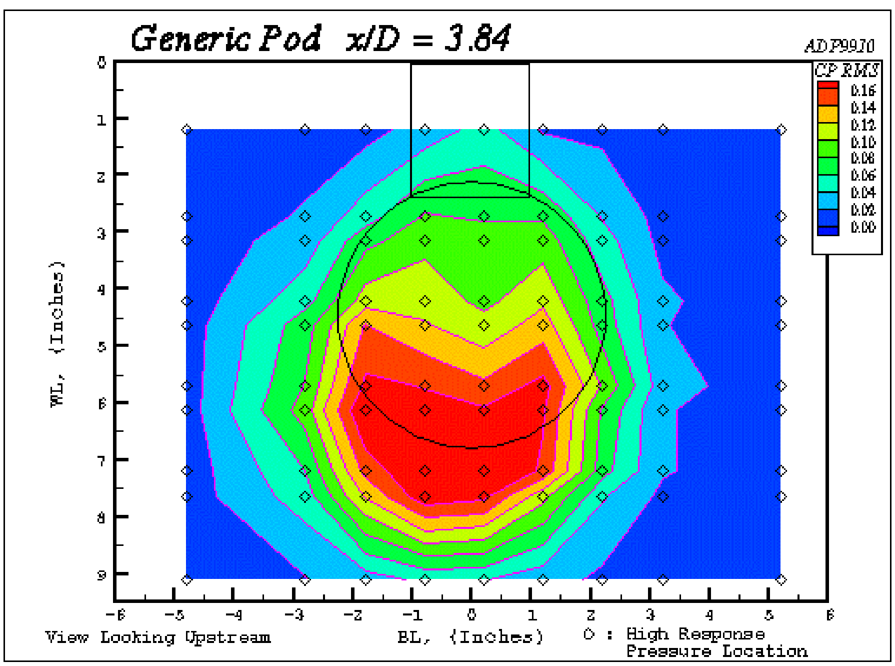

Figure 22. RMS pressure coefficients downstream of the baseline pod
(Data are referenced to tunnel static pressure)

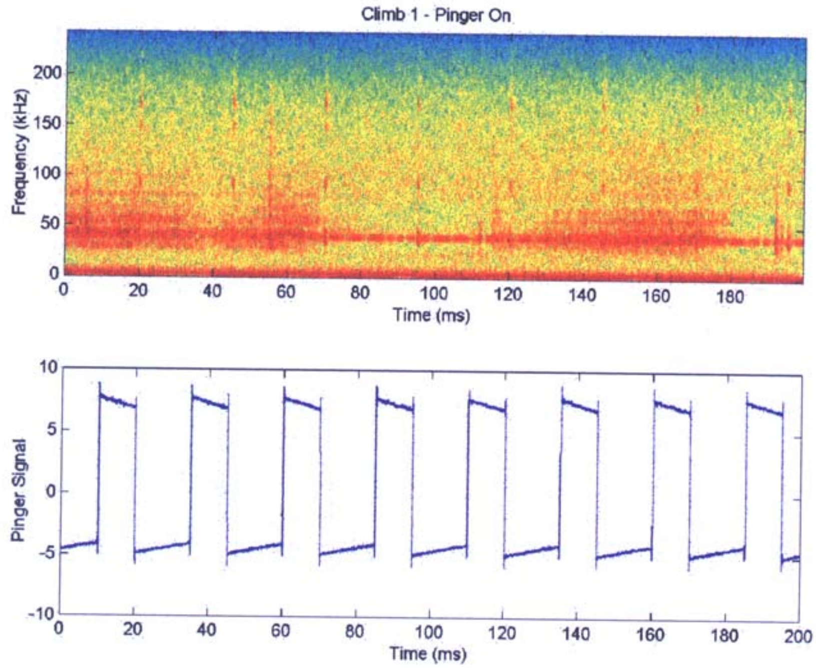

Figure 23. Spectrogram for climb maneuver

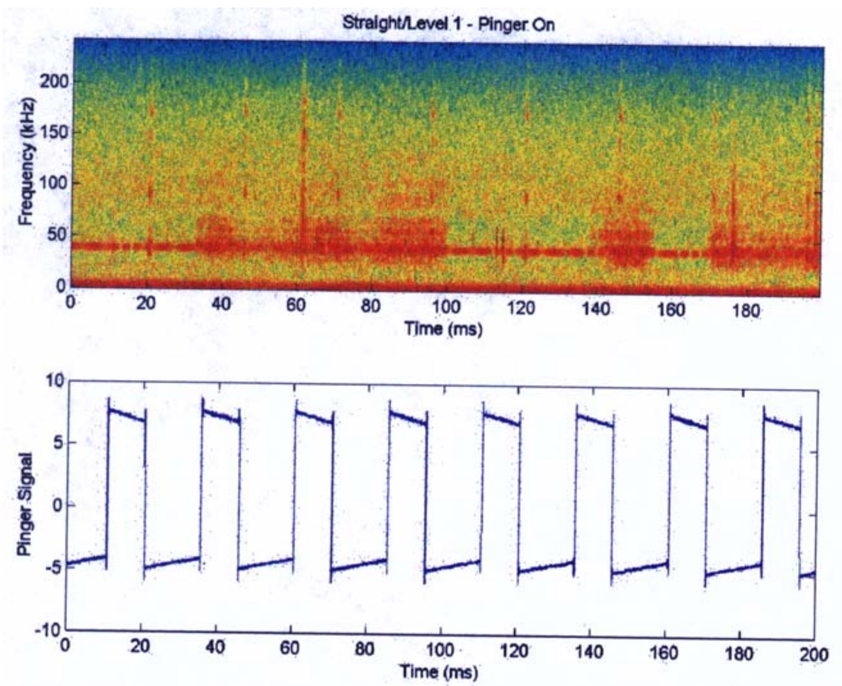

Figure 24. Spectrogram for straight and level maneuver

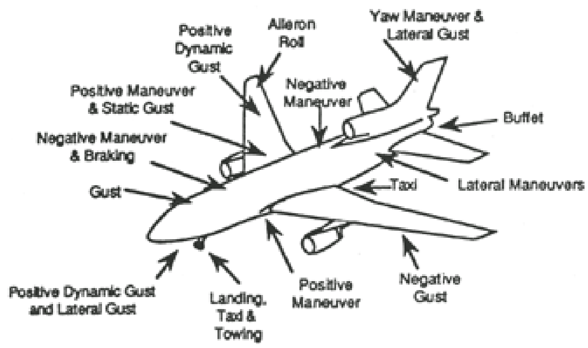

Figure 25. Operational Flight and Ground Loads

Figure 26. Flight Recorder

Figure 27. Instrumented Aircraft

Figure 28. Aircraft Landing Loads

Figure 29. FAA Video Landing Loads Survey Facility

Figure 30. Lightning Environment

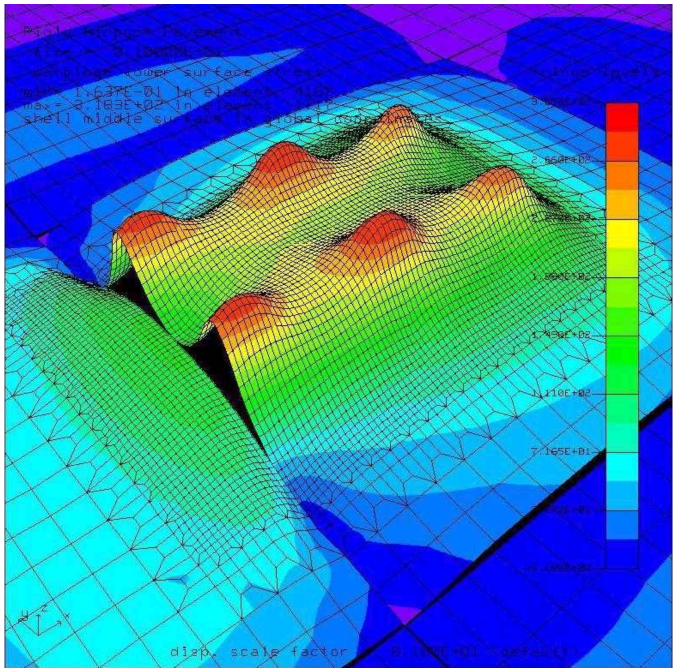

Figure 31. B-777 bending stress on the bottom plane of a rigid pavement slab

Figure 32. Cellular cement arrestor bed brings aircraft to a safe stop at JFK airport (May 8, 1999)

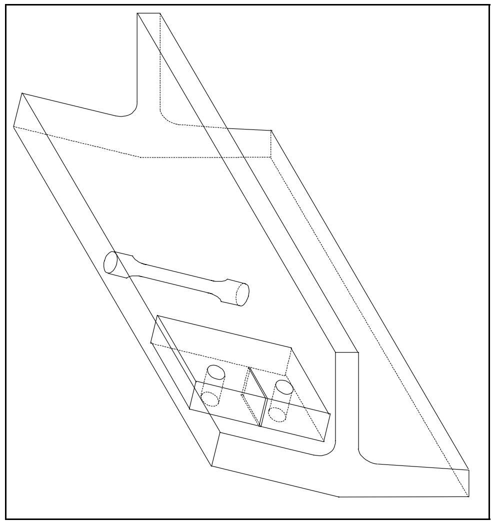

Figure 33. Specimen orientation

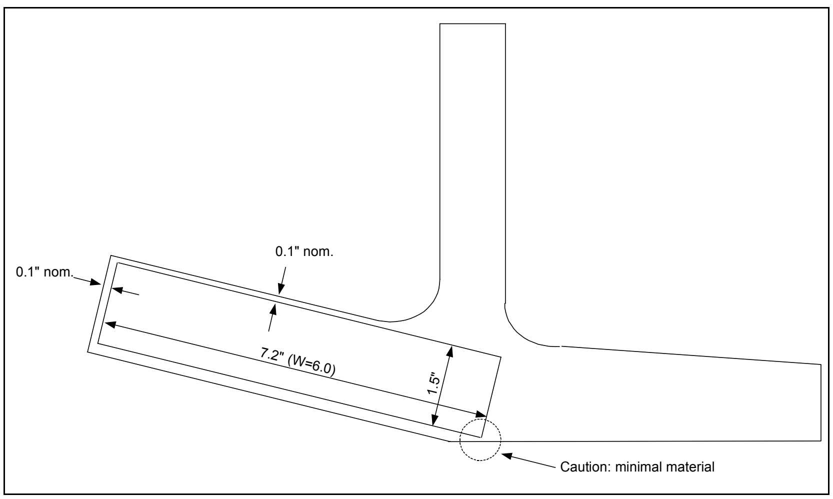

Figure 34. Suggested location for 1.5" thick specimens

Material/Thickness	Crack Growth (K_{FCG}) ksi-in^0.5	Plane Stress Toughness (K_{app}) ksi-in^0.5	Plane Strain Toughness (K_Q) ksi-in^0.5
2024-T3511 (1.2")	20.6	54.8	n/a
2024-T3511 (1.5")	20.2	53.5	n/a
2024-T3511 (1.75")	n/a	n/a	32.5
2224-T3511 (1.2")	22.4	63.1	n/a
2224-T3511 (1.5")	23.1	61.9	n/a
2224-T3511 (1.75")	n/a	n/a	45.1

Table 1. Phase I preliminary crack growth K_{FCG} (in air) and toughness values (K_{app} and K_Q) for the 2024-T3511 and 2224-T3511 T-chord extrusions. K_{FCG} is the normalized stress intensity at a crack growth rate of 10^{-4} in/cycle. K_{app} is similar to K_C, based on R-curve test results.

Material/Thickness	Crack Growth (K_{FCG}) % difference	Plane Stress Toughness (K_{app}) % difference	Plane Strain Toughness (K_Q) % difference
2224-T3511 (1.2") **vs.** 2024-T3511 (1.2")	+ 8.7	+ 15.1	n/a
2224-T3511 (1.5") **vs.** 2024-T3511 (1.5")	+ 14.4	+ 15.7	n/a
2224-T3511 (1.75") **vs.** 2024-T3511 (1.75")	n/a	n/a	+ 38.8

Table 2. Percent difference. 2224-T3511 vs. 2024-T3511 (baseline) from Table 1.

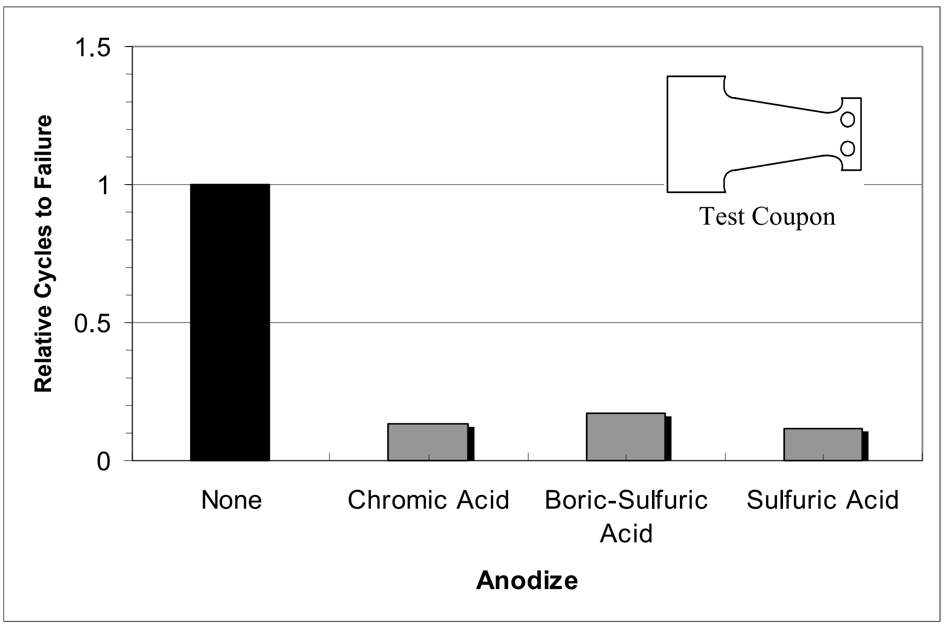

Figure 35. Chromic, boric sulfuric, and sulfuric acid anodize vs. 2024-T3 bare sheet

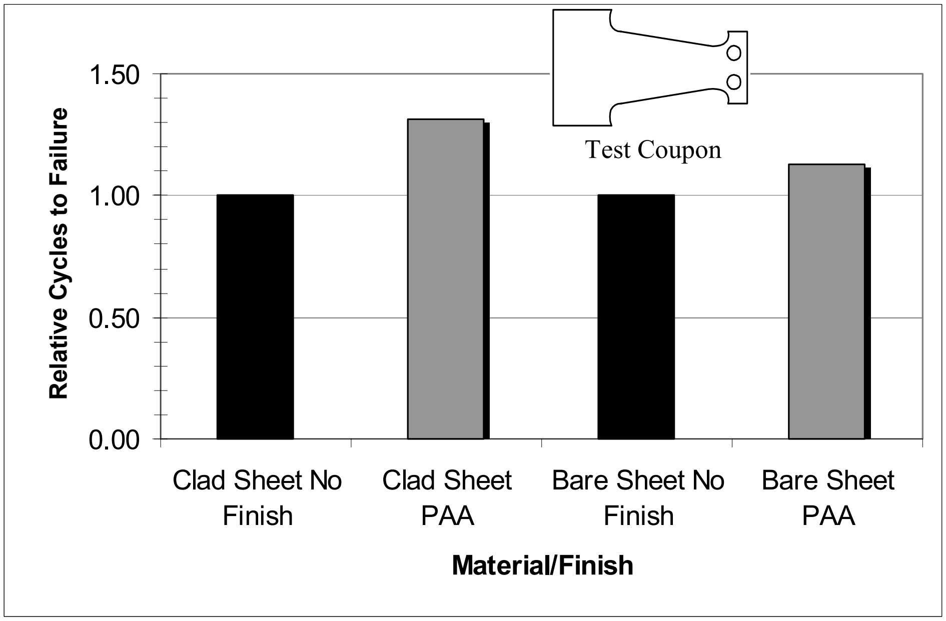

Figure 36. PAA Effects on Fatigue of 2024-T3 clad sheet

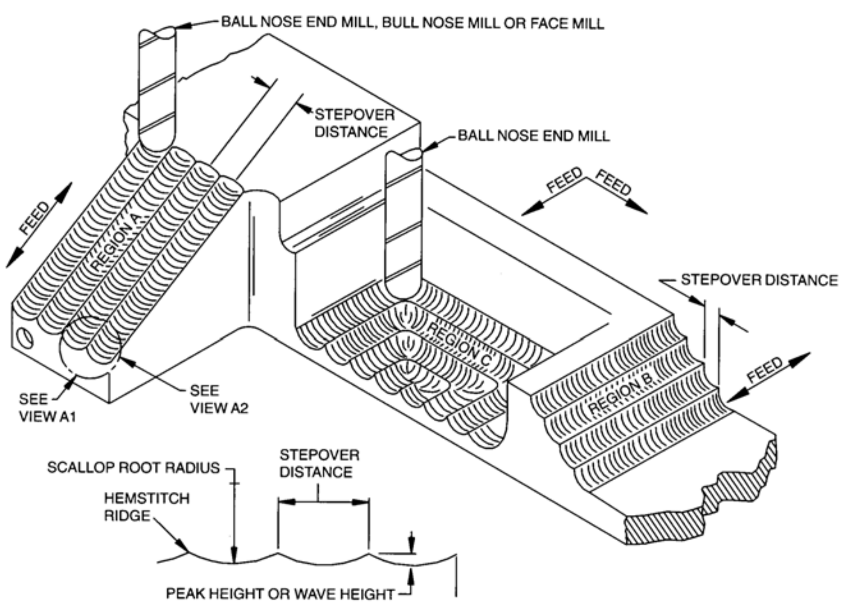

Figure 37. Hemstitch surface

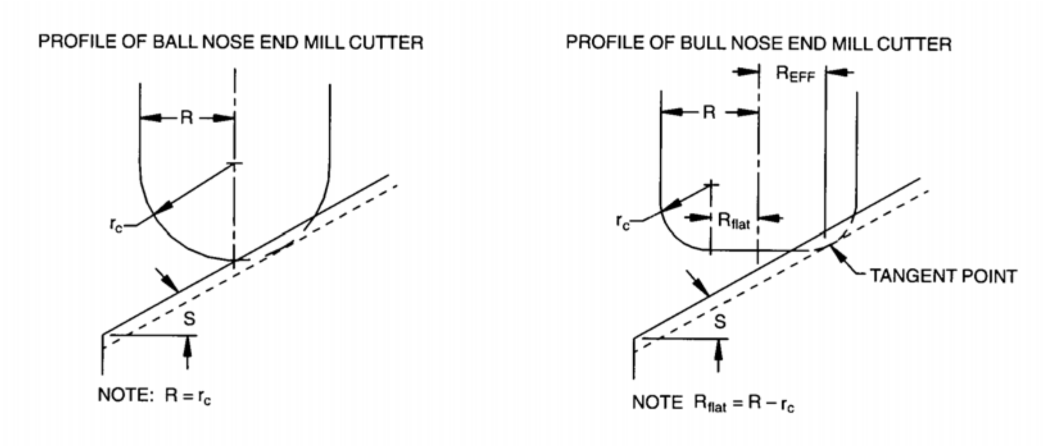

Figure 38. Ballnose and bullnose cutters

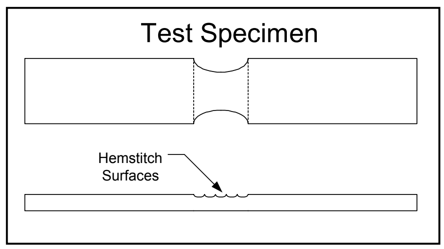

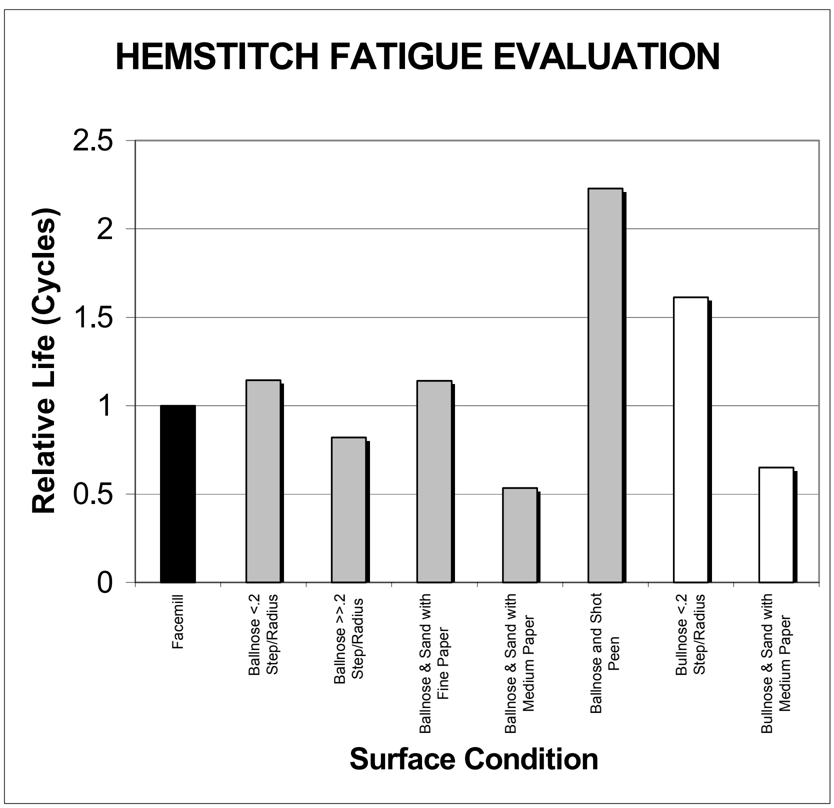

Figure 39. Hemstitch fatigue testing trends

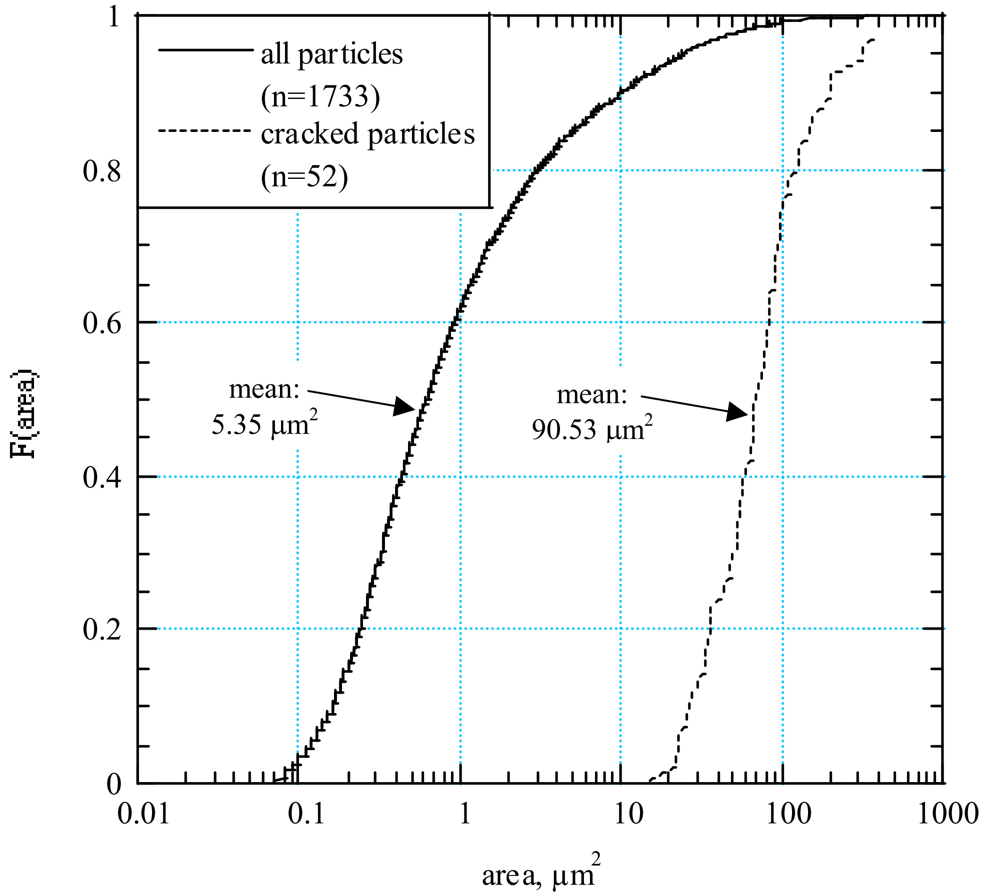

Figure 40. Comparison shows that the distribution of cracked particles for 2024-T3 aluminum comes from the upper tail of the overall particle distribution

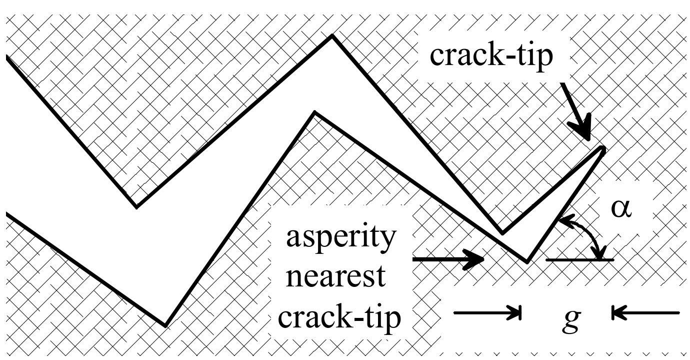

Figure 41. Schematic of rough crack idealized as a sawtooth

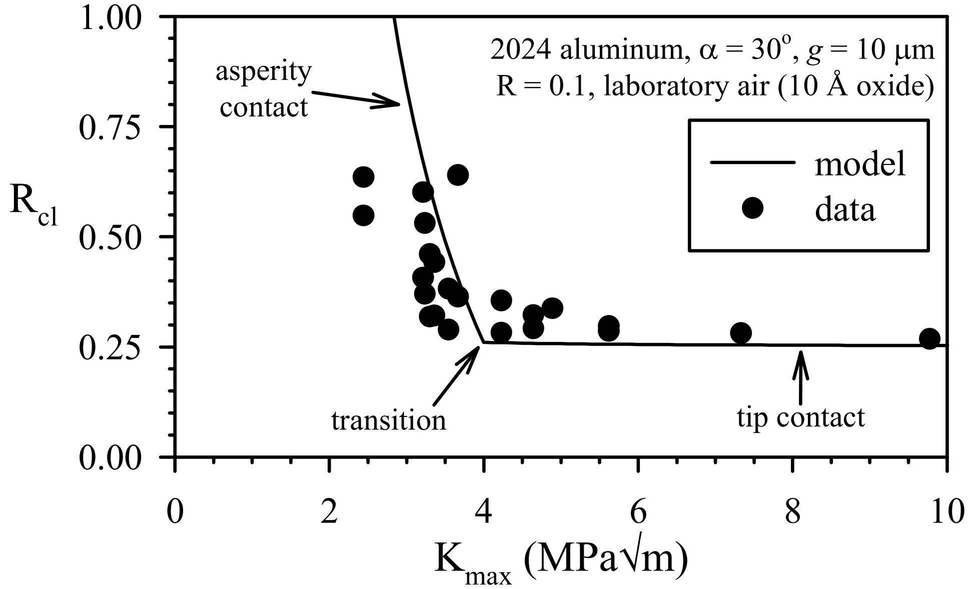

Figure 42. Comparison of model results and experimental data for 2024 aluminum alloy

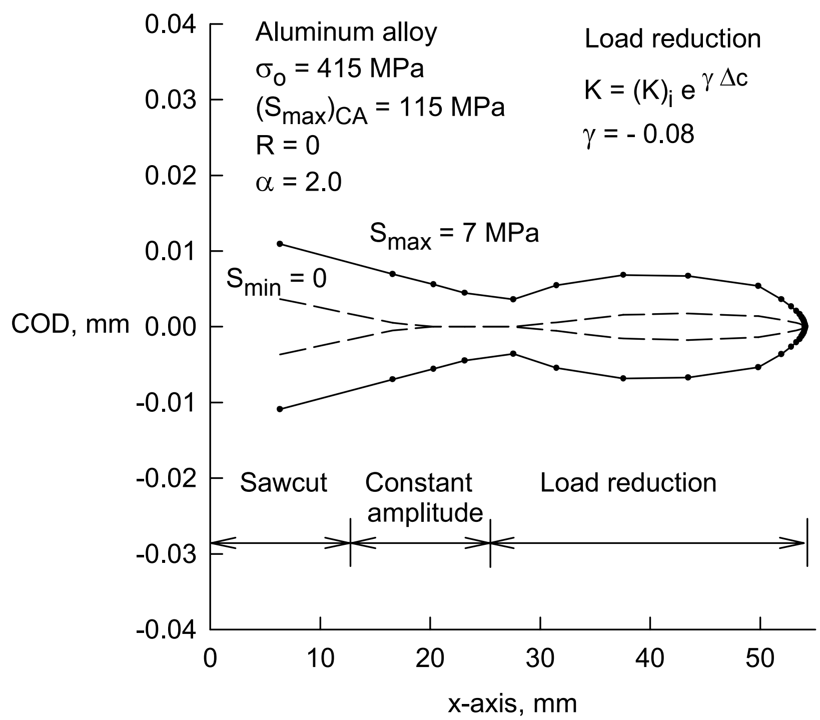

Figure 43. Computed crack-surface displacements after load reduction under high constraint conditions and low-stress ratio (R = 0) conditions

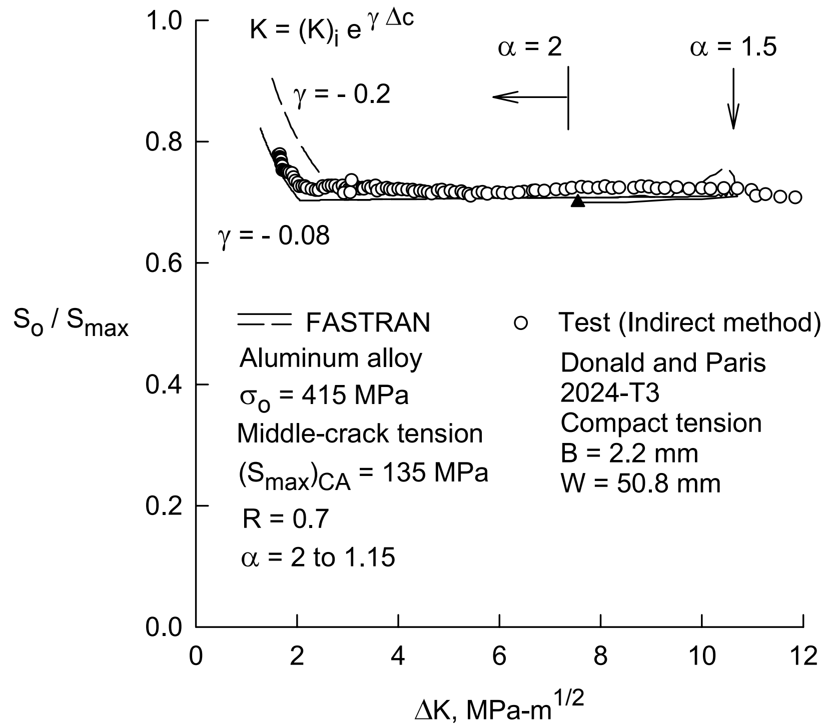

Figure 44. Measured and computed crack-opening behavior for high-stress ratio (R = 0.7) conditions

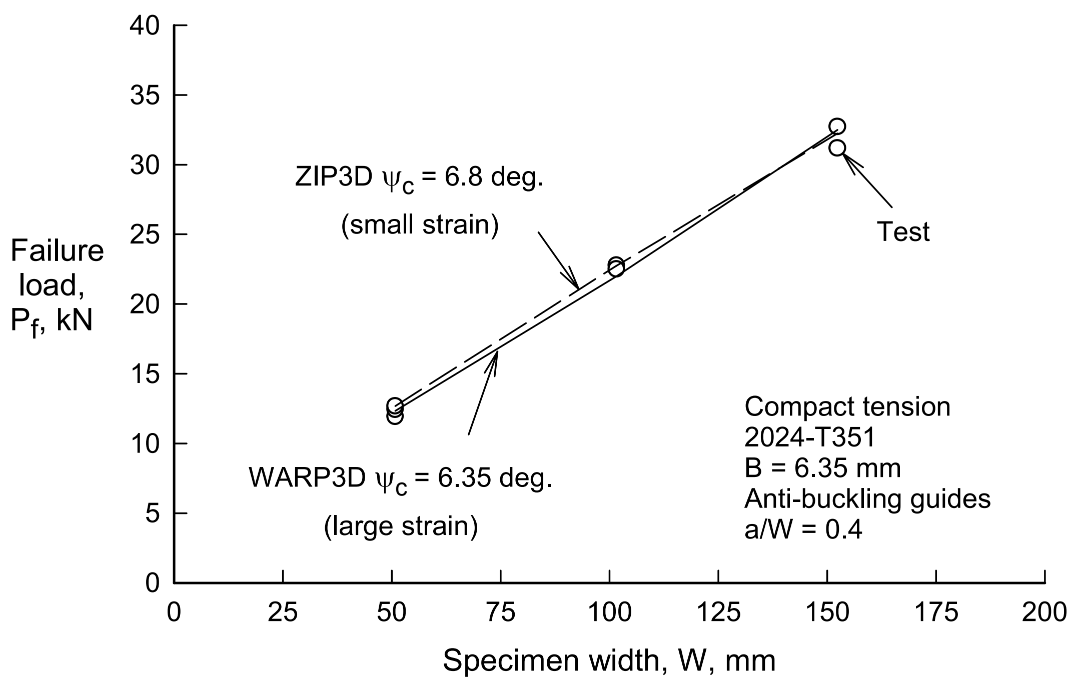

Figure 45. Measured and calculated failure loads for compact tension specimens

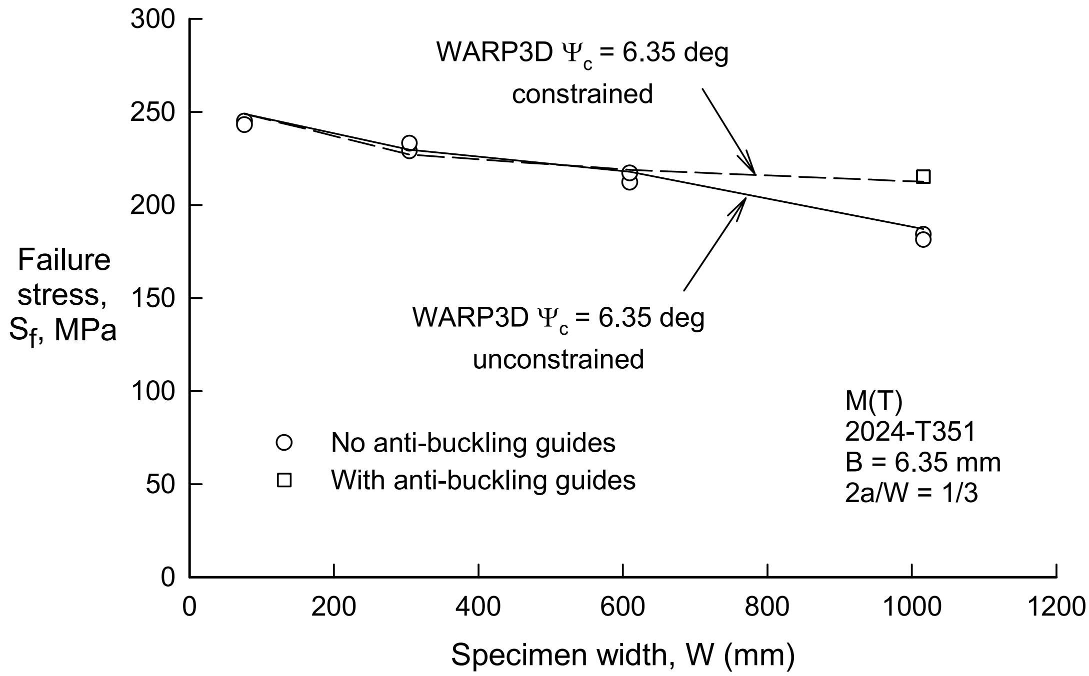

Figure 46. Measured and predicted failure stresses for middle-crack tension panels with and without anti-buckling guides

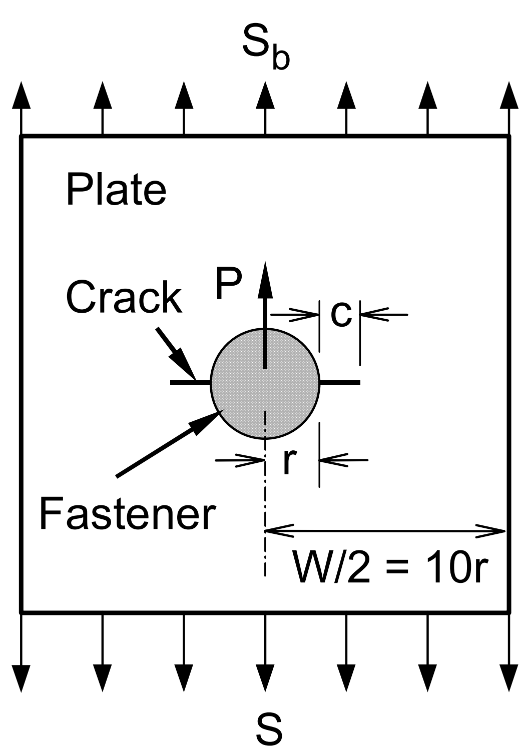

Figure 47. Interference-fit fastener under combined loading

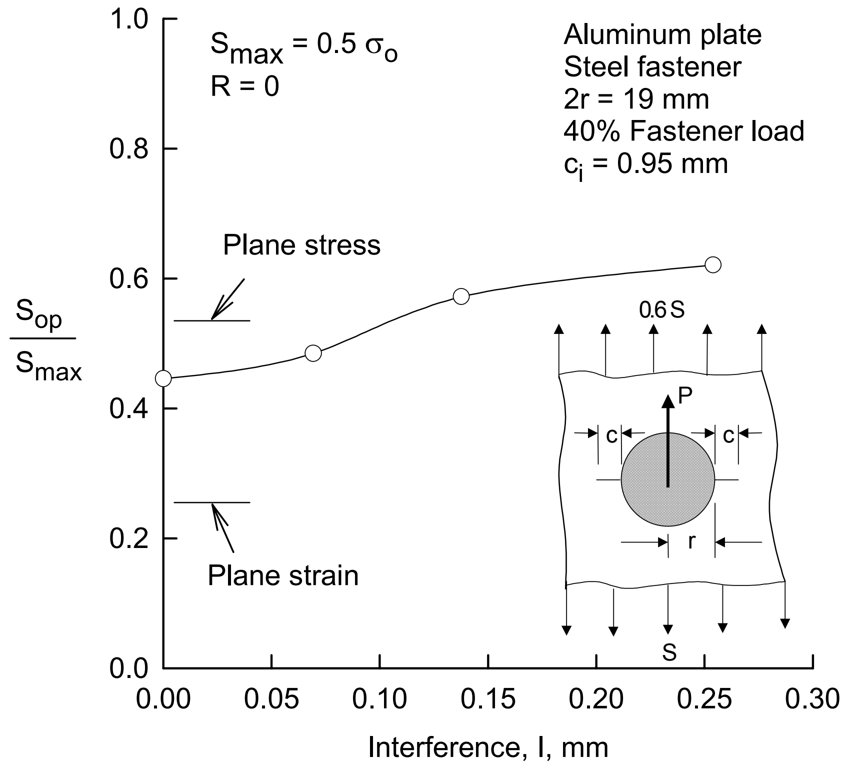

Figure 48. Calculated crack-opening stress levels for cracks growing from various interence-fit fastener holes

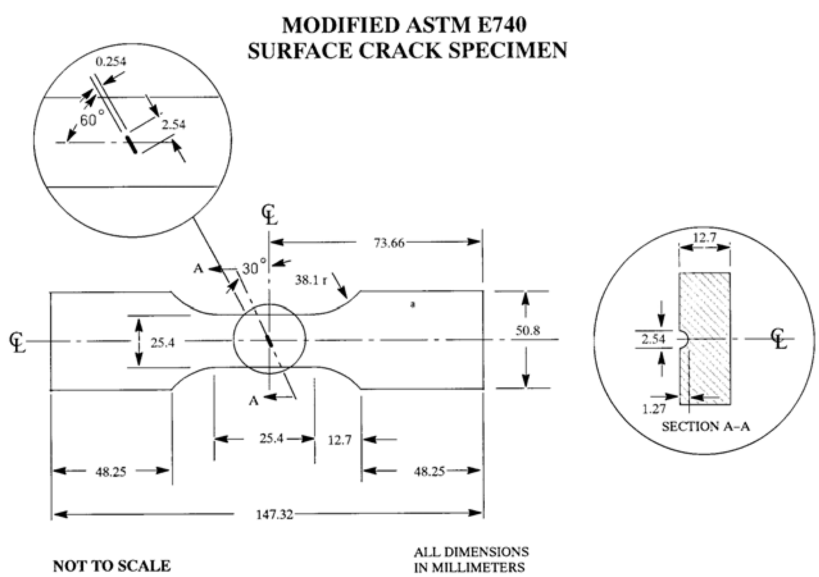

Figure 49. Mixed-mode crack growth specimen design

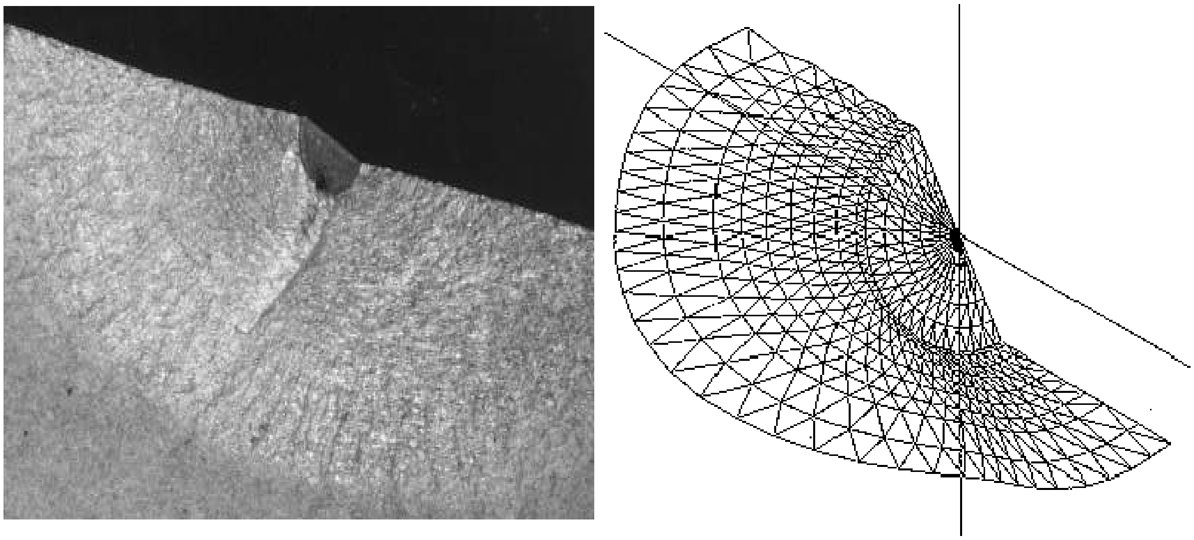

Figure 50. Mixed-mode crack growth for 60-degree case (mesh and photo)

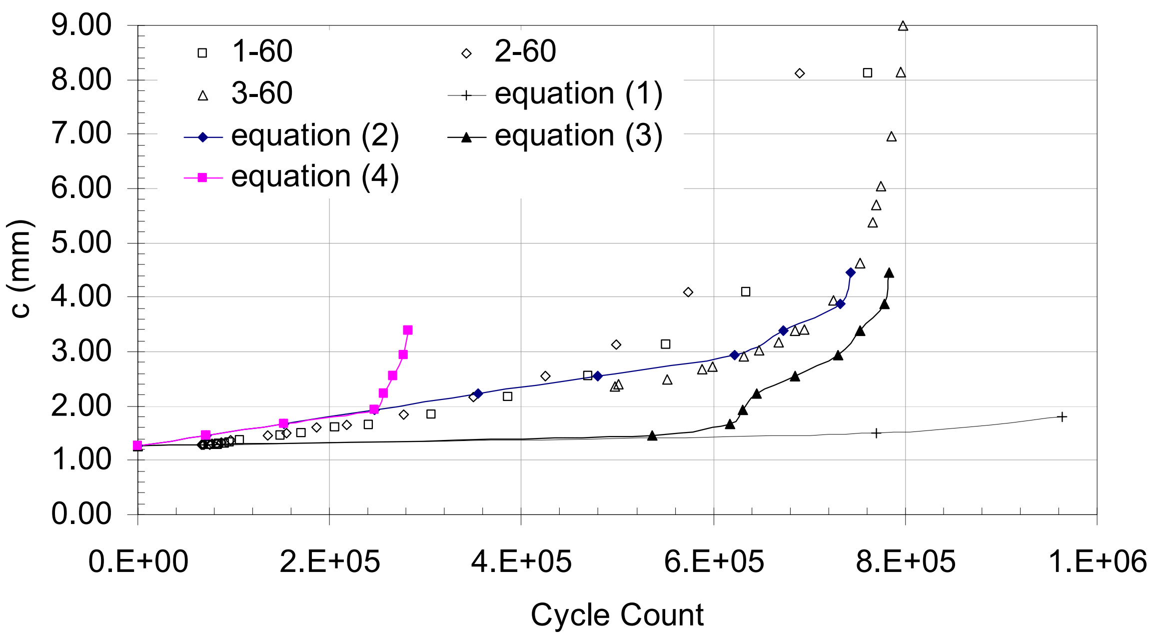

Figure 51. Comparison of energy equivalence theories, θ = 60 degrees

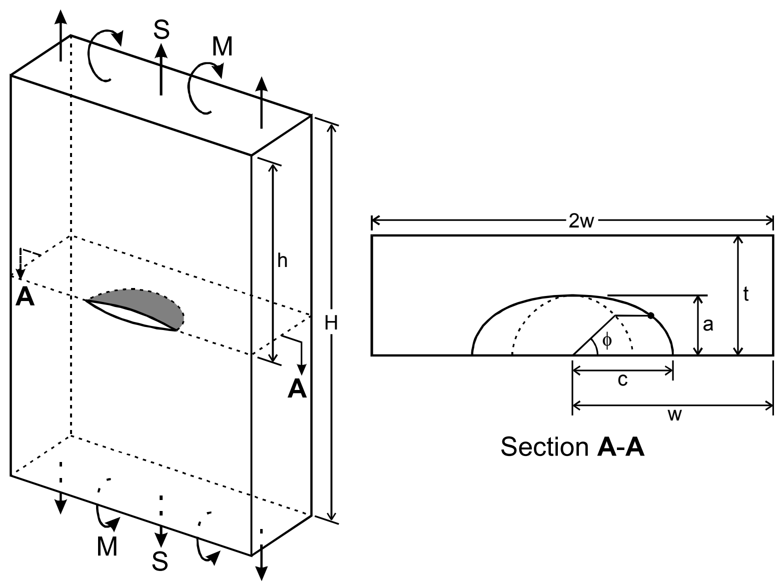

Figure 52. Surface-crack configuration subjected to remote tension and bending

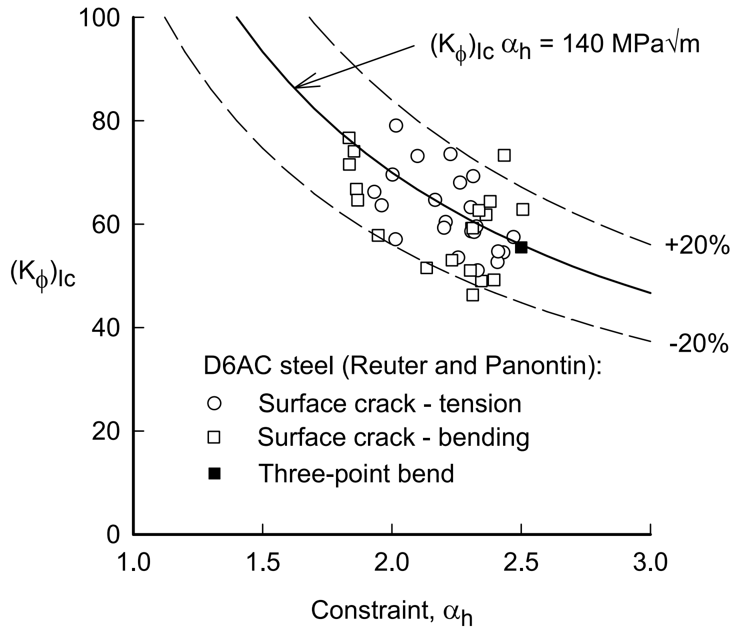

Figure 53. Correlation of fracture toughness from through-the-thickness cracks and surface cracks subjected to tension or bending loads

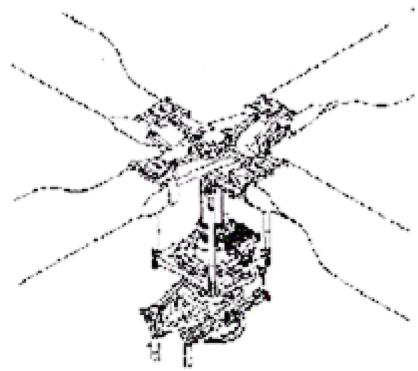

Figure 54. Model 430 main rotor idler link

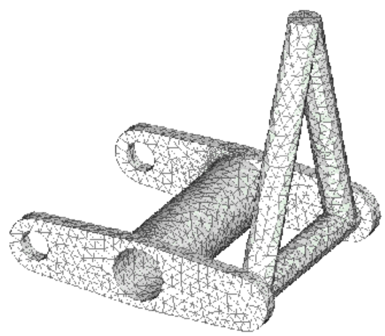

Figure 55. Global mesh of the main rotor idler link consisting of tetrahedral quadratic elements

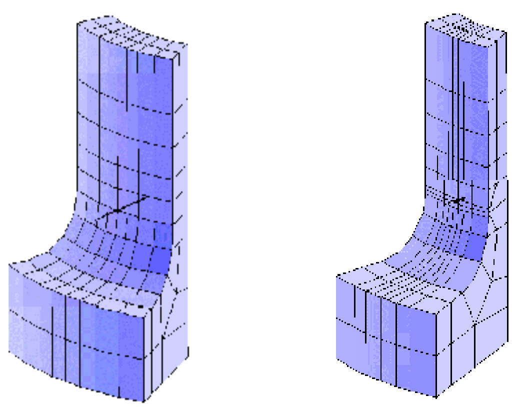

Figure 56. A model for the local analysis of the idler link component for small and large cracks

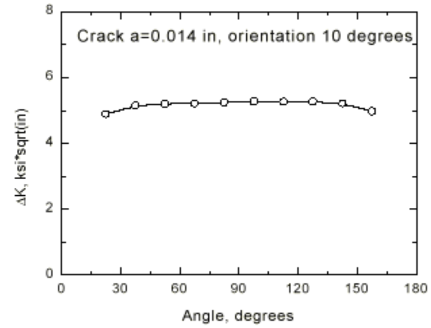

Figure 57. Stress-intensity factors ΔK for crack 2a = 0.028 inch

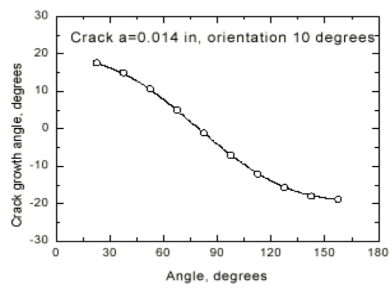

Figure 58. Crack growth angle for crack 2a = 0.028 inch

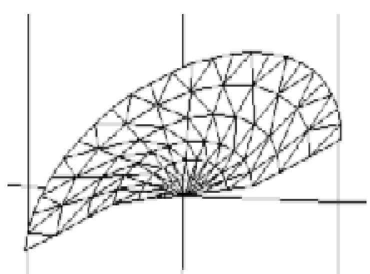

Figure 59. Predicted final crack configuration of the crack after fatigue precracking for the Model 430 main rotor idler link

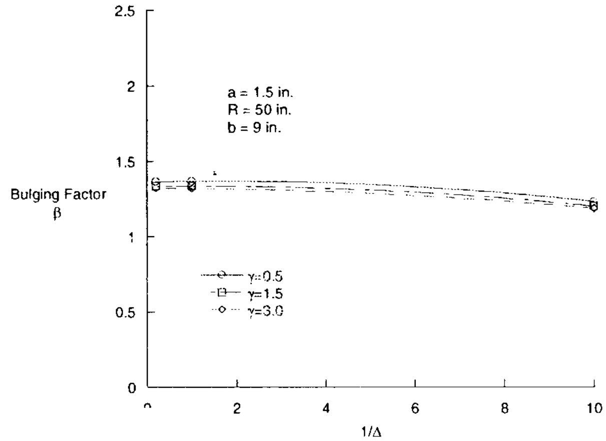

Figure 60. Bulging factors for α = 1.0

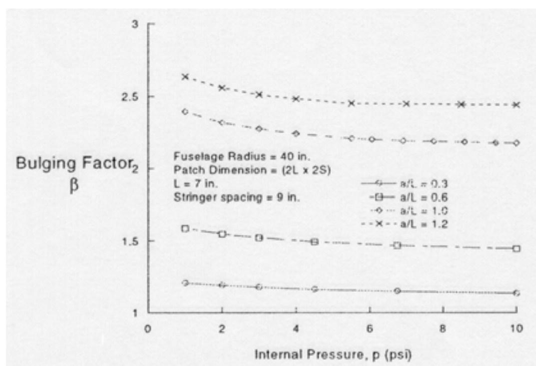

Figure 61. Bulding factor for stiffened fuselage with a repair

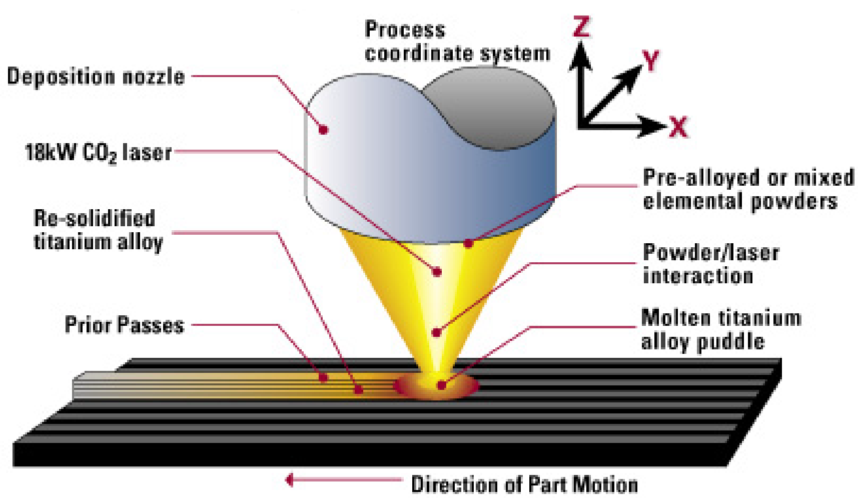

Figure 62. The AeroMet^{TM} laser additive manufacturing process

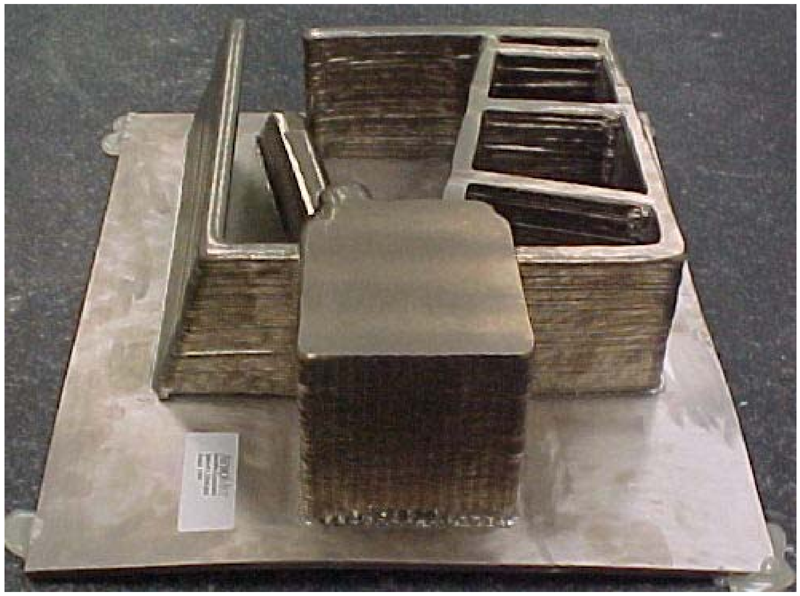

Figure 63. 45cm x 35cm wrought base plate

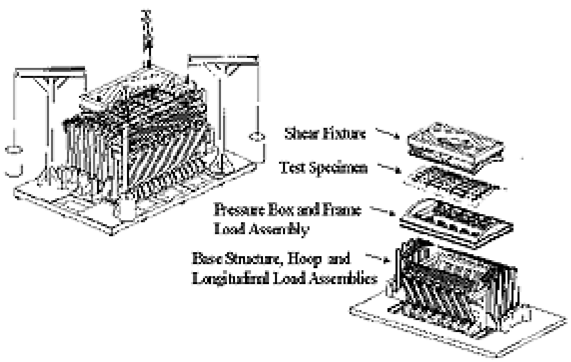

Figure 64. FASTER Facility

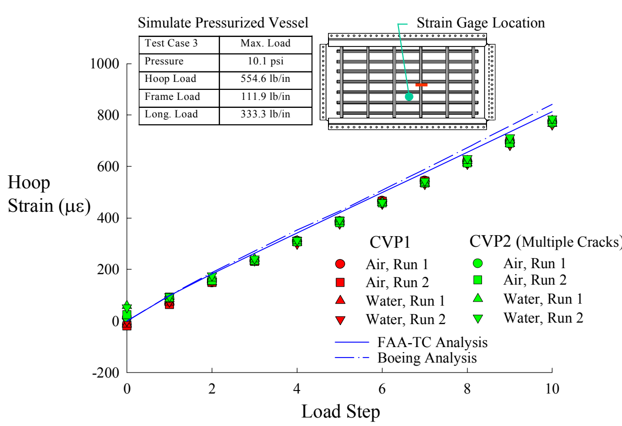

Figure 65. The measured and predicted hoop strain at gages in the middle of a skin bay in CVP1 (lead crack only) and CVP2 (lead crack and multiple cracks) panels are plotted as a function of load step.

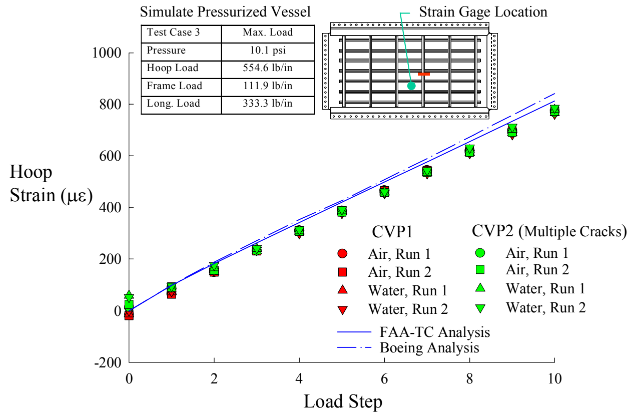

Figure 66. The effect of multiple cracks on the lead crack growth behavior

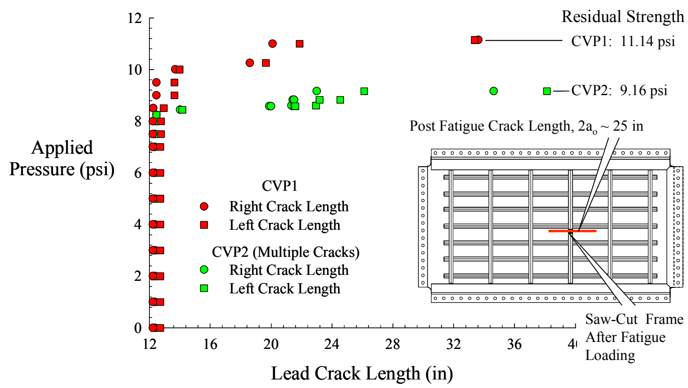

Figure 67. The effect of multiple cracks on the residual strength behavior

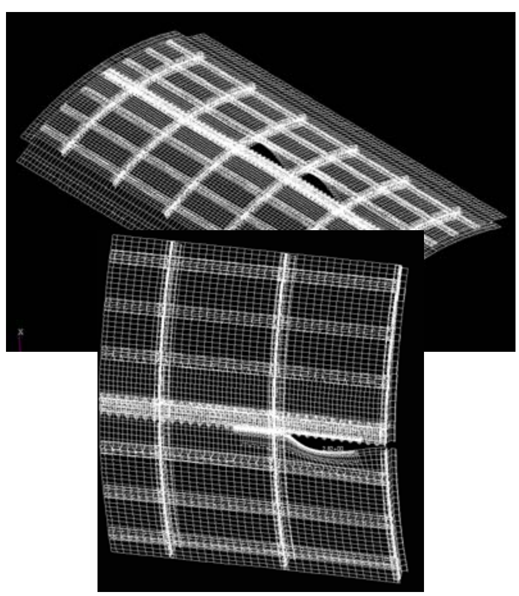

Figure 68. FEM curved panel model

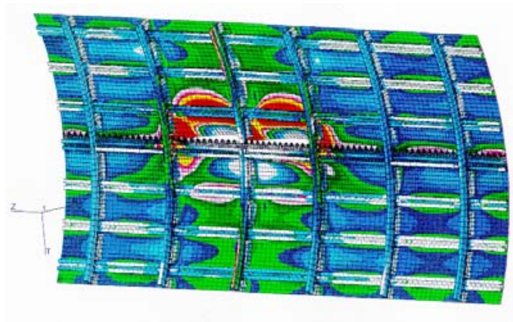

Figure 69. Principle stress at the panel inner surface in deformed shape

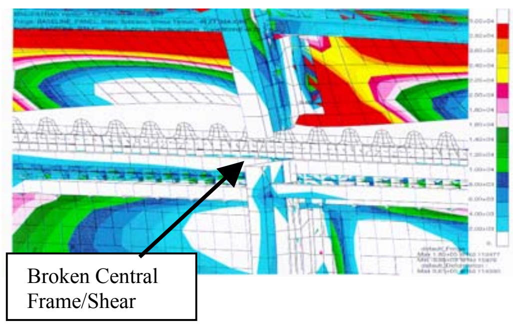

Figure 70. Stress plot at the broken frame

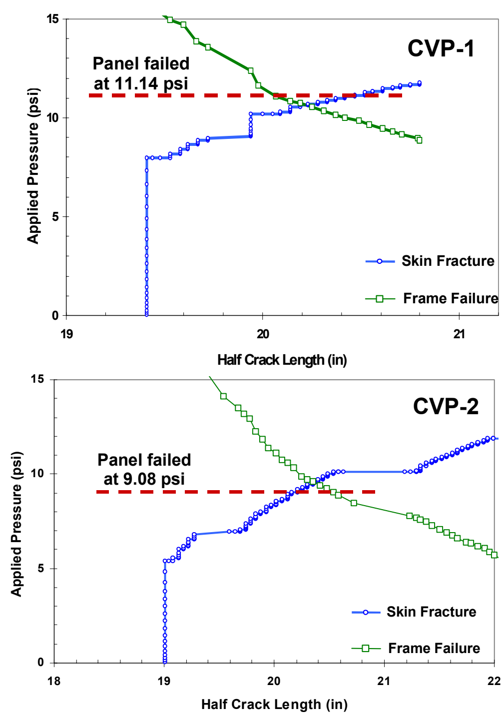

Figure 71. The analysis results for curved panels CVP1 and CVP2

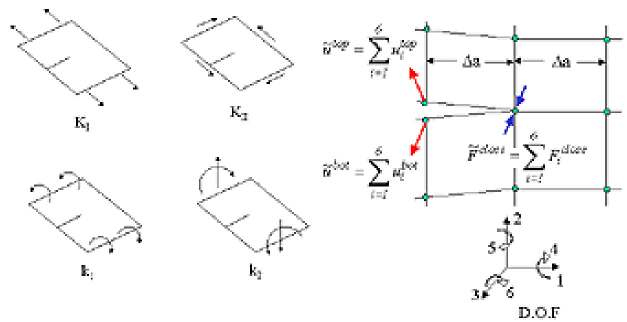

Figure 72. Calculation of the SIF caused by tensile load, K_I, in-plane shear load, K_{II}, symmetric bending loads, k_1, and out-of-plane shear and twist loads, k_2

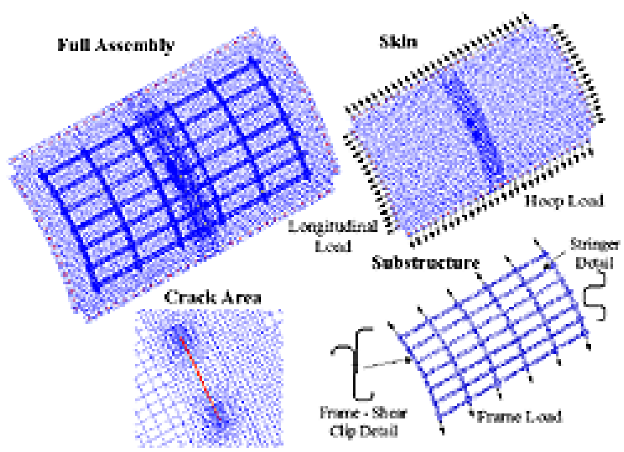

Figure 73. Details of the test panels were modeled using two-dimensional shell elements with each node having six degrees of freedom

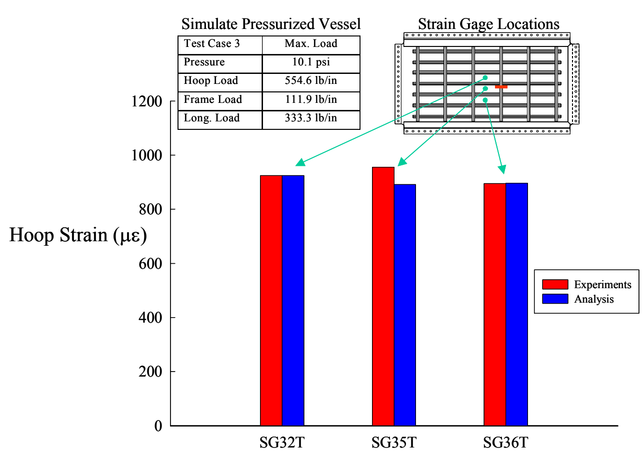

Figure 74. The measured and predicted hoop strain at gages in the middle of a skin bay in CVP1 panels

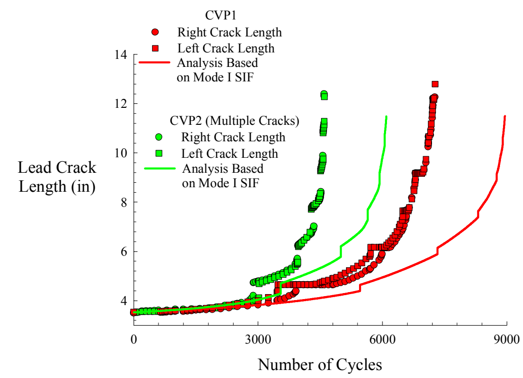

Figure 75. The measured and predicted fatigue crack growth behavior for CVP1 (lead crack only) and CVP2 (lead crack and multiple cracks) panels

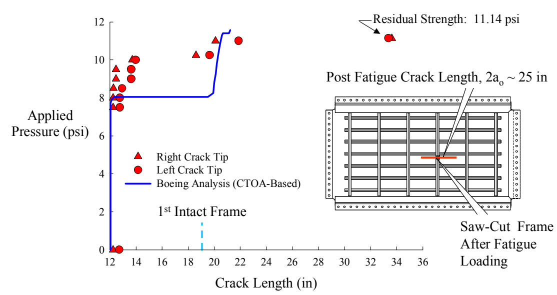

Figure 76. The measured and predicted residual strength behavior for CVP1

Figure 77. Test device consisting of an array of linear variable differential translation (LVDT) displacement transducers oriented normal to the panel surface

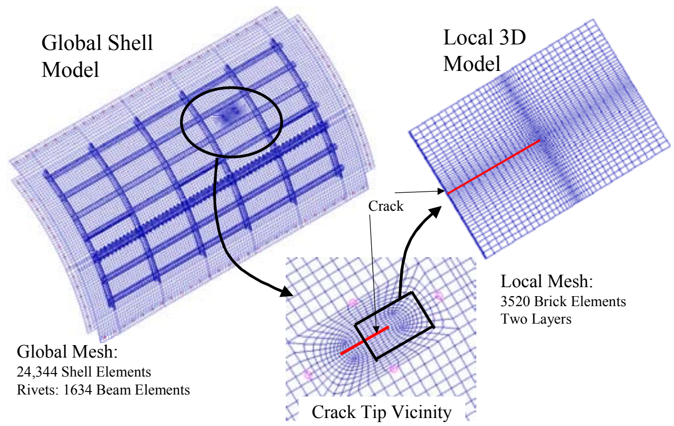

Figure 78. GLH methodology that was used to analyze the test panels

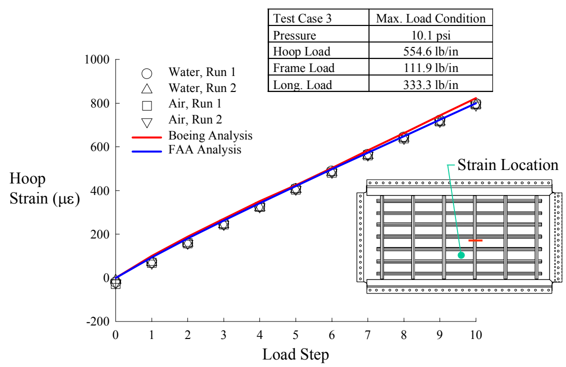

Figure 79. Measured and predicted hoop strains in the middle of a skin bay

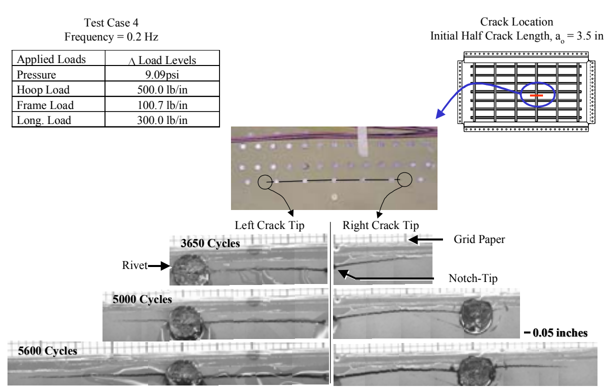

Figure 80. Images from the RCCM system showing the crack extension from the two tips of the crack

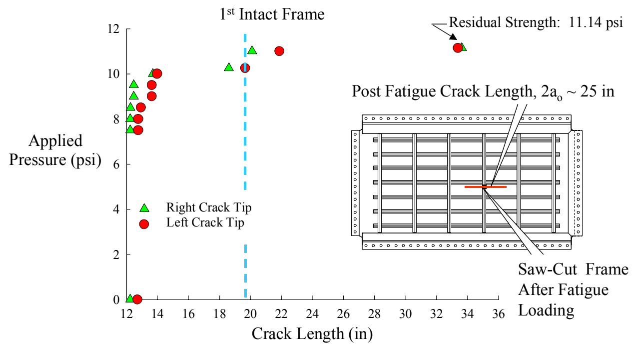

Figure 81. Failed panel at a pressure of 11.14 psi (the residual strength)

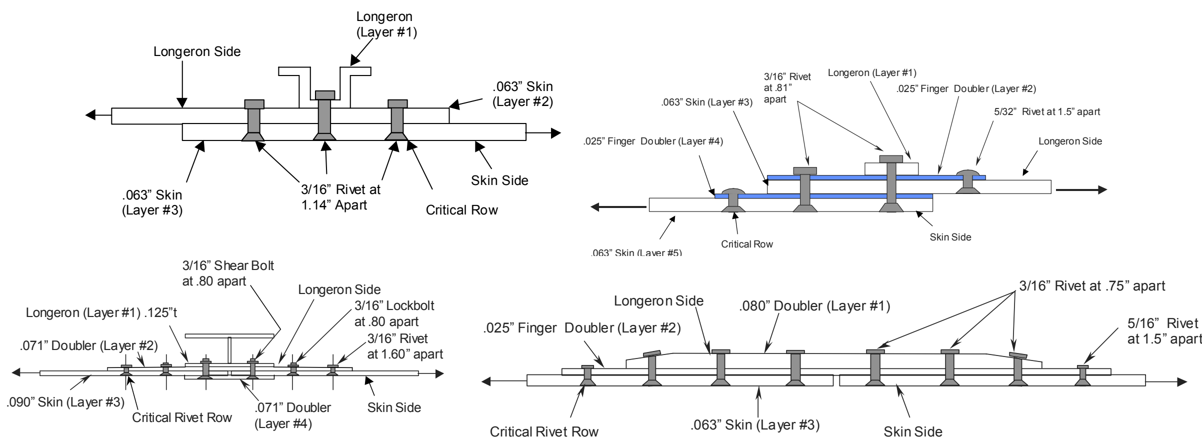

Figure 82. MSD panel joint types

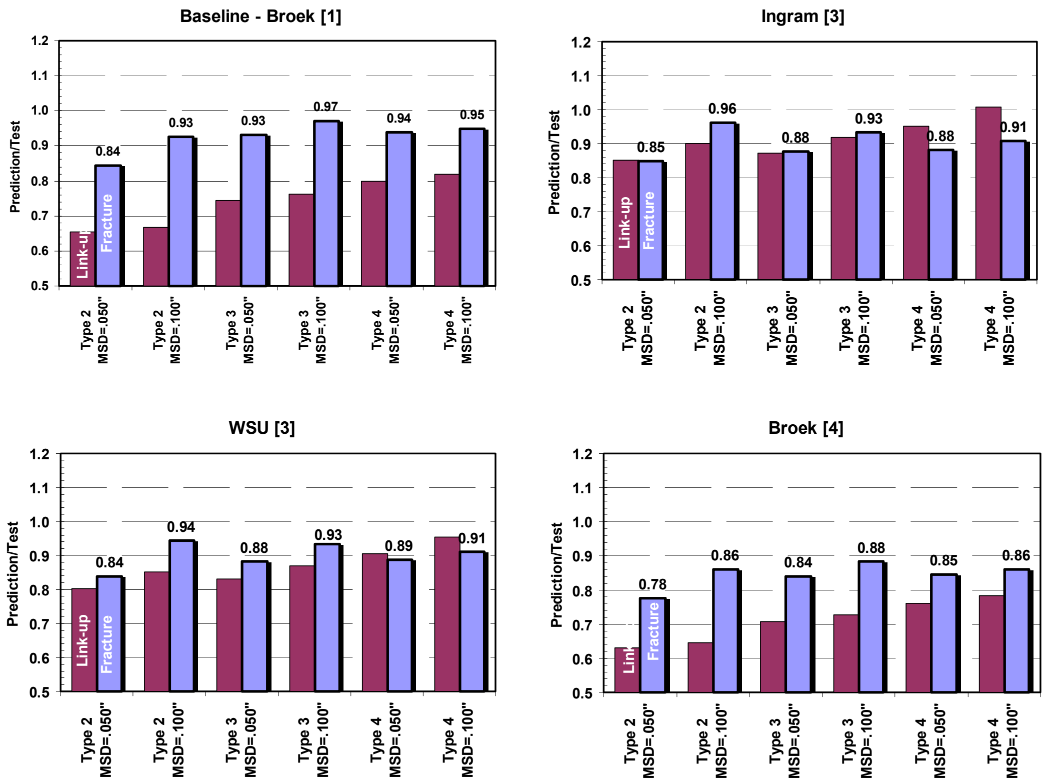

Figure 83. Comparison of residual strength predictions using ligament yield criteria

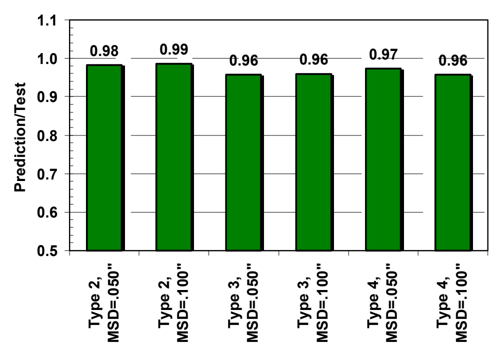

Figure 84. Comparison of residual strength predictions using T* integral criterion

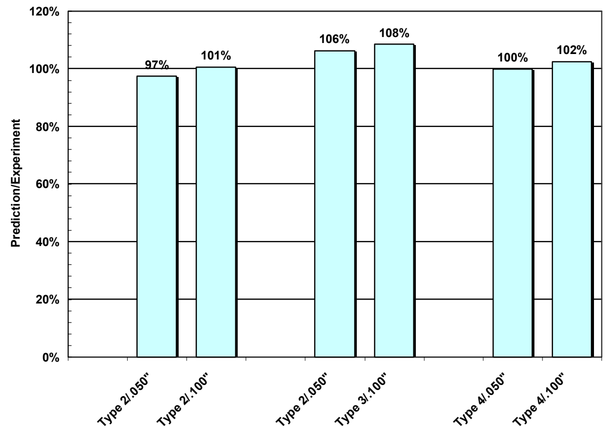

Figure 85. Comparison of residual strength predictions using CTOA criterion

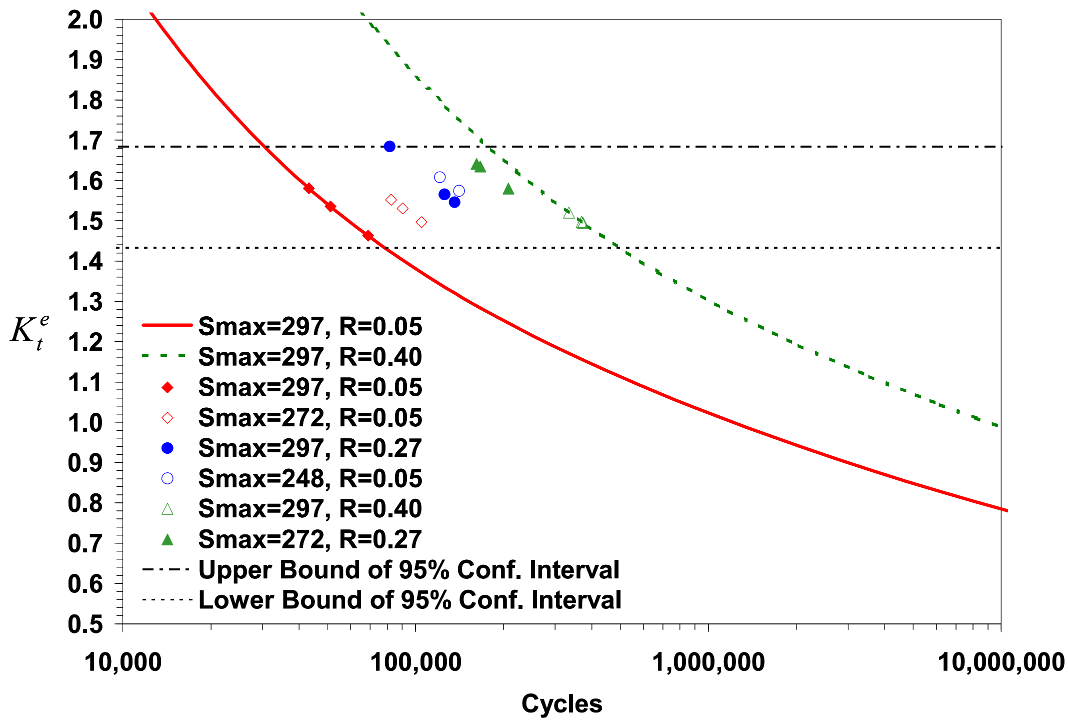

Figure 86. Individual fatigue test results (pre-corroded) and strain-based fatigue analysis using ASM Al 2024-T351 material constants - cycles verses K_t^e

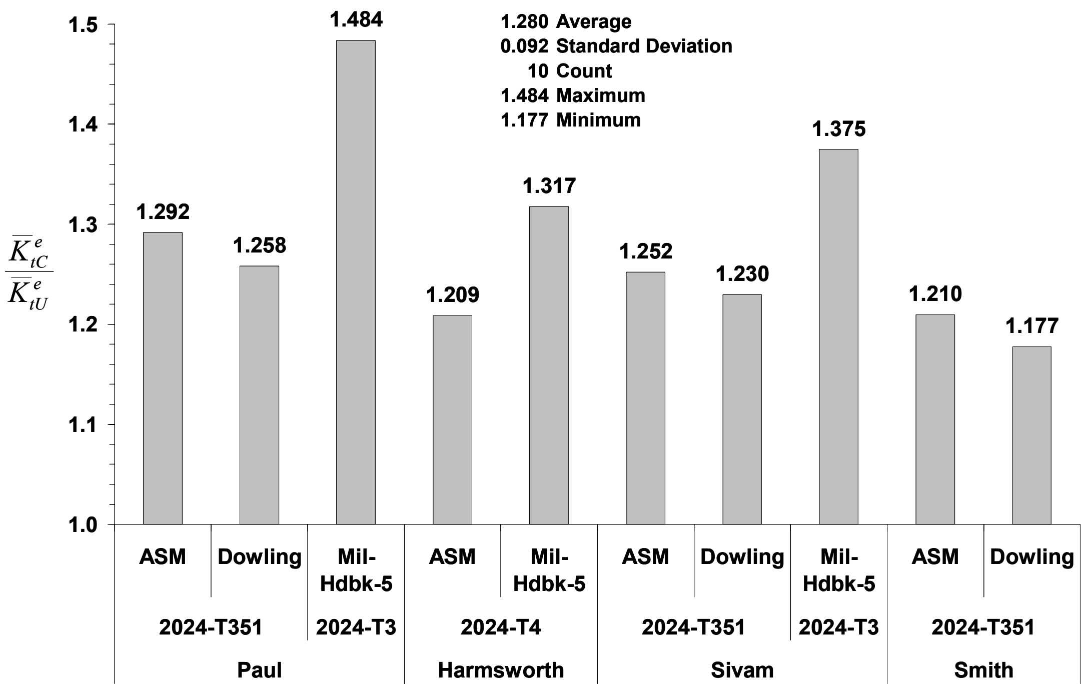

Figure 87. $\overline{K}_{tC}^{e} \big/ \overline{K}_{tU}^{e}$ **values using fatigue life data from author and other studies**

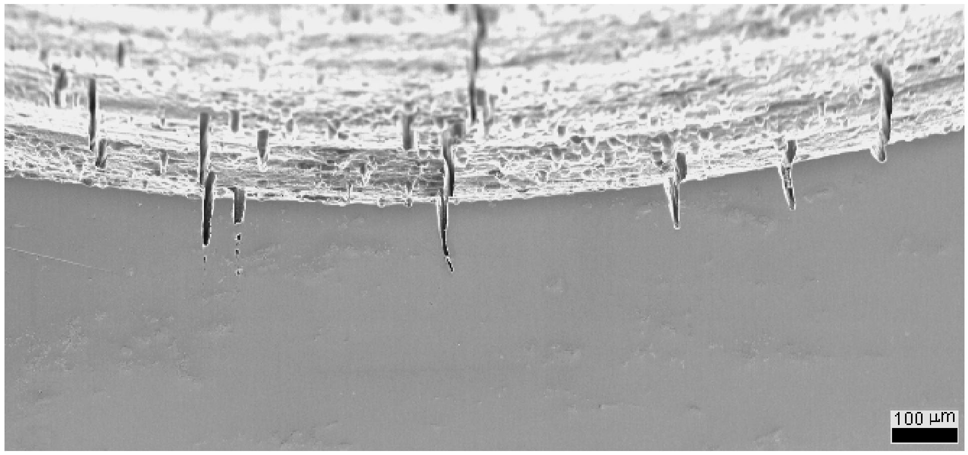

Figure 88. A typical SEM micrograph (at 30° tilt and 50X) showing numerous cracks and corrosion damage in a fastener hole

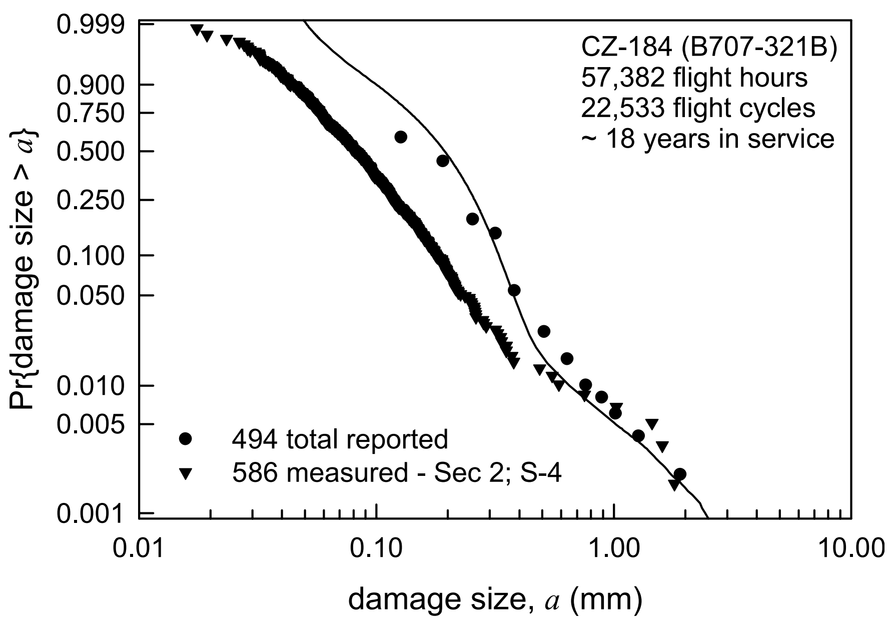

Figure 89. Comparison of the PoO for all MHWC lengths reported by J-STARS and all of those measured using video imaging microscopy for 110 holes along stiffener 4 (with steel fasteners) from the CZ-184 aircraft

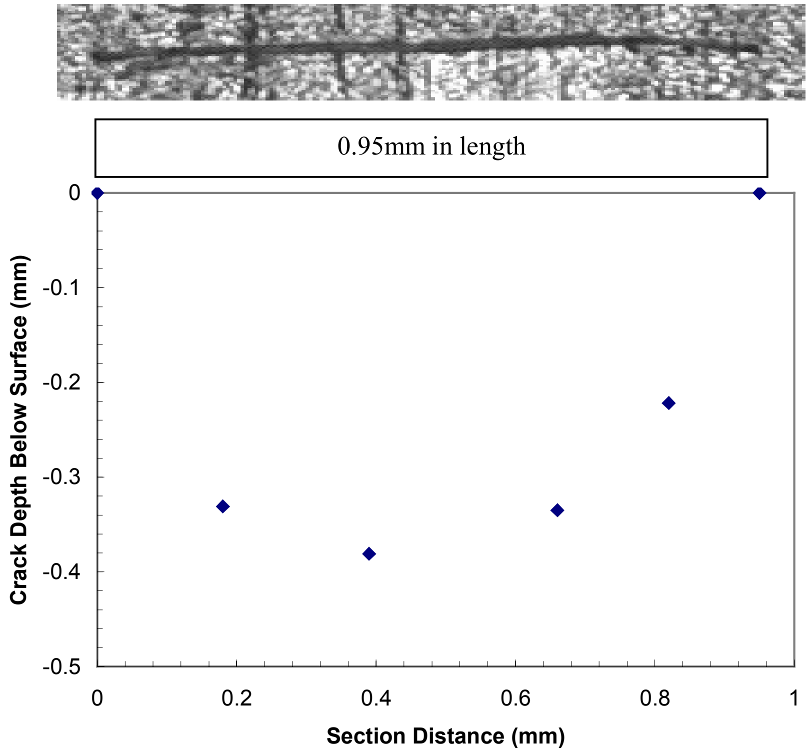

Figure 90. Typical profile of an isolated crack in a fastener hole, obtained from SEM images of serial sections, along with its optical micrographic image

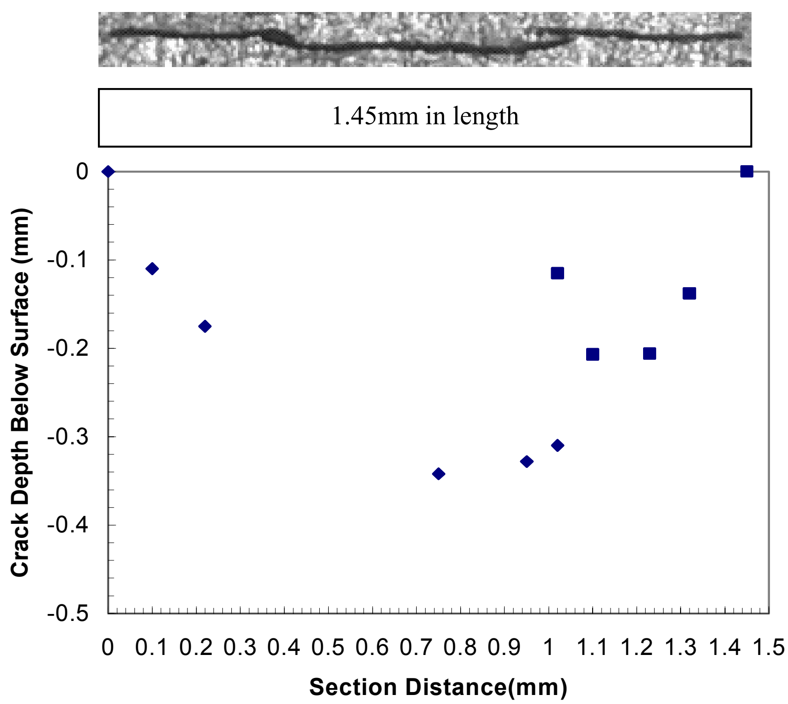

Figure 91. Typical profile showing the linkup of three cracks in a fastener hole, obtained from SEM images of serial sections, along with their optical micrographic image

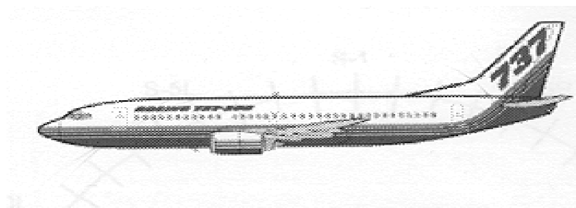

Figure 92.

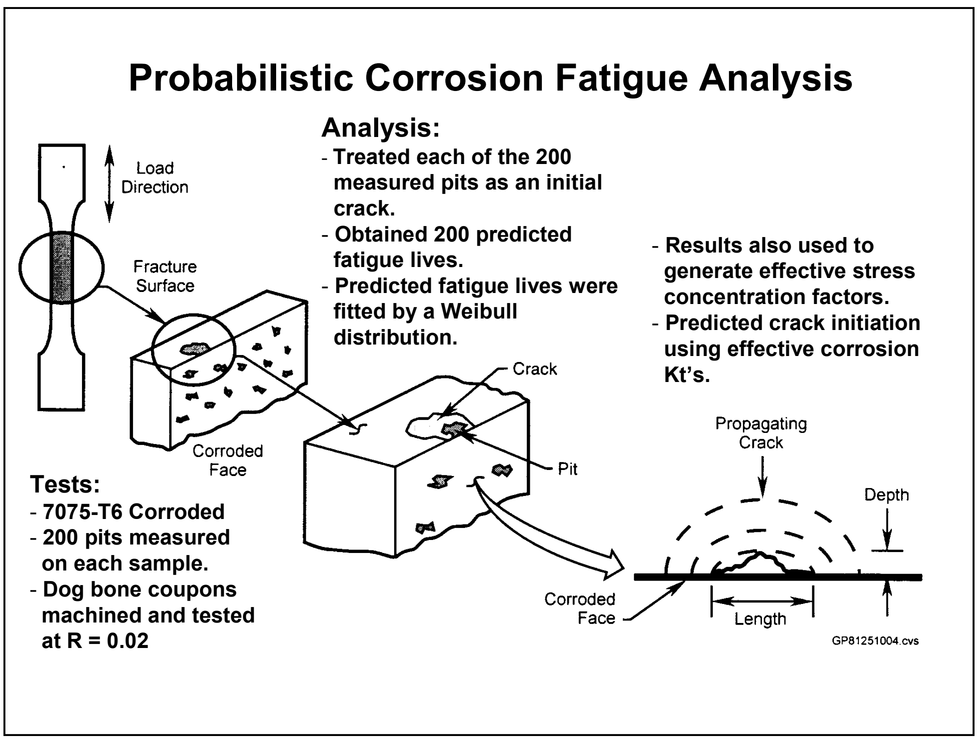

Figure 93. Probabilistic corrosion fatigue analysis

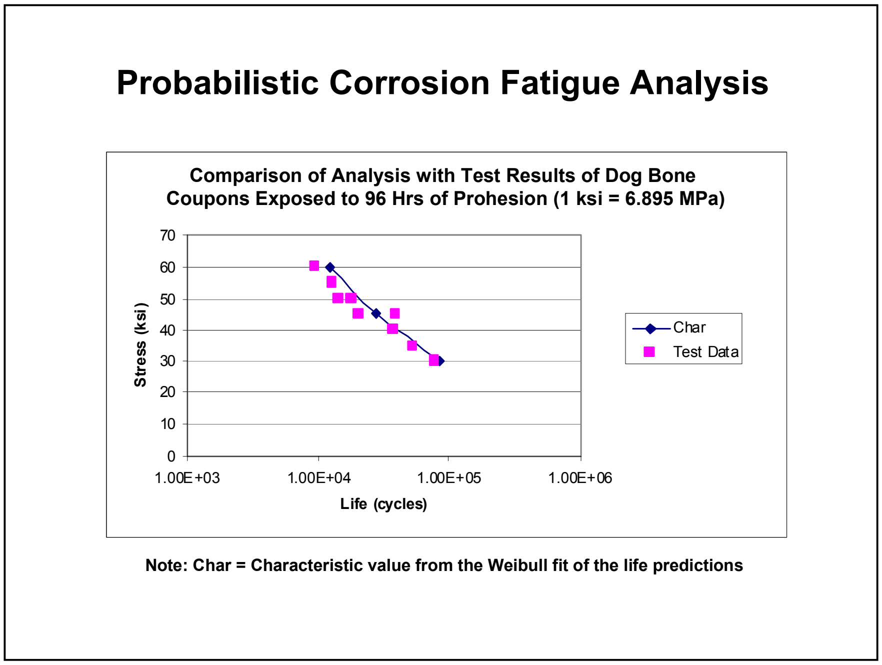

Figure 94. Comparison of analysis with test results

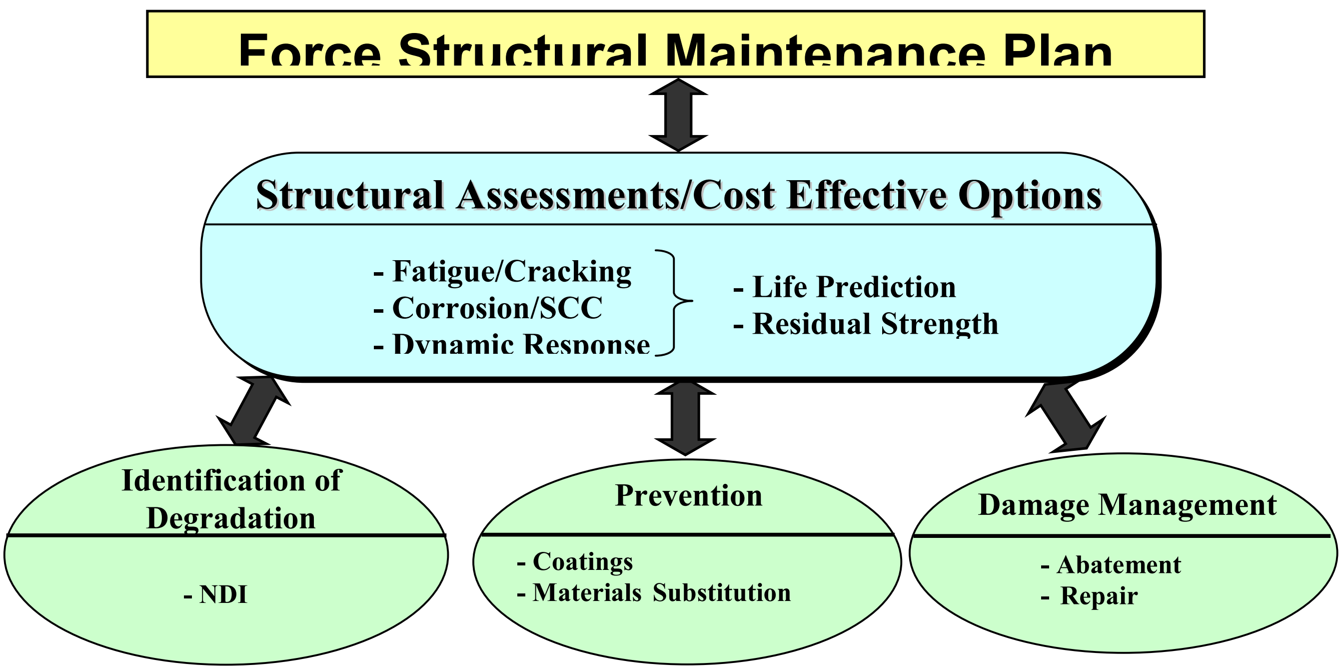

Figure 95. Schematic of corrosion effects on structural integrity strategic technology plan

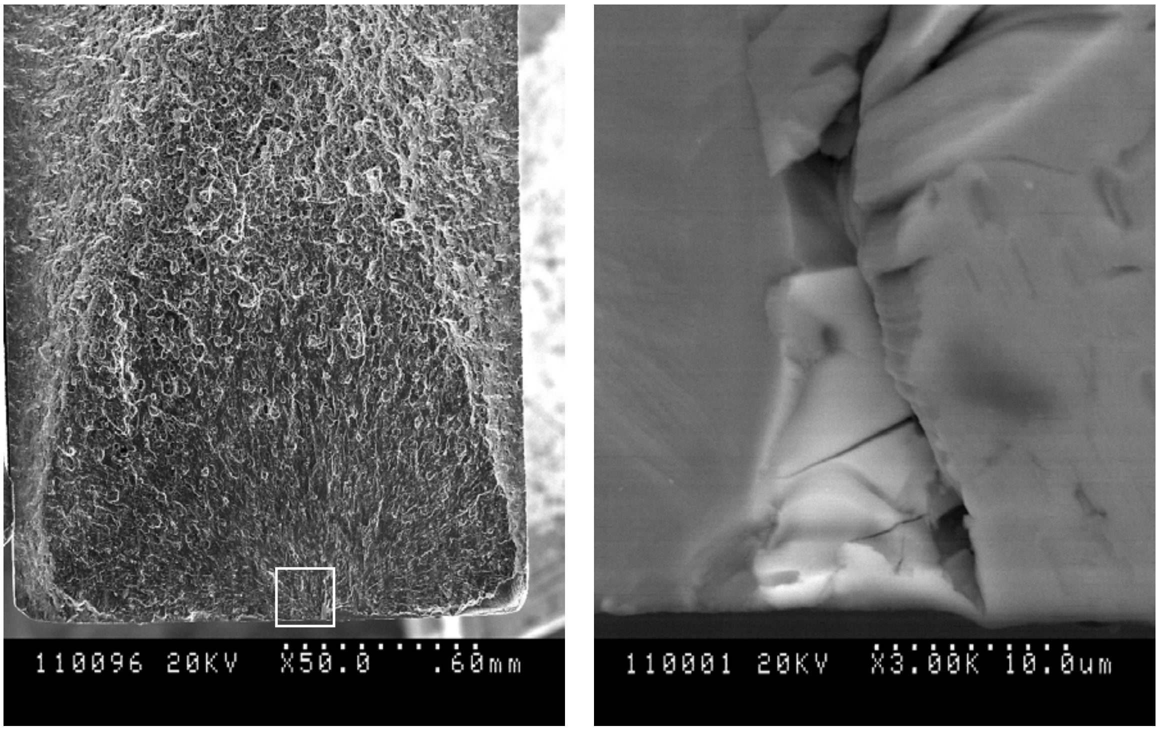

a) b)

Figure 96. Fracture surface of a fatigue test coupon manufactured from 7075-T6 aluminum alloy: a) SEM micrograph at low magnification showing the crack nucleation site (window); b) high magnification view of the window in figure a, showing the crack nucleation site, which is at a constituent particle

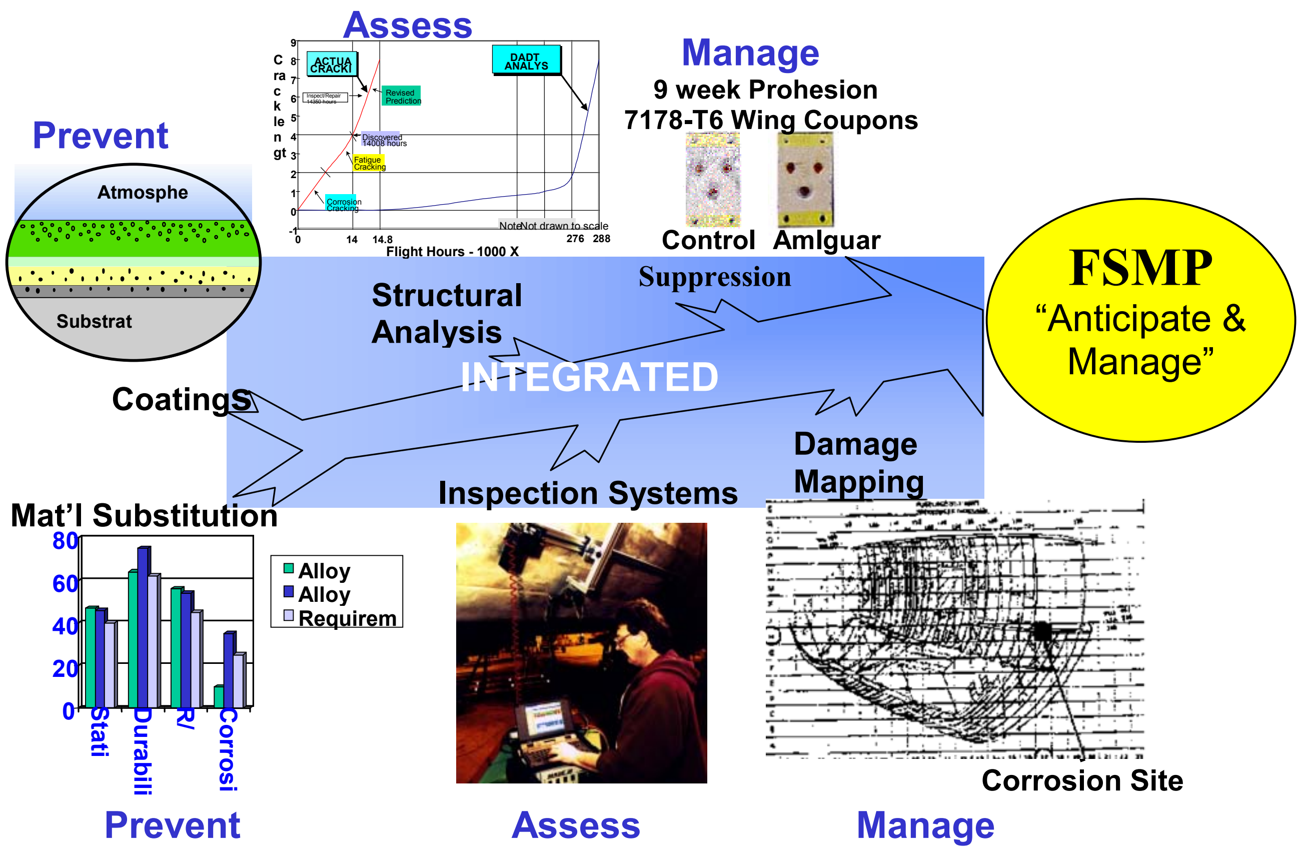

Figure 97. Integration of technologies in corrosion fatigue damage management

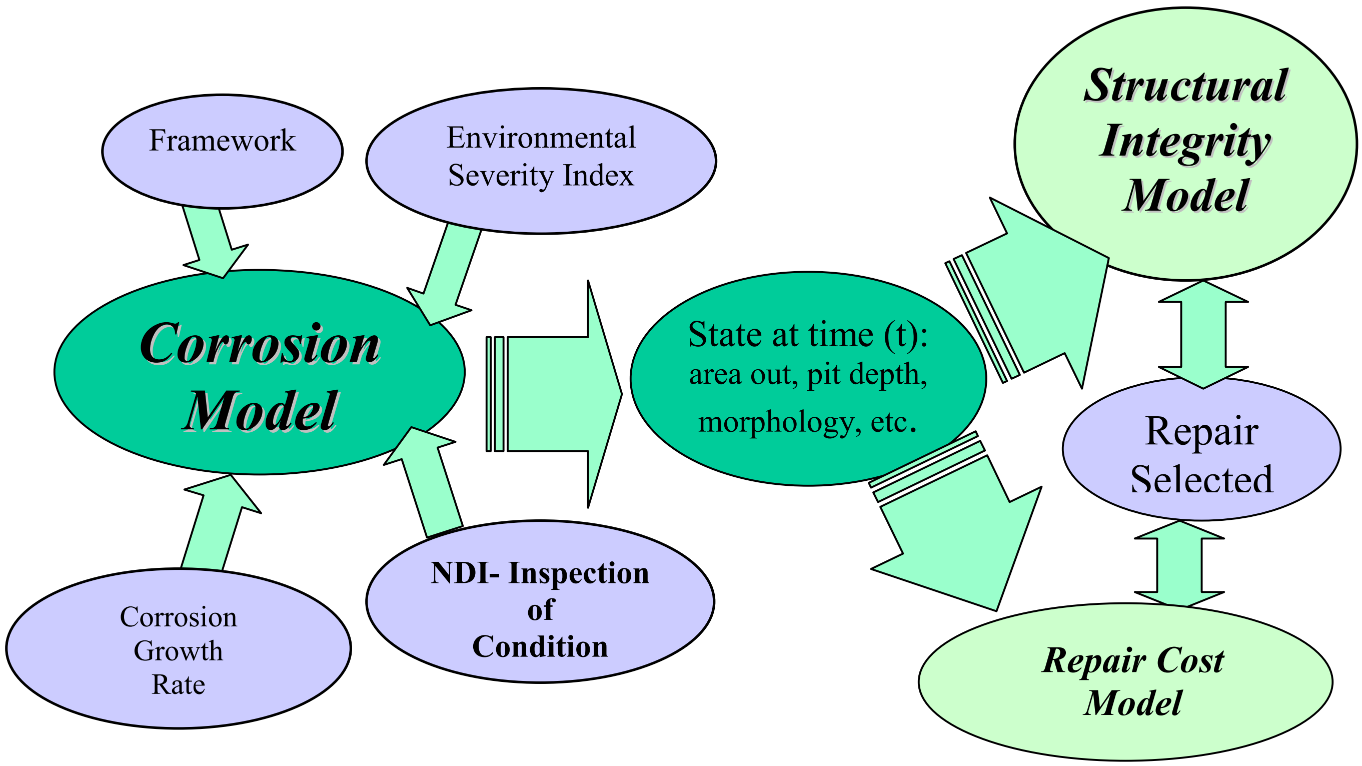

Figure 98. Schematic of integrated "Anticipate & Manage" corrosion fatigue software

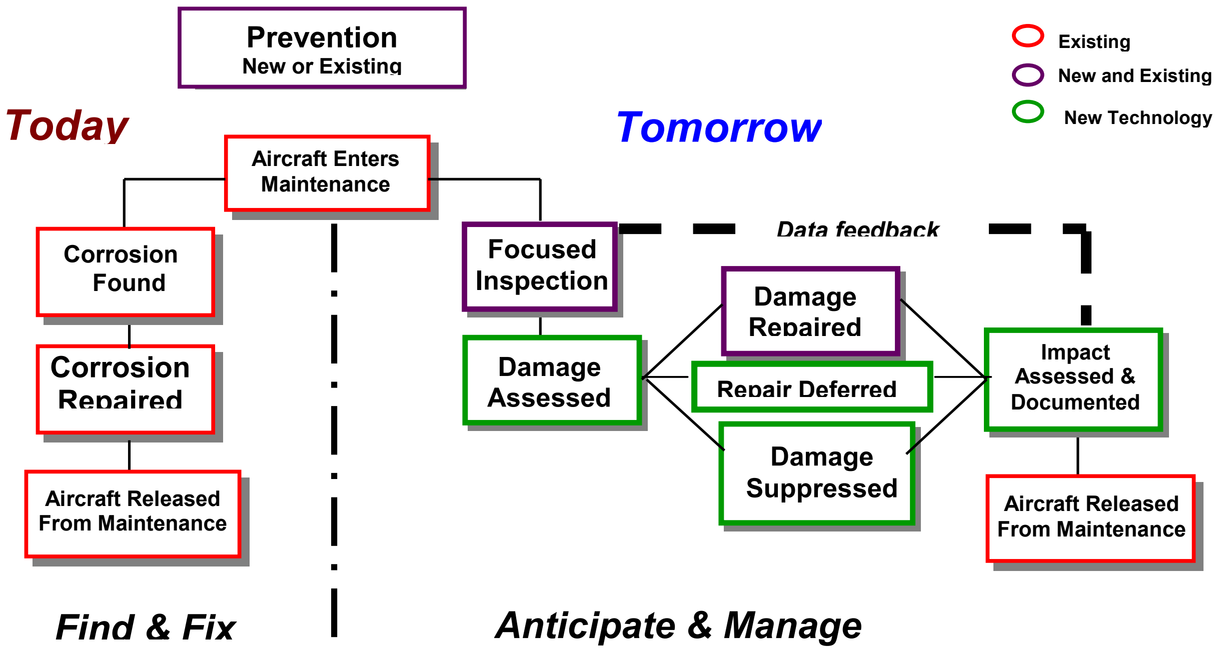

Figure 99. Maintenance process flowchart for "Find & Fix" versus "Anticipate & Manage"

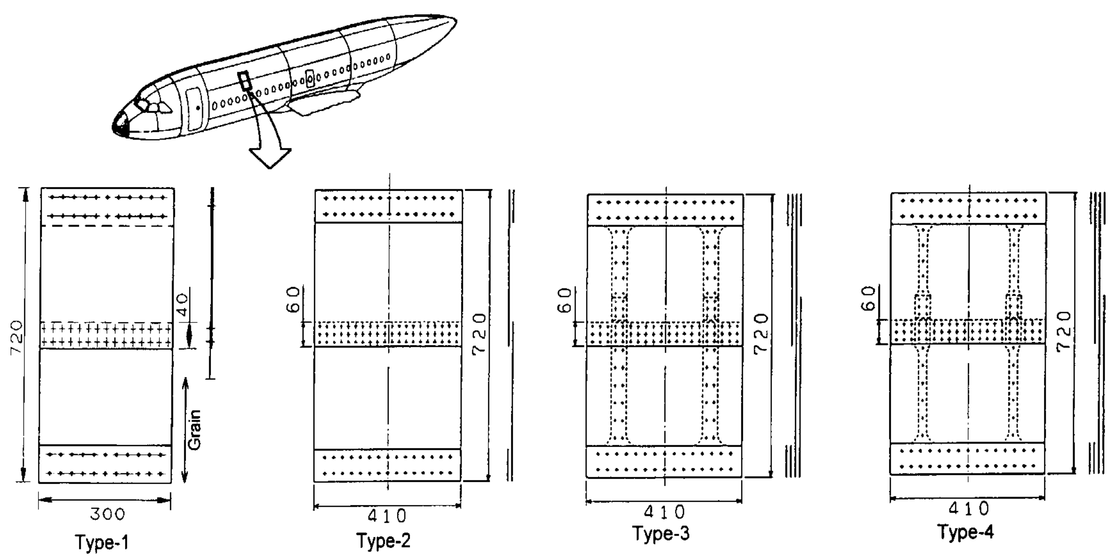

Figure 100. Lap-joint configurations tested by Furuta, Terada and Sashikuma [1]

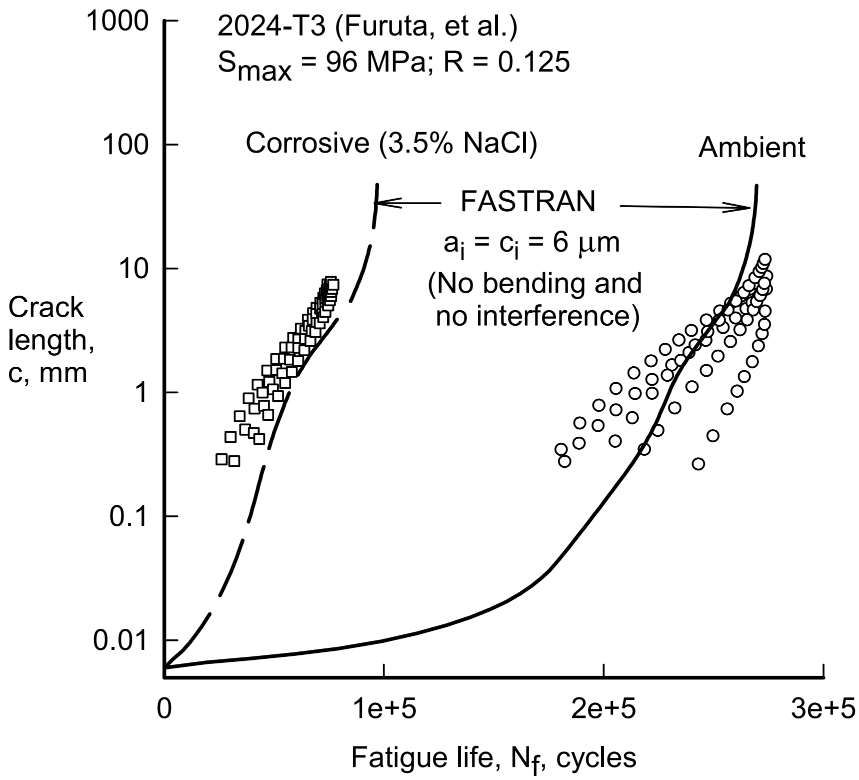

Figure 101. Measured and calculated fatigue crack growth results for Type 1 panels under ambient and salt-water conditions

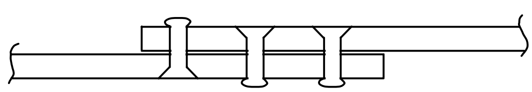

Figure 102. Lap joint schematic showing reversed riveting used to evaluate the fatigue critical location of riveted joints

Figure 103. Small-scale lap joint fatigue test set-up

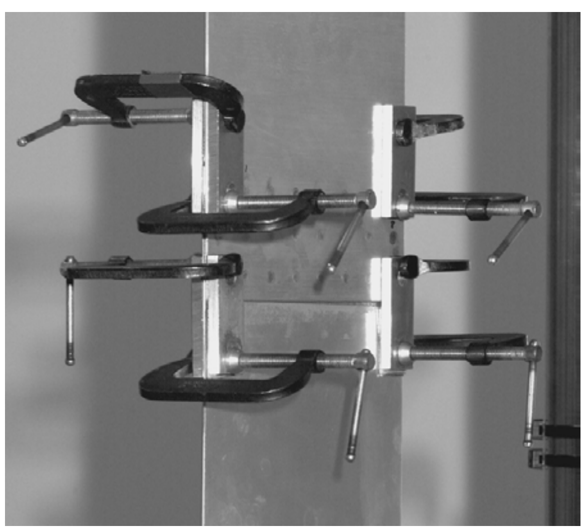

Figure 104. Close-up showing edge clamping of test specimen

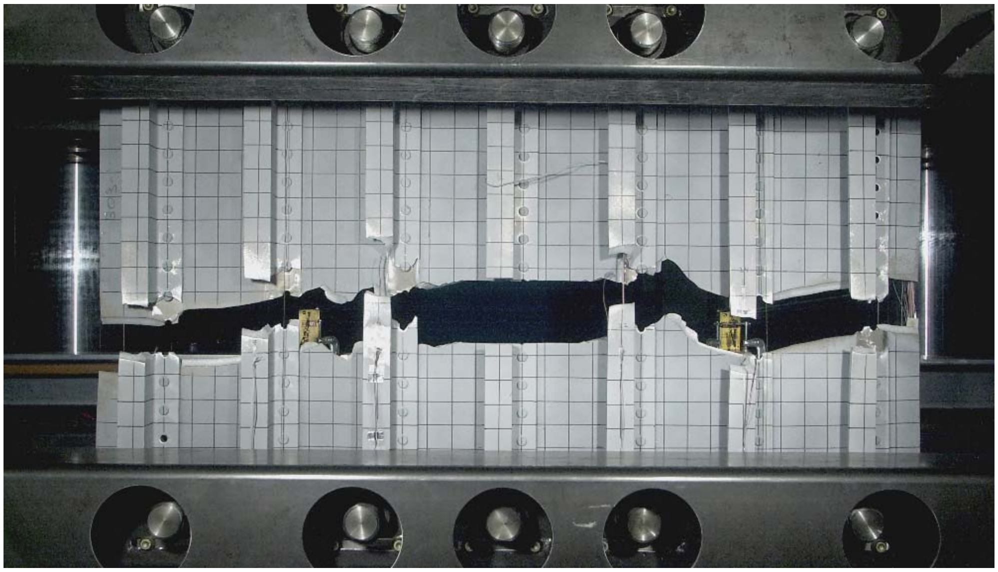

Figure 105. Failed residual strength panel with a 2-bay initial crack

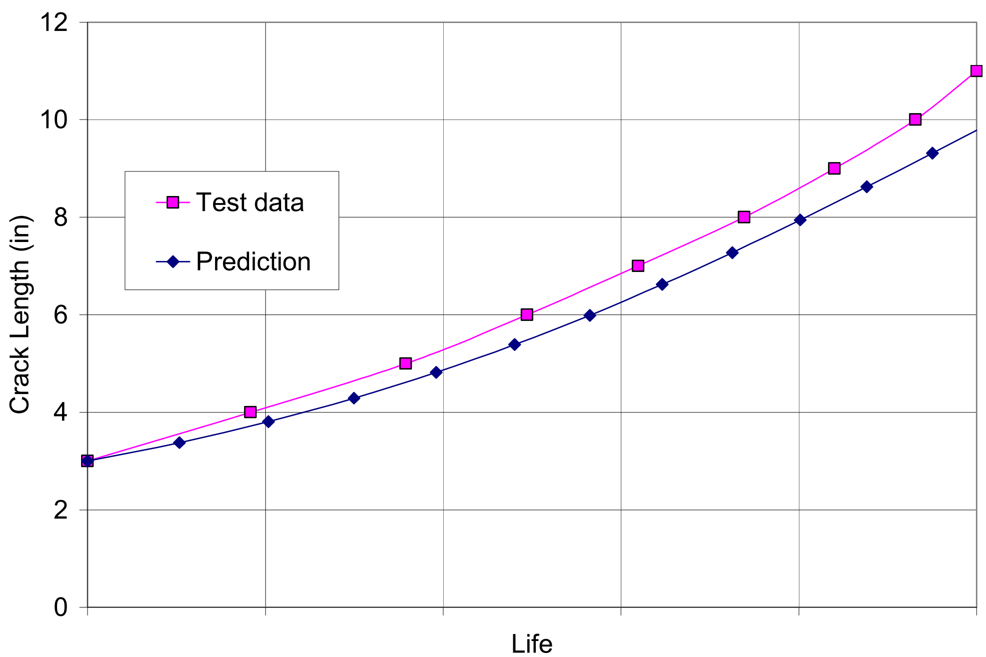

Figure 106. Predicted and actual crack growth curves for the 7-stringer panel

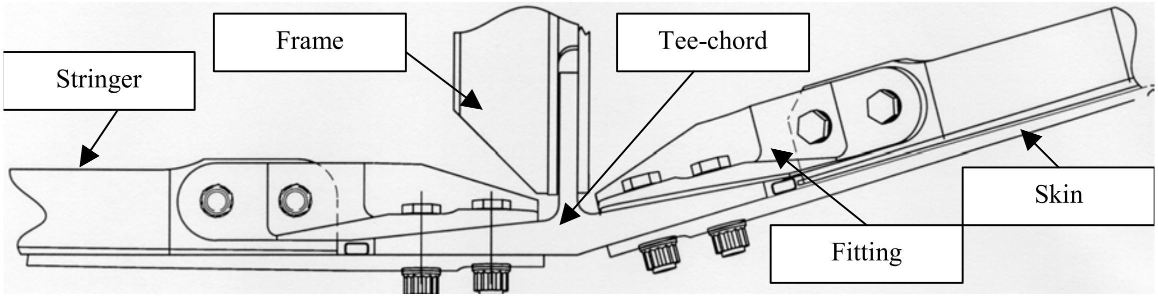

Figure 107. Wing joint

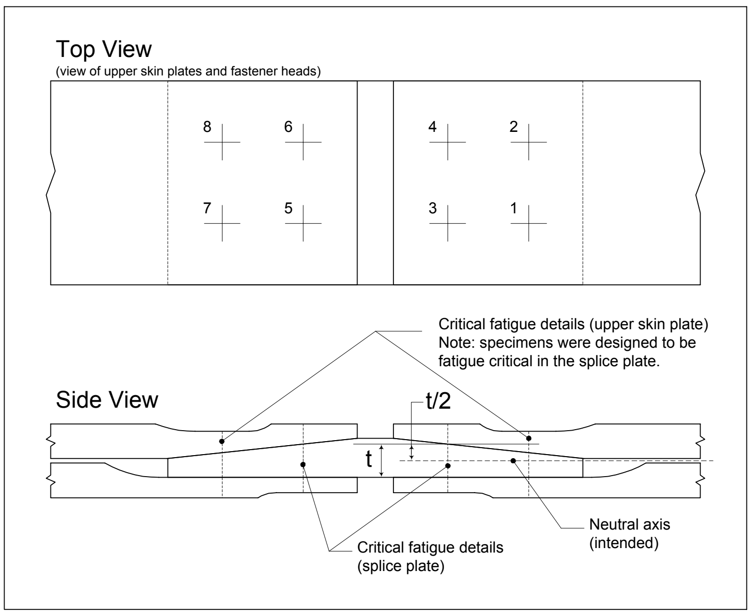

Figure 108. Wing joint coupon - test section details

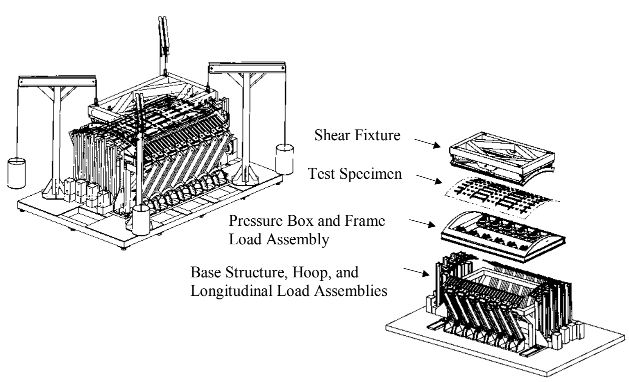

Figure 109. FASTER Facility

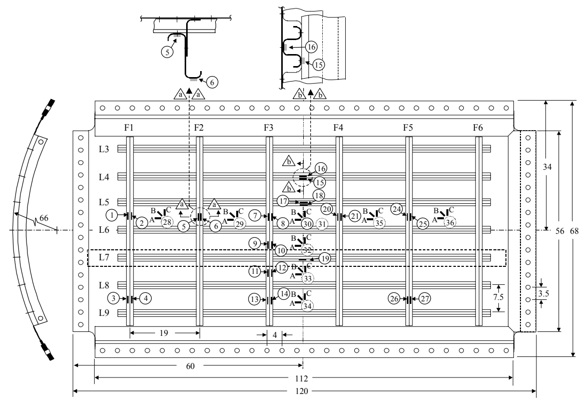

Figure 110. Panel cut from the fuselage of a narrow-body aircraft containing six frames (labeled F1 through F6) and seven stringers (labeled L3 through L9)

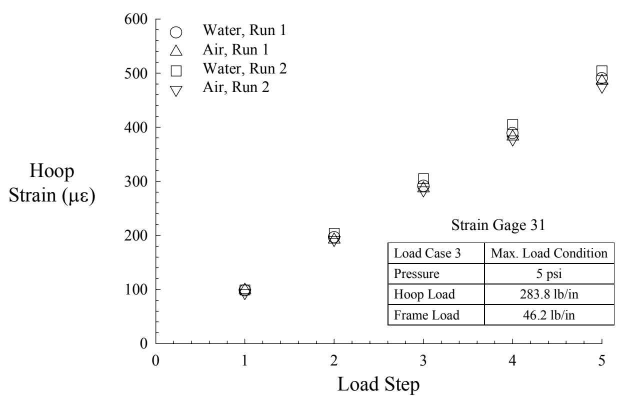

Figure 111. Hoop strain measurements

Figure 112. Aft pressure bulkhead

Figure 113. Saw-cut lead crack and strain gage locations

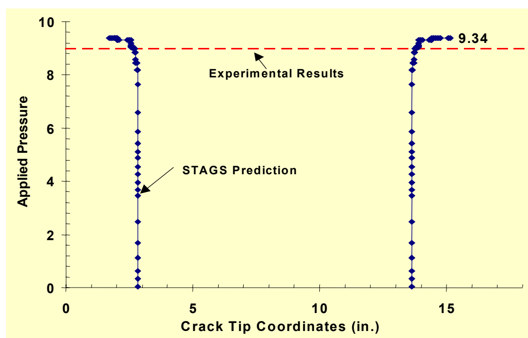

Figure 114. Crack tip coordinates

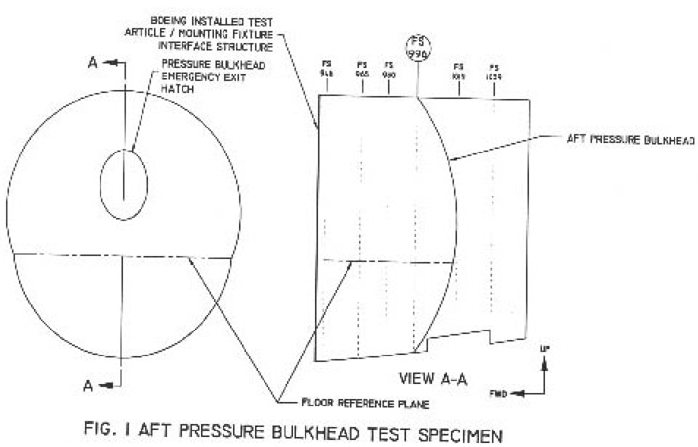

Figure 115. Aft pressure bulkhead test specimen

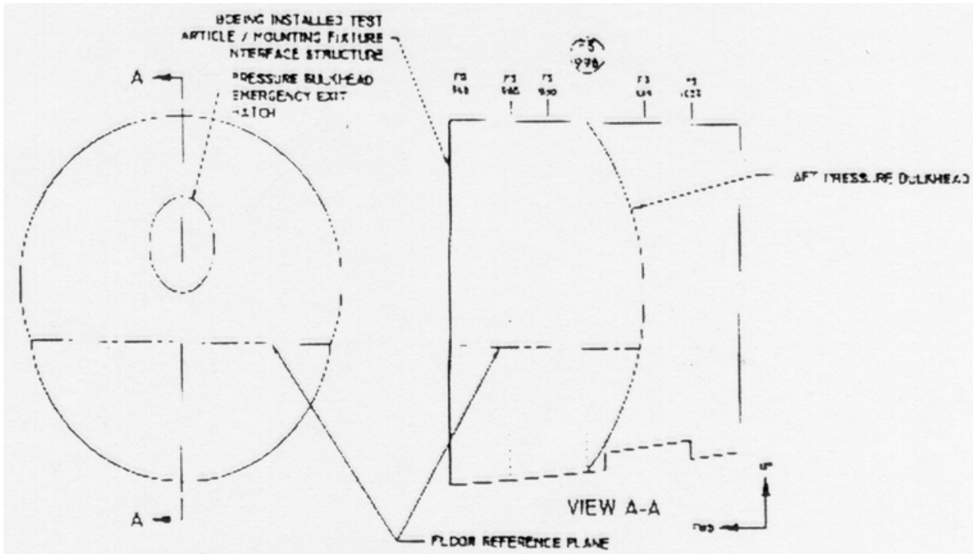

Figure 116. Aft pressure bulkhead initial damage detail

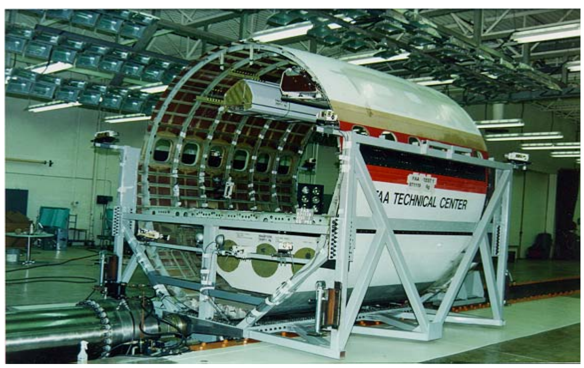

Figure 117. Fuselage section nominally accelerated to 6, 9, and 16 g's


Figure 118. Boeing 737 Model 200 fuselage section

Figure 119. 737-800 fuselage fatigue test setup

Figure 120. 737-800 fuselage fatigue test typical side of body load strap and wiffle tree arrangement

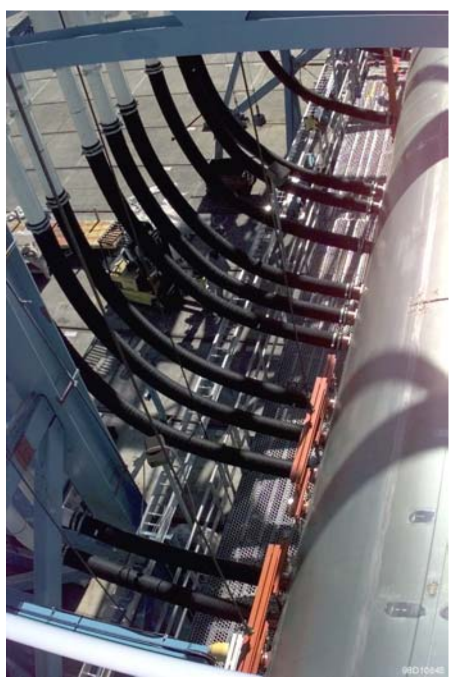

Figure 121. 737-800 Fuselage fatigue test air supply system

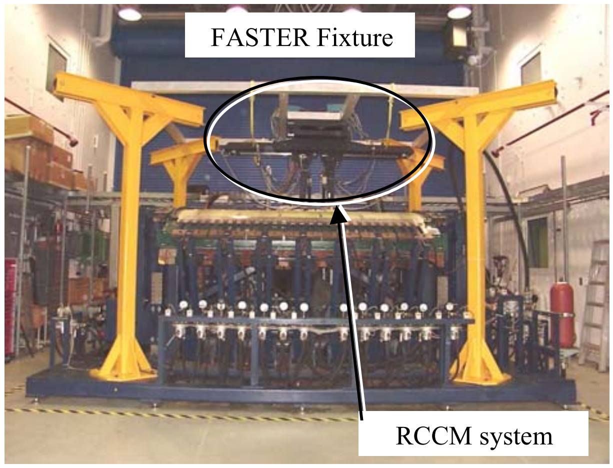

Figure 122. The FASTER facility used to generate data to support and validate analytical models being developed under the sponsorship of the FAA to assess aging aircraft with multiple-cracking scenarios

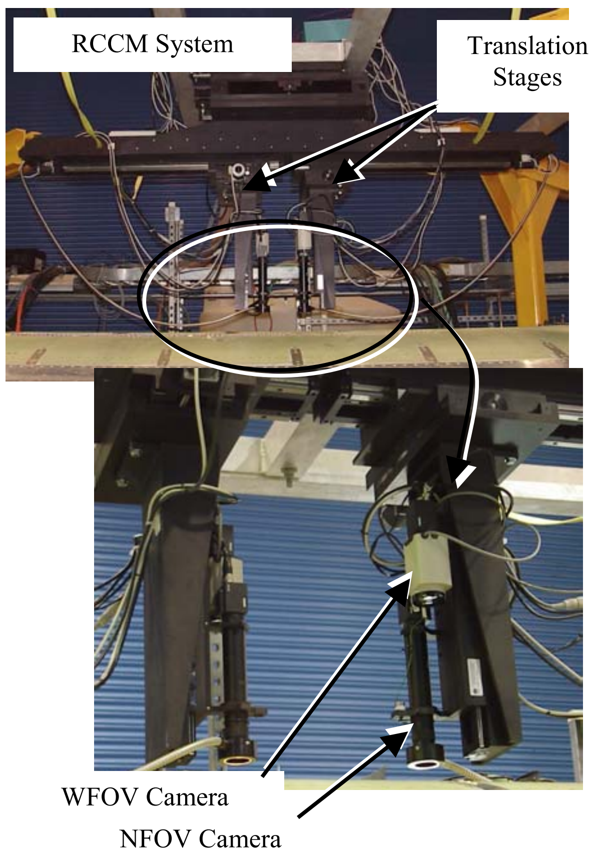

Figure 123. The RCCM system

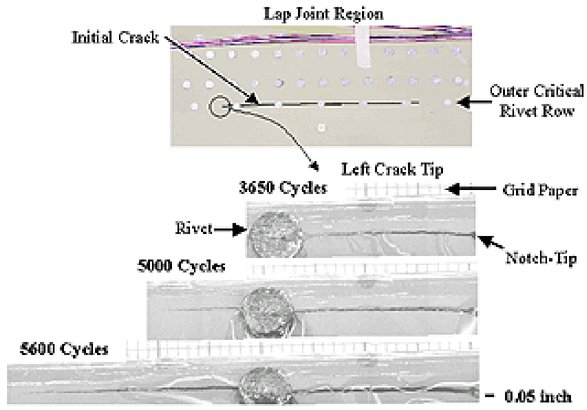

Figure 124. Shows crack growth from the notch in a co-linear manner

Figure 125. Test vehicle applying simulated aircraft loads to concrete pavements during testing at the NAPTF

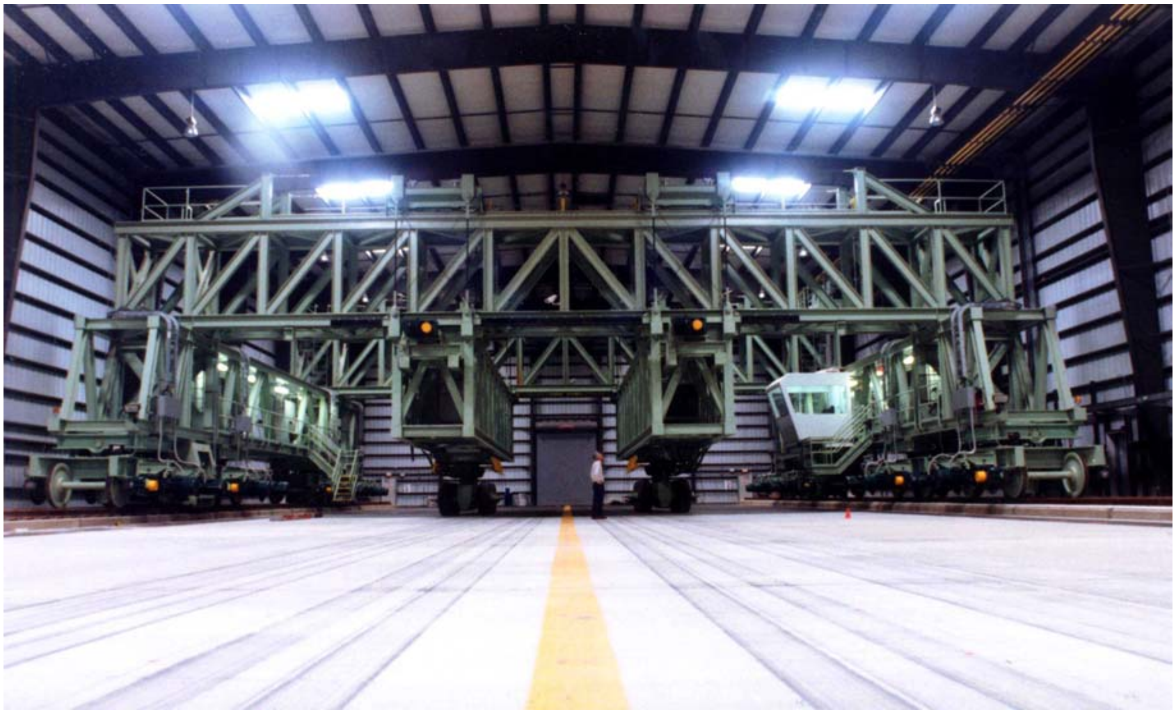

Figure 126. The National Airport pavement test facility

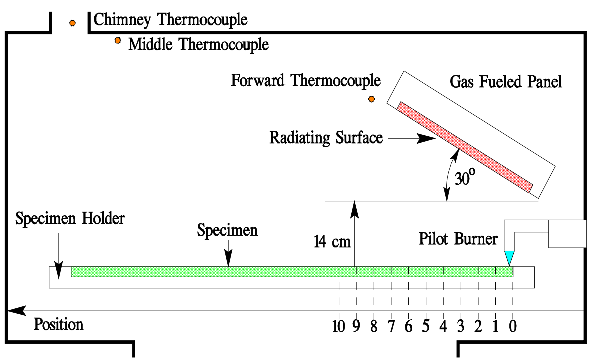

Figure 127. Radiant panel test apparatus for evaluating flammability of thermal acoustical insulation

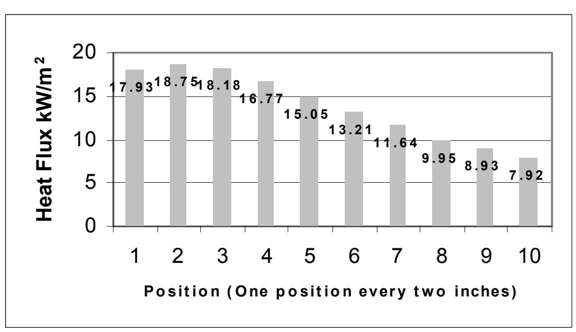

Figure 128. Flux profile curve of incident radiant heat energy versus position on the specimen surface

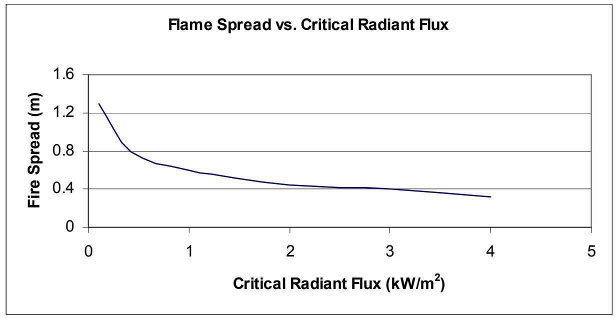

Figure 129. Relationship between flame spread and critical radiant heat flux

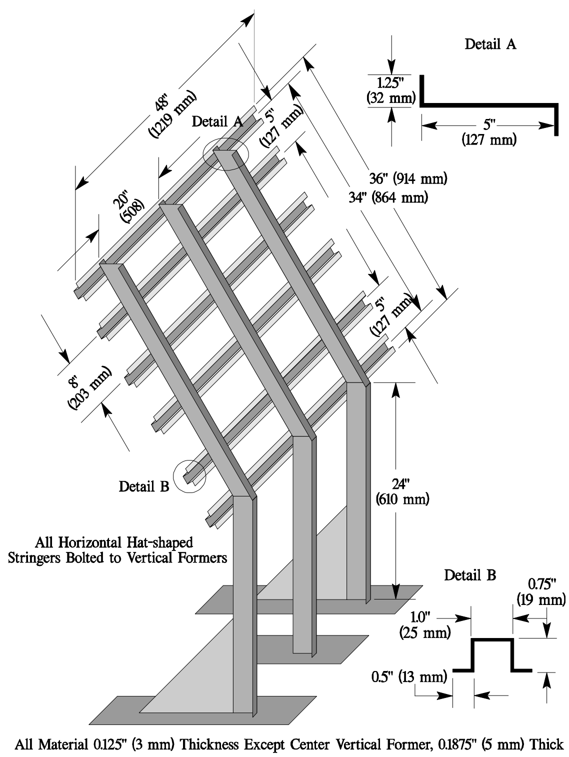

Figure 130. Six horizontal hat-shaped stringers bolted into place

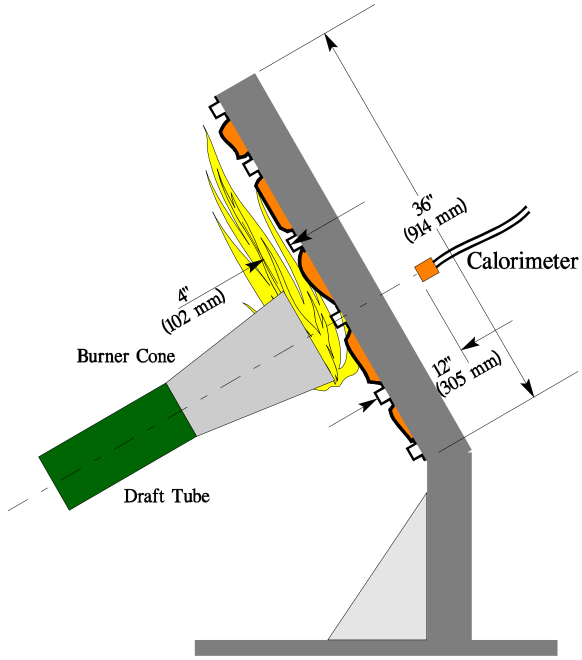

Figure 131. Test burner aimed at the center of the test frame

Test Date	Burner Fuel Flowrate (gal/hr)	Burner Air Velocity (ft/min)	Burner Distance (inches)	Skin Material	Skin Thickness (inches)	Burnthrough Time (seconds)
12/8/98	2	1800	5	5052 Aluminum	0.05	480 +
12/8/98	2	1800	2	5052 Aluminum	0.05	45 to 80
12/8/98	4	2000	4	5052 Aluminum	0.05	120
12/9/98	6	2200	4	5052 Aluminum	0.05	55
12/9/98	6	2200	4	5052 Aluminum	0.05	55

Table 3. During the baseline trails, the burner fuel flowrate, intake air velocity, and position respective to the test frame were modified in order to obtain the appropriate condition

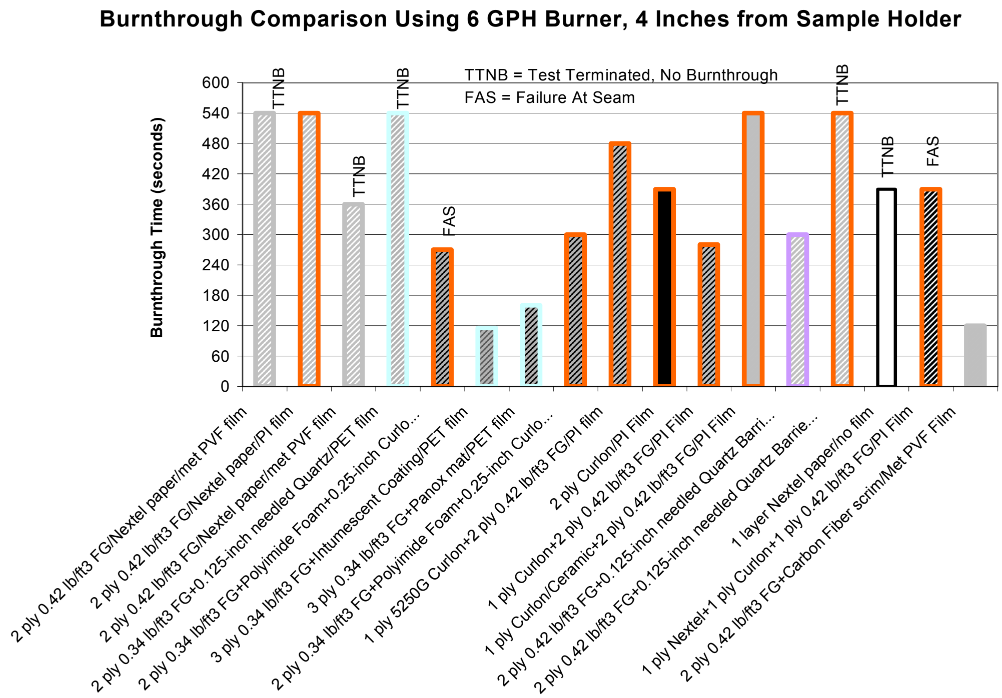

Figure 132. Burnthrough comparison using 6 GPH burner, 4 inches from sample holder

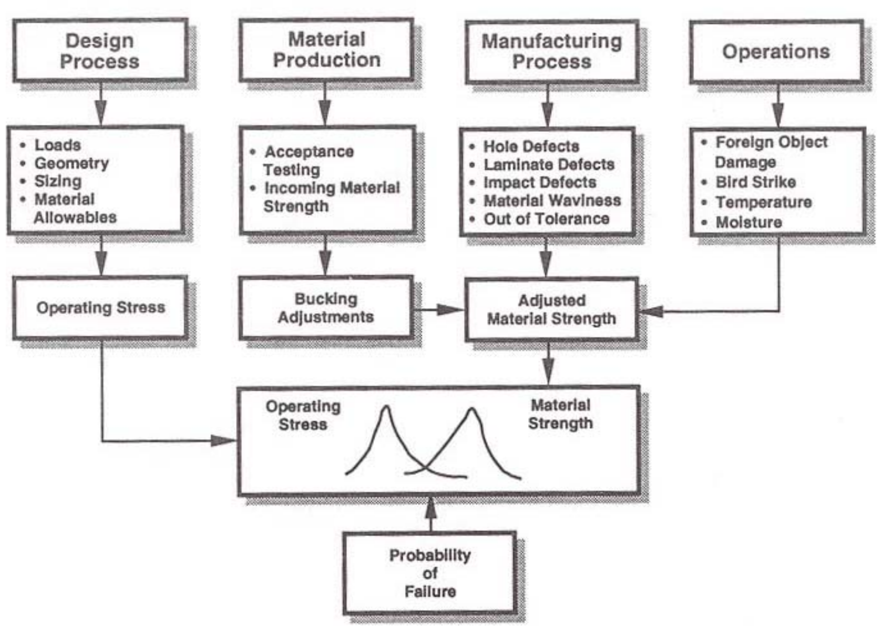

Probabilistic Design Process

Figure 133. Flow chart of the total probabilistic design process

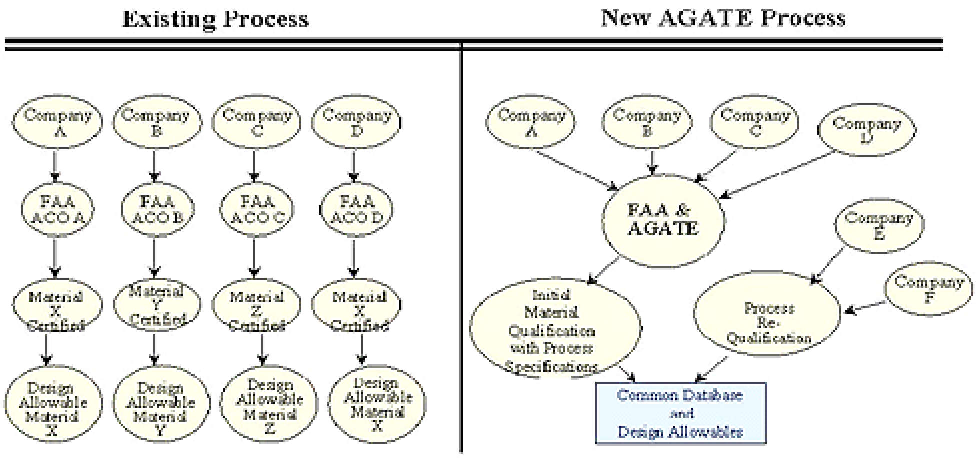

Figure 134. Comparision of conventional and AGATE certification procedures

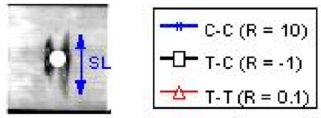

T-Tension
C-Compression

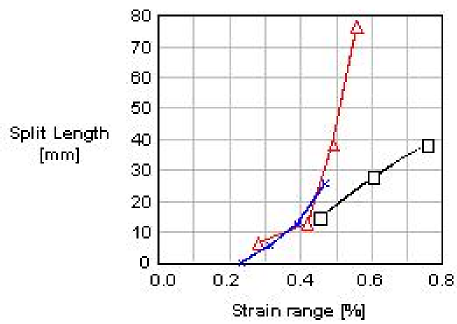

Split Damage at 10^6 Cycles as a Function of Maximum Cyclic Strain and Strain Range

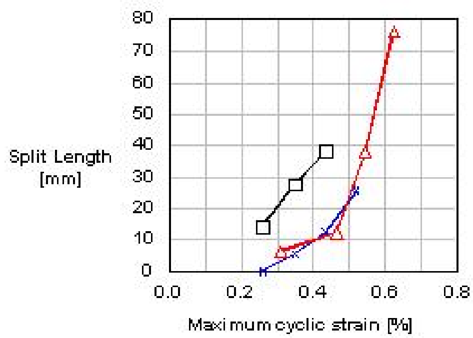

Split Damage at 10^6 Cycles as a Function of Maximum Cyclic Strain in Constant Amplitude Fatigue

Figure 135. Comparison of strain range and constant amplitude fatigue

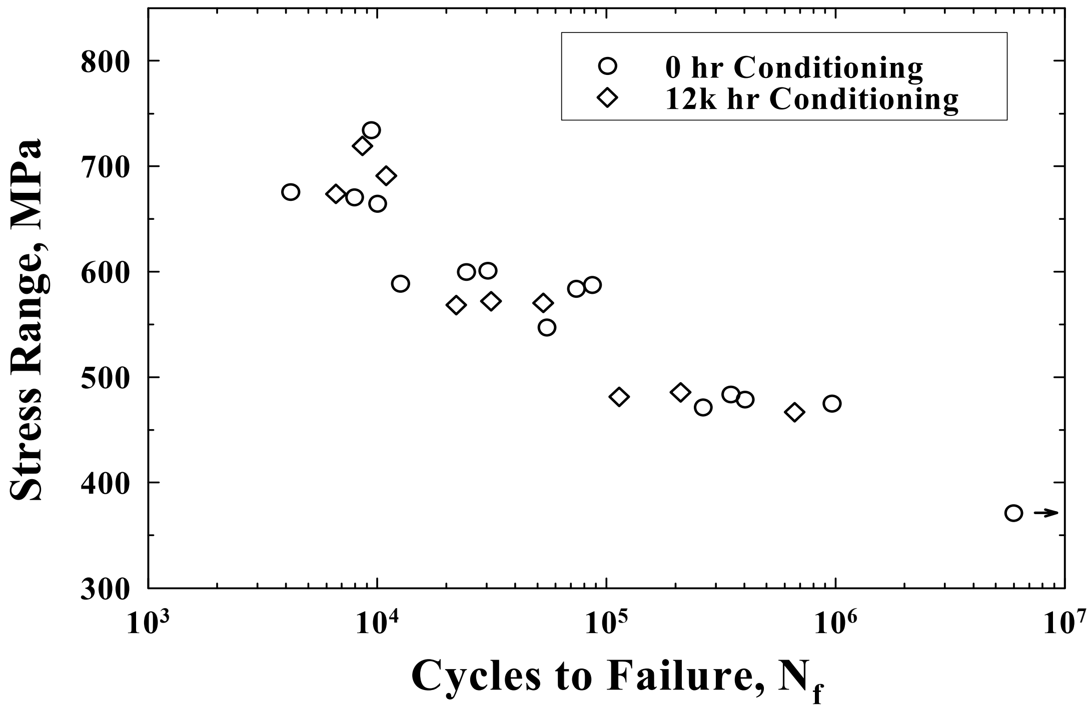

Figure 136. Fatigue strength as a function of cycles to failure

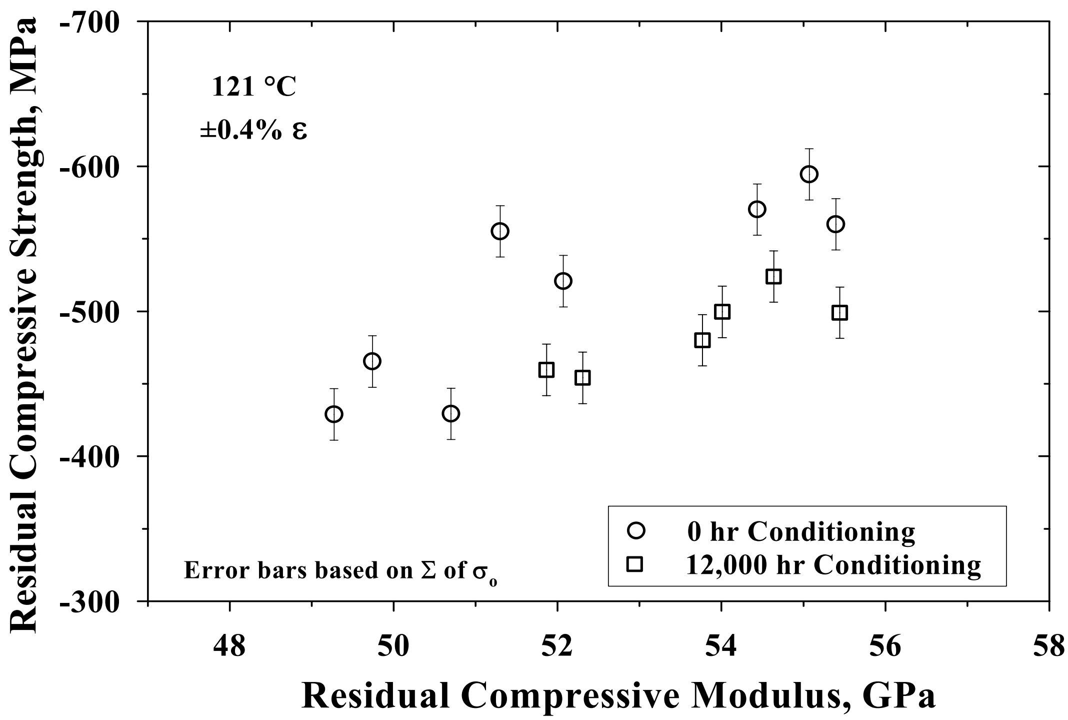

Figure 137. Residual strength/modulus relationship

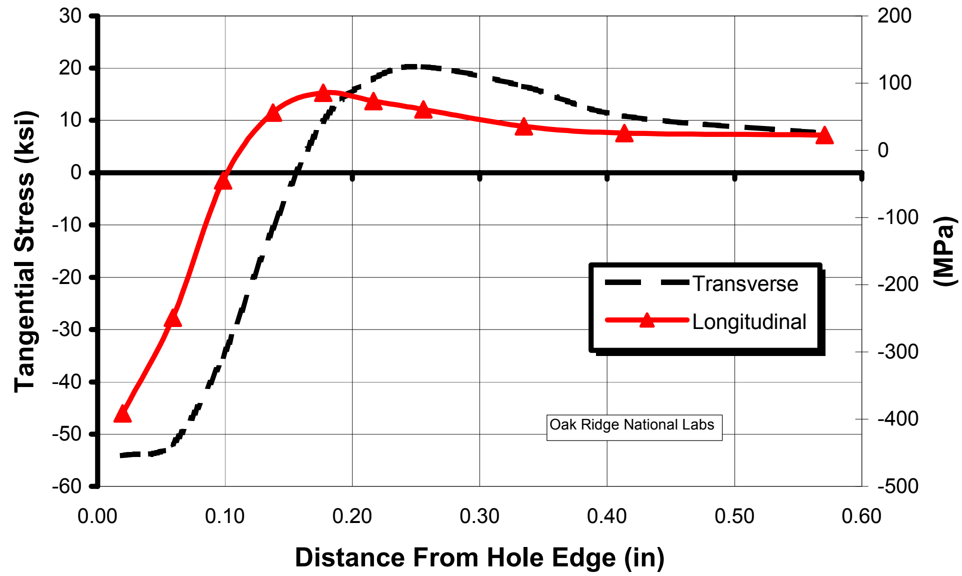

Figure 138. Tangential residual stresses measured at mid-plane using neutron diffraction, 7075-T6 aluminum

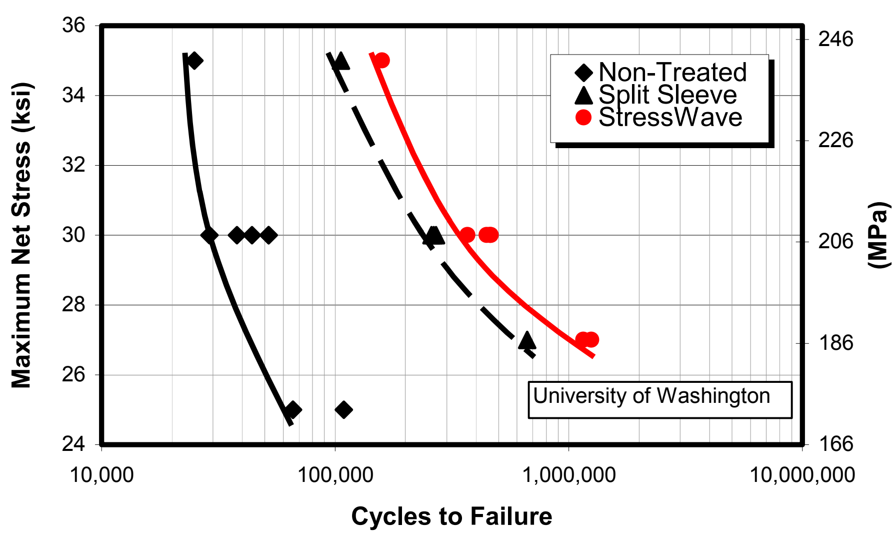

Figure 139. S-N curve for 2024-T3 aluminum, 4.8mm thick, 6.35mm hole diameter

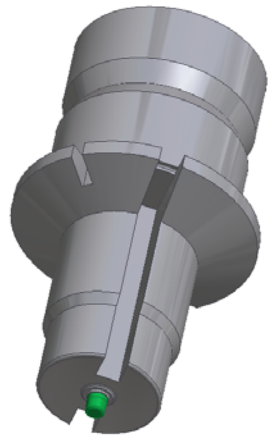

Figure 140. Oblique view of StressWave end effector

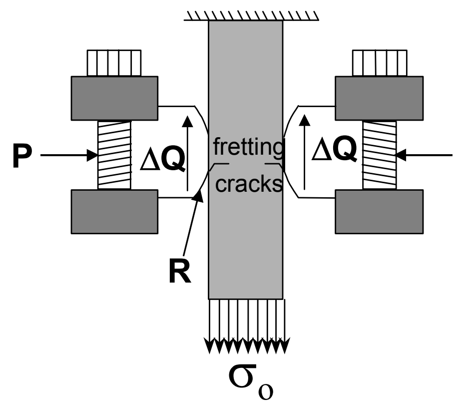

Figure 141. Schematic of the fretting fatigue test setup[1]

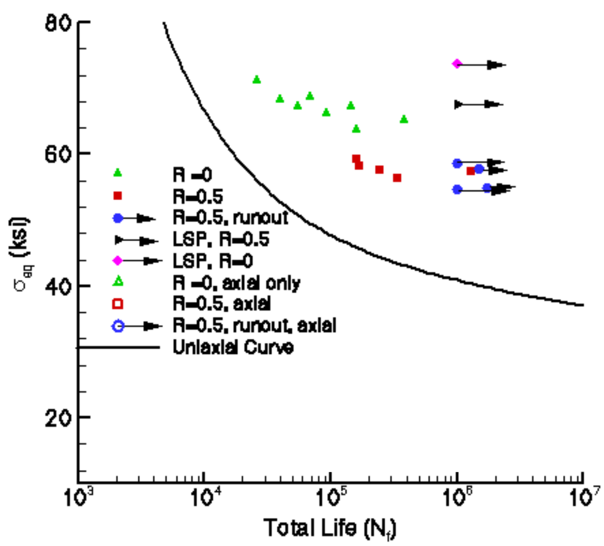

Figure 142. Fretting fatigue results. LSP data points are laser peened, the others are untreated

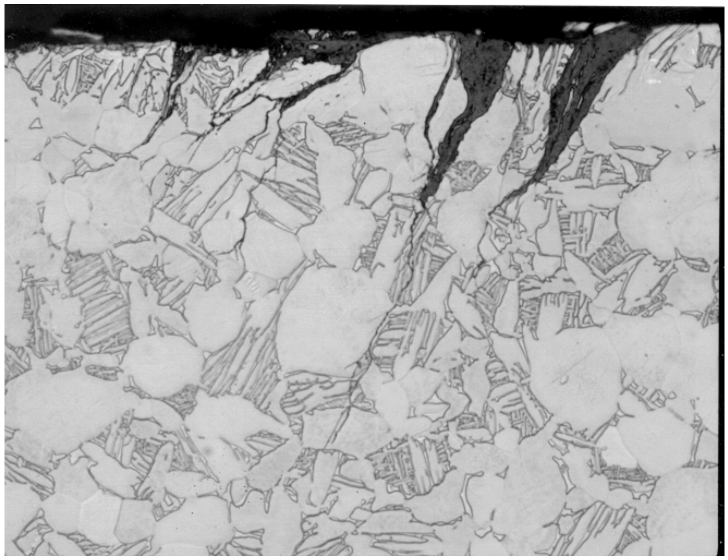

Figure 143. Metallographic section thru surface fretting cracks of LSP2

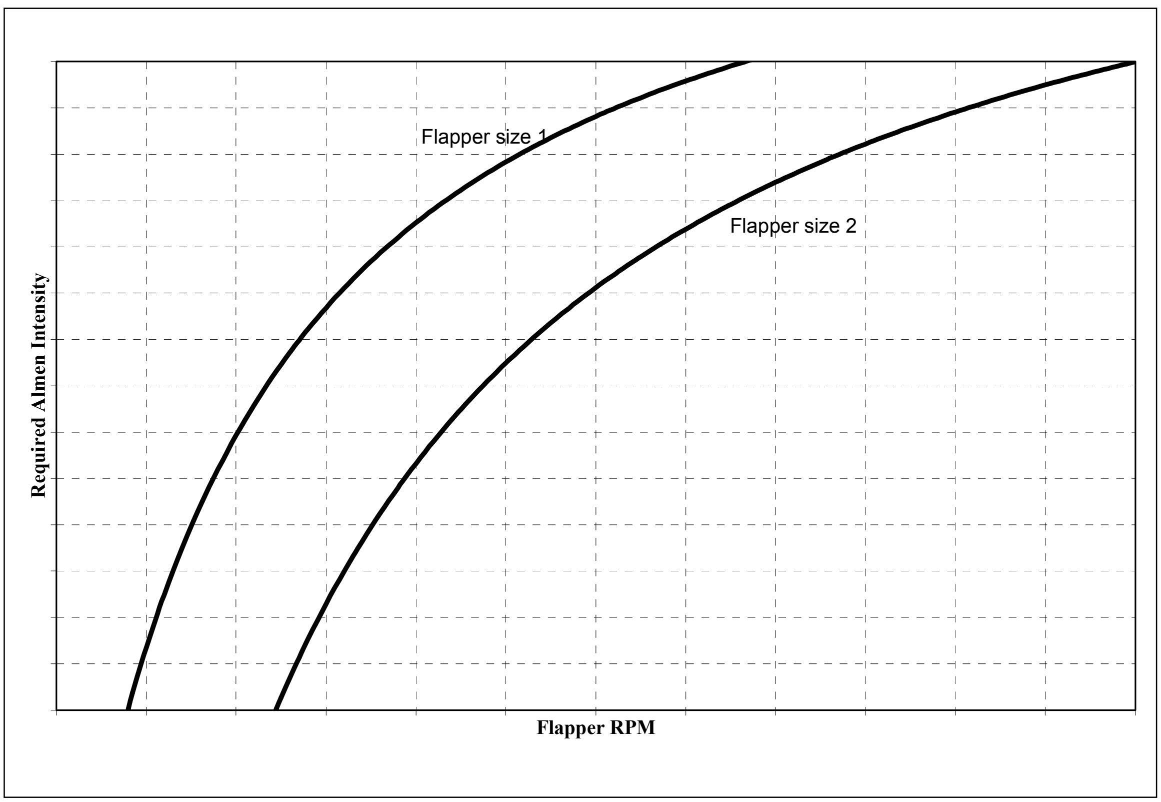

Figure 144. Flapper RPM vs. almen intensity chart

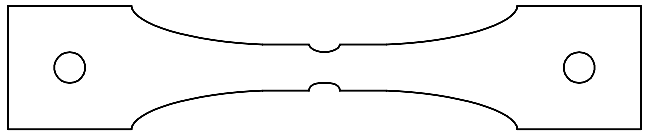

Figure 145. Notch fatigue test specimen

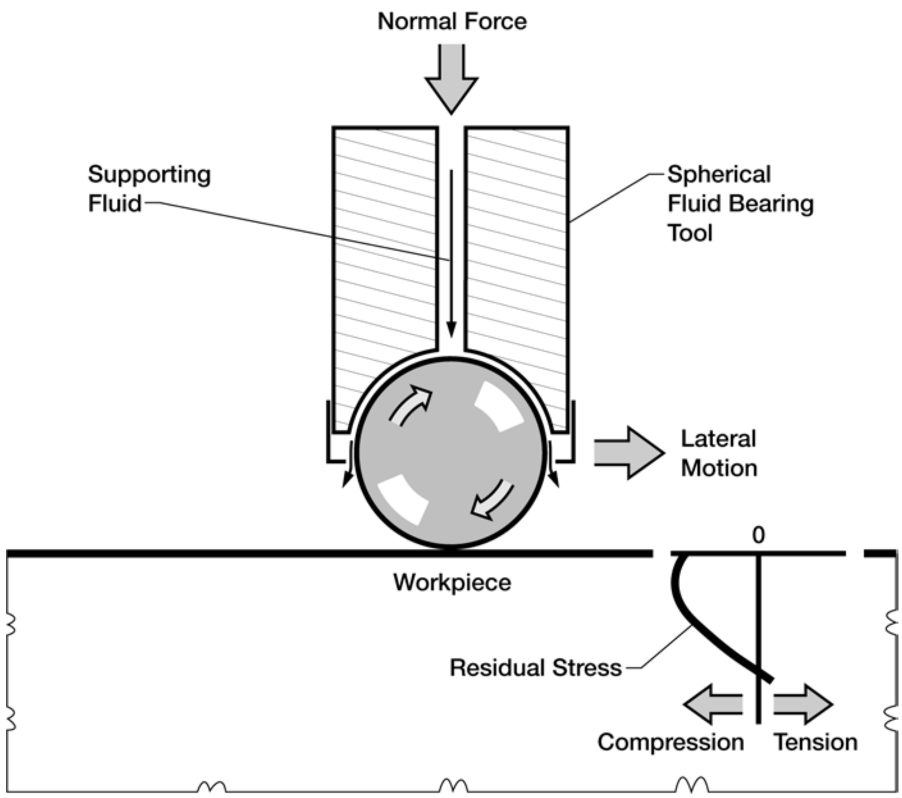

Figure 146. Diagram of the low-plasticity burnishing apparatus: A spherical ballsuspended in a fluid bearing contacts the work piece under a normal force while undergoing lateral motion

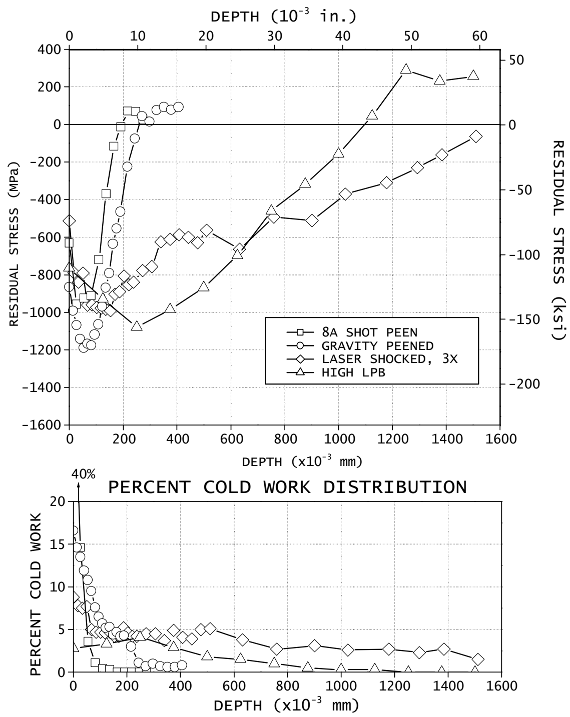

Figure 147. Comparison of the residual stresses and percent cold work produced by shot peening, laser shock treatment, and low-plasticity burnishing in IN718 (ref. 1). Low-plasticity burnishing produces compressive residual stresses to depths of 0.9 to 1.5 mm with cold work of 4 percent or less

Figure 148. Migrated bushing

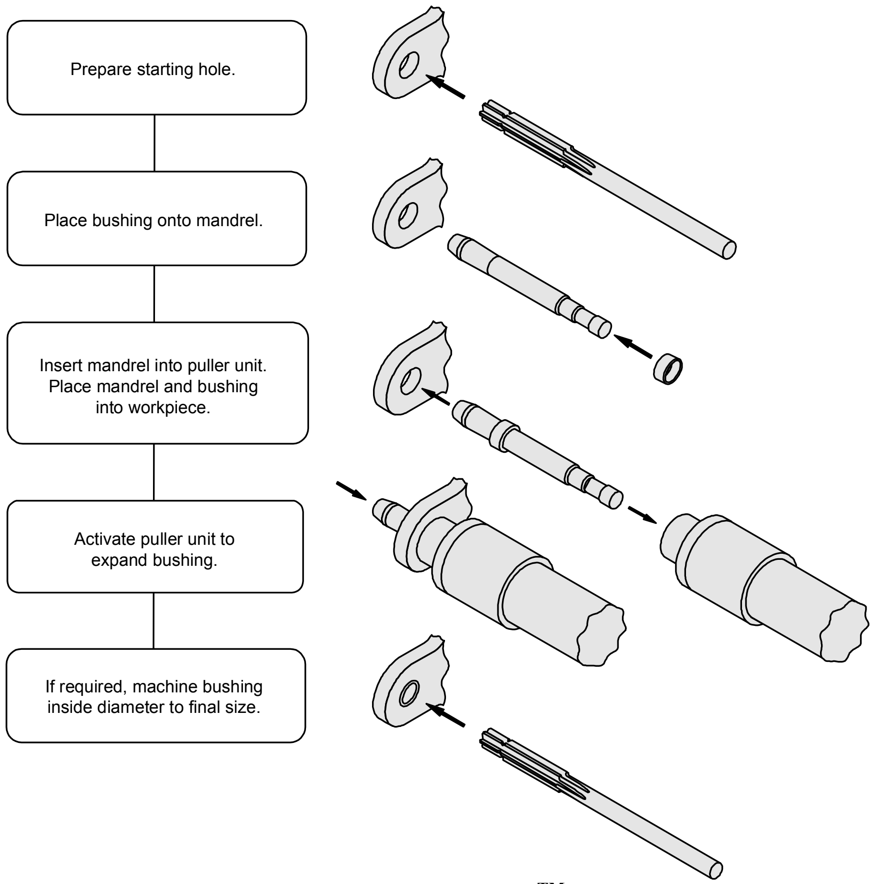

Figure 149. FTI ForceMate™ process

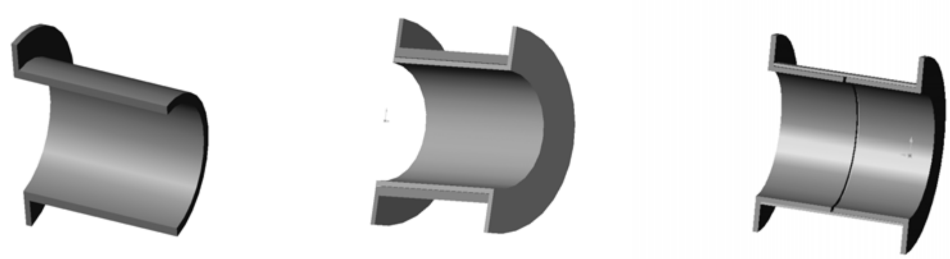

Figure 150. Bushing configurations

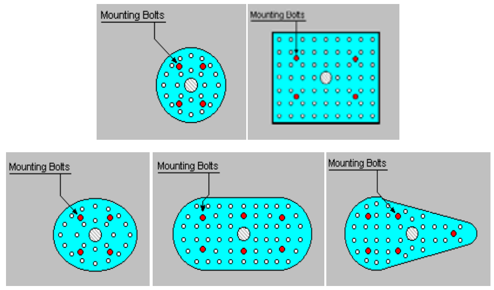

Figure 151.

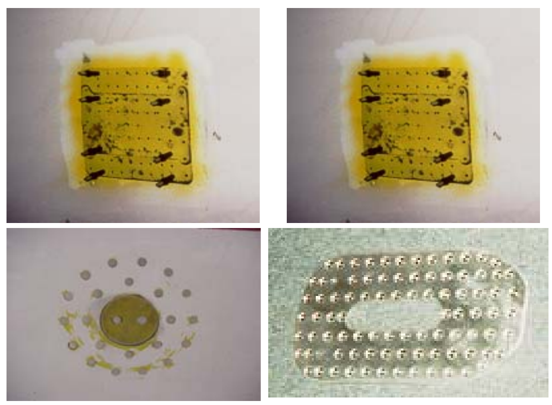

Figure 152. Repairs and a sausage-shaped antenna installation mounting plate

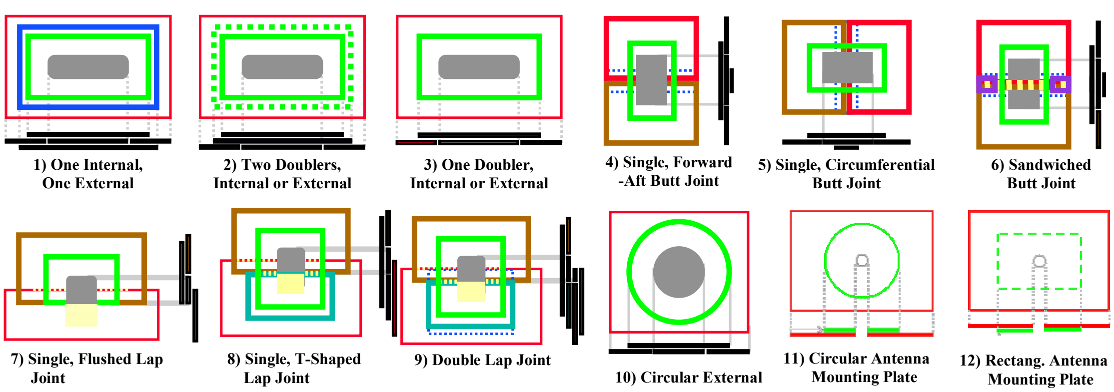

Figure 153. Basic repair types in RAPIDC V1.0

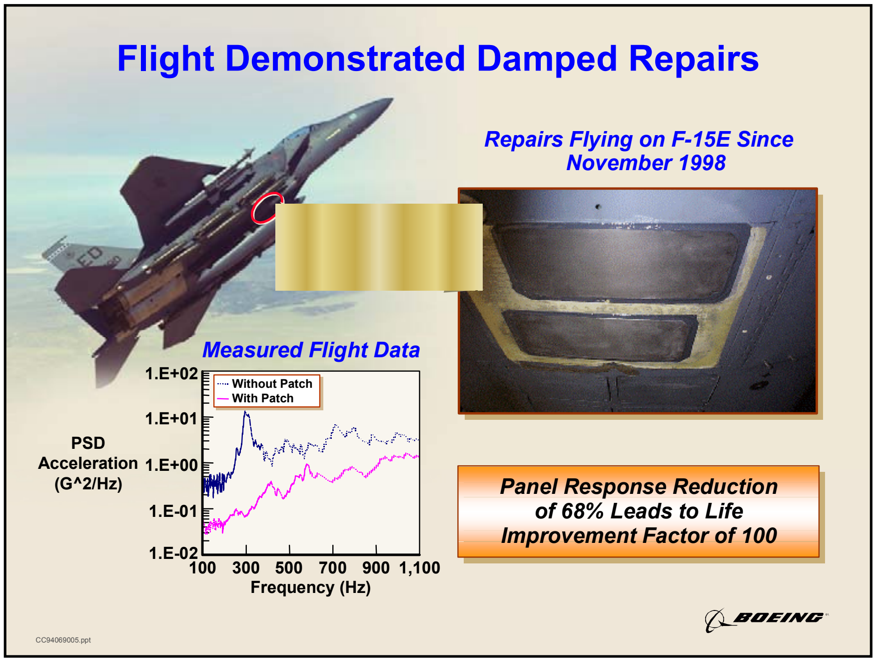

Figure 154. Damped bonded patch repairs

Figure 155. Thermal wave imaging system developed by Wayne State University - CASR

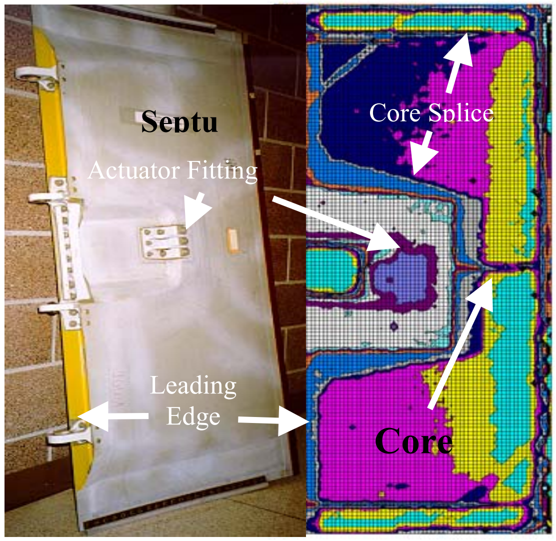

Photo of B767 Outboard Spoiler

Tap Test Image

Figure 156. Tap test image of B-767 outboard spoiler

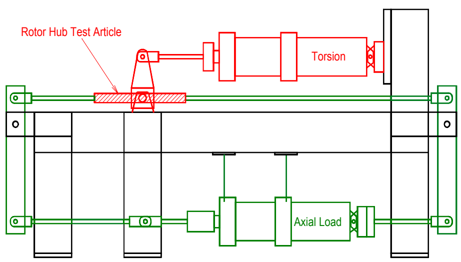

Figure 157. Biaxial flex beam test rig

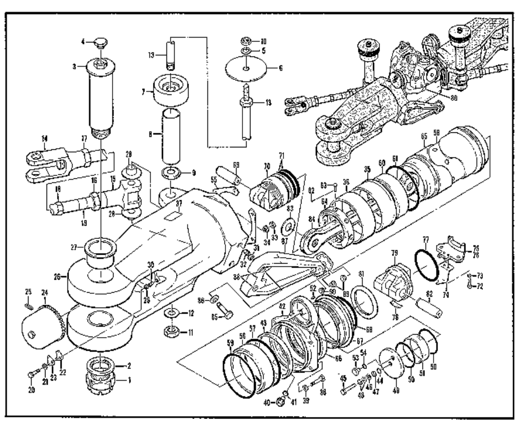

Figure 158. Tension straps

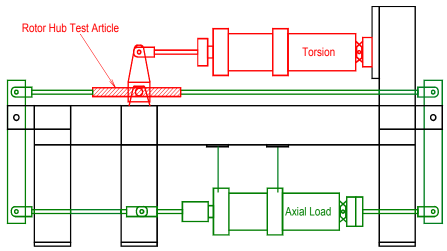

Figure 159. Biaxial flex beam test rig

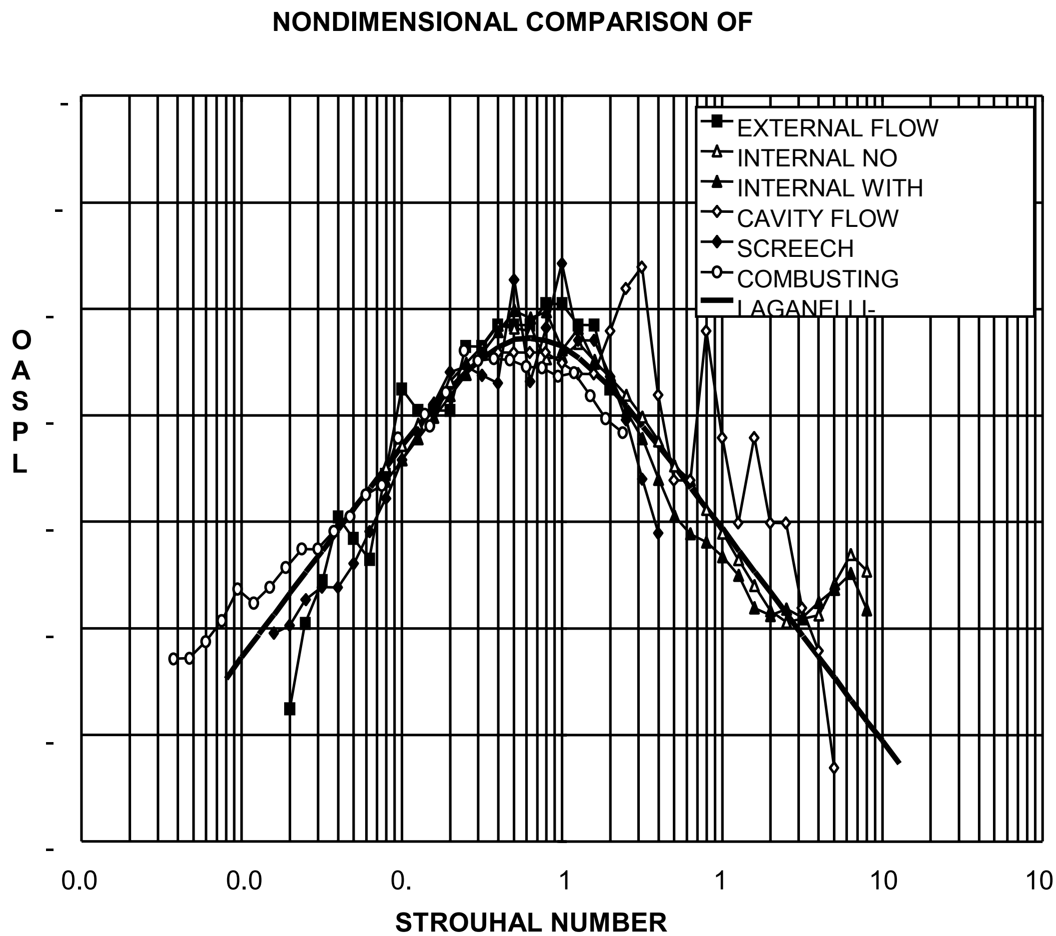

Figure 160. A wide source of aeroacoustic data all normalized to essentially one curve using the novel technique

$$\Phi = a^2(-\cos\alpha\sin\beta\cos\gamma + \sin\alpha\sin\gamma)^2$$
$$+ b^2(\cos\alpha\sin\beta\sin\gamma + \sin\alpha\cos\gamma)^2$$
$$+ c^2(\cos\alpha\cos\beta)^2$$

$$A_{int} = \pi abc\,\frac{\Phi - \rho^2}{[\Phi]^{3/2}} = \pi abc\,\frac{1 - \rho^2/\Phi}{\sqrt{\Phi}}$$

Where:

ρ = distance from sectioning plane to centroid

a, b, c = ellipsoid dimensions

α, β, γ = rotation angles

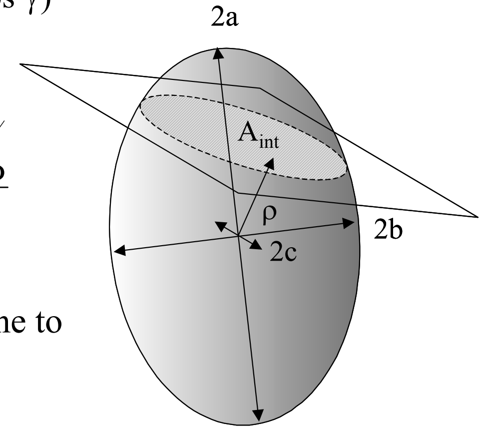

Figure 161. Intercepted area of a randomly oriented ellipsoid cut by a random plane

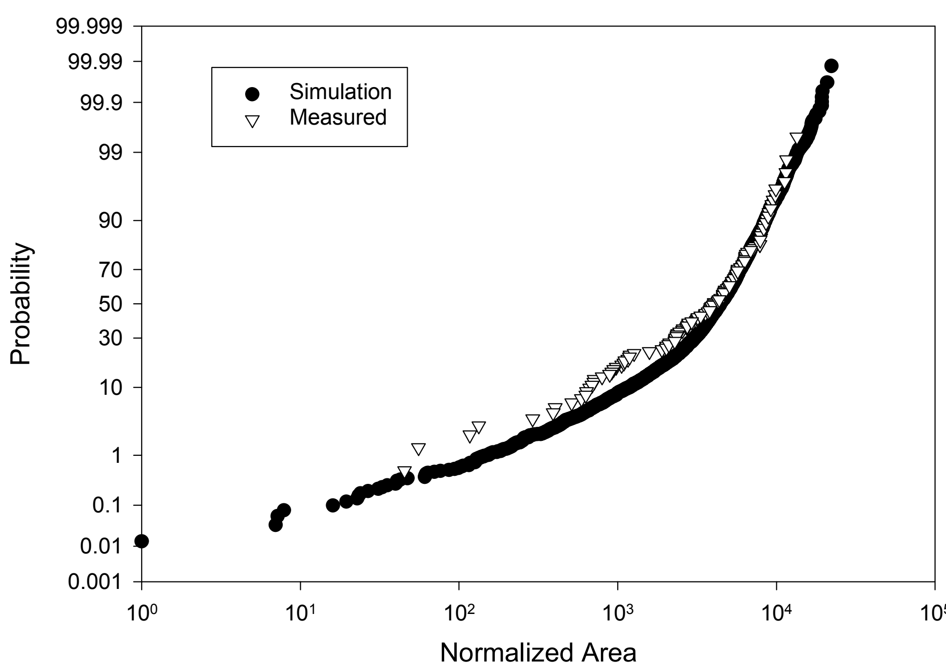

Figure 162. Comparison of observed vs. predicted intercepted surface areas for a seeded sample

Maximum Stress	Fraction of UTS	No. of Cycles	Loss in E^T	Loss in E^C
380 MPa	~47%	50,000	~1%	<1%
448 MPa	~55%	50,000	2%	<1%
517 MPa	~65%	10,000	2%	<1%
		50,000	6%	3.5%
585 MPa	~73%	10,000	8%	6%
		46,000	19%	not measured

Table 4. Tensile and compressive modulus degradation as a function of zero-tension fatigue cycles ate 315°C for dry T650-35/PMR-II-50

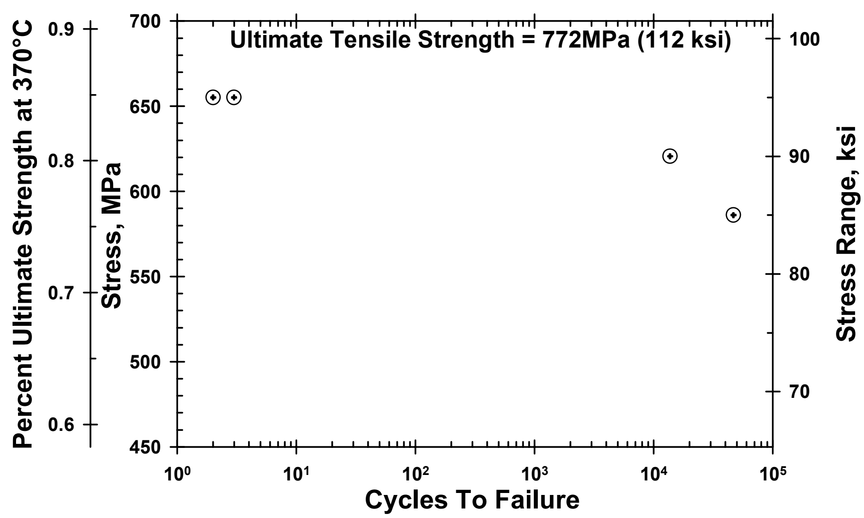

Figure 163. Approximate S-N curve for T650-35/PMR-II-50 tested at R=0 and 370°C

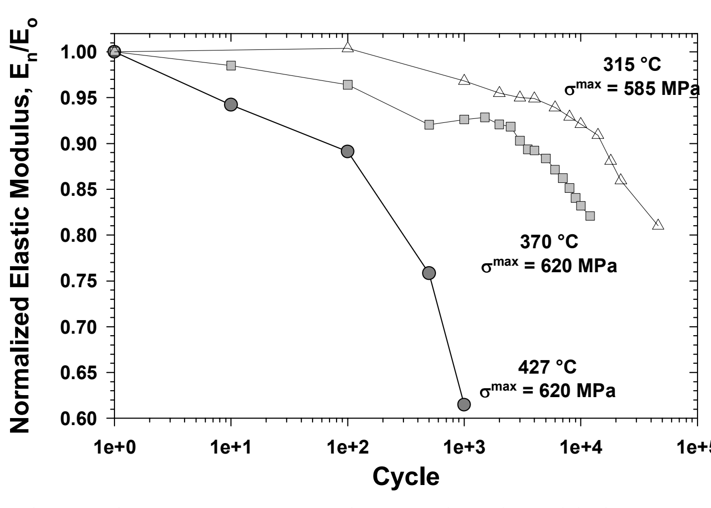

Figure 164. Tensile elastic modulus degradation as a function of fatigue cycles (R=0) for dry T650-35/PMR-II-50

Figure 165. Uncontained engine fan disk debris

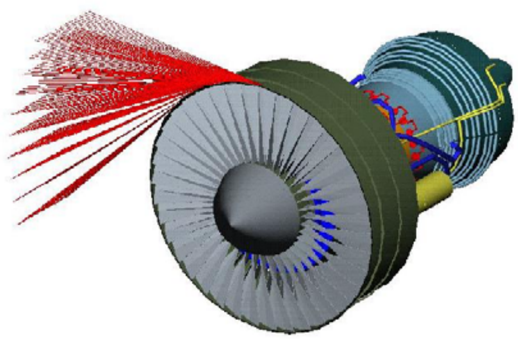

Figure 166. Uncontained engine failure model

Figure 167. Fuselage air-gun test facility

Figure 168. Photograph of Ti-6Al-4v sample after testing in compression

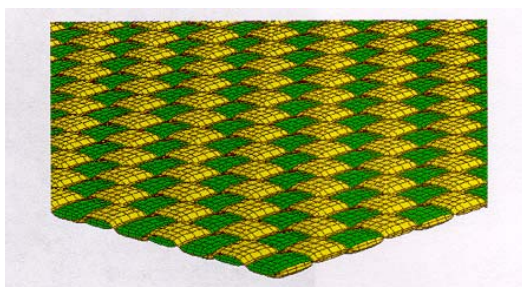

Figure 169. Woven fabric model

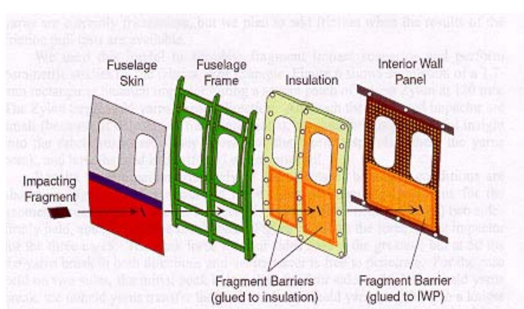

Figure 170. Armor fabric installation schematic

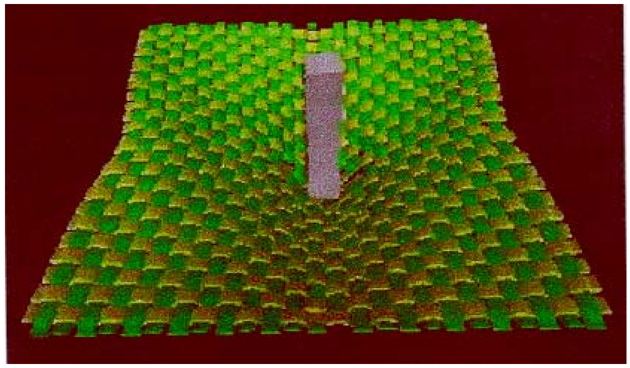

Figure 171. Model of fabric impact by debris

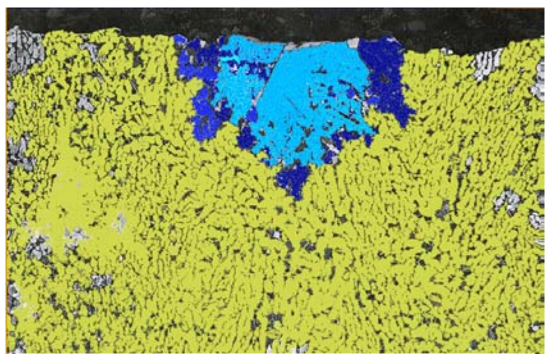

Figure 172. Cutaway of a hard-alpha defect in titanium

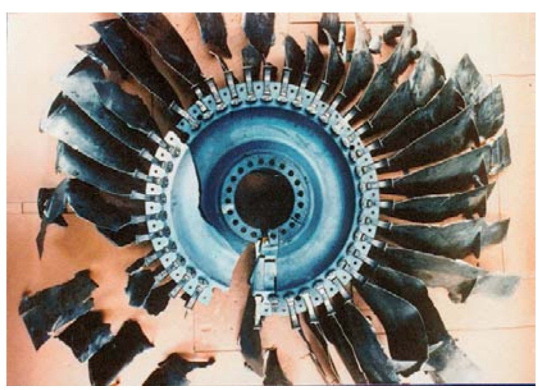

Figure 173. Fragments of an uncontained fan disk failure